Rolf E. Hummel

Electronic Properties of Materials

An Introduction for Engineers

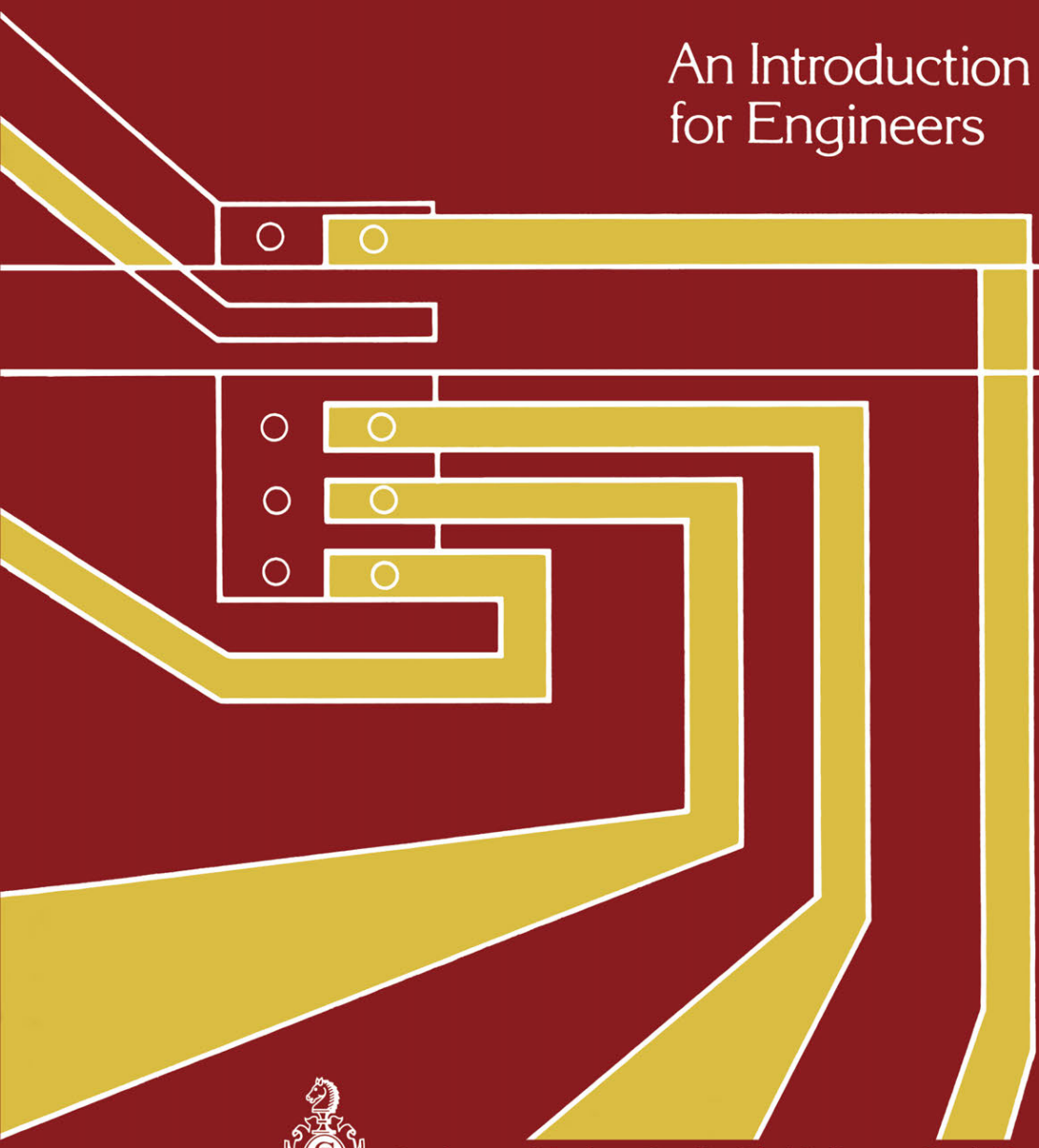

Springer-Verlag Berlin Heidelberg GmbH

Electronic Properties of Materials

Rolf E. Hummel

Electronic Properties of Materials

An Introduction for Engineers

With 219 Illustrations

Springer-Verlag Berlin Heidelberg GmbH

Rolf E. Hummel
Department of Materials Science
and Engineering
University of Florida
Gainesville, FL 32611
U.S.A.

Library of Congress Cataloging-in-Publication Data
Hummel, Rolf E., 1934–
Electronic properties of materials.
Bibliography: p.
Includes index.
1. Solid state physics. 2. Energy-band theory of solids. 3. Electronics—Materials. 4. Electric engineering—Materials. I. Title.
QC176.H86 1985 530.4'1 85-14685

ISBN 978-3-662-02426-3 ISBN 978-3-662-02424-9 (eBook)
DOI 10.1007/978-3-662-02424-9

Originally published by Springer-Verlag Berlin Heidelberg New York Tokyo in 1985
Softcover reprint of the hardcover 1st edition 1985

Typeset by Asco Trade Typesetting Ltd., North Point, Hong Kong.

9 8 7 6 5 4 3 2 1

Preface

The present book on electrical, optical, magnetic and thermal properties of materials is in many aspects different from other introductory texts in solid state physics. First of all, this book is written for engineers, particularly materials and electrical engineers who want to gain a fundamental understanding of semiconductor devices, magnetic materials, lasers, alloys, etc. Second, it stresses concepts rather than mathematical formalism, which should make the presentation relatively easy to understand. Thus, this book provides a thorough preparation for advanced texts, monographs, or specialized journal articles. Third, this book is not an encyclopedia. The selection of topics is restricted to material which is considered to be essential and which can be covered in a 15-week semester course. For those professors who want to teach a two-semester course, supplemental topics can be found which deepen the understanding. (These sections are marked by an asterisk [*].) Fourth, the present text leaves the teaching of crystallography, X-ray diffraction, diffusion, lattice defects, etc., to those courses which specialize in these subjects. As a rule, engineering students learn this material at the beginning of their upper division curriculum. The reader is, however, reminded of some of these topics whenever the need arises. Fifth, this book is distinctly divided into five self-contained parts which may be read independently. All are based on the first part, entitled "Fundamentals of Electron Theory," because the electron theory of materials is a basic tool with which most material properties can be understood. The modern electron theory of solids is relatively involved. It is, however, not my intent to train a student to become proficient in the entire field of quantum theory. This should be left to more specialized texts. Instead, the essential quantum mechanical concepts are introduced only to the extent to which they are needed for the understanding of materials science. Sixth, plenty of practical applications are presented in the text, as well as in the

problem sections, so that the students may gain an understanding of many devices that are used every day. In other words, I tried to bridge the gap between physics and engineering. Finally, I gave the treatment of the optical properties of materials about equal coverage to that of the electrical properties. This is partly due to my personal inclinations and partly because it is felt that a more detailed description of the optical properties is needed since most other texts on solid state physics devote relatively little space on this topic. It should be kept in mind that the optical properties have gained an increasing amount of attention in recent years because of their potential application in communication devices as well as their contributions to the understanding of the electronic structure of materials.

The philosophy and the substance of the present text emerged from lecture notes which I accumulated during more than twenty years of teaching. A preliminary version of Parts I and II appeared several years ago in the *Journal of Educational Modules for Materials Science and Engineering* (**4**, 1 (1982) and **4**, 781 (1982)).

I sincerely hope that the students who read and work with this book will enjoy as much as I the journey through the fascinating field of the physical properties of materials.

Each work benefits greatly from the interaction between author and colleagues or students. I am grateful in particular to Professor R.T. DeHoff, who read the entire manuscript and who helped with his inquisitive mind to clarify many points in the presentation. Professor Ken Watson read the part dealing with magnetism and made many helpful suggestions. Other colleagues to whom I am indebted are Professor Fred Lindholm, Professor Terry Orlando, and Dr. Siegfried Hofmann. My daughter, Sirka Hummel, contributed with her skills as an artist. Last, but not least, I am obliged to my family, to faculty, and to the chairman of the Department of Materials Science and Engineering at the University of Florida for providing the harmonious atmosphere which is of utmost necessity for being creative.

Contents

PART I

FUNDAMENTALS OF ELECTRON THEORY

CHAPTER 1

Introduction

The understanding of the behavior of electrons in solids is one of the keys to understanding materials. The electron theory of solids is capable of explaining optical, magnetic, thermal, as well as electrical properties of materials. In others words, the electron theory provides important fundamentals for a technology which is often considered to be the basis for modern civilization. A few examples will illustrate this. Magnetic materials are used in electric generators, motors, loudspeakers, transformers, tape recorders, and tapes. Optical properties of materials are utilized in lasers, windows, lenses, optical coatings, solar collectors, and reflectors. Thermal properties play a role in refrigeration and heating devices and in heat shields for spacecraft. Some materials are extremely good electrical conductors, such as silver and copper; others are good insulators, such as porcelain or quartz. Semiconductors are generally poor conductors at room temperature. However if traces of certain elements are added, the electrical conductivity increases.

Since the invention of the transistor in the late 1940s, the electronic industry has grown to an annual sales level of about one trillion dollars. From the very beginning, materials and materials research have been the lifeblood of the electronics industry.

For the understanding of the electronic properties of materials three approaches have been developed during the past hundred years or so which differ considerably in their philosophy and their level of sophistication. In the last century, a phenomenological description of the experimental observation was widely used. The laws which were eventually discovered were empirically derived. This "continuum theory" considered only macroscopic quantities and interrelated experimental data. No assumptions were made about the structure of matter when the equations were formulated. The conclusions which can be drawn from the empirical laws still have validity, at least as long

as no oversimplifications are made during their interpretation. Ohm's law, the Maxwell equations, Newton's law, or the Hagen–Rubens equation may serve as examples.

A refinement in understanding the properties of materials was accomplished at the turn of this century by introducing atomistic principles into the description of matter. The "classical electron theory" postulated that free electrons in metals drift as a response to an external force and interact with certain lattice atoms. Paul Drude was the principal proponent of this approach. He developed several fundamental equations which are still widely utilized today. We shall make extensive use of the Drude equations in subsequent parts of this book.

A further refinement was accomplished at the beginning of this century by quantum theory. This approach was able to explain important experimental observations which could not be readily interpreted by classical means. Quantum theory, however, lacks vivid visualization of the phenomena which it describes. Thus, a considerable effort needs to be undertaken to comprehend its basic concepts; but mastering its principles leads to a much deeper understanding of the electronic properties of materials.

The first part of the present book introduces the reader to the fundamentals of quantum theory. Upon completion of this part the reader should be comfortable with terms such as Fermi energy, density of states, Fermi distribution function, band structure, Brillouin zones, effective mass of electrons, uncertainty principle, and quantization of energy levels. These concepts will be needed in the following parts of the book.

It is assumed that the reader has taken courses in freshman physics, chemistry, and differential equations. From these courses the reader should be familiar with the necessary mathematics and relevant equations and definitions, such as:

Newton's law: force equals mass times acceleration ($F = ma$), (1.1)

Kinetic energy: $E_{\text{kin}} = \frac{1}{2}mv^2$ (v is the particle velocity), (1.2)

Momentum: $p = mv$, (1.3)

Combining (1.2) and (1.3) yields $E_{\text{kin}} = \dfrac{p^2}{2m}$, (1.4)

Speed of light: $c = \nu\lambda$ (ν = frequency of the light wave, and λ its wavelength), (1.5)

Velocity of a wave: $u = \nu\lambda$, (1.6)

Angular frequency: $\omega = 2\pi\nu$, (1.7)

Einstein's mass–energy equivalence: $E = mc^2$. (1.8)

In order to keep the book as self-contained as possible, some fundamentals in mathematics and physics are summarized in the Appendices.

CHAPTER 2

Wave Properties of Electrons

We start our discussion with a thought which might be familiar to the reader: "Waves and particles are merely two forms of the same physical reality." This statement is true for light as well as for matter. For example, light can be described as having wave properties or, alternately, particle properties. A particle, or quantum of *light* is called a *photon* whose energy is

$$E = \nu h = \omega \hbar, \tag{2.1}$$

where h is the Planck constant and

$$\hbar = \frac{h}{2\pi}. \tag{2.2}$$

The particle property of the *electron* with mass m and charge e was discovered in 1897 by Thomson in an experiment in which he observed the deviation of a cathode ray by electric and magnetic fields. The proof for the free mobility of the electrons in a metal was accomplished by measurement of inertia effects by Tolman.

In 1924 de Broglie introduced the thought that electrons should also have wave properties. He connected the wavelength λ of an electron wave and the momentum p of the particle by the relation

$$\lambda = \frac{h}{p} = \frac{2\pi\hbar}{p}. \tag{2.3}$$

In 1926 Schrödinger gave this thought by de Broglie a mathematical form. In 1927, Davisson, Germer, and G.P. Thomson discovered electron diffraction by a crystal which finally proved the wave nature of electrons.

The property of the electron shall be described in the following by a de Broglie wave, or by a wave function Ψ. This wave function does not represent

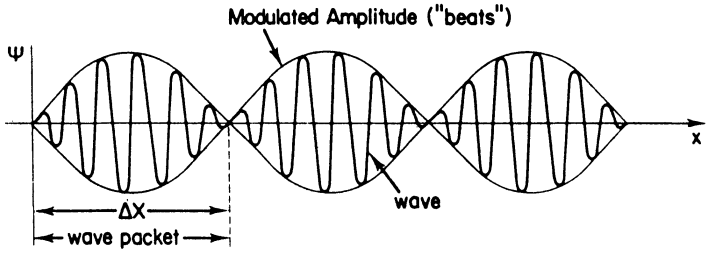

Figure 2.1. Combination of two waves of slightly different frequencies. ΔX is the distance over which the particle can be found.

physical waves or other physical quantities. It should be understood merely as a mathematical description of a particle (the electron) which enables us to calculate its actual behavior in a convenient way. This thought probably sounds unfamiliar to a beginner in quantum physics. However, by repeated exposure, one can become accustomed to it.

The wave–particle duality can be better understood by realizing that the electron, described as a particle, can be represented by a combination of several wave trains having slightly different frequencies between ω and $\omega + \Delta\omega$. Let us study this, assuming at first only *two* waves, which shall be written as

$$\Psi_1 = \sin(kx - \omega t) \tag{2.4a}$$

and

$$\Psi_2 = \sin[kx - (\omega + \Delta\omega)t]. \tag{2.4b}$$

Superposition of Ψ_1 and Ψ_2 yields a new wave Ψ. With $\sin\alpha + \sin\beta = 2\cos\frac{1}{2}(\alpha - \beta) \cdot \sin\frac{1}{2}(\alpha + \beta)$ we obtain

$$\Psi_1 + \Psi_2 = \Psi = \underbrace{2\cos\frac{\Delta\omega}{2}t}_{\substack{\text{Modulated} \\ \text{amplitude}}} \cdot \underbrace{\sin\left[kx - \left(\omega + \frac{\Delta\omega}{2}\right)t\right]}_{\substack{\text{Sine wave} \\ \text{amplitude}}}. \tag{2.5}$$

Equation (2.5) describes a sine wave (having a frequency intermediately between ω and $\omega + \Delta\omega$) whose amplitude is slowly modulated by a cosine function. (This familiar effect in acoustics can be heard in the form of "beats" when two strings of a piano have a slightly different pitch. The beats become less rapid the smaller the difference in frequency $\Delta\omega$ between the two strings until they finally cease once both strings have the same pitch, (2.5).) Each of the "beats" represents a "wave packet" (Fig. 2.1). The wave packet becomes "larger" the slower the beats, i.e., the smaller $\Delta\omega$. The extreme conditions are as follows: (a) no variation in ω (i.e., $\Delta\omega = 0$), which yields an "infinitely long" wave packet, i.e., a monochromatic wave. This corresponds to the wave

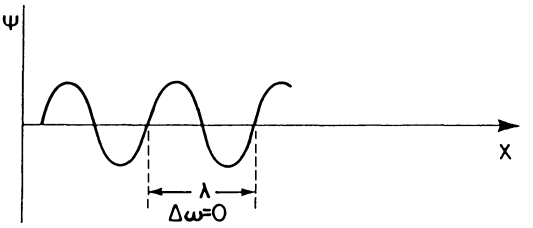

Figure 2.2. Monochromatic matter wave ($\Delta\omega = 0$). The wave has constant amplitude. The matter wave travels with the phase velocity u.

picture of an electron (see Fig. 2.2). (b) alternately, $\Delta\omega$ could be assumed to be very large. This yields small wave packets. If a large number of different waves are considered (rather than two waves Ψ_1 and Ψ_2), filling the frequencies between ω and $\Delta\omega$, the string of wave packets shown in Fig. 2.1 reduces to *one* wave packet. The electron is then represented by a particle.

Different velocities are involved:

(a) The velocity of the *matter wave* is called the wave velocity or "*phase velocity*," u. As we saw above, the matter wave is a monochromatic wave (or a stream of particles of equal velocity) whose frequency ω, wavelength λ, momentum p or energy E can be exactly determined (Fig. 2.2). The location of the particles, however, is undetermined. The phase velocity can be calculated with $E = vh$ (2.1), $E = mc^2$ (1.8), $h = p\lambda$ (2.3), and (1.6) to

$$u = v\lambda = \frac{Eh}{hp} = \frac{mc^2}{mv_g} = \frac{c^2}{v_g} \tag{2.6}$$

(v_g is the group velocity; see below). We can deduce from this equation that matter waves show dispersion and that the phase velocity of an electron wave has a velocity larger than the speed of light, i.e., $u > c$. (This latter result is not a contradiction of the theory of relativity because matter waves, due to the identity of their amplitudes, cannot be used for the transmittance of information.)

(b) We mentioned above that a *particle* can be understood to be "composed of" a group of waves or a "wave packet." Each wave has a slightly different frequency ranging between ω and $\omega + \Delta\omega$. Appropriately, the velocity of a particle is called "*group velocity*," v_g. The "envelope" (modulated amplitude; see Fig. 2.1) propagates with the group velocity v_g. The sine wave inside of the envelope propagates with a velocity u which is larger than v_g (Eqn. 2.6). The location X of a particle is precisely known, whereas the frequency is not. This is due to the fact that a wave packet can be thought to "consist" of several wave functions $\Psi_1, \Psi_2, \ldots, \Psi_n$ with different frequencies between ω and $\omega + \Delta\omega$. Another way of looking at it is to perform a Fourier analysis of a single disturbance (Fig. 2.3) which results in a series of sine and cosine functions (waves) which have different

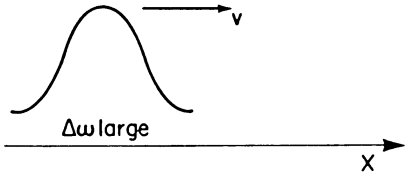

Figure 2.3. Particle moving with group velocity v_g ($\Delta\omega$ is large).

wavelengths. The better the location, ΔX, of a particle can be determined, the wider the frequency range, $\Delta\omega$, of its waves. This is one form of Heisenberg's uncertainty principle,

$$\Delta p \cdot \Delta X \geqslant h, \tag{2.7}$$

stating that the distance over which there is a finite probability of finding an electron, ΔX, and the range of momenta of the electron wave (which is proportional to the frequency) is a constant. This means that location and frequency of an electron cannot be accurately determined at the same time.

In summary, we can define the phase velocity as

$$u = \frac{\omega}{k} \tag{2.8}$$

and the group velocity as

$$v_g = \frac{d\omega}{dk}, \tag{2.9}$$

where $|\mathbf{k}|$ is the wave vector which we shall introduce in Chapter 4. Equations (2.8) and (2.9) show in mathematical form that the group velocity describes the velocity of a wave pulse (quantum) whereas the phase velocity describes the velocity of a monochromatic wave.

After this discussion of the wave–particle duality and the general behavior of electron waves, we turn now to practical applications.

We have already mentioned that the Ψ-waves cannot be understood in terms of real physical quantities. For the interpretation of the wave functions, we shall therefore use Born's postulate which states that the square of the wave function (or because Ψ is generally a complex function, the quantity $\Psi\Psi^*$) is the probability of finding a particle at a certain location. (Ψ^* is the complex conjugate quantity of Ψ.) In other words,

$$\Psi\Psi^* \, dx \, dy \, dz = \Psi\Psi^* \, d\tau \tag{2.10}$$

is the probability of finding an electron in the volume element $d\tau$.

We are interested in the following question: How do the electrons behave in a potential field of an atomic nucleus or an arrangement of atoms within a crystal? To answer this, we have to write an expression for the potential

field in terms of a potential energy V. The general method for the solution of wave mechanical problems which we will apply below is, therefore: At first, an expression for the potential V has to be found which describes the actual situation. Then, one inserts this expression into the Schrödinger equation and solves it with the aid of "boundary conditions." In this way, one obtains solutions for Ψ as a function of space (and time) which one interprets by means of (2.10).

The description of the method of solution just described makes it clear that in wave mechanics probability statements are obtained, whereas in classical mechanics the location of a particle can be exactly determined. We will see, however, that this does not affect the value of our results.

Problems

1. Calculate the wavelength of an electron in a metal which has a kinetic energy of 4 eV.
2. What should be the energy of an electron so that the associated electron waves have a wavelength of 600 nm?
3. Since the visible region spans between approximately 400 nm and 700 nm, why can the electron wave mentioned in Problem 2 not be seen with human eyes? What kind of device is necessary to detect electron waves?
4. What is the energy of a light quantum (photon) which has a wavelength of 600 nm? Compare the energy with the electron wave energy calculated in Problem 2 and discuss the difference.

CHAPTER 3

The Schrödinger Equation

All "derivations" of the Schrödinger equation start in one way or another from certain assumptions which cause the uninitiated reader to ask the legitimate question, "Why just in this way?"

It is, therefore, not intended here to "derive" the Schrödinger equation. We consider this relation as a fundamental equation for the description of wave properties of electrons, just as Newton's equations describe the matter properties of large particles.

The *time independent* Schrödinger equation will always be applied when the properties of atomic systems have to be calculated in stationary conditions, i.e., when the property of the surroundings of the electron does not change with time. In this case the potential energy V depends only on the location (and not, in addition, on the time). Therefore the time independent Schrödinger equation is an equation of a *vibration*. It has the following form:

$$\boxed{\nabla^2\psi + \frac{2m}{\hbar^2}(E - V)\psi = 0,} \tag{3.1}$$

where

$$\nabla^2\psi = \frac{\partial^2\psi}{\partial x^2} + \frac{\partial^2\psi}{\partial y^2} + \frac{\partial^2\psi}{\partial z^2}, \tag{3.2}$$

m is the mass of the electron, and

$$E = E_{\text{kin}} + V \tag{3.3}$$

is the total energy of the system.

In (3.1) we wrote for the wave function a lower case ψ which we shall always use from now on when we want to state explicitly that the wave function is only space dependent. Thus, we split from Ψ a time dependent part:

$$\Psi(x, y, z, t) = \psi(x, y, z) \cdot e^{i\omega t}. \tag{3.4}$$

The *time dependent* Schrödinger equation is a *wave* equation because it contains derivatives of Ψ with respect to space *and* time. One obtains this equation from (3.1) by eliminating the total energy,

$$E = vh = \omega\hbar, \tag{3.5}$$

where ω is obtained by differentiating (3.4) with respect to time:

$$\frac{\partial \Psi}{\partial t} = \psi i\omega e^{i\omega t} = \Psi i\omega. \tag{3.6}$$

This yields

$$\omega = -\frac{i}{\Psi}\frac{d\Psi}{dt} \tag{3.7}$$

and

$$\boxed{\nabla^2\Psi - \frac{2mV}{\hbar^2}\Psi - \frac{2mi}{\hbar}\frac{\partial \Psi}{\partial t} = 0.} \tag{3.8}$$

It should be noted here that quantum mechanical equations can be obtained from classical equations by applying two differential operators upon the wave function Ψ (Hamiltonian operators). They are

$$E \triangleq \hbar i\frac{\partial}{\partial t} \tag{3.9}$$

and

$$\mathbf{p} \triangleq -\hbar i\nabla. \tag{3.10}$$

When these operators are applied to

$$E_{\text{total}} = E_{\text{kin}} + E_{\text{pot}} = \frac{p^2}{2m} + V \tag{3.11}$$

we obtain

$$\hbar i\frac{\partial \Psi}{\partial t} = \frac{\hbar^2 i^2}{2m}\nabla^2\Psi + V\Psi, \tag{3.12}$$

which yields, after rearranging, the time dependent Schrödinger equation (3.8).

3.1. Special Properties of Vibrational Problems

The solution of an equation for vibration is determined except for certain constants. These constants are calculated by using boundary or starting conditions,

$$(\text{e.g., } \psi = 0 \text{ at } x = 0). \tag{3.13}$$

As we will see in Section 4.2, only certain vibrational forms are possible when boundary conditions are imposed. This is similar to the vibrational forms of a vibrating string, where the fixed ends cannot undergo vibrations. Vibrational problems which are determined by boundary conditions are called *boundary* or *eigenvalue problems*. It is the peculiarity of vibrational problems with boundary conditions that not all frequency values are possible and, therefore, because of

$$E = vh \tag{3.14}$$

not all values for the energy are allowed. One calls the values which are allowed, eigenvalues. The functions ψ which belong to the eigenvalues, and which are a solution of the vibration equation and in addition satisfy the boundary conditions, are called *eigenfunctions* of the differential equation.

In Section 2 we have related the product $\psi\psi^*$ (which is called the "norm") to the probability of finding a particle at a given location. The probability of finding a particle somewhere in space is one, or

$$\int \psi\psi^* \, d\tau = \int |\psi|^2 \, d\tau = 1. \tag{3.15}$$

Equation (3.15) is called the normalized eigenfunction.

Problems

1. Write a mathematical expression for a vibration (vibrating string, for example) and for a wave. (See Appendix 1.) Familiarize yourself with the way these differential equations are solved. What is a "trial solution?" What is a boundary condition?
2. Define the terms "vibration" and "wave."
3. What is the difference between a damped and an undamped vibration? Write the appropriate equations.
4. What is the complex conjugate function of
   a) $\hat{x} = a + bi$,
   b) $\Psi = 2Ai \sin \alpha x$.

CHAPTER 4

Solution of the Schrödinger Equation for Four Specific Problems

4.1. Free Electrons

At first we solve the Schrödinger equation for a simple but nevertheless very important case. We consider electrons which propagate freely, that is, in a potential free space in the positive x direction. The potential energy V is then zero and the Schrödinger equation (3.1) assumes the following form:

$$\frac{d^2\psi}{dx^2} + \frac{2m}{\hbar^2} E\psi = 0. \tag{4.1}$$

This is a differential equation for an undamped vibration[1] with spatial periodicity whose solution is known to be[1]

$$\psi(x) = Ae^{ikx} \equiv A\cos kx + iA\sin kx, \tag{4.2}$$

where

$$k = \sqrt{\frac{2m}{\hbar^2} E}. \tag{4.3}$$

For our special case we do not write the second term in (A.5)[1]

$$u = Ae^{i\alpha x} + Be^{-i\alpha x} \tag{4.4}$$

because we stipulated above that the electron wave[1]

$$\Psi(x) = Ae^{ikx} \cdot e^{-i\omega t} \tag{4.5}$$

propagates only in the positive x direction and not, in addition, in the negative x direction.

---

[1] See Appendix 1.

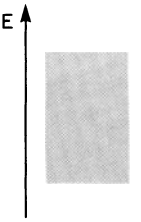

Figure 4.1. Energy continuum of a free electron (compare to Fig. 4.3).

From (4.3), it follows that

$$E = \frac{\hbar^2}{2m} k^2. \tag{4.6}$$

Combining (4.3), (2.3) and (1.4), that is,

$$E = \frac{p^2}{2m}, \tag{4.7}$$

yields

$$k = \sqrt{\frac{2mE}{\hbar^2}} = \frac{p}{\hbar} = \frac{2\pi}{\lambda}. \tag{4.8}$$

We see from (4.8) that the quantity k is proportional to the momentum p and, because of $\mathbf{p} = m\mathbf{v}$, also proportional to the velocity of the electrons. Since both momentum and velocity are vectors, it follows that k is a vector too. Therefore, we actually should write k as a vector which has the components k_x, k_y, and k_z:

$$|\mathbf{k}| = \frac{2\pi}{\lambda}. \tag{4.9}$$

Since $\mathbf{k}$ is inversely proportional to the wave length λ, it is usually called the "wave vector." We shall use the wave vector in the following sections frequently. The $\mathbf{k}$-vector describes the wave properties of an electron just as one describes in classical mechanics the particle property of an electron with the momentum. $\mathbf{k}$ and $\mathbf{p}$ are mutually proportional, as one can see from (4.8). The proportionality factor is $1/\hbar$.

We come back now to (4.2). Since no boundary condition had to be considered for the calculation of the free flying electron, all values of the energy are "allowed," i.e., one obtains an energy continuum (Fig. 4.1). According to (4.2), free electrons are equivalent in wave mechanics to sine or cosine waves.

4.2. Electron in a Potential Well

We now consider an electron which is bound to its atomic nucleus. For simplicity, we assume that the electron can move freely only between two infinitely high potential barriers (Fig. 4.2). Therefore, the potential barriers do not allow the electron to escape from this potential well, which means that $\psi = 0$ for $x \leqq 0$ and $x \geqq a$. We first treat the one-dimensional case just as in Section 4.1, i.e., we assume that the electron propagates only along the x-axis. However, because the electron is reflected on the walls of the well, it can now propagate in the positive as well as in the negative x direction. In this respect, the present problem is different from the preceding one. The potential energy inside of the well is zero, as before, so that the Schrödinger equation for an electron in this region can be written as before as

$$\frac{d^2\psi}{dx^2} + \frac{2m}{\hbar^2} E\psi = 0. \tag{4.10}$$

Because of the two propagation directions of the electron, the solution of (4.10) is

$$\psi = Ae^{i\alpha x} + Be^{-i\alpha x}, \tag{4.11}$$

(see Appendix 1), where

$$\alpha = \sqrt{\frac{2m}{\hbar^2} E}. \tag{4.12}$$

We determine now the constants A and B by means of boundary conditions. We just mentioned that at $x \leqq 0$ and $x \geqq a$ the ψ function is zero. This boundary condition is similar to that known for a vibrating string which does not vibrate at the two points where it is clamped down. (See also Fig. 4.4(a).) Thus, for $x = 0$ we stipulate $\psi = 0$. Then we obtain from (4.11)

$$B = -A. \tag{4.13}$$

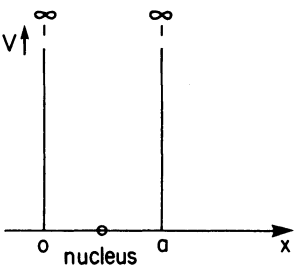

Figure 4.2. One-dimensional potential well. The walls consist of infinitely high potential barriers.

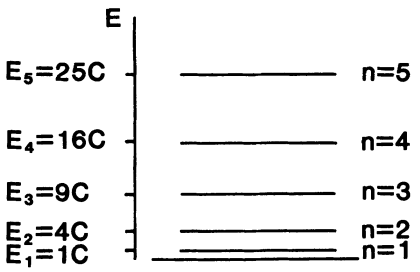

Figure 4.3. Allowed energy values of an electron which is bound to its atomic nucleus. E is the excitation energy in the present case. $C = \hbar^2\pi^2/2ma^2$, see (4.18). (E_1 is the zero point energy.)

Similarly, we obtain $\psi = 0$ for $x = a$, which gives

$$0 = Ae^{i\alpha a} + Be^{-i\alpha a}. \tag{4.14}$$

With (4.13) and Euler's equation

$$\sin\rho = \frac{1}{2i}(e^{i\rho} - e^{-i\rho}) \tag{4.15}$$

(see Appendix 2), we write

$$A[e^{i\alpha a} - e^{-i\alpha a}] = 2Ai \cdot \sin\alpha a = 0. \tag{4.16}$$

Equation (4.16) is only valid if $\sin\alpha a = 0$, i.e., if

$$\alpha a = n\pi, \qquad n = 0, 1, 2, 3, \ldots. \tag{4.17}$$

Substituting the value of α from (4.12) into (4.17) provides

$$E_n = \frac{\hbar^2}{2m}\alpha^2 = \frac{\hbar^2\pi^2}{2ma^2}n^2, \qquad n = 1, 2, 3, \ldots. \tag{4.18}$$

(We exclude the solution $n = 0$ because for $n = 0$ it follows that $\psi = 0$ and thus $\psi\psi^* = 0$.) We notice immediately a striking difference from the problem in Section 4.1. Because of the boundary conditions, only certain solutions of the Schrödinger equation exist, namely those for which n is an integer. In the present case the energy assumes only those values which are determined by (4.18). All other energies are not allowed. The allowed values are called "energy levels." They are shown in Fig. 4.3 for a one-dimensional case. Because of the fact that an electron of an isolated atom can assume only certain energy levels, it follows that the energies which are excited or absorbed also possess only discrete values.

We determine now the wave function ψ, and the probability ($\psi\psi^*$) for finding an electron within the potential well. We apply the method described in Section 2. According to (4.11), (4.13), and Euler's equation (4.15) we obtain within the well

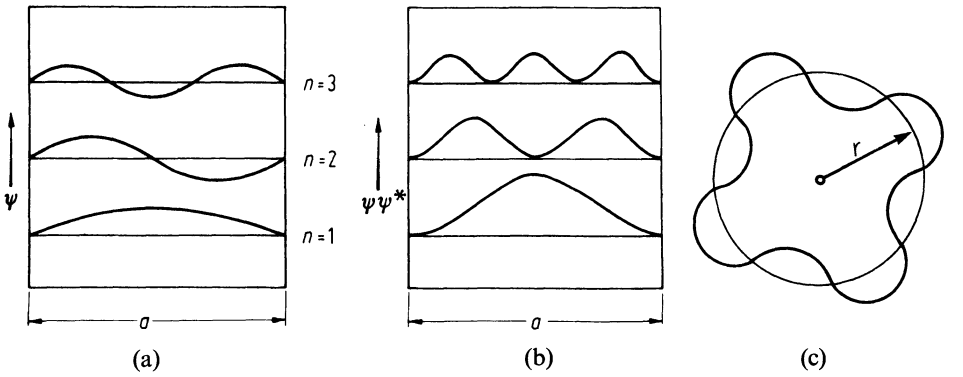

Figure 4.4. (a) ψ function and (b) probability function $\psi\psi^*$ for an electron in a potential well for different n-values. (c) Allowed electron orbit of an atom.

$$\psi = 2Ai \cdot \sin \alpha x, \tag{4.19}$$

and the complex conjugate of ψ

$$\psi^* = -2Ai \sin \alpha x. \tag{4.20}$$

The product $\psi\psi^*$ is then

$$\psi\psi^* = 4A^2 \sin^2 \alpha x. \tag{4.21}$$

This equation is rewritten by making use of (3.15):

$$\int_0^a \psi\psi^* \, dx = 4A^2 \int_0^a \sin^2(\alpha x) \, dx = \frac{4A^2}{\alpha}\left[-\frac{1}{2}\sin \alpha x \cos \alpha x + \frac{\alpha x}{2}\right]_0^a = 1. \tag{4.22}$$

Inserting the boundaries in (4.22) and using (4.17) provides

$$A = \sqrt{\frac{1}{2a}}. \tag{4.23}$$

Then one obtains from (4.19)

$$|\psi| = \sqrt{\frac{2}{a}} \sin \frac{n\pi}{a} x, \tag{4.24}$$

and from (4.21)

$$\psi\psi^* = \frac{2}{a} \sin^2 \frac{n\pi}{a} x. \tag{4.25}$$

Equations (4.24) and (4.25) are plotted for various n-values in Fig. 4.4. From Fig. 4.4(a), we see that standing electron waves are created between the walls of the potential well. Note that integer multiples of half a wave length are equal to the length a of the potential well. The present case, in its mathematical treatment as well as in its result, is analogous to that of a vibrating string.

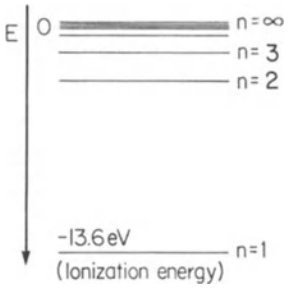

Figure 4.5. Energy levels of atomic hydrogen. E is the binding energy.

Of special interest is the behavior of the function $\psi\psi^*$, i.e., the probability of finding the electron at a certain place within the well (Fig. 4.4(b)). In the classical case the electron travels back and forth between the walls. Its probability function is therefore equally distributed along the whole length of the well. In wave mechanics the deviation from the classical case is most pronounced for $n = 1$. In this case, $\psi\psi^*$ is largest in the middle of the well and vanishes at the boundary. For higher n-values, i.e., for higher energies, the wave mechanical values for $\psi\psi^*$ are approaching the classical value.

The results which are obtained by considering an electron in a square well are similar to the ones which one receives when the wave mechanical properties of a hydrogen atom are calculated. As above, one considers an electron with charge $-e$ to be bound to its nucleus. The potential V in which the electron propagates is taken as the Coulombic potential $V = -e^2/r$. Since V is a function of the radius r, the Schrödinger equation is more conveniently expressed in polar coordinates. Of main interest are, again, the conditions under which solutions to this Schrödinger equation exist. The treatment leads, similarly as above, to discrete energy levels:

$$E = -\frac{me^4}{2\hbar^2}\frac{1}{n^2}. \tag{4.18a}$$

The main difference compared to the square well model is, however, that the energy is now proportional to $1/n^2$ (and not as in (4.18) to n^2). This results in a "crowding" of energy levels at higher energies. The energy at the lowest level is called the ionization energy, which has to be supplied to remove an electron from its nucleus. Energy diagrams, as in Fig. 4.5, are common in spectroscopy. The origin of the energy scale is arbitrarily set at $n = \infty$ and the ionization energies are counted negative. Since we are mainly concerned with the solid state, the detailed calculation of the hydrogen atom is not treated here.

It was implied above that an electron can be considered to orbit around its nucleus. Similarly as shown in Fig. 4.4(a), the electron waves associated with an orbiting electron have to be standing waves. If this would not be the case, the wave would be out of phase with itself after one orbit. After a large number of orbits, all possible phases would be obtained and the wave would be

annihilated by destructive interference (Fig. 4.4(c)). This can only be avoided if a radius is chosen so that the wave joins on itself. In this case the circumference $2\pi r$ of the orbit is an integer multiple n of the wave length λ or

$$2\pi r = n\lambda$$

which yields

$$r = \frac{\lambda}{2\pi} n.$$

This means that only certain orbits are allowed, which brings us back to the allowed energy levels which we discussed above.

So far we considered the electron to be confined into a one-dimensional well. A similar calculation for a three-dimensional potential well ("electron in a box") leads to an equation which is analogous to (4.18):

$$E_n = \frac{\hbar^2 \pi^2}{2ma^2}(n_x^2 + n_y^2 + n_z^2). \tag{4.26}$$

The smallest allowed energy in a three-dimensional potential well is occupied by an electron if $n_x = n_y = n_z = 1$. For the next higher energy there are three different possibilities for combining the n-values; namely, $(n_x, n_y, n_z) = (1, 1, 2)$, $(1, 2, 1)$, or $(2, 1, 1)$. One calls the states which have the same energy but different quantum numbers "degenerate" states. The example just given describes a threefold degenerate energy state.

*4.3. Finite Potential Barrier (Tunnel Effect)

Let us assume that a free electron, propagating in the positive x direction, encounters a potential barrier whose potential energy V_0 ("height" of the barrier) is larger than the total energy E of the electron, but is still finite (Fig. 4.6). For this case we have to write two Schrödinger equations which take into account the two different areas. In region I ($x < 0$) the electron is assumed to be free and we can write

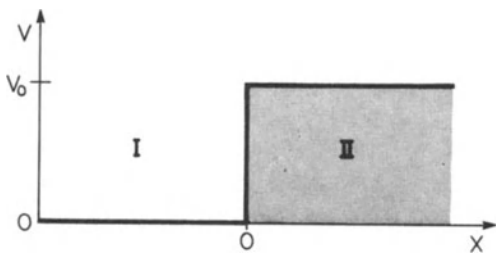

Figure 4.6. Potential barrier.

$$\text{I)} \quad \frac{d^2\psi}{dx^2} + \frac{2m}{\hbar^2} E\psi = 0. \tag{4.27}$$

Inside the potential barrier ($x > 0$) the Schrödinger equation reads

$$\text{II)} \quad \frac{d^2\psi}{dx^2} + \frac{2m}{\hbar^2}(E - V_0)\psi = 0. \tag{4.28}$$

The solution to these equations is as before (see Appendix 1):

$$\text{I)} \quad \psi_\text{I} = Ae^{i\alpha x} + Be^{-i\alpha x}, \tag{4.29}$$

where

$$\text{II)} \quad \alpha = \sqrt{\frac{2mE}{\hbar^2}} \tag{4.30}$$

and

$$\psi_\text{II} = Ce^{i\beta x} + De^{-i\beta x} \tag{4.31}$$

with

$$\beta = \sqrt{\frac{2m}{\hbar^2}(E - V_0)}. \tag{4.32}$$

A word of caution has to be said here. We stipulated above that V_0 shall be larger than E. As a consequence of this $(E - V_0)$ becomes negative and β imaginary. Therefore, we define a new constant

$$\gamma = -i\beta. \tag{4.33}$$

With (4.33), equation (4.31) becomes

$$\text{II)} \quad \psi_\text{II} = Ce^{-\gamma x} + De^{\gamma x}. \tag{4.34}$$

Next, the four constants A, B, C, D need to be determined by means of the boundary conditions:

(1) For $x \to \infty$ it follows from (4.34) that

$$\psi_\text{II} = C \cdot 0 + D \cdot \infty. \tag{4.35}$$

The consequence of (4.35) could be that ψ_II and therefore $\psi_\text{II}\psi_\text{II}^*$ are infinity. Since the probability $\psi\psi^*$ can never be larger than one (certainty) $\psi_\text{II} \to \infty$ is no solution. To avoid this, D has to go to zero:

$$D \to 0. \tag{4.36}$$

(2) The functions ψ_I and ψ_II are continuous at $x = 0$. As a consequence $\psi_\text{I} \equiv \psi_\text{II}$ at $x = 0$. This yields with (4.29), (4.34), and (4.36)

$$Ae^{i\alpha x} + Be^{-i\alpha x} = Ce^{-\gamma x}. \tag{4.37}$$

With $x = 0$, we obtain

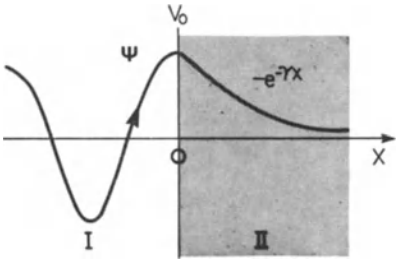

Figure 4.7. ψ function meeting a potential barrier.

$$A + B = C. \tag{4.38}$$

(3) The slopes of the wave functions in regions I and II are continuous at $x = 0$, i.e., $(d\psi_I/dx) \equiv (d\psi_{II}/dx)$. This yields:

$$Ai\alpha e^{i\alpha x} - Bi\alpha e^{-i\alpha x} = -\gamma C e^{-\gamma x}. \tag{4.39}$$

With $x = 0$, one can write

$$Ai\alpha - Bi\alpha = -\gamma C. \tag{4.40}$$

Inserting (4.38) yields

$$A = \frac{C}{2}\left(1 + i\frac{\gamma}{\alpha}\right) \tag{4.41}$$

and

$$B = \frac{C}{2}\left(1 - i\frac{\gamma}{\alpha}\right). \tag{4.42}$$

From this, the ψ function in regions I and II can be expressed in terms of an amplitude C. Of particular interest is the modified equation (4.34),

$$\psi_{II} = Ce^{-\gamma x}, \tag{4.43}$$

which expresses that the amplitude decreases in region II exponentially, as shown in Fig. 4.7. The decrease is faster the larger γ is chosen, that is, for large potential barriers V_0. If the potential barrier is only moderately high and the barrier relatively narrow, the electron wave ψ_{II} continues on the opposite side. This penetration of a potential barrier by an electron wave is called "tunneling" and has important applications in solid state physics (tunnel diode, field ion microscope). Tunneling is a quantum mechanical effect. In classical physics, only the equivalent to (4.29), i.e., a wave running towards a wall and its reflection, is observed.

If an electron is confined to a square well (Section 4.2) with *finite* potential barriers, the penetration of the electron wave into this barrier has to be considered as shown in Fig. 4.8.

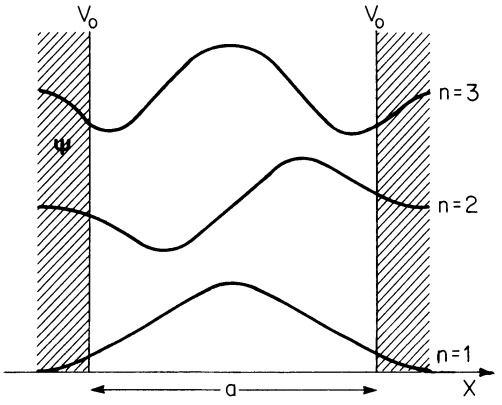

Figure 4.8. Square well with finite potential barriers.

4.4. Electron in a Periodic Field of a Crystal

In the preceding sections we got acquainted with some special cases, namely the completely free electron and the electron which is confined to a potential well. The goal of this section is to study the behavior of an electron in a crystal. We shall eventually see that the extreme cases which we treated previously can be derived from this general case.

Our first task is to find a potential distribution which is suitable for a solid. From *X*-ray diffraction investigations it is known that the atoms in a crystal are arranged periodically. Thus, for the treatment of our problem a periodic repetition of the potential well of Fig. 4.2, i.e., a periodic arrangement of potential wells and potential barriers, is most probably very close to reality and is also best suited for a calculation. Such a periodic potential is shown in Fig. 4.9 for the one-dimensional case.[2]

[2] Kronig, R. De L., Penney, W.G., *Proc. Roy. Soc.*, London, **130**, 499 (1931).

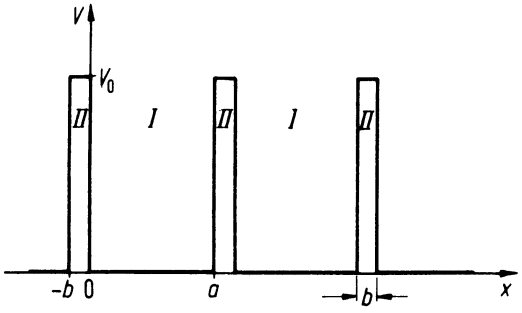

Figure 4.9. One-dimensional periodic potential distribution (simplified).

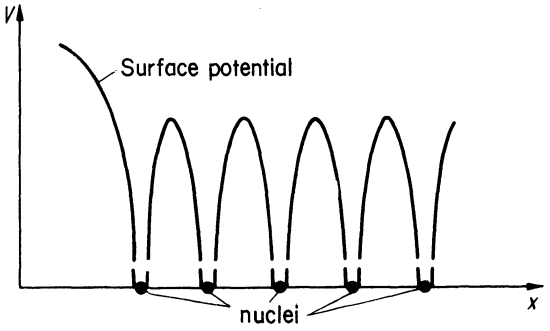

Figure 4.10. One-dimensional period potential distribution for a crystal (muffin tin potential).

The potential distribution shows potential wells of length a which we call region I. These wells are separated by potential barriers of height V_0 and width b (region II), which V_0 is assumed to be larger than the energy E of the electron.

This model is certainly a coarse simplification of the actual potential distribution in a crystal. It does not take into consideration that the inner electrons are more strongly bound to the core, i.e., that the potential function of a point charge varies as $1/r$. It also does not consider that the individual potentials from each lattice site overlap. A potential distribution which takes these features into consideration is shown in Fig. 4.10. It is immediately evident, however, that the latter model is less suitable for a simple calculation than the one which is shown in Fig. 4.9.

We write now the Schrödinger equation for regions I and II:

$$\text{I)} \quad \frac{d^2\psi}{dx^2} + \frac{2m}{\hbar^2}E\psi = 0 \tag{4.44}$$

$$\text{II)} \quad \frac{d^2\psi}{dx^2} + \frac{2m}{\hbar^2}(E - V_0)\psi = 0. \tag{4.45}$$

For abbreviation we write as before

$$\alpha^2 = \frac{2m}{\hbar^2}E \tag{4.46}$$

and

$$\beta^2 = \frac{2m}{\hbar^2}(V_0 - E). \tag{4.47}$$

(β^2 is chosen in a way to avoid β becoming imaginary.) Equations (4.44) and (4.45) need to be solved simultaneously, a task which can be achieved only with considerable mathematical effort. Bloch[3] showed that the solution of this type of equation has the following form:

[3] Bloch, F., *Z. Phys.* **52**, 555 (1928); **59**, 208 (1930).

$$\psi(x) = u(x) \cdot e^{ikx} \tag{4.48}$$

(Bloch function), where $u(x)$ is a periodic function which possesses the periodicity of the lattice in the x direction. Therefore, $u(x)$ is no longer a constant (amplitude A) as in (4.5), but changes periodically with increasing x (modulated amplitude). Of course $u(x)$ is different for various directions in the crystal lattice.

The reader who is basically interested in the results and their implications to the electronic structure of crystals may skip the mathematical treatment given below and may refer directly to (4.67).

Differentiating the Bloch function (4.48) twice with respect to x provides

$$\frac{d^2\psi}{dx^2} = \left(\frac{d^2u}{dx^2} + \frac{du}{dx}2ik - k^2u\right)e^{ikx}. \tag{4.49}$$

We insert (4.49) into (4.44) and (4.45) and take into account the abbreviations (4.46) and (4.47):

$$\text{I)} \quad \frac{d^2u}{dx^2} + 2ik\frac{du}{dx} - (k^2 - \alpha^2)u = 0 \tag{4.50}$$

$$\text{II)} \quad \frac{d^2u}{dx^2} + 2ik\frac{du}{dx} - (k^2 + \beta^2)u = 0. \tag{4.51}$$

Equations (4.50) and (4.51) have the form of an equation of a damped vibration. The solution[4] to (4.50) and (4.51) is

$$\text{I)} \quad u = e^{-ikx}(Ae^{i\alpha x} + Be^{-i\alpha x}) \tag{4.55}$$

$$\text{II)} \quad u = e^{-ikx}(Ce^{-\beta x} + De^{\beta x}). \tag{4.56}$$

We have four constants A, B, C, D which we need to dispose of by means of four boundary conditions: The functions ψ and $d\psi/dx$ pass over continuously from region I into region II at the point $x = 0$. Equation I = Equation II for $x = 0$ yields:

$$A + B = C + D. \tag{4.57}$$

(du/dx) for I = (du/dx) for II at $x = 0$ provides

$$A(i\alpha - ik) + B(-i\alpha - ik) = C(-\beta - ik) + D(\beta - ik). \tag{4.58}$$

---

[4] Differential equation of a damped vibration for spatial periodicity (see Appendix 1)

$$\frac{d^2u}{dx^2} + D\frac{du}{dx} + Cu = 0. \tag{4.52}$$

Solution:

$$u = e^{-(D/2)x}(Ae^{i\delta x} + Be^{-i\delta x}), \tag{4.53}$$

where

$$\delta = \sqrt{C - \frac{D^2}{4}}. \tag{4.54}$$

Further, ψ and therefore u shall be continuous at the distance $(a + b)$. This means that equation I at $x = 0$ must be equal to equation II at $x = a + b$, or, more simply, equation I at $x = a$ is equal to equation II at $x = -b$ (see Fig. 4.9). This yields:

$$Ae^{(i\alpha - ik)a} + Be^{(-i\alpha - ik)a} = Ce^{(ik+\beta)b} + De^{(ik-\beta)b}. \tag{4.59}$$

Finally, (du/dx) shall be periodic in $a + b$:

$$\begin{aligned} &Ai(\alpha - k)e^{ia(\alpha-k)} - Bi(\alpha + k)e^{-ia(\alpha+k)} \\ &\quad = -C(\beta + ik)e^{(ik+\beta)b} + D(\beta - ik)e^{(ik-\beta)b}. \end{aligned} \tag{4.60}$$

The constants A, B, C, and D can be determined by means of these four equations which, when inserted in (4.55) and (4.56), provide values for u. This also means that solutions for the function ψ can be given by using (4.48). However, as in the preceding sections, the knowledge of the ψ function is not of primary interest. We are searching instead for a condition which tells us where solutions to the Schrödinger equations (4.44) and (4.45) exist. We recall that just these limiting conditions were leading to the energy levels in Section 4.2. We proceed here in the same manner.

If equations (4.57)–(4.60) are consistent in themselves, it follows that the determinant formed out of the coefficients of A, B, C, and D has to be zero. The lengthy calculation provides, using Euler's equations[5]

$$\frac{\beta^2 - \alpha^2}{2\alpha\beta}\sinh(\beta b)\cdot\sin(\alpha a) + \cosh(\beta b)\cos(\alpha a) = \cos k(a + b). \tag{4.61}$$

For simplification of the discussion of this equation we make the following stipulation. The potential barriers in Fig. 4.9 shall be of the kind such that b is very small and V_0 is very large. It is further assumed that the product $V_0 b$, i.e., the area of this potential barrier, remains finite. In other words, if V_0 grows, b diminishes accordingly. The product $V_0 b$ is called the potential barrier strength.

If V_0 is very large, then E in (4.47) can be considered to be small compared to V_0 and can therefore be neglected so that

$$\beta = \sqrt{\frac{2m}{\hbar^2}}\sqrt{V_0}. \tag{4.62}$$

Multiplication of (4.62) with b yields:

$$\beta b = \sqrt{\frac{2m}{\hbar^2}}\sqrt{(V_0 b)b}. \tag{4.63}$$

Since $V_0 b$ has to remain finite (see above) and $b \to 0$ it follows that βb becomes very small. For a small βb we obtain (see tables of the hyperbolic functions)

[5] See Appendix 2.

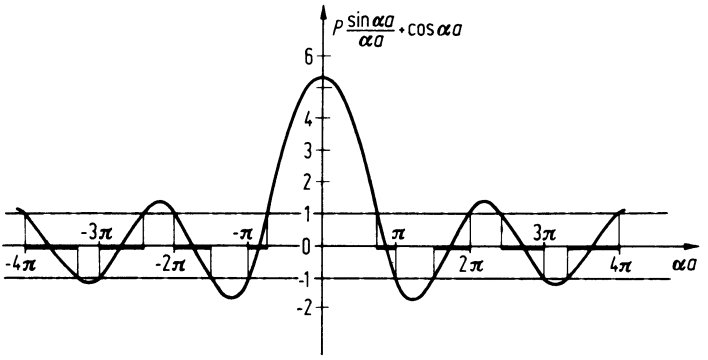

Figure 4.11. Function $P(\sin\alpha a/\alpha a) + \cos\alpha a$ versus αa. P was arbitrarily set to be $(3/2)\pi$.

$$\cosh(\beta b) \approx 1 \quad \text{and} \quad \sinh(\beta b) \approx \beta b. \tag{4.64}$$

Finally, one can neglect α^2 compared to β^2 and b compared to a (see (4.46), (4.47), and Fig. 4.9) so that (4.61) reads as follows:

$$\frac{m}{\alpha\hbar^2} V_0 b \sin\alpha a + \cos\alpha a = \cos ka. \tag{4.65}$$

With the abbreviation

$$P = \frac{maV_0 b}{\hbar^2} \tag{4.66}$$

we finally get from (4.65)

$$\boxed{P\frac{\sin\alpha a}{\alpha a} + \cos\alpha a = \cos ka.} \tag{4.67}$$

This is the desired relation which provides the allowed solutions to the Schrödinger equations (4.44) and (4.45). We notice that the boundary conditions lead to an equation with trigonometric functions. Therefore, only certain values of α are possible. This in turn means that because of (4.46), only certain values for the energy E are defined. This is quite similar to the case in Section 4.2. One can assess the situation best if one plots the function $P(\sin\alpha a/\alpha a) + \cos\alpha a$ versus αa which is done in Fig. 4.11 with $P = (3/2)\alpha$. It is of particular significance that the right-hand side of (4.67) allows only certain values of this function because $\cos ka$ is only defined between $+1$ and -1 (except for imaginary k values). This is shown in Fig. 4.11 in which the allowed values of the function $P(\sin\alpha a/\alpha a) + \cos\alpha a$ are marked by heavy lines on the αa-axis.

We arrive herewith at the following, very important result: Because αa is a function of the energy, the above-mentioned limitation means that an

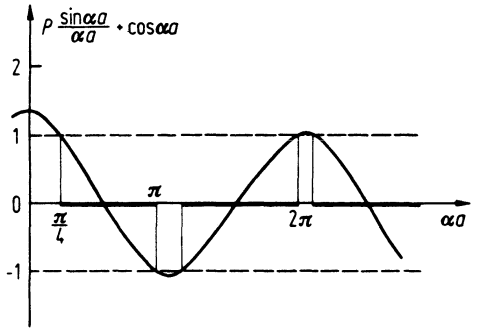

Figure 4.12. Function $P(\sin \alpha a/\alpha a) + \cos \alpha a$ versus αa with $P = \pi/10$.

electron, which moves in a periodically varying potential field, can only occupy certain allowed energy zones. Energies outside of these allowed zones or "bands" are prohibited. One sees from Fig. 4.11 that with increasing values of αa (i.e., with increasing energy), the disallowed (or forbidden) bands become narrower. The size of the allowed and forbidden energy bands varies with the variation of P. Below, four special cases will be discussed.

(a) The "potential barrier strength" $V_0 b$ (see Fig. 4.9) shall be large. Then, according to (4.66), P is also large and the curve in Fig. 4.11 proceeds more steeply. The allowed bands are narrow.

(b) If the potential barrier strength and therefore P is small, the allowed bands become wider (see Fig. 4.12).

(c) If the potential barrier strength becomes smaller and smaller and finally disappears completely, P goes toward zero, and one obtains from (4.67)

$$\cos \alpha a = \cos ka \tag{4.68}$$

or $\alpha = k$. From this it follows with (4.46), that

$$E = \frac{\hbar^2 k^2}{2m}.$$

This is the well-known equation (4.6) for free electrons which we derived in Section 4.1.

(d) If the potential barrier strength is very large, P approaches infinity. However, because the left-hand side of (4.67) has to stay within the limits ± 1, i.e., it has to remain finite, it follows that

$$\frac{\sin \alpha a}{\alpha a} \to 0$$

that is, $\sin \alpha a \to 0$. This is only possible if $\alpha a = n\pi$ or

$$\alpha^2 = \frac{n^2 \pi^2}{a^2}, \quad \text{for } n = 1, 2, 3, \ldots. \tag{4.69}$$

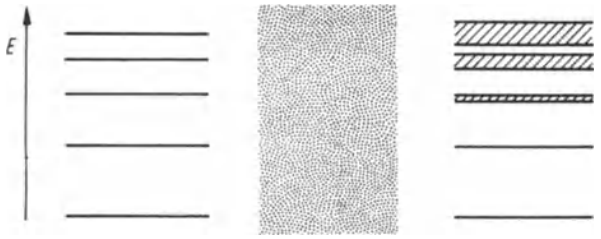

Figure 4.13. Allowed energy levels for (a) bound electrons, (b) free electrons, and (c) electrons in a solid.

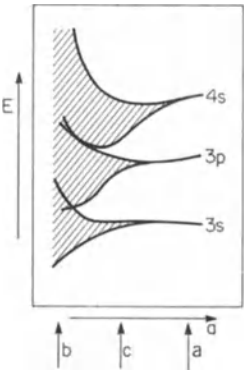

Figure 4.14. Widening of the sharp energy levels into bands and finally into a quasi-continuous energy region with decreasing atomic distance a for a metal (after calculations of Slater). The quantum numbers are explained in Appendix 3.

Combining (4.46) with (4.69) yields

$$E = \frac{\pi^2 \hbar^2}{2ma^2} \cdot n^2,$$

which is the result of Section 4.2, equation (4.18).

We summarize (Fig. 4.13): If the electrons are strongly bound, i.e., if the potential barrier is very large, one obtains sharp energy levels. (Electron in the potential field of *one* ion.) If the electron is not bound, one obtains a continuous energy region (free electrons). If the electron moves in a periodic potential field one receives energy bands (solid).

The widening of the energy levels into energy bands and the transition into a quasicontinuous energy region is shown in Fig. 4.14. This widening occurs because the atoms increasingly interact as their mutual distance decreases. The arrows a, b, and c refer to the three sketches of Fig. 4.13.

Problems

1. Describe the energy for
   a) A free electron;
   b) A strongly bound electron;
   c) An electron in a periodic potential;
   Why do we get these different band schemes?

2. Sketch $\psi\psi^*$ for $n = 78$ for an electron in a potential well. What conclusions can be drawn from this sketch?

3. State the two Schrödinger equations for electrons in a periodic potential field (Kronig–Penny model). Use for their solutions, instead of the Bloch function, the trial solution

$$\psi(x) = Ae^{ikx}.$$

   Discuss the result. (*Hint:* For free electrons $V_0 = 0$.)

*4. When treating the Kronig–Penny model, we arrived at four equations for the constants A, B, C, D. Write the determinant and confirm (4.61):

$$\frac{\beta^2 - \alpha^2}{2\alpha\beta}\sinh(\beta b)\cdot\sin(\alpha a) + \cosh(\beta b)\cos(\alpha a) = \cos k(a + b).$$

5. The differential equation for an undamped vibration is

$$a\frac{d^2u}{dx^2} + bu = 0 \tag{1}$$

   whose solution is

$$u = Ae^{ikx} + Be^{-ikx}, \tag{2}$$

   where

$$k = \sqrt{b/a}. \tag{3}$$

   Prove that (2) is indeed a solution of (1).

CHAPTER 5

Energy Bands in Crystals

5.1. One-Dimensional Zone Schemes

We are now in a position to make additional important statements which contribute considerably to the understanding of the properties of crystals. For this we plot the energy versus the momentum of the electrons or, because of (4.8), versus the wave vector $\mathbf{k}$. As before we first discuss the one-dimensional case.

The relation between E and k_x is particularly simple in the case of free electrons as can be seen from (4.3),

$$k_x = \text{const. } E^{1/2}. \tag{5.1}$$

The plot of E versus k_x is a parabola (Fig. 5.1).

We return now to (4.68) which we obtained from (4.67) for $P = 0$ (free electrons). Because the cosine function is periodic in 2π, (4.68) should be written in the more general form:

$$\cos \alpha a = \cos k_x a \equiv \cos(k_x a + n2\pi), \tag{5.2}$$

where $n = 0, \pm 1, \pm 2, \ldots$. This gives

$$\alpha a = k_x a + n2\pi. \tag{5.3}$$

Combining (4.12),

$$\alpha = \sqrt{\frac{2m}{\hbar^2}} E^{1/2},$$

with (5.3) yields:

$$k_x + n\frac{2\pi}{a} = \sqrt{\frac{2m}{\hbar^2}} E^{1/2}. \tag{5.4}$$

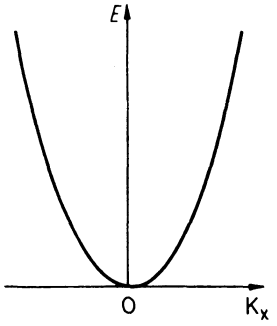

Figure 5.1. Electron energy E versus the wave vector k_x for free electrons.

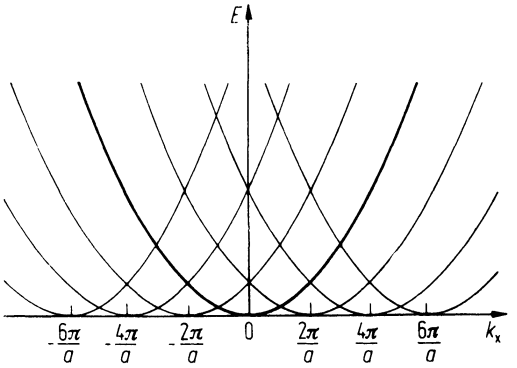

Figure 5.2. Periodic repetition of Fig. 5.1 at the points $k_x = n \cdot 2\pi/a$.

We see from (5.4) that in the general case the parabola, shown in Fig. 5.1, is repeated periodically in intervals of $n \cdot 2\pi/a$ (Fig. 5.2). The energy is thus a periodic function of k_x with the periodicity $2\pi/a$.

We noted when discussing Fig. 4.11 that if an electron propagates in a periodic potential we always observe discontinuities of the energies when $\cos k_x a$ has a maximum or a minimum, i.e., when $\cos k_x a = 1$. This is only the case when

$$k_x a = n\pi, \qquad n = \pm 1, \pm 2, \pm 3, \ldots \tag{5.5}$$

or

$$k_x = n \cdot \frac{\pi}{a}. \tag{5.6}$$

At these singularities a deviation from the parabolic E versus k_x curve occurs and the branches of the individual parabolas merge into the neighboring ones.[6] This is shown in Fig. 5.3.

[6] If two energy functions with equal symmetry cross, the quantum mechanical "noncrossing rule" requires that the eigenfunctions be split, so that they do not cross.

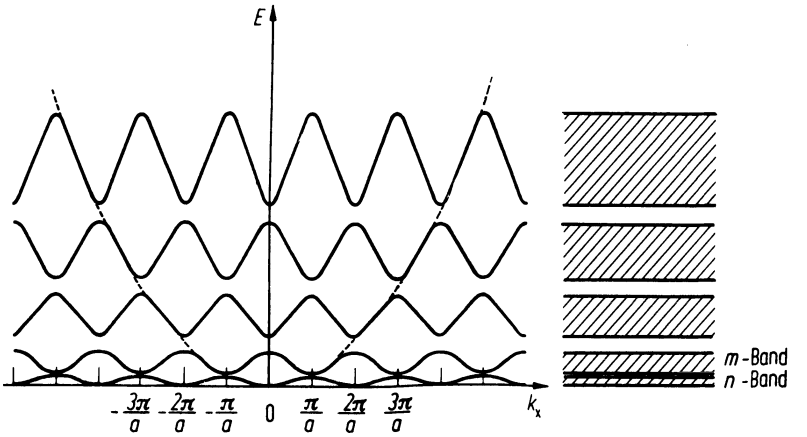

Figure 5.3. Periodic zone scheme.

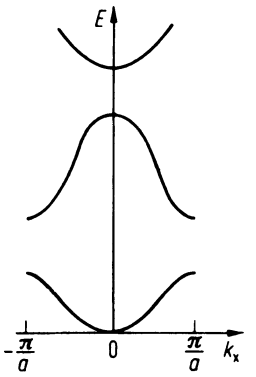

Figure 5.4. Reduced zone scheme. (This is a section of Fig. 5.3 between $-\pi/a$ and $+\pi/a$.)

The aforementioned consideration leads to a very important result. The electrons in a crystal behave for most k_x values like free electrons except when k_x approaches the value $n \cdot \pi/a$.

Besides this "periodic zone scheme" (Fig. 5.3), two further zone schemes are common. In the future we shall use mostly the "reduced zone scheme" (Fig. 5.4) which is a section of Fig. 5.3 between the limits $\pm\pi/a$. In the "extended zone scheme" (Fig. 5.5), the deviations from the free electron parabola at the critical points $k_x = n \cdot \pi/a$ are particularly easy to identify.

Occasionally it is useful to plot *free* electrons in a reduced zone scheme. In doing so, one considers the width of the forbidden bands to be reduced until the energy gap between the individual branches disappears completely. This leads to the "free electron bands" which are shown in Fig. 5.6 for a special case. The well-known band character disappears for free electrons, however,

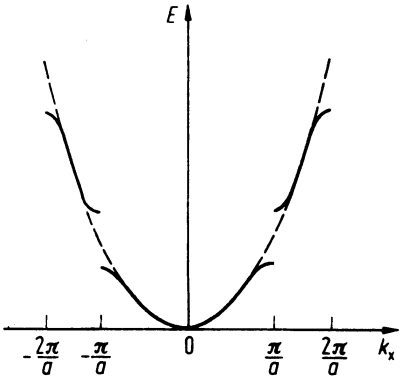

Figure 5.5. Extended zone scheme.

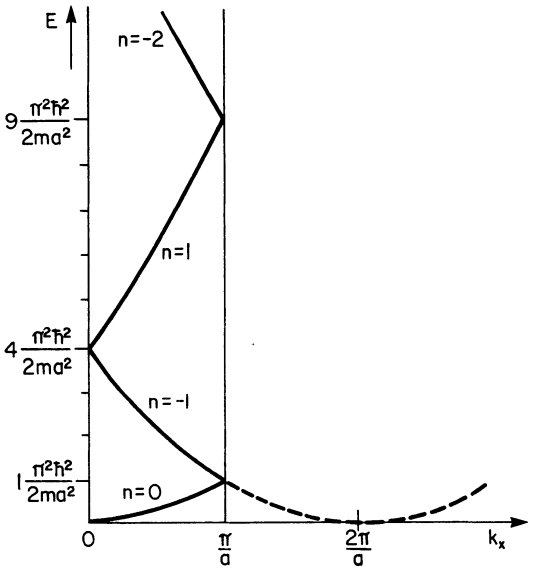

Figure 5.6. "Free electron bands" plotted in the reduced zone scheme (cubic primitive crystal structure).

and one obtains a continuous energy region as explained in Section 4.1. As before, the shape of the individual branches in Fig. 5.6 is due to the $2\pi/a$ periodicity as a comparison with Fig. 5.2 shows. From (5.4), it follows that

$$E = \frac{\hbar^2}{2m}\left(k_x + n\frac{2\pi}{a}\right)^2, \qquad n = 0, \pm 1, \pm 2, \ldots . \tag{5.7}$$

By inserting different n-values in (5.7), one can calculate the shape of the branches of the free electron band. A few examples might illustrate this:

$$\mathbf{n = 0} \text{ yields } E = \frac{\hbar^2}{2m} k_x^2 \text{ (parabola with 0 as origin);}$$

$$\mathbf{n = -1} \text{ yields } E = \frac{\hbar^2}{2m}\left(k_x - \frac{2\pi}{a}\right)^2 \left(\text{parabola with } \frac{2\pi}{a} \text{ as origin}\right);$$

$$\text{for } k_x = 0 \text{ follows } E = 4\frac{\pi^2\hbar^2}{2ma^2};$$

$$\text{for } k_x = \frac{\pi}{a} \text{ follows } E = 1\frac{\pi^2\hbar^2}{2ma^2}.$$

The calculated data are depicted in Fig. 5.6.

One important question has remained essentially unanswered: What do these E versus $|\mathbf{k}|$ curves really mean? Simply spoken, they relate the energy of an electron with its **k**-vector, that is, with its momentum. We shall eventually learn to appreciate complete band diagrams in later chapters in which we shall draw from these diagrams important conclusions about the electronic properties of materials.

An additional item needs to be mentioned: It is quite common to use the word "band" for both the allowed energy regions, such as the n-band or the m-band in Fig. 5.3, as well as for the individual branches within a band as seen in Fig. 5.6. As a rule this does not cause any confusion.

Finally, we need to stress one more point: The wave vector **k** is inversely proportional to the wavelength of the electrons (see equation (4.9)). Thus, **k** has the unit of a reciprocal length and is therefore defined in "reciprocal space." The reader might recall from a course in crystallography that each crystal structure has two lattices associated with it, one of them being the crystal (or real) lattice and the other the reciprocal lattice. We shall show in Section 5.5 how these two lattices are related. The following may suffice for the moment: each lattice plane in real space can be represented by a vector which is normal to this plane and whose length is made proportional to the reciprocal of the interplanar distance. The tips of all such vectors from different planes form the points in a reciprocal lattice. An X-ray diffraction pattern is a map of such a reciprocal lattice.

5.2. Two-Dimensional Brillouin Zones

We now consider the behavior of an electron in the potential of a two-dimensional lattice. The electron movement in two dimensions can be described as before by the wave vector **k** which has the components k_x and k_y which are parallel to the x- and the y-axis, in reciprocal space. Points in the k_x–k_y coordinate system form a two-dimensional reciprocal lattice (see Fig. 5.7).

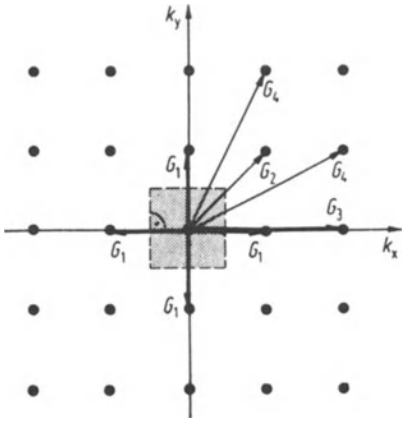

Figure 5.7. Four shortest lattice vectors in a k_x–k_y coordinate system and first Brillouin zone in a two-dimensional reciprocal lattice.

One obtains in the two-dimensional case a two-dimensional field of allowed energy regions which corresponds to the allowed energy bands. They are called Brillouin zones. The electrons can only arrive by jumps from one energy band to the next or from one Brillouin zone to the next.

We shall illustrate the construction of the Brillouin zones for a two-dimensional reciprocal lattice (Fig. 5.7). For the first zone one constructs the perpendicular bisectors on the shortest lattice vectors, G_1. The enclosed area is the first Brillouin zone. For the following zones the bisectors of the next shortest lattice vectors are constructed. It is essential that for the zones of higher order the extended limiting lines of the zones of lower order have to be used as additional limiting lines. The first four Brillouin zones are shown in Fig. 5.8. Note that all the zones have the same area. The first four shortest lattice vectors G_1 through G_4 are drawn in Fig. 5.7.

Three-dimensional Brillouin zones form volumes. The significance of the Brillouin zones, particularly the first Brillouin zone, will become evident in Section 5.4 when the energy bands of solids are discussed.

The Brillouin zones are useful if one wants to calculate the acceleration of an electron which may travel in a specific direction in reciprocal space. For example, if in a two-dimensional lattice, an electron travels at 45° to the k_x-axis, the limit of the Brillouin zone is reached according to (5.6) or Fig. 5.8 at

$$k_{\text{crit}} = \frac{\pi}{a}\sqrt{2}. \tag{5.8}$$

In contrast to this the boundary of a Brillouin zone is reached at

$$k_{\text{crit}} = \frac{\pi}{a} \tag{5.9}$$

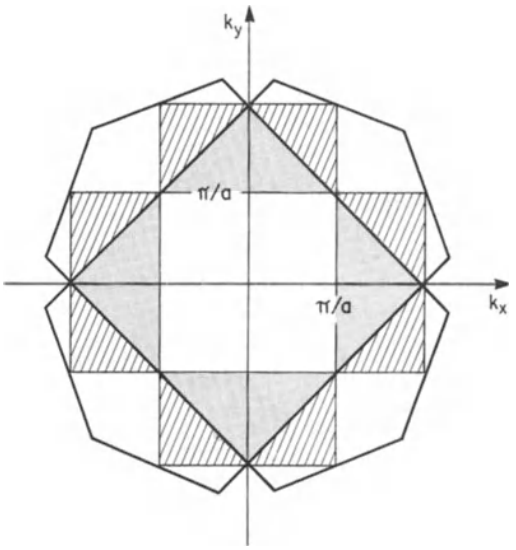

Figure 5.8. The four first Brillouin zones of a two-dimensional reciprocal lattice.

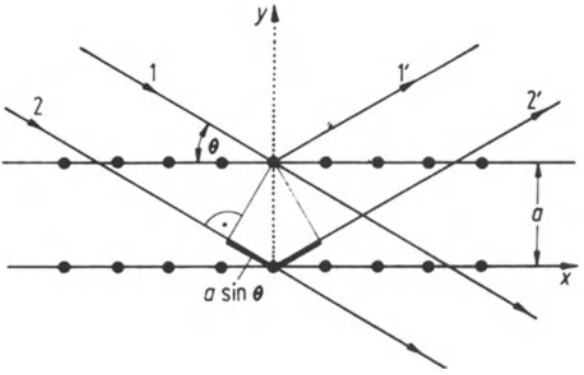

Figure 5.9. Bragg reflection of an electron wave in a lattice. The critical angle of incidence is θ.

when an electron moves parallel to the k_x- or k_y-axis. The largest momenta which electrons can assume in these two examples are $p_{max} = (\pi/a)\hbar\sqrt{2}$ and $p_{max} = (\pi/a)\hbar$, respectively (4.8). The overlapping of energy bands which we will treat in Section 6 can be explained by means of the Brillouin zones without difficulty.

The occurrence of allowed and forbidden energy zones for the electron movement in a crystal can be illustrated in a completely different way. This shall be done here briefly because of its immediate intuitive power. We consider an electron wave which propagates in a lattice at an angle θ to the lattice plane (Fig. 5.9). At a certain angle of incidence constructive inter-

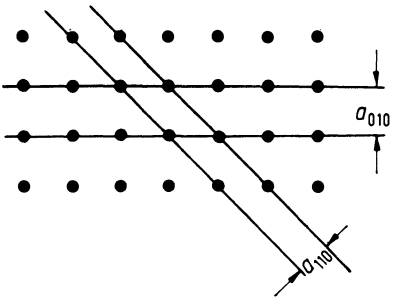

Figure 5.10. Lattice planes of a square lattice.

ference of rays 1 and 2 occur because of interference of the electron waves which are diffracted on the lattice atoms. It has been shown by Bragg that each ray which is diffracted in this way can be considered as being reflected by a mirror parallel to the lattice planes. At this critical angle the transmitted ray will be weakened considerably. This is always the case when the path difference $2a \sin\theta$ is an integer multiple of the electron wave length λ, i.e., when

$$2a \sin\theta = n\lambda, \qquad n = 1, 2, 3, \ldots \tag{5.10}$$

(Bragg Relation). With (4.9) one obtains from (5.10)

$$2a \sin\theta = n\frac{2\pi}{k}$$

and therefore

$$k_{\text{crit}} = n\frac{\pi}{a \sin\theta}. \tag{5.11}$$

For an electron movement parallel to a coordinate axis, i.e., for perpendicular incidence, (5.9) follows from (5.11); if $\theta = 45°$, one obtains (5.8).

Equation (5.11) leads to the result that for increasing electron energies a critical $\mathbf{k}$ value is finally reached; for which "reflection" of the electron wave at the lattice planes occurs. At this critical $\mathbf{k}$ value the transmission of an electron beam through the lattice is prevented. Then, the incident and the Bragg-reflected electron wave form a standing wave. The critical $\mathbf{k}$ value is inversely proportional to the lattice constant a, as seen in (5.11). As a consequence, critical $\mathbf{k}$- (or energy) values for which "reflection" occurs are reached first at planes with small Miller indices (Fig. 5.10).

*5.3. Three-Dimensional Brillouin Zones

In the previous section, the physical significance of the Brillouin zones was discussed. It was shown that at the boundaries of these zones the electron waves were Bragg-reflected by the crystal. The wave vector $|\mathbf{k}| = 2\pi/\lambda$ was

seen to have the unit of a reciprocal length and is therefore defined in the reciprocal lattice. We shall attempt now to construct three-dimensional Brillouin zones for two important crystal structures, namely, the face-centered cubic (fcc) and the body-centered cubic (bcc) crystals. Since the Brillouin zones for these structures have some important features in common with the so-called Wigner–Seitz cells, it is appropriate to discuss, at first, the Wigner–Seitz cells and also certain features of the reciprocal lattice before we return to the Brillouin zones at the end of Section 5.5.

*5.4. Wigner–Seitz Cells

Crystals have symmetrical properties. Therefore, a crystal can be described as an accumulation of "unit cells." The smaller such a unit cell, i.e., the fewer atoms it contains, the simpler its description. The smallest possible cell is called a "primitive unit cell." Frequently, however, a larger, nonprimitive unit cell is used, which might have the advantage that the symmetry can be better recognized. Body-centered cubic and face-centered cubic are characterisic representatives of such "conventional" unit cells.[7]

The Wigner–Seitz cell is a special type of primitive unit cell which shows the cubic symmetry of the cubic cells. For its construction, one bisects the vectors from a given atom to its nearest neighbors and places a plane perpendicular to these vectors at the bisecting points. This is shown in Fig. 5.11 for the bcc lattice.

In the fcc lattice, the atoms are arranged on the corners and faces of a cube, which is equivalent with the center points of the edges (Fig. 5.12). The Wigner–Seitz cell for this structure is shown in Fig. 5.13.

[7] A lattice is a regular periodic arrangement of points in space; it is, consequently, a mathematical abstraction. All crystal structures can be traced to one of the 14 types of Bravais lattices (see textbooks on crystallography).

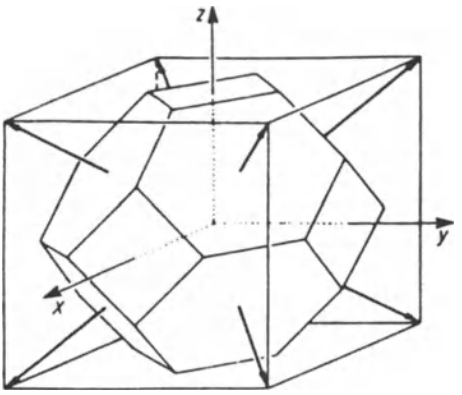

Figure 5.11. Wigner–Seitz cell for the body-centered structure.

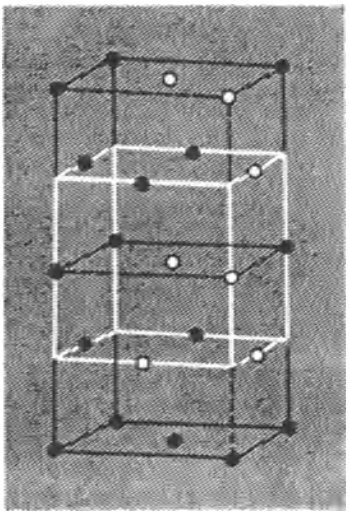

Figure 5.12. Conventional unit cell of the fcc structure. In the cell which is marked black, the atoms are situated on the corners and faces of the cubes. In the white cell, the atoms are at the centers of the edges.

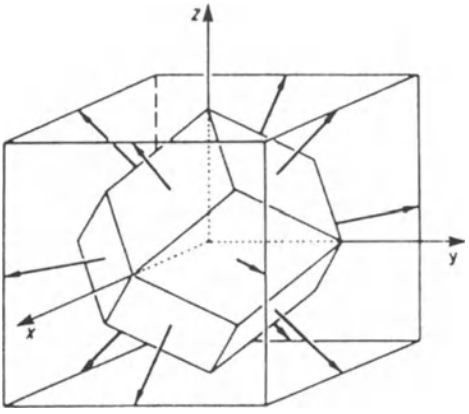

Figure 5.13. Wigner–Seitz cell for the fcc structure. It is constructed from the white cell which is marked in Fig. 5.12.

*5.5. Translation Vectors and the Reciprocal Lattice

In Fig. 5.14(a) the fundamental vectors $\mathbf{t}_1, \mathbf{t}_2, \mathbf{t}_3$ are inserted in a unit cell of a cubic primitive lattice. By combination of these "primitive vectors" a translation vector,

$$\mathbf{R} = n_1\mathbf{t}_1 + n_2\mathbf{t}_2 + n_3\mathbf{t}_3, \tag{5.12}$$

can be defined. Using this translation vector it is possible to reach from a given

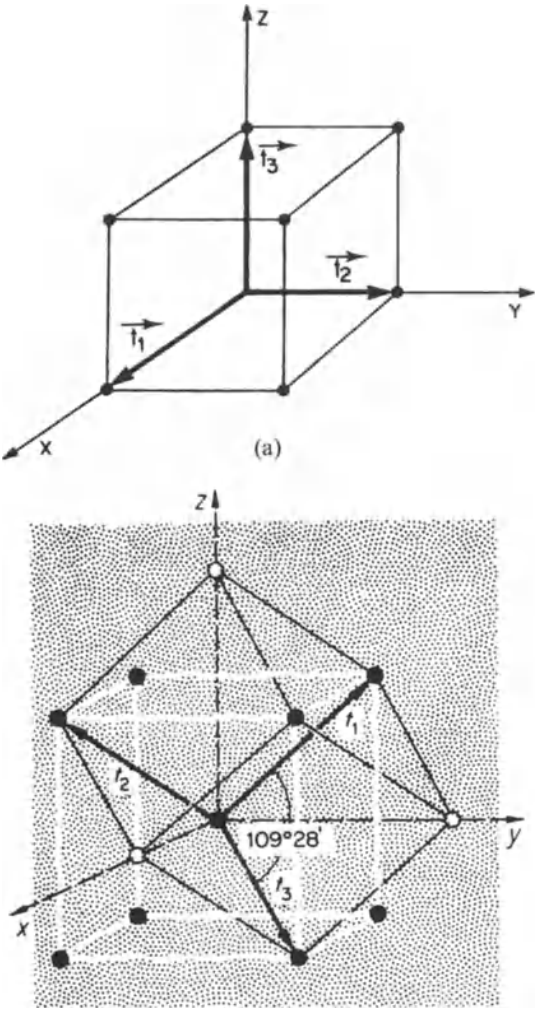

Figure 5.14. (a) Fundamental lattice vectors $\mathbf{t}_1, \mathbf{t}_2, \mathbf{t}_3$ in a cubic primitive lattice. (b) Fundamental lattice vectors in a conventional (white) and primitive, noncubic unit cell (black) of a bcc lattice. The axes of the primitive (noncubic) unit cell form angles of 109° 28′.

lattice point any other equivalent lattice point. For this, the factors n_1, n_2, n_3 have to be integers. In Fig. 5.14(b) the fundamental vectors $\mathbf{t}_1, \mathbf{t}_2, \mathbf{t}_3$ are shown in a conventional unit cell of a bcc lattice.

Similarly, as above, we now introduce for the reciprocal lattice three vectors, $\mathbf{b}_1, \mathbf{b}_2, \mathbf{b}_3$, and a translation vector

$$\mathbf{G} = 2\pi(h_1\mathbf{b}_1 + h_2\mathbf{b}_2 + h_3\mathbf{b}_3), \tag{5.13}$$

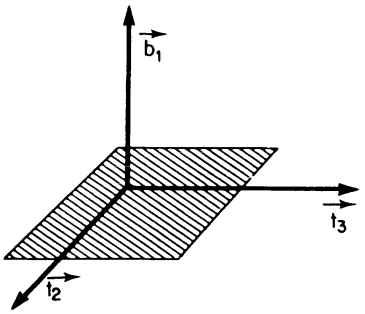

Figure 5.15. Plane formed by $\mathbf{t}_2$ and $\mathbf{t}_3$ with perpendicular vector $\mathbf{b}_1$.

where h_1, h_2, and h_3 are, again, integers. (The factor 2π is introduced for convenience. In X-ray crystallography, this factor is omitted.)

The real and reciprocal lattices are related by a definition which states that the scalar product of the vectors $\mathbf{t}_1$ and $\mathbf{b}_1$ should be unity, whereas the scalar products of $\mathbf{b}_1$ and $\mathbf{t}_2$ or $\mathbf{b}_1$ and $\mathbf{t}_3$ are zero:

$$\mathbf{b}_1 \cdot \mathbf{t}_1 = 1 \tag{5.14}$$

$$\mathbf{b}_1 \cdot \mathbf{t}_2 = 0 \tag{5.15}$$

$$\mathbf{b}_1 \cdot \mathbf{t}_3 = 0. \tag{5.16}$$

Equivalent equations are defined for $\mathbf{b}_2$ and $\mathbf{b}_3$. These nine equations can be combined by using the Kronecker-Delta symbol,

$$\mathbf{b}_n \cdot \mathbf{t}_m = \delta_{nm}, \tag{5.17}$$

where $\delta_{nm} = 1$ for $n = m$ and $\delta_{nm} = 0$ for $n \neq m$. Equation (5.17) is from now on our *definition* for the three vectors $\mathbf{b}_n$, which are reciprocal to the vectors $\mathbf{t}_m$. From (5.15) and (5.16) it follows[8] that $\mathbf{b}_1$ is perpendicular to $\mathbf{t}_2$ and to $\mathbf{t}_3$ which means that $\mathbf{t}_2$ and $\mathbf{t}_3$ form a plane perpendicular to the vector $\mathbf{b}_1$ (Fig. 5.15). We therefore write[9]

$$\mathbf{b}_1 = \text{const}\ \mathbf{t}_2 \times \mathbf{t}_3. \tag{5.18}$$

To evaluate the constant, we form the scalar product of $\mathbf{t}_1$ and $\mathbf{b}_1$ (5.18) and make use of (5.14):

$$\mathbf{b}_1 \cdot \mathbf{t}_1 = \text{const}\ \mathbf{t}_1 \cdot \mathbf{t}_2 \times \mathbf{t}_3 = 1. \tag{5.19}$$

This yields

$$\text{const} = \frac{1}{\mathbf{t}_1 \cdot \mathbf{t}_2 \times \mathbf{t}_3}. \tag{5.20}$$

---

[8] The *scalar product* of two vectors $\mathbf{a}$ and $\mathbf{b}$ is $\mathbf{a} \cdot \mathbf{b} = ab\cos(\mathbf{ab})$. If $\mathbf{i}$, $\mathbf{j}$ and $\mathbf{l}$ are mutually perpendicular unit vectors, then we can write $\mathbf{i} \cdot \mathbf{j} = \mathbf{j} \cdot \mathbf{l} = \mathbf{l} \cdot \mathbf{i} = 0$ and $\mathbf{i} \cdot \mathbf{i} = \mathbf{jj} = \mathbf{ll} = 1$.

[9] The *vector product* of two vectors $\mathbf{a}$ and $\mathbf{b}$ is a vector which stands perpendicular to the plane formed by $\mathbf{a}$ and $\mathbf{b}$. It is $\mathbf{i} \times \mathbf{i} = \mathbf{j} \times \mathbf{j} = \mathbf{l} \times \mathbf{l} = 0$ and $\mathbf{i} \times \mathbf{j} = \mathbf{l}$ and $\mathbf{j} \times \mathbf{i} = -\mathbf{l}$.

Combining (5.18) with (5.20) gives

$$\mathbf{b}_1 = \frac{\mathbf{t}_2 \times \mathbf{t}_3}{\mathbf{t}_1 \cdot \mathbf{t}_2 \times \mathbf{t}_3}. \tag{5.21}$$

Equivalent equations can be obtained for $\mathbf{b}_2$ and $\mathbf{b}_3$:

$$\mathbf{b}_2 = \frac{\mathbf{t}_3 \times \mathbf{t}_1}{\mathbf{t}_1 \cdot \mathbf{t}_2 \times \mathbf{t}_3} \tag{5.22}$$

$$\mathbf{b}_3 = \frac{\mathbf{t}_1 \times \mathbf{t}_2}{\mathbf{t}_1 \cdot \mathbf{t}_2 \times \mathbf{t}_3}. \tag{5.23}$$

Equations (5.21)–(5.23) are the transformation equations which express the fundamental vectors $\mathbf{b}_1$, $\mathbf{b}_2$, and $\mathbf{b}_3$ of the reciprocal lattice in terms of real lattice vectors.

As an example of how these transformations are performed, we calculate now the reciprocal lattice of a bcc crystal. The real crystal may have the lattice constant "a." We express the lattice vectors $\mathbf{t}_1$, $\mathbf{t}_2$, $\mathbf{t}_3$ in terms of the unit vectors, $\mathbf{i}$, $\mathbf{j}$, $\mathbf{l}$ in the x, y, z coordinate system (see Fig. 5.14(b)):

$$\mathbf{t}_1 = \frac{a}{2}(-\mathbf{i} + \mathbf{j} + \mathbf{l}) \tag{5.24}$$

or, abbreviated,

$$\mathbf{t}_1 = \frac{a}{2}(\bar{1}11) \tag{5.25}$$

and

$$\mathbf{t}_2 = \frac{a}{2}(1\bar{1}1) \tag{5.26}$$

$$\mathbf{t}_3 = \frac{a}{2}(11\bar{1}). \tag{5.27}$$

To calculate $\mathbf{b}_1$, using (5.21), we form at first the vector product[10]

$$\mathbf{t}_2 \times \mathbf{t}_3 = \frac{a^2}{4}\begin{vmatrix} \mathbf{i} & \mathbf{j} & \mathbf{l} \\ 1 & -1 & 1 \\ 1 & 1 & -1 \end{vmatrix} = \frac{a^2}{4}(\mathbf{i} + \mathbf{j} + \mathbf{l} + \mathbf{l} - \mathbf{i} + \mathbf{j}) = \frac{a^2}{4}(2\mathbf{j} + 2\mathbf{l})$$
$$= \frac{a^2}{2}(\mathbf{j} + \mathbf{l}) \tag{5.28}$$

and the scalar[11] product

---

[10] $\mathbf{a} \times \mathbf{b} = \begin{vmatrix} \mathbf{i} & \mathbf{j} & \mathbf{l} \\ a_x & a_y & a_z \\ b_x & b_y & b_z \end{vmatrix}$.

[11] $\mathbf{a} \cdot \mathbf{b} = a_x b_x + a_y b_y + a_z b_z$.

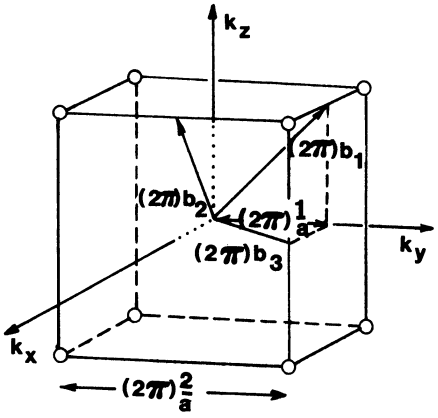

Figure 5.16. Lattice vectors in reciprocal space of a bcc crystal. The primitive vectors in the reciprocal lattice are (because of (5.13)) larger by a factor of 2π. The lattice constant of the cube then becomes $2\pi \cdot 2/a$.

$$\mathbf{t}_1 \cdot \mathbf{t}_2 \times \mathbf{t}_3 = \frac{a^3}{4}(-\mathbf{i} + \mathbf{j} + \mathbf{l}) \cdot (0 + \mathbf{j} + \mathbf{l}) = \frac{a^3}{4}(0 + 1 + 1) = \frac{a^3}{2}. \tag{5.29}$$

Combining (5.21) with (5.28) and (5.29) yields:

$$\mathbf{b}_1 = \frac{\frac{a^2}{2}(\mathbf{j} + \mathbf{l})}{\frac{a^3}{2}} = \frac{1}{a}(\mathbf{j} + \mathbf{l}) \tag{5.30}$$

or

$$\mathbf{b}_1 = \frac{1}{a}(011). \tag{5.31}$$

Similar calculaltions yield

$$\mathbf{b}_2 = \frac{1}{a}(101) \tag{5.32}$$

$$\mathbf{b}_3 = \frac{1}{a}(110). \tag{5.33}$$

In Fig. 5.16, the vectors $\mathbf{b}_1$, $\mathbf{b}_2$, $\mathbf{b}_3$ are inserted into a cube of length $2/a$. We note immediately an important result. The end points of the reciprocal lattice vectors of a bcc crystal are at the center of the edges of a cube. This means that points of the reciprocal lattice of the bcc structure are identical with the lattice points in a real lattice of the fcc structure. Conversely, the reciprocal lattice points of the fcc structure and the real lattice points of the bcc structure are identical.

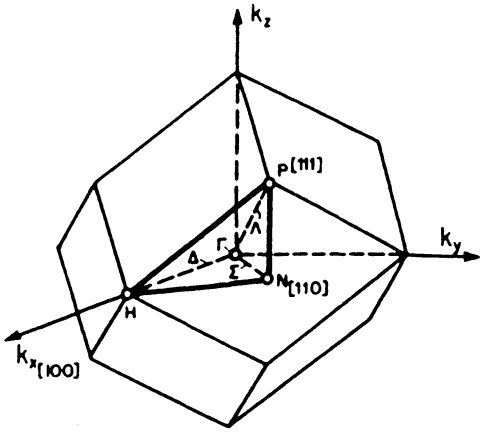

Figure 5.17. First Brillouin zone of the body-centered cubic crystal structure.

In Section 5.2, we constructed two-dimensional Brillouin zones by drawing perpendicular bisectors on the shortest lattice vectors. Similarly, a three-dimensional Brillouin zone can be obtained by bisecting all lattice vectors **b** and placing planes perpendicular on these points. As has been shown in Section 5.4, this construction is identical for a Wigner–Seitz cell. A comparison of the fundamental lattice vectors **b** and **t** gives the striking result that the Wigner–Seitz cell for an fcc crystal and the first Brillouin zone for a bcc crystal are identical. The same is true for the Wigner–Seitz cell for bcc and the first Brillouin zone for fcc. Thus, a Brillouin zone can be defined as a Wigner–Seitz cell in the reciprocal lattice.

From (5.31) it can again be seen that the reciprocal lattice vector has the unit of a reciprocal length.

*5.6. Complete Energy Bands for Metals and Semiconductors

We mentioned in Section 5.1 that, because of the $E(\mathbf{k})$ periodicity, all information pertaining to the electronic properties of materials is contained in the first Brillouin zone. In other words, the energy $E_{\mathbf{k}'}$ for $\mathbf{k}'$ outside of the first zone is identical with the energy $E_{\mathbf{k}}$ within the first zone if a suitable translation vector **G** can be found so that a wave vector $\mathbf{k}'$ becomes:

$$\mathbf{k}' = \mathbf{k} + \mathbf{G}. \tag{5.34}$$

We have already used this feature in Section 5.1, where we plotted one-dimensional energy bands in the form of a reduced zone scheme. We proceed now to three-dimensional zone pictures. We might correctly expect that the energy bands are not alike in different directions in **k** space. This can be

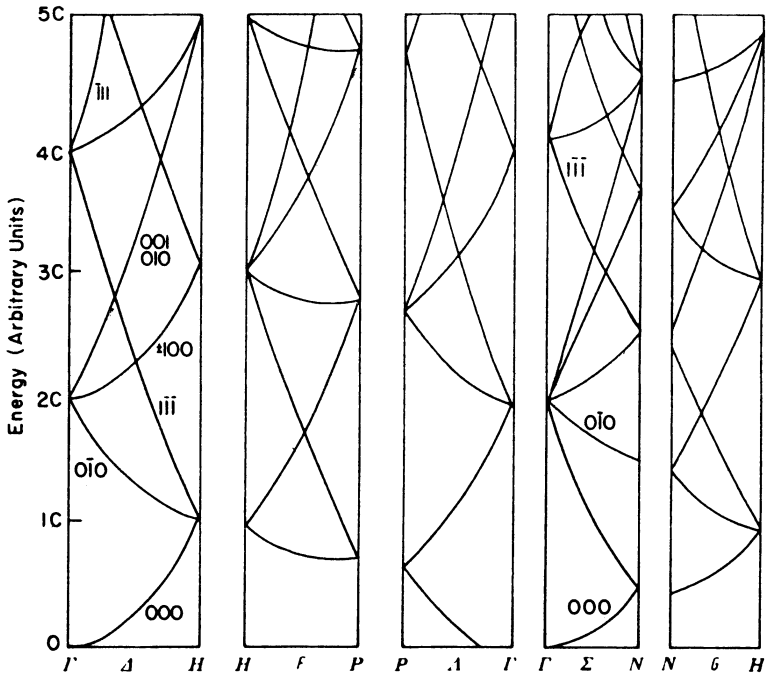

Figure 5.18. Energy bands of the free electrons for the bcc structure. The numbers given on the branches are the respective h_i values (see the calculation in the text). Compare to Fig. 5.6. $C = \hbar^2 2\pi^2/ma^2$, see (5.37).

demonstrated by using the "free electron bands" which we introduced in Fig. 5.6. We explain the details using the bcc crystal structure as an example.

In three dimensions the equation analogous to (5.7) reads

$$E_{\mathbf{k}} = \frac{\hbar^2}{2m}(\mathbf{k} + \mathbf{G})^2. \tag{5.35}$$

In Fig. 5.17 three important directions in $\mathbf{k}$ space are inserted into the first Brillouin zone of a bcc lattice. They are the [100] direction from the origin (Γ) to point H, the [110] direction from Γ to N and the [111] direction from Γ to P. These directions are commonly labeled by the symbols Δ, Σ and Λ, respectively. Figure 5.18 depicts the bands, calculated by using (5.35), for these distinct directions in $\mathbf{k}$ space. The sequence of the individual subgraphs is established by convention and can be followed using Fig. 5.17.

We now show how some of these bands are calculated for a simple case. We select the Γ–H direction as an example. We vary the modulus of the vector $\mathbf{k}_{\Gamma H} \equiv \mathbf{k}_x$ between 0 and $2\pi/a$, the latter being the boundary of the Brillouin zone (see Fig. 5.16). For this direction, (5.35) becomes

$$E = \frac{\hbar^2}{2m}\left(\frac{2\pi}{a}x\mathbf{i} + \mathbf{G}\right)^2 \tag{5.36}$$

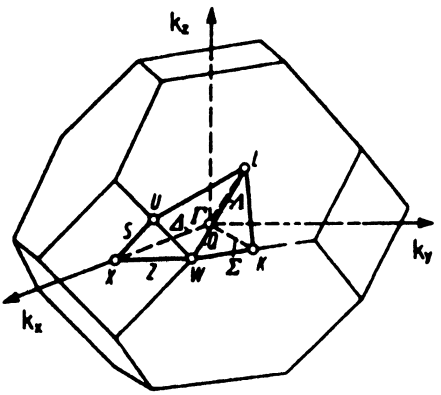

Figure 5.19. First Brillouin zone of the fcc structure.

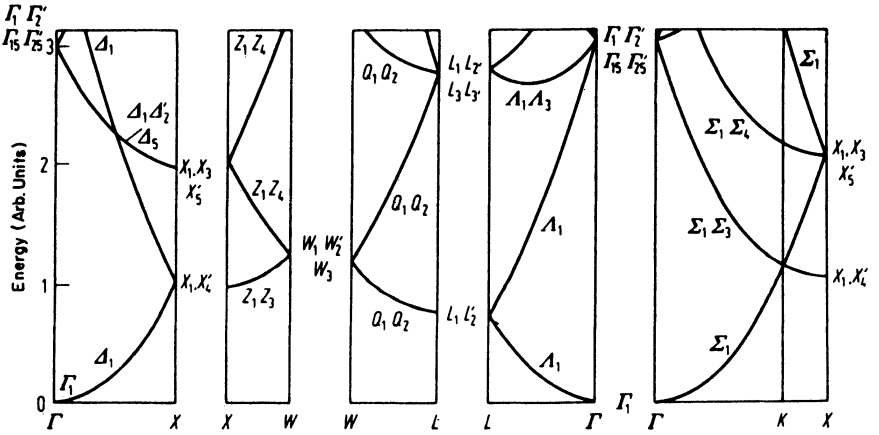

Figure 5.20. Free electron bands of the fcc structure.

whereas x may take values between 0 and 1. To start with, let $\mathbf{G}$ be 0. Then (5.36) reads

$$E = \frac{\hbar^2}{2m}\left(\frac{2\pi}{a}\right)^2 (x\mathbf{i})^2 \equiv Cx^2. \tag{5.37}$$

This yields the well-known parabolic $E(\mathbf{k})$ dependence. The curve which represents (5.37) is labeled (000) in Fig. 5.18.

Now we let $h_1 = 0$, $h_2 = -1$, and $h_3 = 0$. Then we obtain by using (5.13) and (5.32),

$$\mathbf{G} = -\frac{2\pi}{a}(\mathbf{i} + \mathbf{l}). \tag{5.38}$$

Combining (5.36) with (5.38) provides

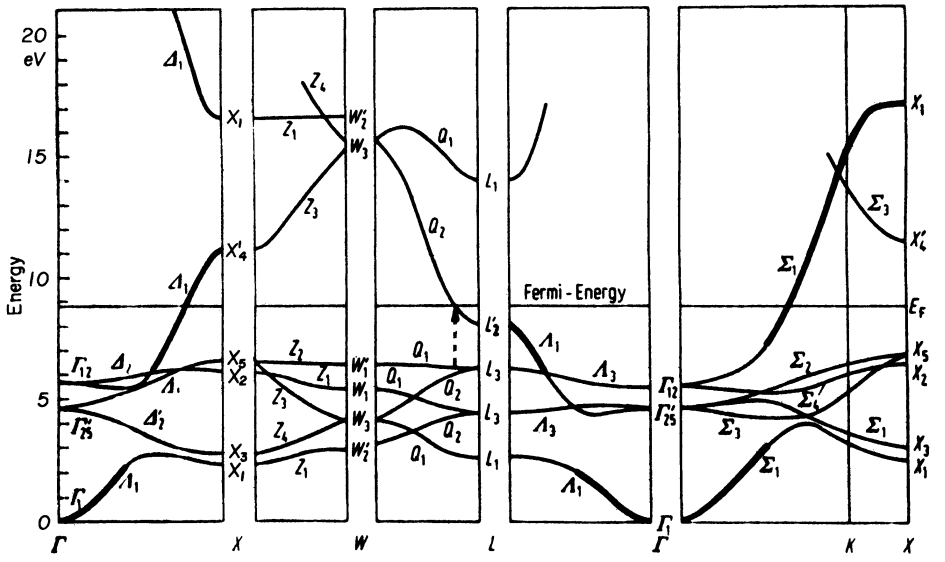

Figure 5.21. Band structure of copper (fcc). (Adapted from Segal, B. (1962) *Phys. Rev.* **125**, 109). The calculation was made using the *l*-dependent potential. (For the definition of the Fermi energy, see Section 6.1.)

$$E = \frac{\hbar^2}{2m}\left[\frac{2\pi x}{a}\mathbf{i} - \frac{2\pi}{a}(\mathbf{i}+\mathbf{l})\right]^2 = C[\mathbf{i}(x-1) - \mathbf{l}]^2$$
$$= C[(x-1)^2 + 1] = C(x^2 - 2x + 2) \tag{5.39}$$

which yields for

$$x = 0 \rightarrow E = 2C$$

and for

$$x = 1 \rightarrow E = 1C.$$

We obtain the band labeled $(0\bar{1}0)$ in Fig. 5.18. Similarly, all bands in Fig. 5.18 can be calculated by variation of the h values, $\mathbf{k}$ directions and by using (5.35).

The free electron bands are very useful for the following reason: by comparing them with the band structures of actual materials, an assessment is possible if and to what degree the electrons in that material can be considered to be free.

In Figs. 5.19 and 5.20 the first Brillouin zone and the free electron bands of an fcc structure are shown.

At the end of this section, four band structures of important solids are shown and discussed. We start with the band structure for copper (Fig. 5.21). Comparing Figs. 5.21 and 5.20 shows immediately that the copper bands do not completely resemble those for free electrons. In the lower half of the band structure, closely spaced and flat running bands can be seen. Calculations show that these can be attributed to the 3*d*-bands of copper (see Appendix 3).

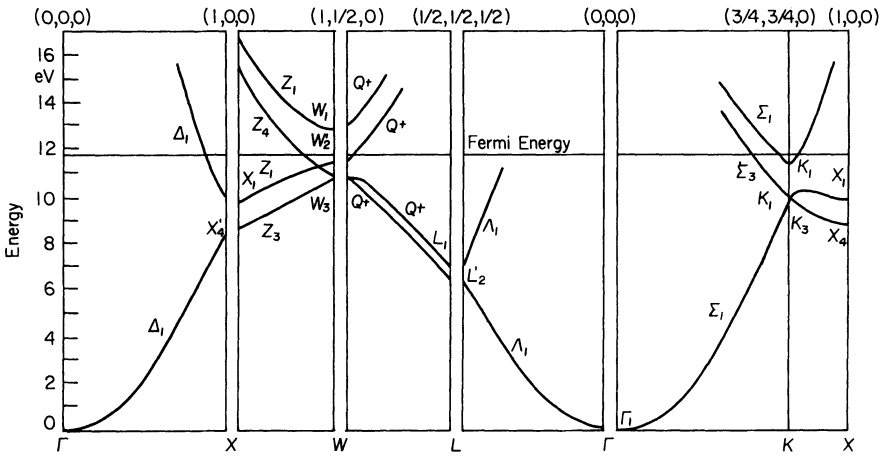

Figure 5.22. Energy bands for aluminum. Adapted from Segal, B. (1961) *Phys. Rev.* **124**, 1797.

They superimpose the 4*s*-bands (which are heavily marked in Fig. 5.21). The band which starts at Γ is, at first, *s*-electron-like, and becomes *d*-electron-like while approaching point *X*. The first half of this band is continued at higher energies. It is likewise heavily marked. It can be seen, therefore, that the *d*-bands overlap the *s*-bands. The origin of the energy scale is positioned for convenience in the lower end of the *s*-band.

As a second example, consider the band diagram of aluminum (fcc), Fig. 5.22. Comparison with Fig. 5.20 shows that the energy bands of aluminum are essentially free-electron-like. The band gap between the points X_4' and X_1, which was about 5 eV in copper, is here only about 1 eV. Further, no overlapping of *d*- and *s*-bands can be seen.

As a third example, the band structure of silicon is shown (Fig. 5.23). Here, any similarity to free electron bands (Fig. 5.20) is completely gone. Of particular interest is the area between 0 and approximately 1 eV in which no energy bands are shown. This "energy gap," which is responsible for the well-known semiconductor properties, will be the subject of detailed discussion in a later chapter.

Finally, the band structure of gallium–arsenide is shown in Fig. 5.24. The so-called III–V semiconductor compounds such as GaAs may become of great technical importance, as we shall discuss in Section 8.5. They have the same crystal structure and the same total number of valence electrons as the element silicon.

It should be mentioned in closing that the band structures of actual solids, as shown in Figs. 5.21–5.24, are the result of extensive, computer-aided calculations and that various investigators using different starting potentials arrive at slightly different band structures. Experimental investigations, such as measurements of the frequency dependence of the optical properties, can decide which of the various calculated band structures are closest to reality.

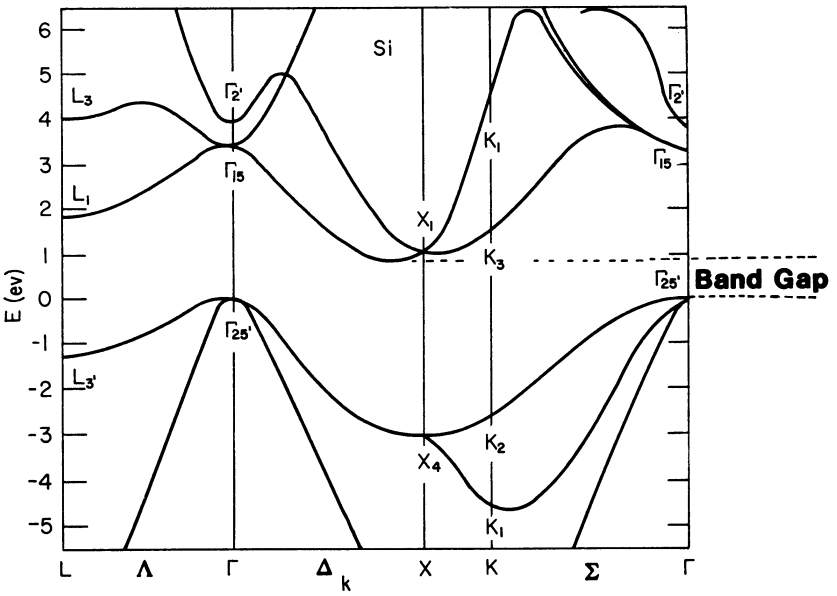

Figure 5.23. Calculated energy band structure of silicon (diamond-cubic crystal structure). Adapted from Cohen, M.L., and Bergstresser, T.K. (1966) *Phys. Rev.* **142**, 789.

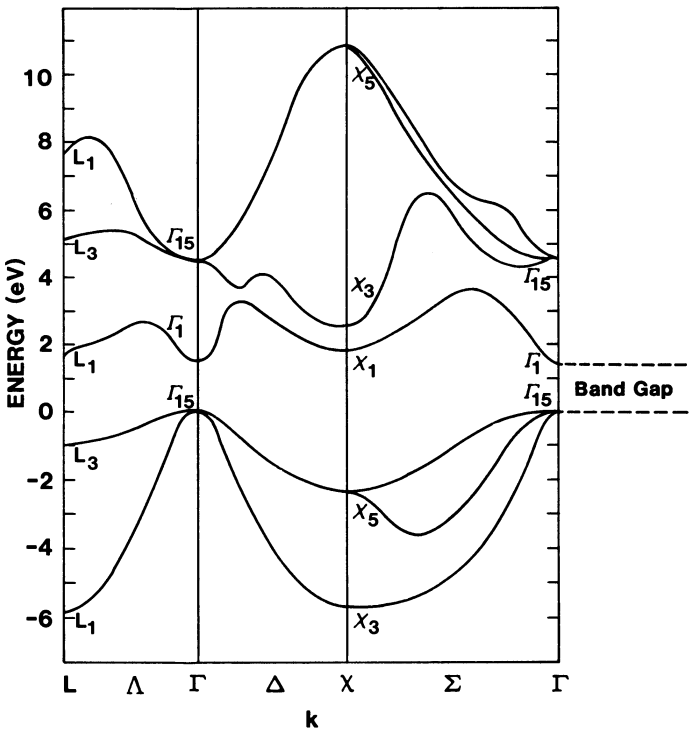

Figure 5.24. Calculated energy band structure of GaAs. Adapted from Herman, F., and Spicer, W.E. (1968), *Phys. Rev.* **174**, 906.

5.7. Curves and Planes of Equal Energy

We conclude this chapter by discussing another interesting aspect of the energy versus wave vector relationship.

In one-dimensional **k**-"space" there is only *one* **k**-value which is connected with a given energy (see Fig. 5.1). In the two-dimensional case, that is, when we plot the electron energy over a k_x–k_y plane, more than one **k**-value can be assigned to a given energy. This leads to curves of equal energy, as shown in Fig. 5.25. For a two-dimensional square lattice and for small electron energies, the curves of equal energy are circles. However, if the energy of the electrons is approaching the energy of the boundary of a Brillouin zone, then a deviation from the circular form is known to occur. This is shown in Fig. 5.26, where curves of equal energy for a two-dimensional square lattice are inserted into the first Brillouin zone. It is of particular interest that the energy which belongs to point *A* in Fig. 5.26 is larger than the energy which belongs to point *B*. Consequently, the curves of equal energy for the first Brillouin zone may extend into the second zone (marked with dotted lines in Fig. 5.26). This leads to an overlapping of energy bands as schematically shown in Fig. 5.27, and in the band structures of Figs. 5.21–5.24. For copper and aluminum the band overlapping leads to quasicontinuous allowed energies (in different directions of **k**-space). For semiconductors the band overlapping is not complete, which results in the already mentioned energy gap (Figs. 5.23 and 5.24).

In three-dimensional **k**-space one obtains *surfaces* of equal energy. For the free electron case and for a cubic lattice they are spheres. For a nonparabolic E-(**k**) behavior these surfaces become more involved. This is demonstrated in Fig. 5.28 for a special case.

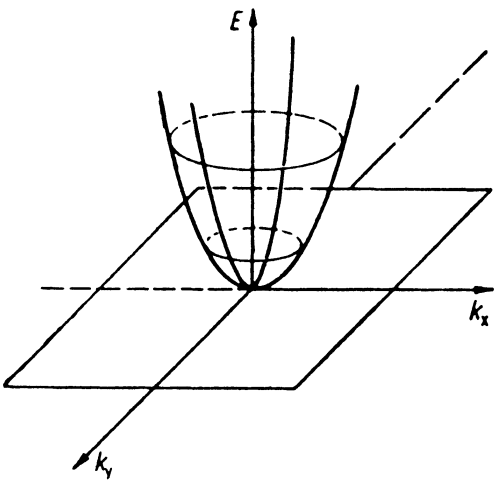

Figure 5.25. Electron energy E versus wave vector **k** (two dimensional). This figure demonstrates various curves of equal energy for free electrons.

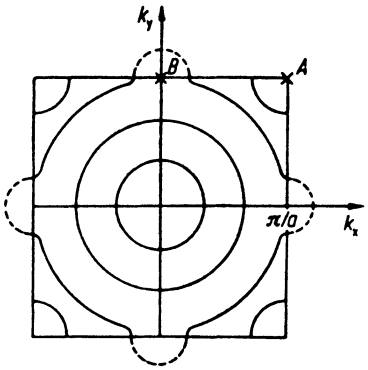

Figure 5.26. Curves of equal energy inserted into the first Brillouin zone for a two-dimensional square lattice.

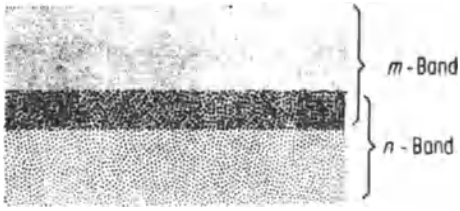

Figure 5.27. Overlapping of energy bands.

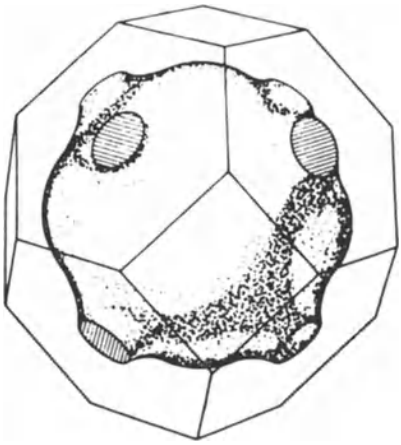

Figure 5.28. A particular surface of equal energy (Fermi surface, see Section 6.1) and the first Brillouin zone for copper. Adapted from Pippard, A.B. (1957) *Phil. Trans. Royal Soc. London* **A 250**, 325.

Problems

1. Calculate the free energy bands for a bcc structure in the $\mathbf{k}_x$ direction having the following values for $h_1/h_2/h_3$: a) $1\bar{1}\bar{1}$, b) 001, c) 010. Plot the bands in k-space. Compare with Fig. 5.18.
2. What is the energy difference between the points L_2' and L_1 (upper) in the band diagram for copper?
3. How large is the "gap energy" for silicon? (*Hint*: Consult the band diagram for silicon.)
4. Calculate the main lattice vectors in reciprocal space of an fcc crystal.
5. a) Calculate how much the kinetic energy of a free electron at the corner of the first Brillouin zone of a simple cubic lattice (three dimensions!) is larger than that of an electron at the midpoint of the face.
   b) What consequences might this result have on the conductivity of a divalent metal?
6. Construct the fourth and fifth Brillouin zones for a simple cubic lattice in two dimensions.
7. Calculate the shape of the free electron bands for the cubic primitive crystal structure for $n = 1$ and $n = -2$ (see Fig. 5.6)
8. Calculate the bands for the bcc structure in the 110 [Γ–N] direction for a) (000); b) $(0\bar{1}0)$; c) $(1\bar{1}\bar{1})$.

CHAPTER 6

Electrons in a Crystal

In the preceding chapters we considered essentially only *one* electron which was confined to the field of the atoms of a solid. This electron was in most cases an outer, i.e., a valence, electron. However, in a solid of one cubic centimeter at least 10^{22} electrons can be found. In this section we shall describe how these electrons are distributed among the available energy levels. It is impossible to calculate the exact place and the kinetic energy of each individual electron. We will see, however, that probability statements nevertheless give satisfying results.

6.1. Fermi Energy and Fermi Surface

The Fermi energy, E_F, is often defined as the "highest energy which an electron assumes at $T = 0$ K." However, this definition, even though convenient, can be misleading, particularly when dealing with semiconductors. Therefore, a more accurate definition of the Fermi energy will be given in Section 6.2. We will see there that at the Fermi energy the Fermi function $F(E)$, equals 1/2. An equation for the Fermi energy is given in (6.11).

In three-dimensional **k**-space the one-dimensional Fermi energy is replaced by a Fermi surface. The energy surface which is shown in Fig. 5.28 is the Fermi surface for copper.

Fermi energies are an important part of electron band diagrams. Many of the electronic properties of materials such as optical, electrical, or magnetic properties are related to the location of E_F within a band. The Fermi energies for copper and aluminum are shown in Figs. 5.21 and 5.22. Numerical values for the Fermi energies for some materials are given in Appendix 4. They range typically from 2 to 12 eV.

6.2. Fermi Distribution Function

The distribution of the energies of a large amount of particles, and its change with increasing temperature can be calculated by means of statistical mechanics. The kinetic energy of an electron gas is governed by Fermi–Dirac statistics which states that the probability that a certain energy level is occupied by an electron is given by the Fermi function, $F(E)$

$$F(E) = \frac{1}{\exp\left(\frac{E - E_F}{k_B T}\right) + 1}. \tag{6.1}$$

If an energy level E is completely occupied by electrons, the Fermi distribution function $F(E)$ equals 1; for an empty energy level one obtains $F(E) = 0$. E_F is the Fermi energy which we introduced in Section 6.1, k_B is the Boltzmann constant and T is the absolute temperature. In Fig. 6.1, the Fermi function is plotted versus the energy for $T = 0$ by using (6.1). One sees from this figure that at $T = 0$ all levels which have an energy smaller than E_F are completely filled with electrons, whereas higher energy states are empty.

The Fermi distribution function for higher temperatures ($T \neq 0$) is shown in Fig. 6.2. The decrease of the function $F(E)$ from 1 to 0 at higher temperatures is "smeared out," i.e., it is extended to an energy interval $2\Delta E$. This decrease is heavily exaggerated in Fig. 6.2. ΔE at room temperature is in reality only about 1% of E_F.

At high energies the upper end of the Fermi distribution function can be approximated by the classical (Boltzmann) distribution function. This is best seen from (6.1) in which for large energies the exponential factor becomes significantly larger compared to 1. Then $F(E)$ is approximately

$$F(E) \approx \exp\left[-\left(\frac{E - E_F}{k_B T}\right)\right]. \tag{6.1a}$$

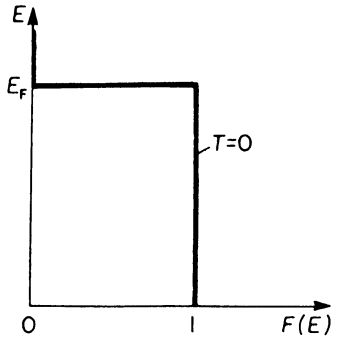

Figure 6.1. Fermi distribution function, $F(E)$, versus energy, E, for $T = 0$.

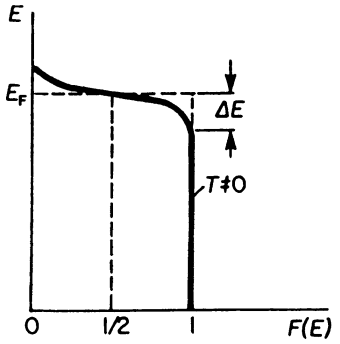

Figure 6.2. Fermi distribution function for $T \neq 0$.

This expression is known to be the Boltzmann factor which gives, in classical thermodynamics, the probability that a given energy state is occupied. The $F(E)$ curve for high energies is thus referred to as the "Boltzmann tail" of the Fermi distribution function.

Of particular interest is the value of the Fermi function $F(E)$ at $E = E_F$ and $T \neq 0$. As can be seen from (6.1), $F(E)$ is in this particular case 1/2. This serves as a definition for the Fermi energy.

6.3. Density of States

We are now interested in the question of how energy levels are distributed over a band. We restrict our discussion to the lower part of the valence band (the *s*-band in copper for example) because there the electrons can be considered to be essentially free due to their weak binding force to the nucleus. We assume that the free electrons (or the "electron gas") are confined into a square potential well from which they cannot escape. The dimensions of this potential well are thought to be identical to the dimensions of the crystal under consideration. Then our problem is similar to the case of *one* electron in a potential well of size a which we treated in Section 4.2. By using the appropriate boundary conditions the solution of the Schrödinger equation yields an equation which is analogous to (4.26):

$$E_n = \frac{\pi^2 \hbar^2}{2ma^2}(n_x^2 + n_y^2 + n_z^2), \tag{6.2}$$

where n_x, n_y, and n_z are the principal quantum numbers. Now we pick an arbitrary set of quantum numbers n_x, n_y, n_z. To each such set we can find a specific energy level E_n, frequently called "energy state." An energy state can therefore be represented by a point in quantum number space (Fig. 6.3). In this space n is the radius from the origin of the coordinate system to a point

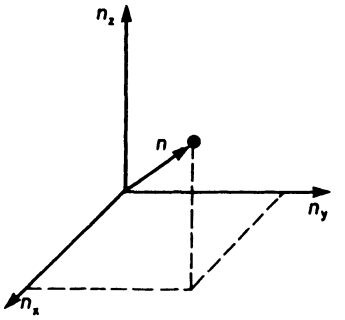

Figure 6.3. Representation of an energy state in quantum number space.

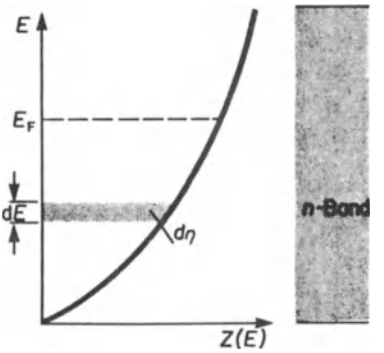

Figure 6.4. Density of states $Z(E)$ within a band. The electrons in this band are considered to be free.

(n_x, n_y, n_z) where

$$n^2 = n_x^2 + n_y^2 + n_z^2. \tag{6.3}$$

Equal values of the energy E_n are lying on the surface of a sphere with radius n. All points within the sphere represent therefore quantum states with energies smaller than E_n. The number of quantum states, η, with an energy equal to or smaller than E_n is proportional to the volume of the sphere. Since the quantum numbers are positive integers, the n values can only be defined in the positive octant of the n space. One-eighth of the volume of the sphere with the radius n gives therefore the number of energy states, η, the energy of which is equal to or smaller than E_n. Thus, with (6.2) and (6.3) we obtain

$$\eta = \frac{1}{8} \cdot \frac{4}{3} \pi n^3 = \frac{\pi}{6} \left(\frac{2ma^2}{\pi^2 \hbar^2} \right)^{3/2} E^{3/2}. \tag{6.4}$$

Differentiation of η with respect to the energy E provides the number of energy states per unit energy in the energy interval dE, that is, the density of the energy states, briefly called density of states $Z(E)$:

$$\frac{d\eta}{dE} = Z(E) = \frac{\pi}{4}\left(\frac{2ma^2}{\pi^2\hbar^2}\right)^{3/2} E^{1/2} = \frac{V}{4\pi^2}\left(\frac{2m}{\hbar^2}\right)^{3/2} E^{1/2} \tag{6.5}$$

(a^3 = volume, V, which the electron can occupy).

The density of states plotted versus the energy gives, according to (6.5), a parabola. Figure 6.4 shows that at the lower end of the band considerably less energy levels are available than at higher energies. The area within the curve in Fig. 6.4 is, by definition, the number of states which have an energy equal to or smaller than E_n. Therefore, one obtains for an area element $d\eta$

$$d\eta = Z(E) \cdot dE \tag{6.6}$$

as can be seen from (6.5) and Fig. 6.4.

6.4. Population Density

The number of electrons per unit energy, $N(E)$, within an energy interval dE can be calculated by multiplying the number of possible energy levels, $Z(E)$, with the probability for the occupation of these energy levels. We have to note, however, that because of the Pauli Principle, each energy state can be occupied by one electron of positive and one of negative spin, i.e., each energy state can be occupied by two electrons. Therefore,

$$N(E) = 2 \cdot Z(E) \cdot F(E) \tag{6.7}$$

or with (6.1) and (6.5)

$$N(E) = \frac{V}{2\pi^2}\left(\frac{2m}{\hbar^2}\right)^{3/2} E^{1/2} \frac{1}{\exp\left(\dfrac{E - E_F}{k_B T}\right) + 1}. \tag{6.8}$$

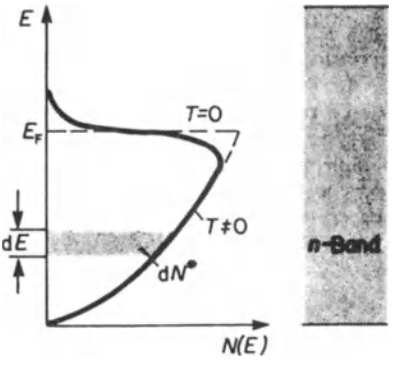

Figure 6.5. Population density $N(E)$ within a band for free electrons. dN^* is the number of electrons in the energy interval dE.

$N(E)$ is called the (electron) population density. We see immediately that for $T \to 0$ and $E < E_F$, the function $N(E)$ equals $2 \cdot Z(E)$ because $F(E)$ is unity in this case. For $T \neq 0$ and $E \simeq E_F$, the Fermi distribution function (6.1) causes a smearing out of $N(E)$, (Fig. 6.5).

The area within the curve in Fig. 6.5 represents the number of electrons, N^*, which has an energy equal to or smaller than the energy E_n. For an energy interval between E and $E + dE$, one obtains

$$dN^* = N(E)\,dE. \tag{6.9}$$

We are now in a position to calculate the Fermi energy by making use of (6.8) and (6.9). We consider the simple case $T \to 0$ and $E < E_F$. Integration from the lower end of the band to the Fermi energy E_F provides

$$N^* = \int_0^{E_F} N(E)\,dE = \int_0^{E_F} \frac{V}{2\pi^2}\left(\frac{2m}{\hbar^2}\right)^{3/2} E^{1/2}\,dE = \frac{V}{3\pi^2}\left(\frac{2m}{\hbar^2}\right)^{3/2} E_F^{3/2}. \tag{6.10}$$

We define $N' = N^*/V$ the number of electrons per unit volume. Then we obtain by rearranging (6.10):

$$E_F = (3\pi^2 N')^{2/3}\frac{\hbar^2}{2m}. \tag{6.11}$$

6.5. Complete Density of States Function Within a Band

We have seen in Section 6.3 that for the free electron case the density of states has a parabolic E versus $Z(E)$ relationship. In actual crystals, however, the density of states is modified by the energy conditions within the first Brillouin zone. Let us consider, for example the curves of equal energy depicted in Fig. 5.26. For low energies, the equal energy curves are circles. Thus, the electrons behave free-electron-like for these low energies. The density of states curve is then, as before, a parabola. For larger energies, however, less energy states are available as seen in Fig. 5.26. Thus, $Z(E)$ decreases with increasing E, until eventually the corners of the Brillouin zones are filled. At this point $Z(E)$ has dropped to zero. The largest number of energy states is thus found near the center of a band, as schematically shown in Fig. 6.6.

6.6. Consequences of the Band Model

We mentioned in Section 6.4 that because of the Pauli Principle, each energy band of a crystal, consisting of N atoms, has space for $2N$ electrons, i.e., for two electrons per atom. If the highest filled band of a crystal is occupied by 2

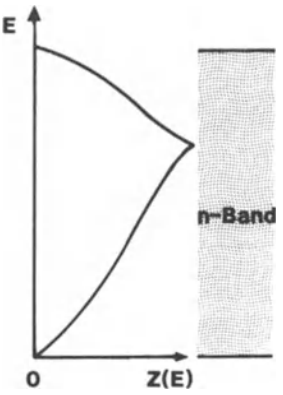

Figure 6.6. Schematic representation of the complete density of states function within a band.

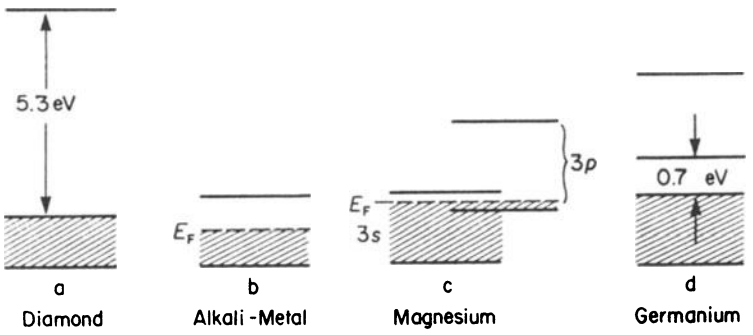

Figure 6.7. Simplified representation for energy bands for (a) insulators, (b) alkali metals, (c) bivalent metals, and (d) intrinsic semiconductors.

electrons per atom, i.e., if the band is completely filled, we would expect that the electrons cannot drift through the crystal when an external electric field is applied (similarly as it is impossible to move a car in a completely occupied parking lot). An electron has to absorb energy in order to move. Keep in mind that for a completely occupied band, higher energy levels are not allowed. (We exclude the possibility of electron jumps into higher bands.) Solids in which the highest filled band is completely occupied by electrons are, therefore, insulators (Fig. 6.7(a)).

In solids with one valence electron per atom (for example, alkali metals) the valence band is essentially half filled. An electron drift upon application of an external field is possible; the crystal shows metallic behavior (Fig. 6.7(b)).

Bivalent metals should be insulators according to this consideration, which is not the case. The reason for this lies in the fact that the upper bands partially overlap, which occurs because of the weak binding forces of the valence

electrons on their atomic nuclei (see Fig. 5.27). If such an overlapping of bands occurs, the valence electrons flow in the lower portion of the next higher band because the electrons tend to assume the lowest potential energy (Fig. 6.7(c)). As a result, bivalent solids may also possess partially filled bands. Thus, they are also conductors.

We shall see in Chapter 8 that valence as well as the conduction bands of semiconductors can accommodate $4N$ electrons. Because germanium or silicon possess 4 valence electrons, the valence band is completely filled with electrons. Intrinsic semiconductors have a relatively narrow forbidden energy zone (Fig. 6.7(d)). A sufficiently large energy can, therefore, excite electrons from the completely filled valence band into the empty conduction band and thus provide some electron conduction.

This preliminary and very qualitative discussion on electronic conduction will be substantially expanded and the understanding will be deepened in Part II of this book.

6.7. Effective Mass

We implied in the previous sections that the mass of an electron in a solid is the same as the mass of a free electron. Experimentally determined physical properties of solids such as optical, thermal, or electrical properties indicate, however, that for some solids the mass is larger while for others it is slightly smaller than the free electron mass. This experimentally determined electron mass is usually called the effective mass m^*. The deviation of m^* from the free electron mass[12] m_0 can be easily appreciated by stating the ratio m^*/m_0 which has values slightly above or below 1 (see Appendix 4). The cause for the deviation of the effective mass from the free electron mass is usually attributed to interactions between the drifting electrons and the atoms in a crystal. For example, an electron which is accelerated in an electric field might be slightly slowed down because of "collisions" with some atoms. The ratio m^*/m_0 is then larger than 1. On the other hand, the electron wave in another crystal might have just the right phase in order that the response to an external electric field be enhanced. In this case m^*/m_0 is smaller than 1.

We shall now attempt to find an expression for the effective mass. For this, we shall compare the acceleration of an electron in an electric field calculated by classical as well as quantum mechanical means. At first, we write an expression for the velocity of an electron in an energy band. We introduced in Chapter 2 the group velocity, i.e., the velocity with which a wave packet moves. Let ω be the angular frequency and $|\mathbf{k}| = 2\pi/\lambda$ the wave number of the electron wave. Then the group velocity is, according to (2.9),

[12] We shall use the symbol m_0 only when we need to distinguish the free electron mass from the effective mass.

$$v_g = \frac{d\omega}{dk} = \frac{d(2\pi\nu)}{dk} = \frac{d(2\pi E/h)}{dk} = \frac{1}{\hbar}\frac{dE}{dk}. \tag{6.12}$$

From this we calculate the acceleration:

$$a = \frac{dv_g}{dt} = \frac{1}{\hbar}\frac{d^2E}{dk^2}\frac{dk}{dt}. \tag{6.13}$$

The relation between the energy E and the wave number $|\mathbf{k}|$ is known from the preceding sections. We want to determine now the factor dk/dt. Forming the first derivative of (4.8) ($p = \hbar k$) with respect to time yields:

$$\frac{dp}{dt} = \hbar\frac{dk}{dt}. \tag{6.14}$$

Combining (6.14) with (6.13) yields:

$$a = \frac{1}{\hbar^2}\frac{d^2E}{dk^2}\frac{dp}{dt} = \frac{1}{\hbar^2}\cdot\frac{d^2E}{dk^2}\cdot\frac{d(mv)}{dt} = \frac{1}{\hbar^2}\frac{d^2E}{dk^2}F, \tag{6.15}$$

where F is the force. The classical acceleration can be calculated from Newton's law (1.1)

$$a = \frac{F}{m}. \tag{6.16}$$

Comparing (6.15) with (6.16) yields the effective mass:

$$m^* = \hbar^2\left(\frac{d^2E}{dk^2}\right)^{-1}. \tag{6.17}$$

We see from (6.17) that the effective mass is inversely proportional to the curvature of an electron band. Specifically, if the curvature of $E = f(k)$ at a given point in k-space is large, then the effective mass is small (and vice versa). When inspecting band structures (Fig. 5.4 or Figs. 5.21–5.24) we notice some regions of high curvature. These regions might be found particularly near the center or near the boundary of a Brillouin zone. At these places, the effective mass is substantially reduced and may be as low as 1% of the free electron mass m_0. At points in k-space for which more than one electron band is found (Γ-point in Fig. 5.23 for example) more than one effective mass needs to be defined.

We shall demonstrate the k-dependence of the effective mass for a simple case and defer discussions about actual cases to Section 8.4. In Fig. 6.8(a) an ideal electron band within the first Brillouin zone is depicted. From this curve both the first derivative and the reciprocal function of the second derivative, that is m^*, have been calculated. These functions are shown in Figs. 6.8(b) and (c). We notice in Fig. 6.8(c) that the effective mass of the electrons is small and positive near the center of the Brillouin zone and eventually increases for larger values of k_x. We likewise observe in Fig. 6.8(c) that electrons in the upper part of the given band have a negative effective mass. An electron with

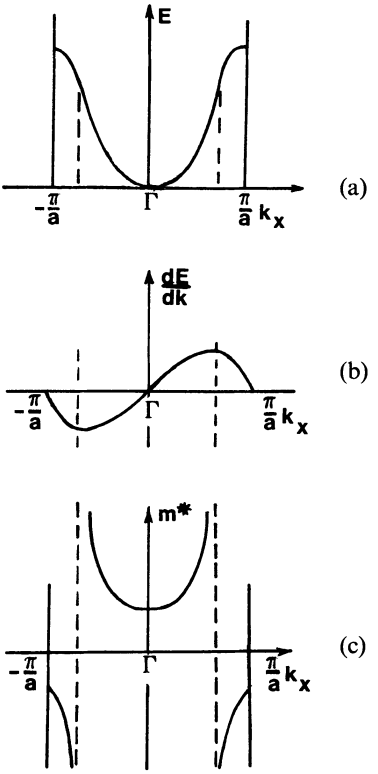

Figure 6.8. (a) Simple bandstructure, as shown in Fig. 5.4. (b) First derivative and (c) inverse function of second derivative of the curve shown in (a).

negative effective mass is called "defect electron" or "electron hole." (It is, however, common to ascribe to the hole a positive effective mass and a positive charge.) Electron holes play an important role in crystals whose valence bands are almost filled, for example, in semiconductors. Solids which possess different properties in various directions (anisotropy) have a different m^* in each direction. The effective mass is a tensor in this case. An electron hole pair is called an "exciton."

6.8. Conclusion

The first part of this book intended to provide the reader with the necessary tools for a better understanding of the electronic properties of materials. We started our discussion by solving the Schrödinger equation for the free electron case, the bound electron case, and for electrons in a crystal. We learned that the distinct energy levels which are characteristic for isolated

atoms widen into energy bands when the atoms are moved closer together and eventually form a solid. We also learned that the electron bands have "fine structure," that is, they consist of individual "branches" in an energy versus momentum (actually **k**) diagram. We further learned that some of these energy bands are filled by electrons, and that the degree of this filling depends upon whether we consider a metal, a semiconductor, or an insulator. Finally, the degree to which electron energy levels are available within a band was found to be nonuniform. We discovered that the density of states is largest near the center of an electron band. All these relatively unfamiliar concepts will become more transparent to the reader when we apply them in the chapters to come.

Problems

1. What velocity has an electron near the Fermi surface of silver? ($E_F = 5.5$ eV).
2. Are there more electrons on the bottom or in the middle of the valence band of a metal? Explain.
3. At what temperature can we expect a 10% probability that electrons in silver have an energy which is 1% above the Fermi energy? ($E_F = 5.5$ eV).
4. Calculate the Fermi energy for silver assuming 6.1×10^{28} free electrons per m^3. (Assume the effective mass equals the free electron mass.)
5. Calculate the density of states of 1 m^3 of copper at the Fermi level ($m^* = m_0$, $T = 0$, $E_F = 7$ eV). *Note*: Take 1 eV as energy interval. (Why?).
6. The density of states per eV at the Fermi level (7 eV) was calculated for a certain metal to be about 10^{27} energy states per eV. Someone is asked to calculate the number of electrons for this metal using the Fermi energy as the maximum kinetic energy which the electrons have. He argues that because of the Pauli Principle, each energy state is occupied by two electrons. Consequently, there are 2×10^{27} electrons in that band.
   a) What is wrong with that argument?
   b) Why is the answer after all not too far off from the correct numerical value?
7. Assuming the electrons to be free, calculate the total number of states below $E =$ 5 eV in a volume of 10^{-5} m^3.
8. a) Calculate the number of electrons per cubic meter in copper, assuming that the maximum energy of these electrons equals the Fermi energy ($m^* = m_0$).
   b) How does this result compare with that determined directly from the density of copper?
   c) How can we correct for the discrepancy?
   d) Does using the effective mass decrease the discrepancy?
9. a) Calculate the density of states for 1 m^3 of Na at the Fermi level for $T = 0$.
   b) Calculate the same quantity for 1 g-mole of Na.
   c) Why are these numbers different?

d) What fraction of the 3*s*-electrons of Na is found within an energy kT of the Fermi level?

10. Calculate the Fermi distribution function for a metal at the Fermi level for $T \neq 0$.

11. Explain why in a simple model a bivalent material could be considered to be an insulator. Explain also why this simple argument is not true.

12. We stated in the text that the Fermi distribution function can be approximated by classical Boltzmann statistics if the exponential factor in the Fermi distribution function is significantly larger than one.
    a) Calculate $E - E_F = nk_BT$ for various values of n and state at which value for n,

$$\exp - \left(\frac{E - E_F}{k_B T} \right)$$

    can be considered to be "significantly larger" then one (assume $T = 300K$).
    b) For what *energy* can we use Boltzmann statistics? (Assume $E_F = 5$ eV and $E - E_F = 4k_BT$).

Suggestions for Further Reading (Part I)

N.W. Ashcroft and N.D. Mermin, *Solid State Physics*, Holt, Rinehart and Winston, New York (1976).
L.V. Azároff and J.J. Brophy, *Electronic Processes in Materials*, McGraw-Hill, New York (1963).
J.S. Blakemore, *Solid State Physics*, W.B. Saunders Comp., West Washington Square, Philadelphia, PA (1969).
R.H. Bube, *Electronic Properties of Crystalline Solids*, Academic Press, New York (1974).
C. Kittel, *Solid State Physics*, J. Wiley and Sons, New York (1976).
N.F. Mott and H. Jones, *The Theory of the Properties of Metals and Alloys*, Dover, New York (1936).
M.A. Omar, *Elementary Solid State Physics*, Addison-Wesley, Reading, MA (1978).
A.B. Pippard, *The Dynamics of Conduction Electrons*, Gordon and Breach, New York, London, Paris (1965).
H.A. Pohl, *Quantum Mechanics for Science and Engineering*, Prentice-Hall Series in Materials Science, Prentice-Hall, Englewood-Cliffs, NJ.
R.M. Rose, L.A. Shepard, and J. Wulff, *The Structure and Properties of Materials*, Vol. IV, Electronic Properties, J. Wiley and Sons, New York (1966).
C.A. Wert and R.M. Thomson, *Physics of Solids*, McGraw-Hill, New York (1964).
P. Wilkes, *Solid State Theory in Metallurgy*, Cambridge University Press, Cambridge (1973).

PART II

ELECTRICAL PROPERTIES OF MATERIALS

CHAPTER 7

Electrical Conduction in Metals and Alloys

7.1. Introduction

The first observations involving electrical phenomena probably began with the study of static electricitiy. Thales of Miletus, a Greek philosopher, discovered around 600 BC that a piece of amber, having been rubbed with a piece of cloth, attracted feathers and other light particles. Very appropriately, the word *electricity* was later coined by incorporating the Greek word *elektron* which means *amber*.

It was apparently not before 2300 years later that man became again interested in electrical phenomena. Stephen Gray found in the early 1700s that some substances conduct electricity whereas others did not. In 1733 DuFay postulated the existence of two types of electricity which he termed *glass electricity* and *amber electricity* dependent on which material was rubbed. From then on a constant stream of well-known scientists contributed to our knowledge of electrical phenomena. Names such as Coulomb, Galvani, Volta, Oersted, Ampère, Ohm, Seebeck, Faraday, Henry, Maxwell, Thomson, and others, come to mind. What started 2600 years ago as a mysterious effect has been applied quite recently in an impressive technology which culminated in large scale integration of electronic devices.

A satisfactory understanding of electrical phenomena on an atomistic basis was achieved by Drude at the turn of this century. A few decades later quantum mechanics refined our understanding. Both the classical as well as the quantum concepts of electrical phenomena shall be covered in the chapters to come. Special emphasis is placed on the description of important applications.

7.2. Survey

The conductivity, σ, of different materials spans about twenty-five orders of magnitude (see Fig. 7.1). This is the largest known variation in a physical property.

It is generally accepted that in metals and alloys the electrons, particularly the outer or valence electrons, play an important role in electrical conduction. Therefore, it seems most appropriate to make use of the electron theory which has been developed in the foregoing chapters. Before doing so, the reader is reminded of some fundamental equations of physics pertaining to electrical conduction. These laws have been extracted from experimental observations. Ohm's law

$$V = RI \tag{7.1}$$

relates the potential difference V (in volts) with the electrical resistance R (in ohms) and the electrical current I (in amps). Another form of Ohm's law,

$$j = \sigma \mathscr{E}, \tag{7.2}$$

links current density

$$j = \frac{I}{A},$$

i.e., the current per unit area (A/m^2), with conductivity σ ($1/\Omega m$) and electric field strength[1]

$$\mathscr{E} = \frac{V}{L} \tag{7.3}$$

(V/m). (In general, $\mathscr{E}$ and j are vectors. For our purpose, however, we need only their moduli.) The current density is frequently expressed by

$$j = Nve, \tag{7.4}$$

[1] We use for the electric field strength a script E to distinguish it from the energy.

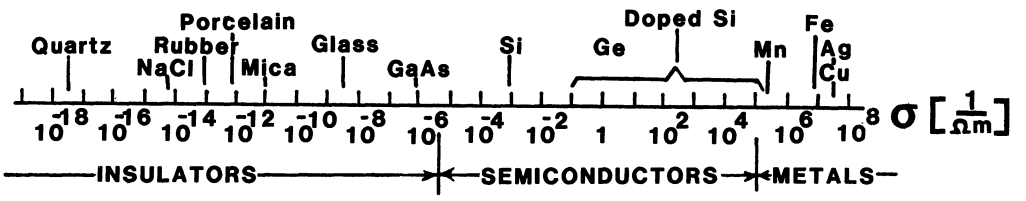

Figure 7.1. Room-temperature conductivity of various materials. (Superconductors, having conductivities of many orders of magnitude larger than copper, near 0 K, are not shown. The conductivity of semiconductors varies substantially with temperature and purity.)

where N is the number of electrons, v their velocity, and e their charge. The resistance of a conductor can be calculated from its physical dimensions by

$$R = \frac{L\rho}{A},$$

where L is the length of the conductor, A is its cross-sectional area, and ρ is the specific resistance, or resistivity (Ωm). We define

$$\rho = \frac{1}{\sigma}.$$

Our first approach towards an understanding of electrical conduction is to postulate, as Drude did, a free "electron gas" or "plasma," consisting of the valence electrons of the individual atoms in a crystal. We assume that in a monovalent metal, such as sodium, each atom contributes *one* electron to this plasma. The number of atoms, N_a, per cubic meter (and therefore the number of free electrons in a monovalent metal) can be obtained by applying

$$N_a = \frac{N_0 \delta}{W}, \tag{7.5}$$

where N_0 is the Avogadro constant, δ the density, and W the atomic weight of the element. One calculates about 10^{28} to 10^{29} atoms per cubic meter, that is, 10^{28} to 10^{29} free electrons per m^3 for a monovalent metal.

The electrons move randomly (in all possible directions) so that their individual velocities in the absence of an electric field cancel and no net velocity results. This situation changes when an electric field is applied. The electrons are then accelerated with the force $e\mathscr{E}$ towards the anode and a net drift of the electrons results which can be expressed by a form of Newton's law ($F = ma$):

$$m\frac{dv}{dt} = e\mathscr{E}, \tag{7.6}$$

where e is the charge of the electrons and m is their mass. Equation (7.6) implies that as long as an electric field persists, the electrons are constantly accelerated. Equation (7.6) also suggests that after the field has been removed, the electrons keep drifting with constant velocity through the crystal. This is generally not observed, however, except for some metals at very low temperatures (superconductors). The *free electron model* needs, therefore, an adjustment to take into account the electrical resistance. We postulate that the resistance in metals and alloys is due to interactions of the drifting electrons with some lattice atoms, that is, essentially with the imperfections in the crystal lattice (such as impurity atoms, vacancies, grain boundaries, dislocations, etc.). Thus, (7.6) is modified as follows:

$$m\frac{dv}{dt} + \gamma v = e\mathscr{E}, \tag{7.7}$$

where γ is a constant. The second term in (7.7) is a damping or *friction* force which contains the drift velocity of the electrons.

We discussed in Chapter 2 the existence of two alternatives to describe an electron. First, we may consider the electrons to have particle nature. The interactions could be envisioned in this case to occur by means of elastic collisions of the drifting electrons with certain lattice atoms. The more collisions are encountered, the higher is the resistance. This concept qualitatively describes the increase in resistance with increasing amount of lattice imperfections. It also explains the observed increase in resistance with increasing temperature: the thermal energy causes the lattice atoms to oscillate about their equilibrium positions (see Part V) thus increasing the probability for collisions with the drifting electrons.

Secondly, one may describe the electrons to have a wave nature. The matter waves may be thought to be scattered by lattice atoms. Scattering is the dissipation of radiation on small particles in all directions. The atoms absorb the energy of an incoming wave and thus become oscillators. These oscillators in turn reemit the energy in the form of spherical waves. If two or more atoms are involved, the phase relationship between the individual reemitted waves has to be taken into consideration. A calculation[2] shows that for a *periodic crystal structure* the individual waves in the forward direction are *in phase*, and thus interfere constructively. As a result, a wave which propagates through an ideal crystal (having periodically arranged atoms) does not suffer any change in intensity or direction. (Only its velocity is modified.) This mechanism is called *coherent scattering*.

If, however, the scattering centers are not periodically arranged (impurity atoms, vacancies, grain boundaries, thermal vibration of atoms, etc.) the scattered waves have no set phase relationship and the wave is said to be *incoherently scattered*. The energy of incoherently scattered waves is smaller in the forward direction.

Finally, diffraction of the incoming waves is always a possibility if certain conditions are fulfilled. The diffracted beam is composed of a large number of coherently scattered rays which mutually reinforce each other. Reinforcement occurs, however, only in certain directions and only if Bragg's law (5.10) is fulfilled, that is, if $\lambda < 2d$. However, the largest distance between lattice planes in metals, d, is typically 2 Å and the wavelength λ of an electron wave having the energy of the electrons at the Fermi surface is around 5 or 6 Ångstroms (Chapter 2, Problem 1). Thus, the electron wave has a wavelength too large to be diffracted by the lattice atoms. (Similarly, light waves having wavelengths between 400 nm and 700 nm are not diffracted by a crystal.)

In summary, the wave picture provides a deeper understanding of the electrical resistance in metals and alloys. In an ideal crystal, the electron waves are coherently scattered in the forward direction. As a consequence the electron wave passes without hindrance through the crystal. If, however,

---

[2] L. Brillouin, *Wave Propagation in Periodic Structures*, Dover Press, New York (1953).

lattice defects, impurities etc., are present, the matter waves lose energy. This energy loss qualitatively explains the resistance. In the following two sections we shall calculate the resistance using, at first, the particle and then the wave concept.

7.3. Conductivity—Classical Electron Theory

We implied above that the drift velocity of electrons, which is caused by an external electric field, is superimposed on the much larger random motion of the electrons. An electron, accelerated by such an electric field, may be described to increase its drift velocity until it encounters a collision. At this time, the electron has acquired the velocity v_{max} which it may lose all or in part at the collision (Fig. 7.2(a)). Alternatively, and more appropriately, one may describe an electron motion to be counteracted by a "friction" force γv which opposes the electrostatic force $e\mathscr{E}$. (See equation 7.7.) The electrons are thought to be accelerated until a final drift velocity v_f is reached (see Fig. 7.2(b)). At that time the electric field force and the friction force are equal in magnitude. In other words, the electrons are thought to move in a "viscous" medium.

For the steady state case $v = v_f$ we obtain $dv/dt = 0$. Then (7.7) reduces to

$$\gamma v_f = e\mathscr{E} \tag{7.8}$$

which yields

$$\gamma = \frac{e\mathscr{E}}{v_f}. \tag{7.9}$$

We insert (7.9) into (7.7) and obtain the complete equation for the drifting electrons under the influence of an electric field force and a friction force:

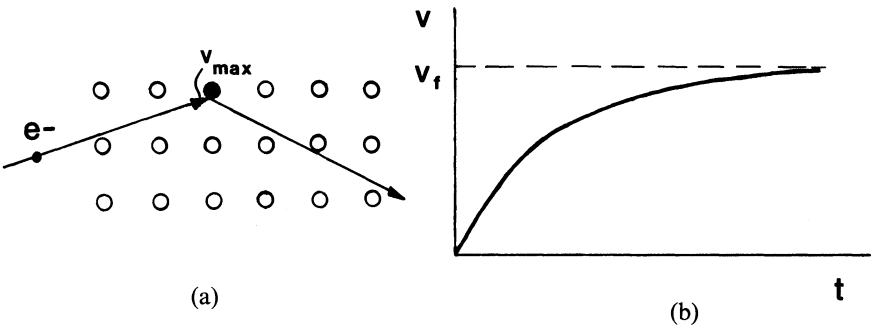

Figure 7.2. (a) Schematic representation of an electron collision with a lattice atom. (b) Velocity distribution of electrons due to an electrostatic force and a counteracting friction force. The electron eventually reaches the final velocity v_f.

$$m\frac{dv}{dt} + \frac{e\mathscr{E}}{v_f}v = e\mathscr{E}. \tag{7.10}$$

The solution to this equation[3] is

$$v = v_f\left[1 - \exp\left(-\left(\frac{e\mathscr{E}}{mv_f}t\right)\right)\right]. \tag{7.11}$$

We note that the factor $mv_f/e\mathscr{E}$ in (7.11) has the unit of a time. It is customary to define this factor

$$\tau = \frac{mv_f}{e\mathscr{E}} \tag{7.12}$$

as a *relaxation time* (which can be interpreted as the average time between two consecutive collisions). Rearranging (7.12) yields

$$v_f = \frac{\tau e\mathscr{E}}{m}. \tag{7.13}$$

We make use of (7.4) which states that the current density j is proportional to the velocity of the drifting electrons and proportional to the number of free electrons N_f (per m^3). This yields with (7.2)

$$j = N_f v_f e = \sigma\mathscr{E}. \tag{7.14}$$

Combining (7.13) with (7.14) provides, finally, the sought-for equation for the conductivity:

$$\boxed{\sigma = \frac{N_f e^2 \tau}{m}}. \tag{7.15}$$

Equation (7.15) teaches us that the conductivity is large for a large number of free electrons and for a large relaxation time. The latter is proportional to the mean free path between two consecutive collisions. The mean free path is defined to be

$$l = v\tau. \tag{7.15a}$$

7.4. Conductivity—Quantum Mechanical Considerations

It was stated above that the valence electrons perform, when in equilibrium, random motions with no preferential velocity in any direction. One can visualize this fact conveniently by plotting the velocities of the electrons in

[3] The reader may convince himself of the correctness of this solution by inserting (7.11) and its first derivative by time into (7.10). Further inserting $t \to \infty$ into (7.11) yields correctly $v = v_f$ (Fig. 7.2(b)). See also Problem 8.

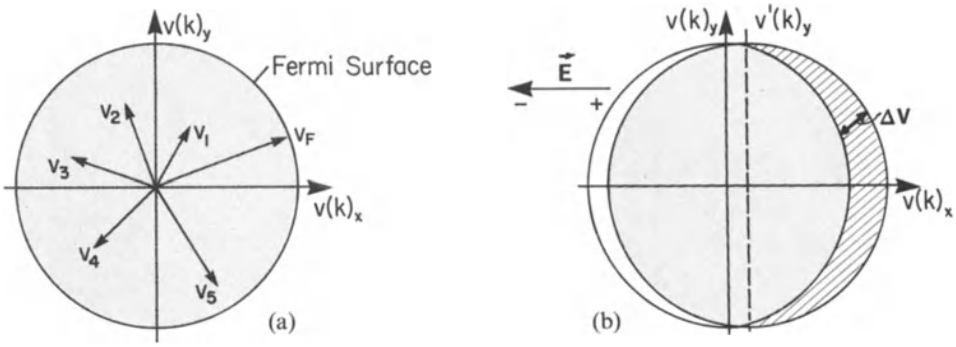

Figure 7.3. Velocity of electrons in two-dimensional velocity space. (a) Equilibrium, (b) when an electric field is applied.

velocity space (Fig. 7.3(a)). The points inside a sphere (or inside a circle when considering two dimensions) correspond to the endpoints of velocity vectors. The maximum velocity which the electrons are able to assume is the Fermi velocity v_F (i.e., the velocity of the electrons at the Fermi energy). The sphere having v_F as a radius represents, therefore, the Fermi surface. All points inside the Fermi sphere are occupied. As a consequence the velocity vectors cancel each other pairwise at equilibrium and no net velocity of the electrons results.

If an electric field is applied, the Fermi sphere is displaced opposite to the field direction, i.e., towards the positive end of the electric field, due to the net velocity gain of the electrons (Fig. 7.3(b)). The great majority of the electron velocities still cancel each other pairwise (shaded area). However, some electrons remain uncompensated; their velocities $v + \Delta v$ are shown cross hatched in Fig. 7.3(b). These electrons cause the observed current. The Drude description of conduction thus needs a modification. In the *classical* picture one would assume that *all* electrons drift, under the influence of an electric field, with a modest velocity. Quantum mechanics, instead, teaches us that *only specific electrons* participate in conduction and that these electrons drift with a high velocity which is approximately the Fermi velocity v_F.

An additional point needs to be discussed and leads to an even deeper understanding. The largest energy which the electrons can assume in a metal at $T = 0$ is the Fermi energy E_F (Chapter 6). A large number of electrons actually possess this very energy since the density of states and thus the population density is highest around E_F (Fig. 7.4). Thus, only a little extra energy ΔE is needed to raise a substantial number of electrons from the Fermi level into slightly higher states. As a consequence, the energy (or the velocity) of electrons accelerated by the electric field $\mathscr{E}$ is only slightly larger than the Fermi energy E_F (or the Fermi velocity v_F) so that for all practical purposes the mean velocity can be approximated by the Fermi velocity v_F. We implied this fact already in our previous discussions.

We calculate now the conductivity by quantum mechanical means and

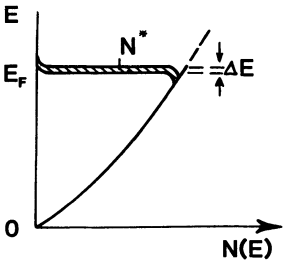

Figure 7.4. Population density $N(E)$ versus energy for free electrons (see Fig. 6.5) and displacement ΔE by an electric field. N^* is the number of displaced electrons in the energy interval ΔE.

apply, as before, Ohm's law $j = \sigma\mathscr{E}$, (7.2). The current density j is, as stated in (7.4), the product of the number of electrons, the electron velocity, and the electron charge. In our present case, we know that the velocity of the electrons which are responsible for the electron conduction is essentially the Fermi velocity v_F. Further, the number of electrons which need to be considered here is N^*, that is the number of displaced electrons, as shown in Fig. 7.4. Thus, (7.4) needs to be modified to read

$$j = v_F e N^*. \tag{7.16}$$

The number of electrons displaced by the electric field $\mathscr{E}$ is

$$N^* = N(E)\Delta E \tag{7.17}$$

(see Fig. 7.4) which yields for the current density

$$j = v_F e N(E)\Delta E = v_F e N(E)\frac{dE}{dk}\Delta k. \tag{7.18}$$

The factor dE/dk is calculated by using the E versus $|\mathbf{k}|$ relationship known for free electrons (4.6), that is,

$$E = \frac{\hbar^2}{2m}k^2. \tag{7.19}$$

Taking the first derivative of (7.19) yields with $k = p/\hbar$ (4.8):

$$\frac{dE}{dk} = \frac{\hbar^2}{m}k = \frac{\hbar^2 p}{m\hbar} = \frac{\hbar m v_F}{m} = \hbar v_F. \tag{7.20}$$

Inserting (7.20) into (7.18) yields

$$j = v_F^2 e N(E)\hbar\Delta k. \tag{7.21}$$

The displacement Δk of the Fermi sphere in k-space under the influence of an electric field can be calculated by using (7.6) and $p = \hbar k$ (4.8):

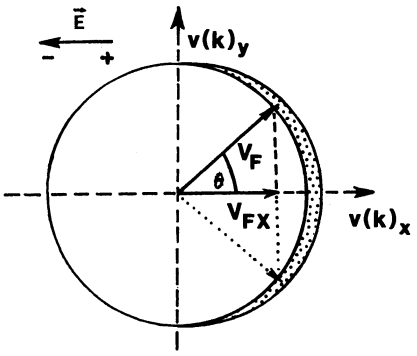

Figure 7.5. Two-dimensional velocity space.

$$F = m\frac{dv}{dt} = \frac{d(mv)}{dt} = \frac{dp}{dt} = \hbar\frac{dk}{dt} = e\mathscr{E}, \tag{7.22}$$

which yields

$$dk = \frac{e\mathscr{E}}{\hbar}dt$$

or

$$\Delta k = \frac{e\mathscr{E}}{\hbar}\Delta t = \frac{e\mathscr{E}}{\hbar}\tau, \tag{7.23}$$

where τ is the time interval Δt between two "collisions" or the relaxation time (see Section 7.3). Inserting (7.23) into (7.21) yields

$$j = v_F^2 e^2 N(E)\mathscr{E}\tau. \tag{7.24}$$

One more consideration needs to be made. If the electric field-vector points into the negative $v(k)_x$ direction, then only the components of those velocities which are parallel to the positive $v(k)_x$ direction contribute to the electric current (Fig. 7.5). The $v(k)_y$ components cancel each other pairwise. In other words, only the projections of the velocities v_F on the positive $v(k)_x$-axis ($v_{Fx} = v_F \cos\theta$) contribute to the current. Thus, we have to sum up all contributions of the velocities in the first and fourth quadrant in Fig. 7.5 which yields

$$\begin{aligned} j &= e^2 N(E)\mathscr{E}\tau \int_{-\pi/2}^{+\pi/2} (v_F \cos\theta)^2 \frac{d\theta}{\pi} \\ &= e^2 N(E)\mathscr{E}\tau \frac{v_F^2}{\pi} \int_{-\pi/2}^{+\pi/2} \cos^2\theta \, d\theta \\ &= e^2 N(E)\mathscr{E}\tau \frac{v_F^2}{\pi}\left[\frac{1}{4}\sin 2\theta + \frac{\theta}{2}\right]_{-\pi/2}^{+\pi/2} \\ j &= \tfrac{1}{2} e^2 N(E)\mathscr{E}\tau v_F^2. \end{aligned}$$

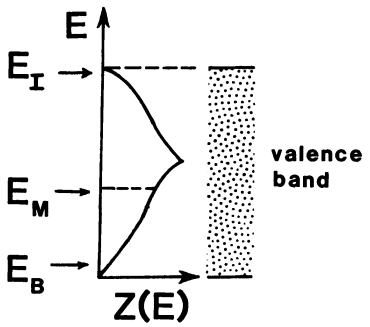

Figure 7.6. Schematic representation of the density of states (Fig. 6.6) and thus with minor modifications, also the population density (6.7). Examples for highest electron energies for a monovalent metal (E_M), for a bivalent metal (E_B), and for an insulator (E_I) are indicated.

A similar calculation for a spherical Fermi surface yields

$$j = \tfrac{1}{3}e^2 N(E)\mathscr{E}\tau v_F^2. \tag{7.25}$$

Thus, the conductivity finally becomes with $\sigma = j/\mathscr{E}$ (7.2)

$$\boxed{\sigma = \tfrac{1}{3}e^2 v_F^2 \tau N(E).} \tag{7.26}$$

This quantum mechanical equation reveals that the conductivity depends on the Fermi velocity, the relaxation time, and the population density. The latter is, as we know, proportional to the density of states. Equation (7.26) is more meaningful than the expression derived from the classical electron theory (7.15). Specifically, (7.26) contains the information that not *all* free electrons N_f are responsible for conduction, that is, the conductivity in metals depends to a large extent on the population density of the electrons near the Fermi surface. For example, monovalent metals (such as copper, silver, or gold) have partially filled valence bands, as shown in Figs. 5.21 or 6.7. Their electron population densities near their Fermi energy are high (Fig. 7.6) which results in a large conductivity according to (7.26). Bivalent metals on the other hand are distinguished by an overlapping of the upper bands and by a small electron concentration near the bottom of the valence band, as shown in Fig. 6.7(c). As a consequence the electron population near the Fermi energy is small (Fig. 7.6) which leads to a comparatively low conductivity. Finally, insulators and semiconductors, have under certain conditions, completely filled electron bands which results in a virtually zero population density near the top of the valence band (Fig. 7.6). Thus, the conductivity in these materials is extremely small.

7.5. Experimental Results and Their Interpretation

7.5.1. Pure Metals

The resistivity of a metal, such as copper, decreases linearly with decreasing temperature until it reaches a finite value (Fig. 7.7). We postulate that thermal energy causes lattice atoms to oscillate about their equilibrium positions, thus increasing the incoherent scattering of the electron waves. The residual resistivity ρ_{res} is interpreted to be due to imperfections in the crystal, such as impurities, vacancies, grain boundaries, or dislocations. The residual resistivity is not temperature dependent. According to Matthiessen's rule the resistivity arises from independent scattering processes which are additive, that is

$$\rho = \rho_{th} + \rho_{imp} + \rho_{def} = \rho_{th} + \rho_{res}. \tag{7.27}$$

The thermally induced part of the resistivity ρ_{th} is called the *ideal* resistivity, whereas the resistivity which has its origin in impurities (ρ_{imp}) and defects (ρ_{def}) is summed up in the residual resistivity. The number of impurity atoms is generally constant in a given metal or alloy. The number of vacancies or grain boundaries, however, can be changed by various heat treatments. For example if a metal is annealed at temperatures close to its melting point and then rapidly quenched into water of room temperature, its room temperature resistivity increases noticeably due to quenched-in vacancies. Frequently, this resistance increase diminishes during room temperature aging or annealing at slightly elevated temperatures due to the annihilation of some vacancies. Likewise, recrystallization, grain growth, and many other metallurgical processes change the resistivity of metals. As a consequence of this and due to its simple measurement, the resistivity is one of the most widely studied properties in materials research.

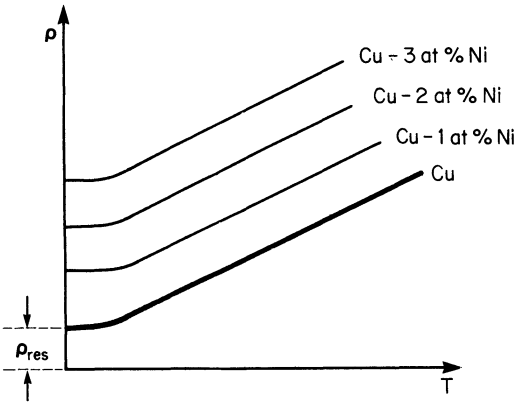

Figure 7.7. Schematic representation of the temperature dependence of the resistivity of copper and various copper–nickel alloys. ρ_{res} is the residual resistivity.

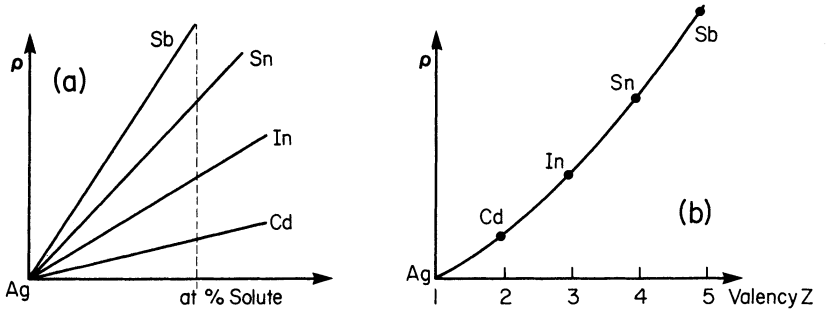

Figure 7.8. Resistivity of various silver alloys (schematic). Solvent and solute are all from the fifth period. (a) Resistivity versus atomic % solute, (b) resistivity change due to 1 atomic % of solute.

7.5.2. Alloys

The resistivity of alloys increases with increasing amount of solute content (Fig. 7.7). The slopes of the individual ρ versus T lines remain, however, constant. Increasing solute concentrations merely cause a linear shift of the ρ versus T curves to higher resistivity values in accordance with Matthiessen's rule.

In Figs. 7.8(a) and (b) the resistivities of various solute elements, having different valences, that is, electron concentrations, are shown. It can be seen that the resistivity increases with the square of increasing electron concentration. The resistivity increase due to solute elements has its origin in two mechanisms. First, atoms of different size cause a variation in the lattice parameter and thus in electron scattering. Second, atoms having different valences introduce a local charge difference which also increases the scattering probability.

Some alloys (copper with small amounts of iron, for example) show a minimum of the resistivity at low temperatures. This anomaly is due to additional scattering of electrons by the magnetic moments of the solutes and is a deviation from the Matthiessen rule (Kondo effect).

7.5.3. Ordering

Solute atoms are generally randomly distributed in the solvent. Thus, the number of centers where incoherent scattering occurs increases proportionally with the number of substitutional atoms. If, however, the solute atoms are periodically arranged in the matrix, i.e., if, for example, in a 50/50 alloy the A and B atoms are alternately occupying successive lattice sites, then the electron waves are coherently scattered. This causes a decrease in resistivity (and an increase in the mean free path) (Fig. 7.9). Only selected alloys such as Cu_3Au, CuAu, Au_3Mn, etc., show a tendency towards long-range ordering.

The ordered state can be achieved by annealing an alloy of appropriate

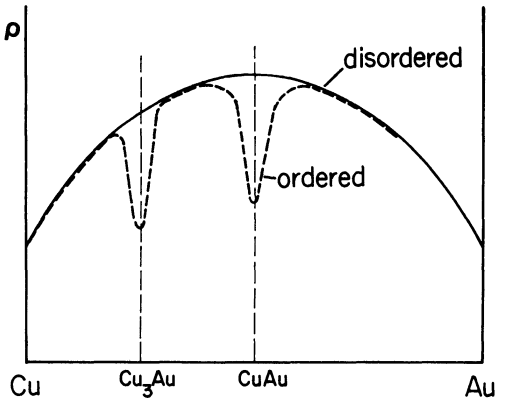

Figure 7.9. Schematic representation of the resistivity of ordered and disordered copper–gold alloys.

composition, below the order–disorder transition temperature (about 395 °C in Cu_3Au) or by slowly cooling from above the transition temperature. Annealing above this transition temperature destroys the ordering effect. In some alloys, however, such as the intermetallic compound CuAu, the tendency towards ordering is so strong that even near the melting point some ordering remains. Long-range ordered alloys cause super lattice lines in X-ray patterns.

The disordered state can be retained at room temperature by quenching the alloy rapidly in ice brine from slightly above the transition temperature.

Some alloys, such as α–copper–aluminum, exhibit a much smaller resistance decrease due to annealing below a certain ordering temperature. This effect is called short-range ordering and has been found to be due to small domains in which the atoms are arranged in an ordered fashion. In the short-range ordered state the A–B interactions are slightly larger than the A–A or B–B interactions. (Short-range ordering can be identified by using small angle X-ray scattering. It causes small and broad intensity increases between the regular diffraction lines.)

The *K*-state is another type of a short-range ordering effect. In this case, however, the resistivity *increases* due to heat treatment below a transition temperature. More information on ordering can be found in its special literature.[4]

7.6. Superconductivity

Superconductors are metals or alloys whose resistivities become immeasurably small or actually become zero below a critical temperature T_c. The most sensitive resistance measurements have shown that the resistance of these

[4] H. Warlimont, ed., *Order–Disorder Transformations in Alloys*, Springer-Verlag, Berlin, Heidelberg, New York (1974).

materials in the superconducting state is at least 10^{16} times smaller than their room temperature values. (See, in this context, Fig. 7.1.) So far, 27 elements and numerous alloys have been discovered to possess superconductivity. Their critical temperatures T_c have values between 23.2 K for Nb_3Ge and 0.01 K for tungsten. Superconductors having a T_c above 20 K are particularly interesting because they do not require liquid helium for cooling. Some metals such as cesium become superconducting only if a large pressure is applied to them. The superconducting state has to be considered as a separate state such as the liquid, the solid, or the gaseous states. It has a higher degree of order—the entropy is zero. The superconducting transition is reversible.

7.6.1. Experimental Results[5]

The transition into the superconducting state is generally quite sharp for pure and structurally perfect elements (Fig. 7.10). A temperature range of less than 10^{-5} K has been observed in pure gallium. In alloys the transition may be spread over a range of about 0.1 K.

Superconductivity can also be destroyed by applying a magnetic field to the solid. The critical field strength H_c which accomplishes this depends upon the temperature to which the metal has been cooled. In general, the lower the sample temperature, the higher the critical field H_c (Fig. 7.11). One finds

$$H_c = H_0\left(1 - \frac{T^2}{T_c^2}\right), \tag{7.28}$$

where H_0 is the critical field stregnth at 0 K. In a *soft superconductor*, the superconducting state can be eliminated by a small magnetic field.

Superconductors are utilized to produce magnets which have high magnetic

[5] This section requires some knowledge on magnetism, see Part IV.

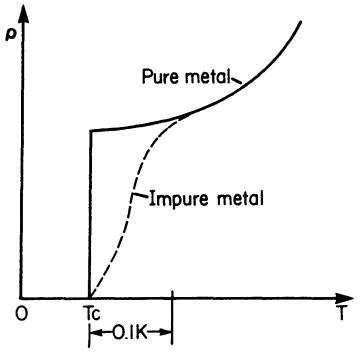

Figure 7.10. Schematic representation of the resistivity of pure and impure superconducting elements. T_c is the transition or critical temperature.

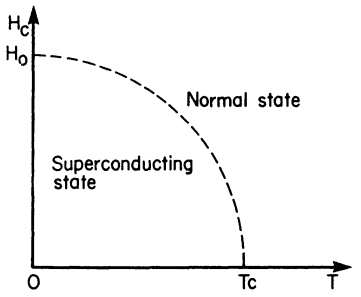

Figure 7.11. Dependence of critical field strength H_c at which superconductivity is destroyed, in relation to the temperature of the specimen.

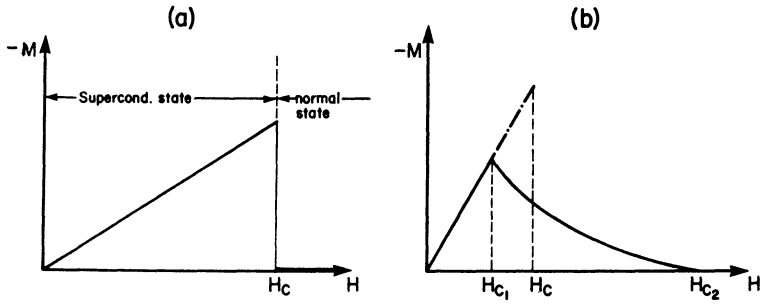

Figure 7.12. Magnetization curves for superconductors. (a) Type I (or soft) superconductors. These solids behave like normal conductors above H_c. (b) Type II (or hard) superconductors. The region between H_{c1} and H_{c2} is called the vortex state. Above H_{c2}, the solid behaves like a normal conductor.

field strengths and no loss in power due to heat dissipation. One limiting factor for ultrahigh field strengths, however, is that the magnetic field thus produced can reach H_c, so that the superconducting state is eventually destroyed by its own magnetic field.

In *type* I *superconductors* the destruction of the superconducting state by a magnetic field, that is, the transition between the superconducting and the normal state, occurs sharply (Fig. 7.12(a)). The critical field strength H_c is relatively low. Thus, type I superconductors are generally not used for coils for superconducting magnets. In *type* II *superconductors* the destruction of the superconducting state by a magnetic field is gradual. The superconducting properties are extended to a field H_{c2} which might be 100 times higher than H_c (Fig. 7.12(b)). Because of this stronger resistance against the magnetically induced destruction of the superconducting state, type II superconductors are mainly utilized for superconducting solenoids. Magnetic fields of several hundred kiloGauss have been achieved with these materials. Among the type II superconductors are transistion metals and alloys consisting of Nb, Al, Si, or V.

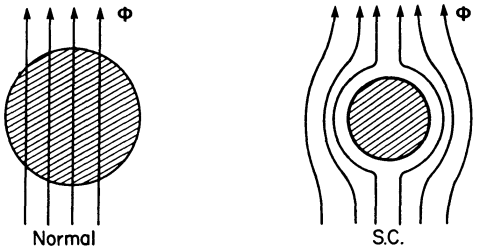

Figure 7.13. Magnetic flux lines in the normal and the superconducting states. The shaded areas represent a cross section of a rod of superconducting material.

The interval between H_{c1} and H_{c2} represents a state in which superconducting and normal conducting areas are mixed in the solid. Specifically, one observes small circular regions, called vortices which are in the normal state. They are surrounded by large, superconducting regions.

It has been observed that superconducting materials expel the magnetic flux lines when in the superconducting state (Fig. 7.13; Meissner effect). We remember from physics that

$$\mathbf{B} = \mathbf{H} + 4\pi\mathbf{M} \tag{7.29}$$

(see also Chapter 14 and particularly (14.11)). **B** is the magnetic induction, **H** is the magnetic field strength and **M** is the magnetization (i.e., the magnetic moment per volume). A superconductor behaves in an external magnetic field as if B would be zero inside the superconductor. Thus,

$$\mathbf{H} = -4\pi\mathbf{M}, \tag{7.30}$$

which means that the magnetization is equal and opposite to the external magnetic field strength. The result is a perfect diamagnet. The susceptibility

$$\chi = \frac{M}{H} \tag{7.31}$$

in superconductors is $-1/4\pi$ compared to -10^{-6} in the normal state. This strong diamagnetism can be used for frictionless bearings, that is, for support of loads by a repelling magnetic field.

The transition temperature T_c varies with the atomic mass m_a according to

$$m_a^{\alpha} \cdot T_c = \text{const}, \tag{7.32}$$

where α is a materials constant (Isotope effect). As an example, T_c for mercury varies from 4.185 K to 4.146 K when m_a changes from 199.5 to 203.4 atomic units.

In short, superconductivity can be destroyed by essentially four mechanisms: 1) high temperatures (above T_c), 2) high magnetic fields (above H_c), 3) high current densities (self-destruction by magnetic field), and 4) ferromagnetic impurities. Potential uses for superconducting materials are: 1) high mag-

netic field solenoids (no power dissipation!), 2) frictionless bearings (strong diamagnet), 3) switching devices called *cryotron* (based on the destruction of the superconducting state in a strong magnetic field), and 4) transmission of power at 100% effeciency.

*7.6.2. Theory

Attempts to explain superconductivity have been made since its discovery in 1911. One of these theories makes use of the two-fluid model which postulates superelectrons, which experience no scattering, have zero entropy (perfect order) and long coherence lengths, i.e., an area 1000 nm wide over which the superelectrons are spread. The London theory, on the other hand, is semi-phenomenological and dwells basically on the electrodynamic properties. The BCS theory (which was developed in 1957 by Bardeen, Cooper, and Schrieffer) is capable of explaining all superconduction properties reasonably well. The theory, however, is quite involved. Phenomenological descriptions of the concepts leading to this theory are probably simplifications of the actual mechanisms which govern superconduction and may thus provide temptations for misleading conclusions. (As so often in quantum mechanics, the mathematics is right—it is only our lack of imagination which holds us back from correctly interpreting the equations.) Nevertheless, a conceptual description of the BCS theory and its results is attempted.

One key to the understanding of the BCS theory is accepting the existence of a pair of electrons (Cooper pair) which has a lower energy than two individual electrons. Imagine an electron in a metal at $T = 0$ K (no lattice vibrations). This electron perturbs the lattice slightly in its neighborhood. When such an electron drifts through a crystal the perturbation is only momentary and, after passing, a displaced ion reverts back into its original position. One can consider this ion to be held by springs in its lattice position so that after the electron has passed by, the ion does not simply return to its original site, but overshoots and eventually oscillates around its rest position. A *phonon* is created.[6] This phonon in turn interacts quickly with a second electron, which takes advantage of the deformation and lowers its energy. Electron 2 finally emits a phonon by itself which interacts with the first electron and so on. It is this passing back and forth of phonons which couples the two electrons together and brings them into a lower energy state (Fig. 7.14). One can visualize that all electrons on the Fermi surface having opposite momentum and opposite spin (that is $k\uparrow$ and $-k\downarrow$) form those Cooper pairs (Fig. 7.15) so that these electrons form a cloud of Cooper pairs which drift cooperatively through the crystal. Thus, the superconducting state is an *ordered* state of the *conduction electrons*. The scattering on the lattice atoms is eliminated, thus

[6] A *phonon* is a lattice vibration quantum. We shall describe the properties of phonons in Chapter 20.

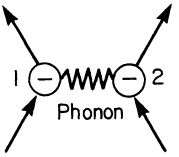

Figure 7.14. Schematic of a Cooper pair.

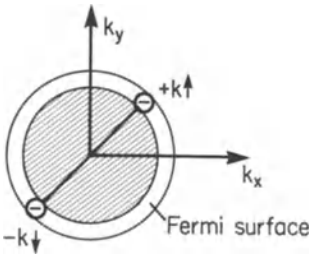

Figure 7.15. Fermi sphere, Fermi surface, and Cooper pair in a metal.

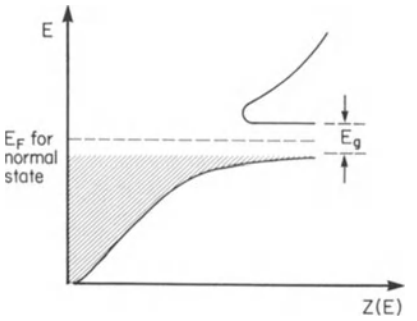

Figure 7.16. Density of states, $Z(E)$, versus electron energy in the superconducting state.

causing a zero resistance, similarly as described in Section 7.5.3 where we observed that ordering of the *atoms* in a crystal lattice reduces the resistivity.

One further aspect has to be considered. We just mentioned that the electrons of a Cooper pair have a lower energy than two unpaired electrons. Thus, the Fermi energy in the superconducting state may be considered to be lower than that for the nonsuperconducting state. This lower state is separated from the normal state by an energy gap E_g (Fig. 7.16). The energy gap stabilizes the Cooper pairs against small changes of net momentum, i.e., prevents them from breaking apart. Such an energy gap of about 10^{-4} eV has been indeed observed by impinging infrared radiation on a superconductor at temperatures below T_c and observing an onset of absorption of the IR radiation.

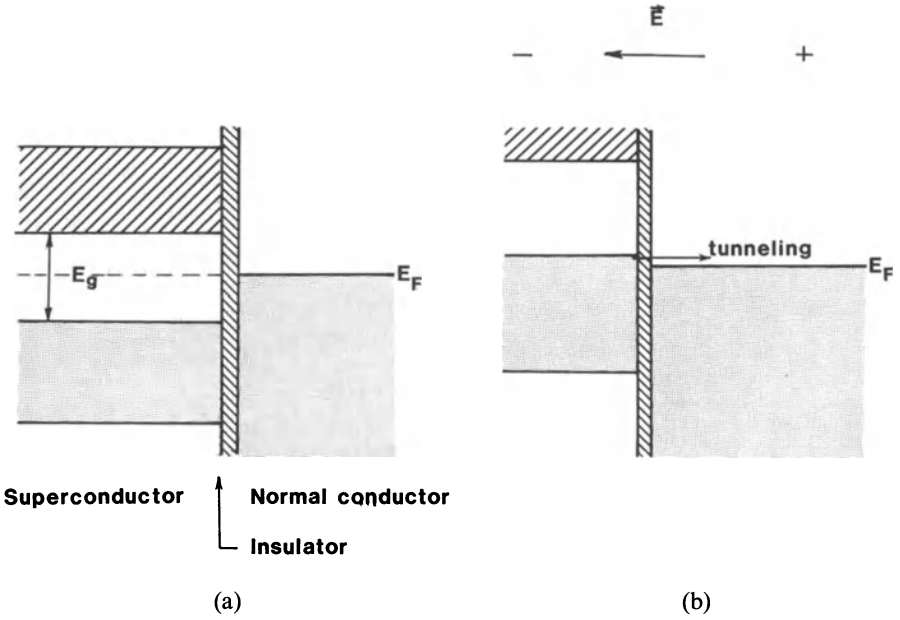

Figure 7.17. Josephson junction (a) in the unbiased state (b) with applied voltage across the junction which facilitates tunnelling in the indicated direction.

An alternate method for measuring this gap energy is by utilizing the Josephson effect. The experiment involves two pieces of metal, one in the superconducting and the other in the normal state. They are separated by a thin insulating film of about 1 nm thickness (Fig. 7.17(a)). A small voltage of proper polarity in the millivolt range applied to this device raises the energy bands in the superconductor. Increasing this voltage eventually leads to a configuration where some filled electron states in the superconductor are opposite to empty states in the normal conductor (Fig. 7.17(b)). Then, the Cooper pairs are capable of tunnelling across the junction as in the description given in Section 4.3. The gap energy is calculated from the threshold voltage eV at which the tunnelling current starts to flow.

It is noted in passing that the insulating film introduces a phase difference in the transmitted wave between both parts of the device. This leads to an alternating current across the junction with a frequency

$$\nu = \frac{2e}{h}\mathrm{V}. \tag{7.33}$$

The "Josephson frequency" is in the microwave range and is, according to (7.33), a function of the applied voltage V. The Josephson effect provides an exact measurement of the ratio $2e/h$ (see (7.33)) and serves as a basis for the international voltage standard.

We just learned that electron–phonon interactions are essential for superconduction. In the normal state of conduction (above T_c), strong interactions between electrons and phonons lead to collisions and thus resistance, whereas at low temperatures they cause Cooper pairs and thus superconduction. This explains why the noble and the alkali metals (which have small electron–phonon interactions) are not superconducting.

Problems

1. Calculate the number of free electrons for gold using its density and its atomic weight.
2. Does the conductivity of an alloy change when long-range ordering takes place? Explain.
3. Calculate the time between two collisions and the mean free path for pure copper at room temperature. Discuss whether or not this result makes sense. *Hint*: Take the velocity to be the Fermi velocity v_F which can be calculated from the Fermi energy of copper $E_F = 7$ eV.
4. Electron waves are "coherently scattered" in ideal crystals at $T = 0$. What does this mean? Explain why in an ideal crystal at $T = 0$ the resistivity is small. State under which conditions the Bragg relation is fulfilled. Insert numbers for λ and d for a typical electron wave in, say, copper. (*Hint*: Calculate the lattice spacing for copper in the (111) direction. Lattice constant $a_{Cu} = 3.61$ Å.) *Note*: Diffraction in an fcc lattice occurs only if the h, k, l's are all even or all odd. Does reinforced coherent scattering occur using electron waves with a wavelength of 6 Å?
5. Calculate the number of free electrons per cubic meter (and per atom) for sodium from resistance data (relaxation time 3.1×10^{-14} sec).
6. Give examples for coherent scattering, incoherent scattering and reinforced coherent scattering.
7. When calculating the population density of electrons for a metal by using (7.26), a value much larger than immediately expected results. Why does the result after all make sense? (Take $\sigma = 5 \times 10^7$ 1/Ωm; $v_F = 10^6$ m/sec and $\tau = 3 \times 10^{-14}$ sec.)
8. Solve the differential equation

$$m\frac{dv}{dt} + \frac{e\mathscr{E}}{v_F}v = e\mathscr{E} \tag{7.10}$$

   and compare your result with (7.11)
9. Calculate the Josephson frequency in (GHz), generated in a normal/superconductor junction for an applied DC voltage of 2mV.

CHAPTER 8

Semiconductors

8.1. Band Structure

We have seen in Chapter 7 that *metals* are characterized by *partially* filled *valence* bands and that the electrons in these bands give rise to electrical conduction. On the other hand, the valence bands of *insulators* are *completely* filled with electrons. Semiconductors finally represent in some respect a position in between metals and insulators. We mentioned in Chapter 6 that semiconductors have, at low temperatures, a completely filled valence band and a narrow gap between this and the next higher, unfilled band. The latter one is called the *conduction band.* We discuss this now in more detail.

Because of band overlapping, the valence as well as the conduction bands of semiconductors consist of mixed (hybrid) s- and p-states. The eight highest $s + p$ states (two s- and six p-states)[7] split into two separate $(s + p)$ bands,[7] each of which consists of one s- and three p-states (see Fig. 8.1). The lower s-state can accommodate one electron per atom, whereas the three lower p-states can accommodate three electrons per atom. The valence band can, therefore, accommodate $4N_a$ electrons. (The same is true for the conduction band.) Because germanium and silicon possess four valence electrons per atom (group IV of the periodic table), the valence band is completely filled with electrons and the conduction band remains empty.

A deeper understanding of this can be gained from Fig. 8.2 which depicts part of a calculated band structure for silicon. Consider at first that electrons are "filled" into these bands like water being poured into a vessel. Then, of course, the lowest s-state will be occupied first. Since no energy gap exists between the top of the s-state and the next higher p-state, additional electrons

[7] See Appendix 3.

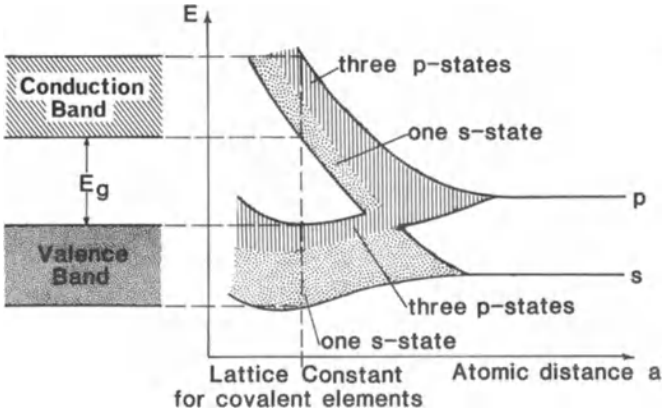

Figure 8.1. Sharp energy levels, widening into bands, and band overlapping with decreasing atomic distance for covalent elements. (Compare with Fig. 4.14.)

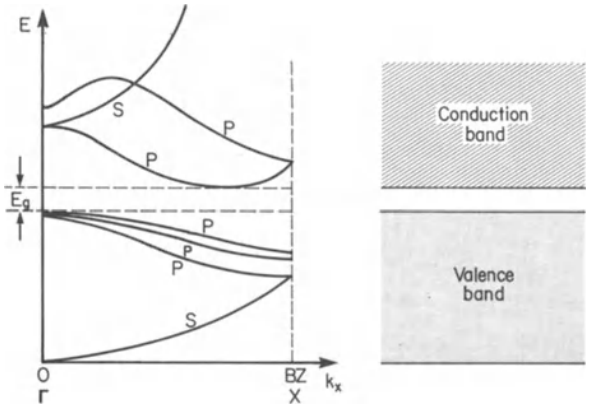

Figure 8.2. Schematic band structure of silicon in the k_x (or X) direction (plotted in the reduced zone scheme). The separation of the two highest p-states in the valence band is strongly exaggerated. Compare with the complete band structure of Fig. 5.23.

will immediately start to occupy the p-states. This process proceeds until all three lower p-states are filled. All of the $4N_a$ electrons of the semiconductor are accommodated now. Note that no higher energy band touches the p-states of the valence band. Thus, an energy gap exists between the filled valence and the empty conduction band. (As was shown in Fig. 5.23 the bands in different directions in k-space usually have a different shape so that a complete assessment can only be made by inspecting the entire band structure.)

All materials which have bonds characterized by electron sharing (covalent bonds) have in common the above-mentioned hybrid bands (Fig. 8.1). An important difference is the magnitude of the gap energy E_g between the conduction band and the valence band. As can be seen from Table 8.1, the gap

Table 8.1. Gap Energies for Some Covalent Elements at 0 K (See also Appendix 4)

Element	E_g[eV]
C (diamond)	5.48
Si	1.1
Ge	0.7
Sn (gray)	0.08

energies for group four elements decrease with increasing atomic number. Diamond, for example, has a gap energy of 5.48 eV and is, therefore, an insulator (at least at room temperature) whereas the E_g for silicon and germanium is around 1 eV. Gray tin, finally, has an energy gap of only 0.08 eV.

8.2. Intrinsic Semiconductors

Semiconductors become conducting at elevated temperatures. In an intrinsic semiconductor, the conduction mechanism is predominated by the properties of the *pure* crystal. In order for a semiconductor to become conducting, electrons have to be excited from the valence band into the conduction band where they can be accelerated by an external electric field. Likewise, the electron holes which are left behind in the valence band contribute to the conduction. They migrate in the opposite direction as the electrons. The energy for the excitation of the electrons from the valence band into the conduction band stems usually from thermal energy. The electrons are transferred from one band into the next by *interband transitions*.

We turn now to a discussion of the *Fermi energy* in semiconductors. We learned in Section 6.2 that the Fermi energy is that energy for which the Fermi distribution function equals 1/2. (It is advisable to keep only this "definition" of the Fermi energy in mind. Any other definition which might give a correct understanding for metals could cause confusion for semiconductors!) The probability that any state in the valence band of an intrinsic semiconductor at $T = 0$ K is occupied by electrons is 100%, i.e., $F(E) = 1$ for $E < E_V$ (Fig. 8.3). At higher temperatures, however, some of the electrons close to the top of the valence band have been excited into the conduction band. As a consequence, the probability function $F(E)$ is slightly reduced at the top of the valence band for $T > 0$ K.

On the other hand, no electrons are found at $T = 0$ K in the conduction band. Thus, the Fermi distribution function for $E > E_0$ must be zero. Again, for higher temperatures a small deviation from $F(E) = 0$ near the bottom of the

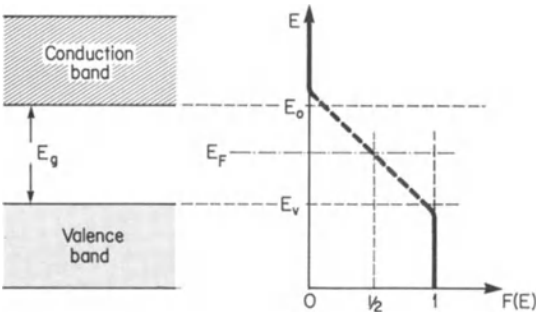

Figure 8.3. Schematic Fermi distribution function and Fermi energy for an intrinsic semiconductor for $T > 0$ K. The "smearing out" of the Fermi distribution function at E_0 and E_V is exaggerated. For reasons of convenience, the zero-point of the energy scale is placed at the bottom of the conduction band.

conduction band is expected (Fig. 8.3). The connection between the two branches of the $F(E)$ curve just discussed is marked with a dashed line in Fig. 8.3. This connecting line does *not* imply that electrons can be found in the forbidden band since $F(E)$ is merely the probability of occupancy of an *available* energy state. (A detailed calculation provides a slightly modified $F(E)$ curve whose vertical branches extend further into the forbidden band.)

Our discussion leads to the conclusion that the Fermi energy, E_F, (i.e., that energy where $F(E) = 1/2$), is located in the center of the forbidden band. In other words, for intrinsic semiconductors we find $E_F = -E_g/2$.

We may argue also somewhat differently: For $T > 0$ K the same amount of current carriers can be found in the valence as well as in the conduction band. Thus, the *average* Fermi energy has to be halfway in between these bands. A simple calculation confirms this statement. (Problem 3 in this chapter should be worked out at this point to deepen the understanding.) We implied in our consideration that the effective masses of electrons and holes are alike (which is not the case; see Appendix 4).

Of special interest to us is the number of electrons in the conduction band. From the discussion carried out above, we immediately suspect that a large number of electrons can be found in the conduction band if E_g is small and, in addition, if the temperature is high. In other words, we suspect that the number of electrons in the conduction band is a function of E_g and T. A detailed calculation, which we will carry out now, verifies this suspicion.

In Section 6.4 we defined N^* to be the number of electrons which have an energy equal to or smaller than a given energy E_n. For an energy interval between E and $E + dE$, we obtained (6.9):

$$dN^* = N(E)\,dE, \tag{8.1}$$

where

$$N(E) = 2 \cdot Z(E) \cdot F(E) \tag{8.2}$$

was called the population density (6.7) and

$$Z(E) = \frac{V}{4\pi^2}\left(\frac{2m}{\hbar^2}\right)^{3/2} E^{1/2} \tag{8.3}$$

is the density of states (6.5). In our particular case the Fermi distribution function $F(E)$ can be approximated by

$$F(E) = \frac{1}{\exp\left(\dfrac{E - E_F}{k_B T}\right) + 1} \simeq \exp\left[-\left(\frac{E - E_F}{k_B T}\right)\right] \tag{8.4}$$

because $E - E_F$ is about 0.5 eV and $k_B T$ at room temperature is in the order of 10^{-2} eV. Therefore, the exponential factor is large compared to 1 (Boltzmann tail). We integrate over all available electrons which have energies larger than the energy at the bottom of the conduction band ($E = 0$), and obtain, with (8.1), (8.3), and (8.4)[8]

$$N^* = \frac{V}{2\pi^2} \cdot \left(\frac{2m}{\hbar^2}\right)^{3/2} \int_0^\infty E^{1/2} \cdot \exp\left[-\left(\frac{E - E_F}{k_B T}\right)\right] dE \tag{8.5}$$

or

$$N^* = \frac{V}{2\pi^2} \cdot \left(\frac{2m}{\hbar^2}\right)^{3/2} \exp\left(\frac{E_F}{k_B T}\right) \int_0^\infty \cdot E^{1/2} \cdot \exp\left[-\left(\frac{E}{k_B T}\right)\right] dE. \tag{8.6}$$

Integration[9] yields

$$\begin{aligned} N^* &= \frac{V}{2\pi^2}\left(\frac{2m}{\hbar^2}\right)^{3/2} \exp\left(\frac{E_F}{k_B T}\right) \frac{k_B T}{2} (\pi k_B T)^{1/2} \\ &= \frac{V}{4}\left(\frac{2mk_B T}{\pi\hbar^2}\right)^{3/2} \exp\left(\frac{E_F}{k_B T}\right). \end{aligned} \tag{8.7}$$

Introducing $E_F = -E_g/2$ (see above) and the effective mass m^* (Section 6.7), we obtain for the number of conduction-band electrons per unit volume $N_e = N^*/V$

$$N_e = \frac{1}{4}\left(\frac{2mk_B}{\pi\hbar^2}\right)^{3/2} \left(\frac{m^*}{m_0}\right)^{3/2} T^{3/2} \exp -\left(\frac{E_g}{2k_B T}\right). \tag{8.8}$$

The constant factor in front of $T^{3/2}$ has the value 4.82×10^{21} ($m^{-3}K^{-3/2}$) so that we can write for (8.8)

$$\boxed{N_e = 4.82 \times 10^{21} \left(\frac{m^*}{m_0}\right)^{3/2} T^{3/2} \exp -\left(\frac{E_g}{2k_B T}\right).} \tag{8.9}$$

---

[8] The integration should actually be done over the states in the conduction band only. However, since the probability factor (F_E) is rapidly approaching zero for energies $E > E_F$, the substitution of infinity for the upper limit does not change the result appreciably. This substitution brings the integral into a standard form.

[9] $\int_0^\infty X^{1/2} e^{-nx}\, dx = 1/2n\sqrt{\pi/n}$.

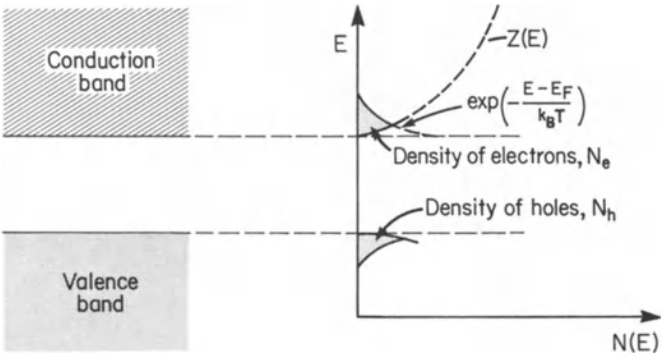

Figure 8.4. Density of electrons (N_e) and holes (N_h) for an intrinsic semiconductor.

We see from (8.9) that the number of electrons in the conduction band is a function of the energy gap and the temperature, as expected. We further notice that the contribution of a temperature increase to N_e is mostly due to the exponential term and only to a lesser extent due to the term $T^{3/2}$. A numerical evaluation of (8.9) tells us that the number of electrons per cubic meter in silicon at room temperature is about 10^{15} (see Problem 4 in this chapter). This means that, at room temperature, only one in every 10^{13} atoms contributes an electron to the conduction. We shall see in the next section that in impurity semiconductors many more electrons can be found in the conduction band.

The electron and hole density is shown in Fig. 8.4 for an intrinsic semiconductor. The number of electrons is given by the area enclosed by the $Z(E)$ curve and $F(E) = \exp[-(E - E_F/k_B T)]$ (8.5).

As implied before, the number of electrons in the conduction band must equal the number of holes in the valence band. This means that an identical equation as (8.8) can be written for the holes if we assume $m_e^* \equiv m_h^*$, which is not strictly true.[10] (An additional term, which is usually neglected, modifies E_F slightly.)

The conductivity[10] of an intrinsic semiconductor is not determined by the number of electrons and holes alone. The mobility[10] (μ) of the current carriers,

$$\mu = \frac{v}{\mathscr{E}}, \tag{8.10}$$

i.e., their velocity per unit electric field, also contributes its share to the conductivity σ. An expression for the conductivity is found by combining (7.2),

$$j = \sigma \mathscr{E}, \tag{8.11}$$

and (7.4),

[10] For numerical values, see the tables in Appendix 4.

$$j = Nve, \tag{8.12}$$

with (8.10), which yields:

$$\sigma = N\frac{v}{\mathscr{E}}e = N\mu e. \tag{8.13}$$

Taking both electrons and holes into consideration we can write

$$\begin{aligned}\sigma &= N_e e\mu_e + N_h e\mu_h \\ &= 4.82 \times 10^{21}\left(\frac{m^*}{m_0}\right)^{3/2} T^{3/2} e(\mu_e + \mu_h)\exp -\left(\frac{E_g}{2k_B T}\right)\end{aligned} \tag{8.14}$$

where the subscripts e and h stand for electrons and holes, respectively. With increasing temperatures, the mobility of the current carriers is reduced by lattice vibrations (Fig. 8.5(a)). On the other hand, around room temperature, an increasing amount of electrons is excited from the valence band into the conduction band, thus increasing the number of current carriers, N_e and N_h (Fig. 8.5(b)). The conductivity is, according to (8.14), a function of these two factors (Fig. 8.5(c)).

At low temperatures the electrons are incoherently scattered by impurity atoms and lattice defects. It is therefore imperative that semiconductor materials are of extreme purity, which can be achieved by zone refining.

8.3. Extrinsic Semiconductors

8.3.1. Donors and Acceptors

We learned in the previous section that in intrinsic semiconductors, only a very small number of electrons (about 10^{15} electrons per m^3) contribute to the conduction of the electric current. In most semiconductor devices, a considerably higher number of charge carriers are, however, present. They are introduced by *doping*, i.e., by adding small amounts of impurities to the semiconductor material. In most cases, elements of group III or V of the periodic table are used as dopants. They replace some regular lattice atoms in a substitutional manner. Let us start our discussion by considering the case where a small amount of phosphorus (for example 0.0001%) is added to silicon. Phosphorus has five valence electrons, i.e., one valence electron more than silicon. Four of these valence electrons form regular electron-pair bonds with their neighboring silicon atoms (Fig. 8.6). The fifth electron, however, is only loosely bound to silicon, that is, the binding energy is about 0.045 eV (see Appendix 4 and Problem 10.) At slightly elevated temperatures this extra electron becomes disassociated from its atom and drifts through the crystal as a conduction electron when a voltage is applied to the crystal. Extra electrons

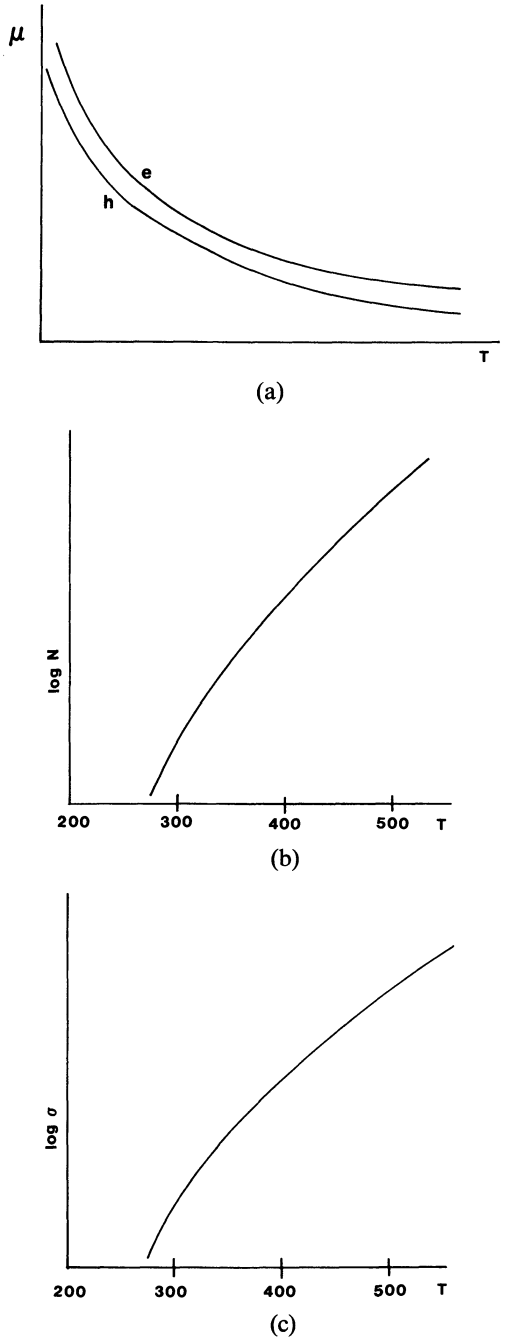

Figure 8.5. Schematic representation of the temperature dependence of (a) electron and hole mobilities, (b) number of carriers in an intrinsic semiconductor, and (c) conductivity for an intrinsic semiconductor. (T is given in K.)

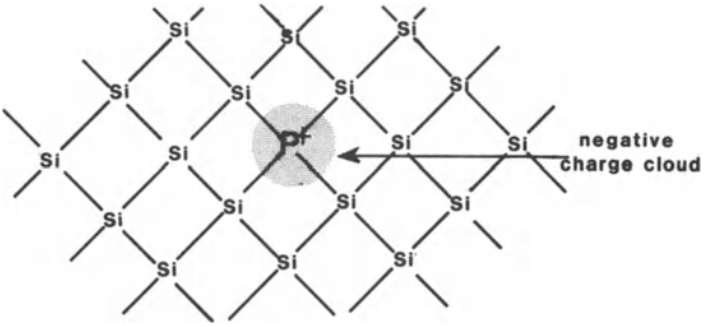

Figure 8.6. Two-dimensional representation of the silicon lattice. An impurity atom of group V of the periodic table (*P*) is shown to replace a silicon atom. The charge cloud around the phosphorus atom stems from the extra phosphorus electron. Each electron pair between two Si atoms constitutes a covalent bond (electron sharing). The two electrons of such a pair are indistinguishable, but must have opposite spin to satisfy the Pauli principle.

of this type are called "donor electrons." They populate the conduction band of a semiconductor, thus providing a contribution to the conduction process.

It has to be noted that at sufficiently high temperatures, in addition to these donor electrons, some electrons from the valence band are also excited into the conduction band in an intrinsic manner. The conduction band contains, therefore, electrons from two sources, the amount of which depends on the device temperature (see Section 8.3.3). Since the conduction mechanism in semiconductors with donor impurities (P, As, Sb) is predominated by negative charge carriers (electrons) these materials are called *n*-type semiconductors. The electrons are the *majority carriers*.

A similar consideration may be done with impurities which stem from the third group of the periodic chart (B, Al, Ga, In). They possess one electron less than silicon and, therefore, introduce a *positive* charge cloud into the crystal around the impurity atom. The conduction mechanism in these semiconductors with *acceptor* impurities is predominated by positive carriers (holes) which are introduced into the valence band. They are, therefore, called *p*-type semiconductors.

8.3.2. Band Structure

The band structure of impurity or *extrinsic* semiconductors is essentially the same as for intrinsic semiconductors. It is desirable. however, to represent in some way the presence of the impurity atoms by *impurity states*. It is common to introduce into the forbidden band so-called donor or acceptor levels (Fig. 8.7). The distance between the donor level and the conduction band represents the energy which is needed to transfer the extra electrons into the conduction

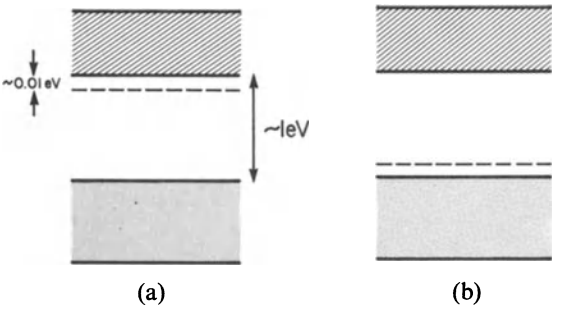

Figure 8.7. (a) Donor and (b) acceptor levels in extrinsic semiconductors.

band. (The same is true for acceptor level and valence band.) It has to be emphasized, however, that the introduction of these impurity levels does not mean that electrons or holes are found in the forbidden band of, say, silicon. The impurity states are only used as a convenient means to remind the reader of the presence of extra electrons or holes in the crystal.

8.3.3. Temperature Dependence of the Number of Carriers

At 0 K the excess electrons of the donor impurities remain in close proximity to the impurity atom and do not contribute to the electric conduction. We express this fact by stating that all donor levels are filled. With increasing temperature, the donor electrons overcome the small potential barrier (Fig. 8.7(a)) and are excited into the conduction band. Thus, the donor levels are increasingly emptied and the number of negative charge carriers in the conduction band increases exponentially, obeying an equation similar to (8.9). Once all electrons are excited from the donor levels into the conduction band, any further temperature increase does not create additional electrons and the N_e versus T curve levels off (Fig. 8.8). As mentioned before, at still higher temperatures intrinsic effects create additional electrons which, depending on the amount of doping, can outnumber the electrons supplied by the impurity atoms.

Similarly, the acceptor levels do not contain any electrons at 0 K. At increasing temperatures, electrons are excited from the valence band into the acceptor levels, leaving behind positive charge carriers. Once all acceptor levels are filled, the number of holes in the valence band is not increased further until intrinsic effects set in.

8.3.4. Conductivity

The conductivity of extrinsic semiconductors can be calculated similarly as in the previous section (8.13) by multiplying the number of carriers with the mobility μ and the electron charge e. Around room temperature, however,

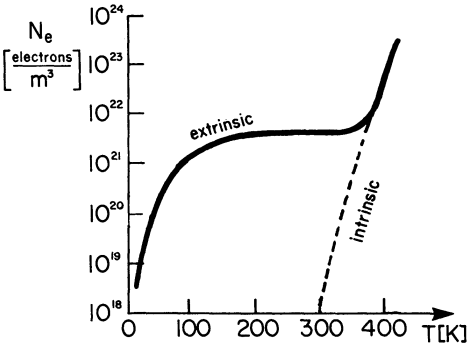

Figure 8.8. Schematic representation of the number of electrons per m^3 in the conduction band versus temperature for an extrinsic semiconductor with low doping.

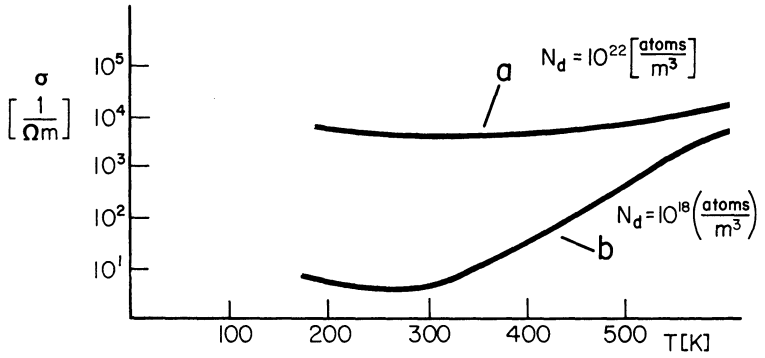

Figure 8.9. Conductivity of two extrinsic semiconductors, (a) high doping and (b) low doping. N_d = number of donor atoms per m^3.

only the majority carriers need to be considered. For electron conduction, for example, one obtains

$$\sigma = N_{de} e \mu_e, \tag{8.15}$$

where N_{de} is the number of donor electrons and μ_e is the mobility of the donor electrons in the conduction band. As mentioned above, it is reasonable to assume that at room temperature, essentially all donor electrons have been excited from the donor levels into the conduction band (Fig. 8.8). Thus, for pure n-type semiconductors, N_{de} is essentially identical with the number of impurities (that is donor) atoms N_d. At substantially lower temperatures, that is at around 100 K, the number of conduction electrons needs to be calculated using an equation similar to (8.8).

Figure 8.9 shows the temperature dependence of the conductivity. We notice that the magnitude of the conductivity, as well as the temperature dependence of σ, is markedly different for various doping levels. For high doping rates, for example, the conductivity decreases with increasing temperature (Fig. 8.9(a)). This is similar to the case of metals where the lattice vibrations present an

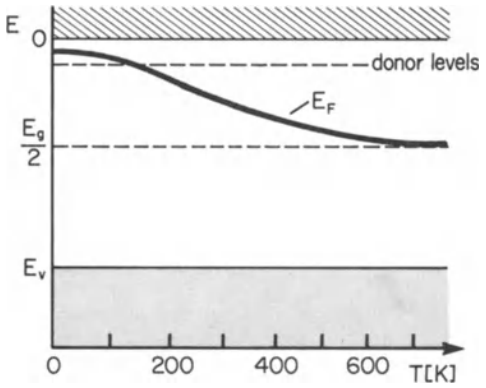

Figure 8.10. Fermi level of an *n*-type semiconductor as a function of temperature. $N_d \approx 10^{22}$ (atoms/m^3).

obstacle to the drifting electrons (or, expressed differently, where the mobility of the carriers is decreased by incoherent scattering of the electrons).

For low doping and low temperatures, we observe a similar temperature dependence of the conductivity as above. However, at room temperature intrinsic effects set in, which increase the number of carriers and therefore enhance the conductivity. As a consequence, two competing effects determine the conductivity above room temperature: an increase of σ due to an increase of the number of electrons, and a decrease of σ due to a decrease of the mobility. (It should be mentioned that the mobility of electrons or holes also decreases slightly when impurity atoms are added to a semiconductor.)

8.3.5. Fermi Energy

In an *n*-type semiconductor, more electrons can be found in the conduction band than holes in the valence band. This is particularly true at low temperatures. The Fermi energy must therefore be between the donor level and the conduction band (Fig. 8.10). With increasing temperatures, an extrinsic semiconductor becomes progressively intrinsic and the Fermi energy approaches the value for an intrinsic semiconductor, i.e., $-(E_g/2)$. [Similarly, the Fermi energy for a *p*-type semiconductor rises with increasing temperature from below the acceptor level to $-(E_g/2)$.]

*8.4. Effective Mass

Some semiconductor properties can be better understood and calculated by evaluating the effective mass of their charge carriers. We mentioned in Section 6.7 that m^* is inversely proportional to the curvature of an electron band. We now make use of this finding.

Let us inspect at first the upper portion of the valence bands for silicon near Γ (Fig. 8.2). We notice that the curvatures of these bands are convex downwards. It is known from Fig. 6.8 that in this case the charge carriers have a negative effective mass, that is, these bands can be considered to be populated by electron holes. Further, we observe that the curvatures of the individual bands are slightly different. Thus, the effective masses of the holes in these bands must likewise be different. One distinguishes appropriately between *light holes* and *heavy holes*. Since two of the bands, namely those having the stronger curvature, are almost identical, we conclude, that two out of the three types of holes are light holes.

We turn now to the *conduction* band of silicon and focus our attention to the lowest band (Fig. 8.2). We notice a minimum (or valley) at about 85% between Γ and X points. Since the curvature at that location is convex upwards, we expect this band to be populated by electrons. (The energy surface near the minimum is actually a spheroid. This leads to *longitudinal* and *transverse* masses m_l^* and m_t^*.) Values for the effective masses are given in Appendix 4. Occasionally, *average effective masses* are listed in the literature. They may be utilized for estimates.

8.5. Hall Effect

The number and type of charge carriers (electrons or holes) which were calculated in the preceeding sections can be elegantly measured by making use of the Hall effect. Actually, it is quite possible to measure concentrations of less than 10^{-18} electrons per m^3 in doped silicon, that is, one can measure one donor electron (and therefore one donor atom) per 10^{10} silicon atoms. This sensitivity is several orders of magnitude better than in any chemical analysis.

We assume for our discussion an n-type semiconductor in which the conduction is predominated by electrons. Suppose an electric current j flows in the positive x-direction and a magnetic field (of magnetic induction B) is applied normal to this electric field in the z-direction (Fig. 8.11). Each electron is then subjected to a force, called the Lorentz force, which causes the electron paths to bend, as shown in Fig. 8.11. As a consequence, the electrons accumulate on one side of the slab (in Fig. 8.11 on the right side) and are deficient on the other side. Thus, an electric field is created in the (negative) y-direction which is called the Hall field. In equilibrium the Hall force

$$F_H = -e\mathscr{E}_y \tag{8.16}$$

balances the above mentioned Lorentz force

$$F_L = vB_z e, \tag{8.17}$$

where v is the velocity of the electrons, and e the electron charge. Combining (8.16) and (8.17) yields for the Hall field

$$\mathscr{E}_y = -v_x B_z \tag{8.18}$$

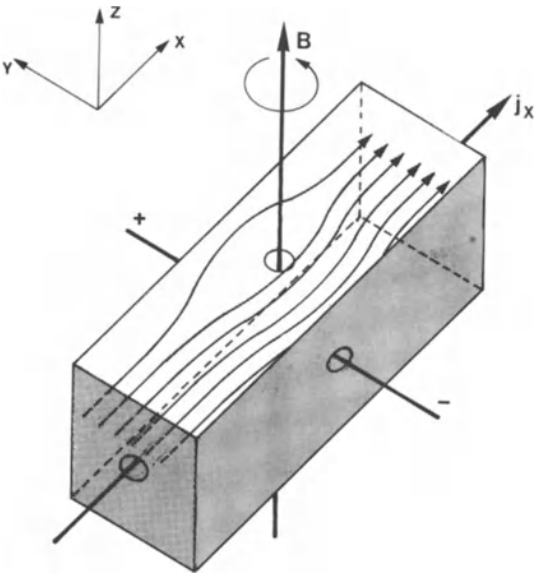

Figure 8.11. Schematic representation of the Hall effect in an *n*-type semiconductor (or a metal).

which becomes with (7.4)

$$j = Nve \tag{8.19}$$

$$\mathscr{E}_y = -\frac{1}{Ne} j_x B_z. \tag{8.20}$$

We define

$$R_H = \frac{1}{Ne} = \frac{\mathscr{E}_y}{j_x B_z} \tag{8.21}$$

as the Hall constant which is inversely proportional to the number of conduction electrons N. The Hall constant can be obtained by measuring the parameters on the right of (8.21). The sign of the Hall constant indicates whether electrons or holes predominate in the conduction process.

8.6. Compound Semiconductors

Gallium arsenide (and other III–V or II–VI semiconductor compounds) are of great technical interest, partially because of their large band gap which essentially prevents intrinsic contributions in impurity semiconductors, partially because of their larger electron mobility which aids in high speed

applications. (Numerical values are given in Appendix 4). The large electron mobility in GaAs is caused by a small value for the electron effective mass which in turn results from a comparatively large convex upward curvature of the conduction electron band near Γ. (See in this context the band structure of GaAs in Fig. 5.24.) The electrons which have been excited into the conduction band (mostly from donor levels) are most likely populating this high curvature region near Γ.

The atomic bonding in III–V and II–VI semiconductors resembles that of the group IV elements with the additional feature that the bonding is partially ionic because of the different valences of the participating elements. The ionization energies[11] of donor and acceptor impurities in GaAs are as a rule one order of magnitude smaller than in Ge or Si which ensures complete ionization even at relatively low temperatures.

8.7. Semiconductor Devices

8.7.1 Metal–Semiconductor Contacts

If a semiconductor is coated on one side with a metal, a *rectifying* contact or an *ohmic* contact is formed, depending on the type of metal used. Both cases are equally important. Rectifiers are widely utilized in electronic devices. However, the type discussed here has been mostly replaced by *p–n* rectifiers. On the other hand, all semiconductor devices need contacts in which the electrons can easily flow in both directions. They are called ohmic contacts.

At the beginning of our discussion let us assume that the surface of an *n*-type semiconductor has been somehow negatively charged. The negative charge repels the free electrons that had been near the surface and leaves positively charged donor ions behind (for example, As^+). Any electron which drifts toward the surface (negative *x*-direction in Fig. 8.12(a)) "feels" this repelling force. As a consequence, the region near the surface has less free electrons than the interior of the solid. This region is called the *depletion layer* (or sometimes *space charge region*).

In order to illustrate the repelling force of an external negative charge it is customary to curve the electron bands near the surface upwards. The depletion can then be understood by stating that the electrons assume the lowest possible energy state (or colloquially expressed: "The electrons like to roll downhill").

Similarly, if a *p*-type semiconductor is positively charged at the surface, the positive carriers (holes) are repelled towards the inner part of the crystal and the band edges are bent downwards (Fig. 8.12(b)). This represents a potential barrier for holes (because holes "want to roll upwards").

[11] See the tables in Appendix 4.

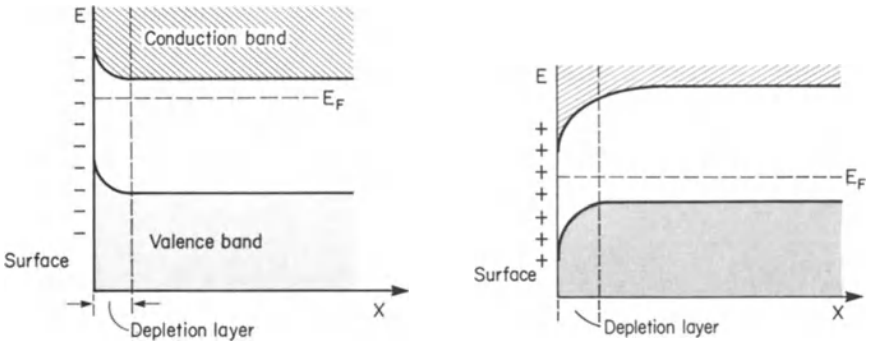

Figure 8.12. (a) Band diagram for an *n*-type semiconductor whose surface has been negatively charged. (b) Band diagram for a *p*-type semiconductor, the surface of which is positively charged. X is the distance from the surface.

8.7.2. Rectifying Contacts (Schottky Barrier Contacts)

It is convenient for our discussion to introduce the work function ϕ which is the energy difference between the Fermi energy and the ionization energy. (Values for ϕ are given in Appendix 4.)

Let us consider a metal and an *n*-type semiconductor before they are brought into contact. In Fig. 8.13(a) the Fermi energy of a metal is shown to be lower than the Fermi energy of the semiconductor, i.e., $\phi_M > \phi_S$. Immediately after the metal and semiconductor have been brought into contact, electrons start to flow from the semiconductor "down" into the metal until the Fermi energies of both solids are equal (Fig. 8.13(b)). As a consequence the

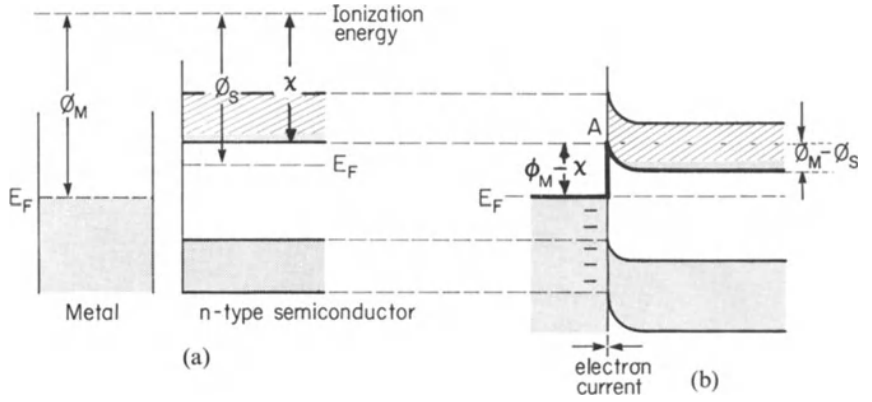

Figure 8.13. Energy bands for a metal and an *n*-type semiconductor (a) before and (b) after contact. $\phi_M > \phi_S$. The potential barrier is marked with heavy lines.

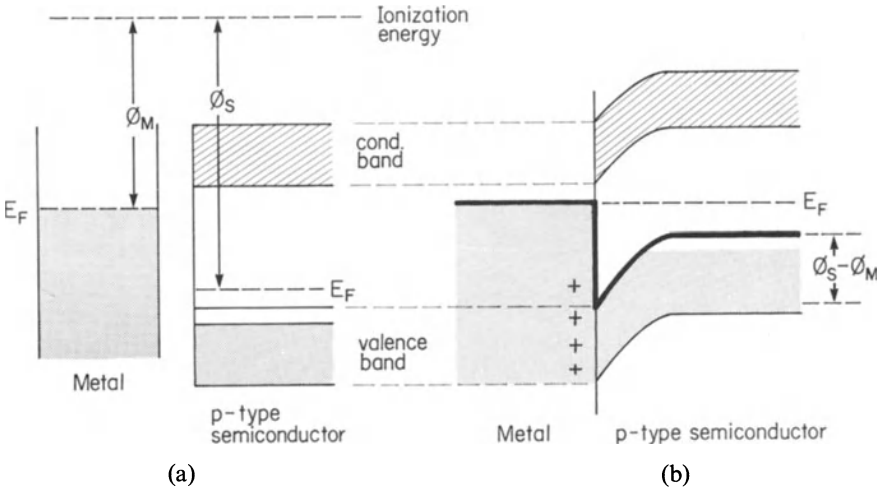

Figure 8.14. Energy bands for a metal and a *p*-type semiconductor (a) before and (b) after contact. $\phi_M < \phi_S$.

metal will be charged negatively and a potential barrier is formed just as shown in Fig. 8.12. This means that the energy bands in the bulk semiconductor are lowered by the amount $\phi_M - \phi_S$ with respect to a point A.

In the equilibrium state electrons from both sides cross the potential barrier. This electron flow constitutes the so called *diffusion current*. The number of electrons diffusing in both directions must be identical for the following reason: the metal contains more free electrons, but these electrons have to climb a higher potential barrier than the electrons in the semiconductor whose conduction band contains less free electrons.

Similarly, if a *p*-type semiconductor is brought into contact with a metal and $\phi_M < \phi_S$, electrons diffuse from the metal into the semiconductor and charge the metal and therefore the surface of the semiconductor positively. Consequently, a "downward" potential barrier (for the holes) is formed (Fig. 8.14).

In addition to the diffusion current just mentioned, a "drift current" needs to be taken into consideration. Let us assume that an electron–hole pair was thermally created in or near the depletion layer of a *p*-type semiconductor (Fig. 8.14(b)). Then the thermally created electron in the conduction band is immediately swept down the barrier, and the hole in the valence band is swept up the barrier. This drift current is usually very small and is relatively insensitive to the height of the potential barrier. The total current across a junction is the sum of drift and diffusion components.

The potential barrier height for an electron diffusing from the semiconductor into the metal is $\phi_M - \phi_S$ (see Fig. 8.13(b)). This potential difference is called the *contact potential*. The height of the potential barrier from the metal

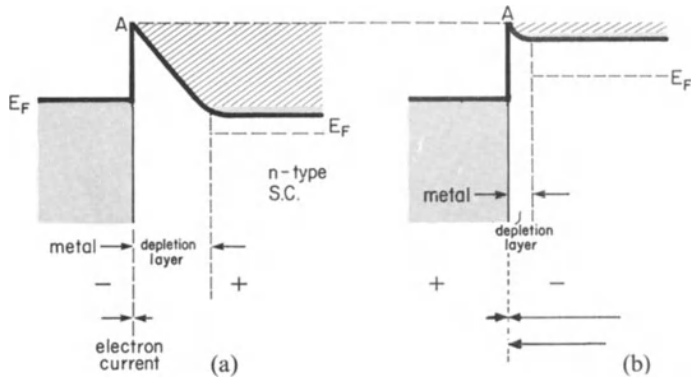

Figure 8.15. Metal–semiconductor contact with two polarities: (a) reverse bias and (b) forward bias. The amount of current in both directions and the net current is indicated by the length of the arrows. The potential barriers are marked with heavy lines.

side is $\phi_M - \chi$, where χ is the *electron affinity* measured from the bottom of the conduction band to the vacuum level (Fig. 8.13(b)).

We shall now estimate the net current which flows across the potential barrier when a metal and an *n*-type semiconductor are connected to a d.c. source (*biasing*). At first the metal is assumed to be connected with the negative terminal of a battery. As a result, the metal is charged even more negatively than without bias. Thus, the electrons in the semiconductor are even more repelled, and the potential barrier is increased (Fig. 8.15(a)). Further, the depletion layer has become wider. Because both barriers are now relatively high, the diffusion currents in both directions are negligible. However, the small and essentially voltage-independent drift current still exists which results in a very small net electron current from the metal into the semiconductor (*reverse bias*, Fig. 8.15(a)).

If the polarity of the battery is reversed, the potential barrier in the semiconductor is reduced, i.e., the electrons are "driven" across the barrier so that a large net current from the semiconductor into the metal results (*forward bias*). The depletion layer is narrow (Fig. 8.15(b)). The voltage–current characteristic of a rectifier is shown in Fig. 8.16. Rectifiers of this type are used to convert alternating current into direct current.

The current which flows from the metal into the semiconductor is

$$I_{MS} = AC'T^2 \exp\left[-\left(\frac{\phi_M - \chi}{k_B T}\right)\right], \tag{8.22}$$

where A is the area of the contact and C' is a constant. The current flowing from the semiconductor into the metal is

$$I_{SM} = AC''T^2 \exp\left[-\left(\frac{\phi_M - \phi_S - eV}{k_B T}\right)\right], \tag{8.23}$$

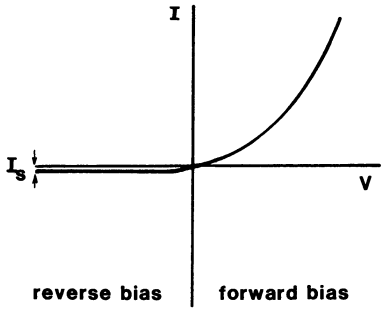

Figure 8.16. Characteristic of a rectifier. The reverse current is grossly exaggerated!

where V is the bias voltage (which has the sign of the polarity of the metal) and e is the electronic charge. The net current $I_{net} = I_{SM} - I_{MS}$ consists of two parts, namely, the saturation current (occasionally called the generation current)

$$I_S = ACT^2 \exp\left[-\left(\frac{\phi_M - \chi}{k_B T}\right)\right] \tag{8.24}$$

and a voltage dependent term. The net current is then obtained by combining (8.22), (8.23), and (8.24):

$$I_{net} = I_S\left[\exp\left(\frac{eV}{k_B T}\right) - 1\right]. \tag{8.25}$$

We see from (8.25) that for forward bias (positive V) the net current increases exponentially with voltage. On the other hand, for reverse bias (negative V) the current is essentially constant and equal to $-I_S$. Figure 8.16 reflects this behavior.

8.7.3. Ohmic Contacts (Metallizations)

In Fig. 8.17 band diagrams are shown for the case where a metal is brought into contact with an n-type semiconductor. It is assumed that $\phi_M < \phi_S$. Thus, electrons flow from the metal into the semiconductor, charging the metal positively. The bands of the semiconductor bend "downwards" and no barrier exists for the flow of electrons in either direction. A similar situation exists for a p-type semiconductor and $\phi_M > \phi_S$.

Aluminum is frequently used for making the contact between a device (for example the p-region of a rectifier) and the external leads. Aluminum bonds readily to Si or SiO_2 if the device is briefly heated at about 550° C after Al-deposition. Since aluminum has a larger work function than silicon (see

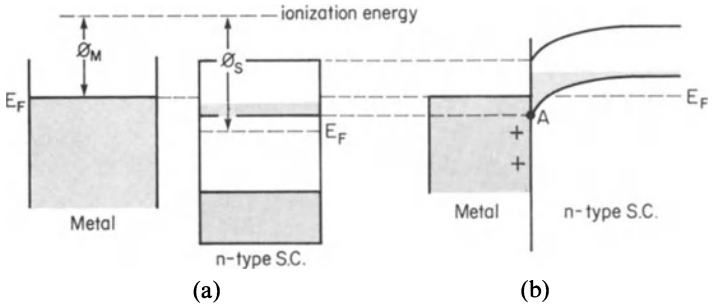

Figure 8.17. Ohmic contact between metal and *n*-type semiconductor ($\phi_M < \phi_S$).

Appendix 4) the contact to a *p*-region is ohmic. Indeed the diffusion of Al into Si yields a shallow and highly conductive p^+-region.[12]

Now, aluminum is likewise used as a contact material for *n*-type silicon. To prevent a rectifying contact in this case, one usually lays down a heavily doped and shallow n^+-layer on top of the *n*-region. Since this n^+-layer is highly conductive and is made to be very thin, tunneling through the barrier accomplishes the unhindered electron flow (see Sections 4.3 and 8.7.8).

We note in passing that aluminum metallizations are particularly used to interconnect many individual electronic devices which are manufactured on one *chip* in order to achieve large scale integration. These thin-film metallizations carry a high current density and are, thus, potentially vulnerable for circuit failure by a mechanism called *electrotransport*. Small additions of copper or silicon to aluminum or alternatively, gold metallizations are used to diminish this problem.

8.7.4. *p–n* Rectifier (Diode)

We learned in Section 8.7.2 that when a metal is brought in contact with an extrinsic semiconductor, a potential barrier may be formed which gives rise to the rectifier action. A similar potential barrier is created when a *p*-type and an *n*-type semiconductor are joined.

As before, electrons flow from the higher level (*n*-type) "down" into the *p*-type semiconductor so that the *p* side is negatively charged. This proceeds until equilibrium is reached and both Fermi energies are at the same level. The resulting band diagram is shown in Fig. 8.18.

Consider at first the conduction band only. The electrons which want to diffuse from the *n*- into the *p*-region encounter a potential barrier near the junction. For statistical reasons, only a few of them have enough energy to climb the barrier and diffuse into the *p*-region. The electrons in the *p*-region, on

[12] The plus superscript means *heavily doped region.*

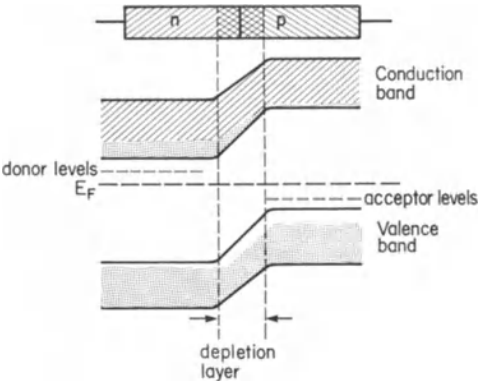

Figure 8.18. Schematic band diagram for a p–n junction (diode) in equilibrium.

the other hand, can easily diffuse "down" the potential barrier into the n-region. Note that only a few electrons exist in the conduction band of the p-region. (They have been thermally excited into this band by intrinsic effects.) In the equilibrium state the number of electrons crossing the junction in both directions is therefore identical. (The same is true for the holes in the valence band.)

When an external potential is applied to this device, effects similar to the ones described in Section 8.7.2 occur: connecting the positive terminal of a d.c. source to the n-side withdraws electrons from the depletion area which becomes wider and the potential barrier grows higher (Fig. 8.19(a)). As a consequence, only a small drift current exists (reverse bias). On the other hand, if the n-side is charged negatively, the barrier decreases in height and the space charge region narrows. A large net electron flow occurs from the n-type to the p-type region (forward bias, Fig. 8.19(b) and (c)).

In Figs. 8.19(a) and (b) "quasi-Fermi levels" for electrons and holes are shown. They are caused by the fact that the electron density varies in the junction from the n side to the p side by many orders of magnitude, while the electron current is almost constant. Consequently, the Fermi level must also be almost constant over the depletion layer.

It has to be emphasized that the current in a p–n rectifier is the sum of both electron and hole current. The net current may be calculated by using an equation similar to (8.25) whereby the saturation current, I_S, in the present case is a function of the equilibrium concentration of the holes in the n-region (C_{hn}), the concentration of electrons in the p-region (C_{ep}), and other device parameters. One finds the *Shockley equation* which is also called the *ideal diode law*:

$$I_S = Ae\left(\frac{C_{ep}D_{ep}}{L_{ep}} + \frac{C_{hn}D_{hn}}{L_{hn}}\right), \tag{8.26}$$

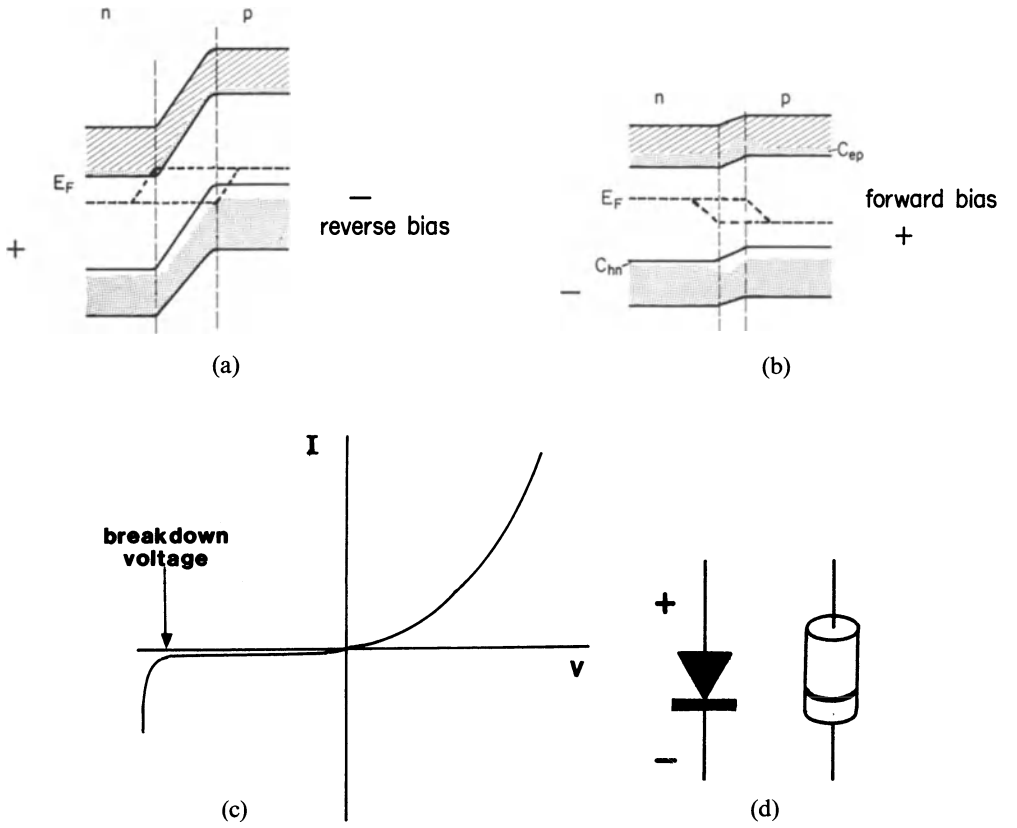

Figure 8.19. (a) Reverse and (b) forward bias of a p–n junction (diode). (c) Voltage–current characteristic of a p–n junction (diode). (d) Symbol of a p–n rectifier in a circuit and designation of polarity in an actual rectifier.

where the D's and L's are diffusion constants and diffusion lengths, respectively. (For example, D_{ep} = diffusion constant for electrons in the p-region, etc.) As before, I_S is the saturation current in the case of reverse bias (see (8.24)). In order to keep the reverse current small, both C_{hn} and C_{ep} (minority carriers) have to be kept at low levels (compared to electrons and holes introduced by doping). This can be accomplished by selecting semiconductors having a large energy gap, such as silicon (Table 8.1), and by high doping.

8.7.5. Zener Diode

When the reverse voltage of a p–n diode is increased above a critical value, the high electric field strength causes the electrons to become accelerated to a velocity at which impact ionization occurs [Fig. 8.20(a)]. The free electrons thus created are likewise accelerated until eventually a *breakdown* occurs and

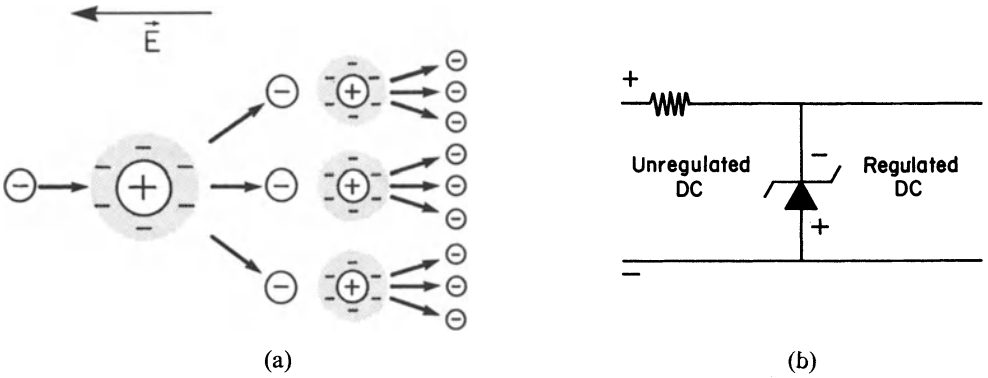

Figure 8.20. (a) Electron avalanche created at breakdown voltage. (b) Zener diode in a circuit for voltage regulation.

the reverse current increases quite rapidly [Fig. 8.19(c)]. This effect is used in a circuit to hold a given voltage constant at a desired level (Fig. 8.20(b)). The Zener diode is generally not destroyed by the breakdown, unless excessive heat generation causes the melting of a device.

8.7.6. Solar Cell (Photo Diode)

A photo diode consists of a p–n junction (Fig. 8.21). If light of sufficiently high energy falls on such a device, electrons are lifted from the valence into the conduction band, leaving holes in the valence band. The electrons in the depleted area immediately "roll down" into the n-region, whereas the holes

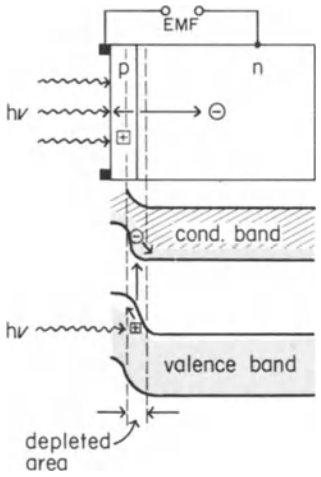

Figure 8.21. Solar cell; the p-region is about 1 μm thick.

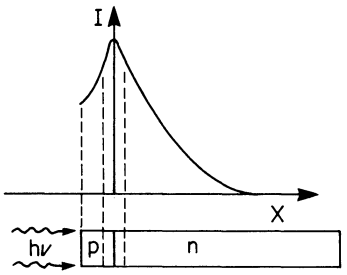

Figure 8.22. Schematic representation of the contribution of electrons and holes to the photo current with respect to the distance x from the p–n junction.

"roll up" into the p-region. These additional carriers can be measured in an external circuit (photographic exposure meter) or used to generate electrical energy. In order to increase the effective area of the junction, the p-type region is made to be extremely thin (1 μm) and the light is radiated through the p-layer (Fig. 8.21).

The electron–hole pairs which are created some distance away from the depleted region are generally not separated by the junction field and eventually recombine; they do not contribute to the electric current. However, some electrons or holes which are within a diffusion length from the depleted region drift into this area and thus contribute to the current. In semiconducting materials which contain only a few defects (such as grain boundaries, dislocations, and impurities) the electrons or holes may diffuse up to 200 μm before they get trapped; whereas in semiconducting materials containing a large number of defects the diffusion length reduces to 10 μm. The closer a carrier was created to the p–n boundary, the larger is its chance to contribute to the current (Fig. 8.22).

The thin p-type layer introduces an internal resistance to the collection current which reduces the efficiency of the energy conversion. At present the efficiency of a photovoltaic device is close to 10%. Intensive research is in progress around the world to improve the efficiency of solar cells and to reduce the cost of this important, pollution-free energy source. The cost may be reduced by using polycrystalline and less zone refined silicon. As discussed above, however, this decreases the photo current. The goal is to produce for terrestrial applications inexpensive solar cells, having 10% efficiency or better and a lifetime of about 20 years. The lifetime is reduced when the metal contacts (grids) to the semiconductor corrode. Silicon-based solar cells have the most uniform junctions. The output of a 2 cm^2 solar cell under *Florida sun* is about 0.5 V at 30 mA.

*8.7.7. Avalanche Photo Diode

This device is a p–n solar cell which is operated in a high reverse bias mode, i.e., at near-breakdown voltage. The electrons or holes which were excited

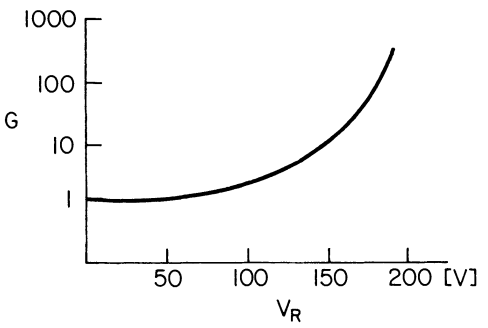

Figure 8.23. Photo current gain G versus reverse voltage V_R for an avalanche photo diode.

from the valence into the conduction band by the incident light are accelerated toward the depleted area with a high velocity. As a consequence, they ionize the lattice atoms and generate secondary hole–electron pairs which in turn are accelerated, generating more hole–electron pairs. The result is a photo current gain, G, which may be between 10 and 1000 (Fig. 8.23). The avalanche photo diode is ideally suited for low light level applications because of its low signal-to-noise ratio, and for very high frequencies (GHz). It is used for detectors in long-distance, fiber-optics telecommunication systems.

*8.7.8. Tunnel Diode

So far, we have restricted our discussion to the case for which the electrons drift from the *n*- to the *p*-type semiconductor be way of "climbing" a potential barrier. Another electron transfer mechanism is, however, possible. If the depleted area is very narrow (approximately 15 nm) and if certain other requirements (see below) are fulfilled, electrons may tunnel *through* the potential barrier. (See in this context Fig. 4.7 and (4.43).) Heavy doping (for example 10^{26} impurity atoms per m^3) yields this condition.

The situation can be best understood by inspecting Fig. 8.24(a) in which a schematic band diagram of a tunnel diode is shown. Because of the high doping level, the Fermi energy extends into the valence band of the *p*-type semiconductor and into the conduction band of the *n*-type semiconductor. In the equilibrium state, the same amount of electrons is tunneling through the potential barrier in both directions, i.e., no net current flows.

If a small *reverse* bias is applied to this device (Fig. 8.24(b)), the potential barrier is increased as usual and the Fermi energy, along with the top and bottom of the bands in the *p*-area, is raised. This creates empty electron spaces in the conduction band of the *n*-type semiconductor, opposite from filled states in the valence band of the *p*-type semiconductor. As a consequence, some electrons tunnel from the *p*- to the *n*-type semiconductor, as indicated by

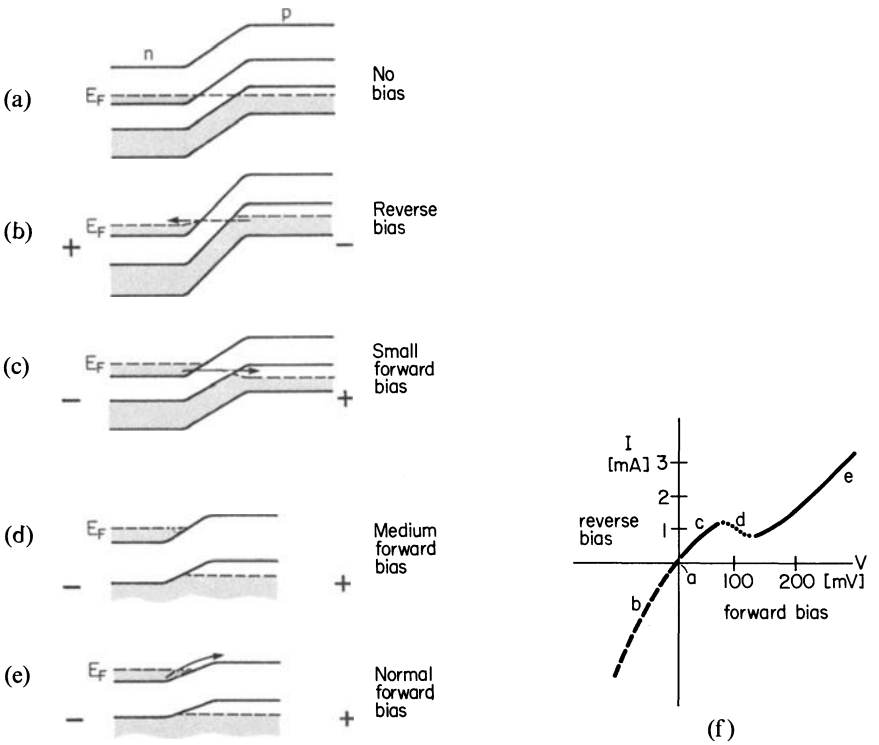

Figure 8.24. (a)–(e) Schematic energy band diagrams for highly doped *n*- and *p*-type semiconductors (tunnel diode). (a) No bias. (b) Reverse bias. (c) Small forward bias. (d) Medium forward bias. (e) "Normal" forward bias. (f) Voltage–current characteristic for a tunnel diode.

an arrow. An increase in the *reverse* voltage yields an increase of the electron current through the device (see Fig. 8.24(f)).

Let us now consider several forward voltages. A small forward bias (Fig. 8.24(c)) creates just the opposite of that seen in Fig. 8.24(b). Electrons are tunneling through the potential barrier from the conduction band of the *n*-type semiconductor into empty states of the valence band of the *p*-type semiconductor. The applied voltage needs to be only of several millivolts and it produces a forward current of about one milliamp.

If, however, the voltage is increased to, say, 100 mV, the potential barrier might be decreased so much that, opposite from the filled *n*-conduction states, no allowed empty states in the *p*-area are present [Fig. 8.24(d)]. (The area opposite to the filled *n*-conduction states may be the forbidden band.) In this case, no tunneling takes place. As a consequence of this, the current decreases with increasing forward voltage, as shown in Fig. 8.24(f). We experience a *negative current–voltage characteristic*.

Finally, if the forward voltage is increased even more, the electrons in the

conduction band of the *n*-type semiconductor obtain enough energy to climb the potential barrier to the *p*-side just like in a regular *p*–*n* junction. As a consequence, the current increases with voltage, just as in Fig. 8.19(c).

Of particular interest is the range in which a negative voltage–current characteristic is experienced. One has to bear in mind that all other electrical devices have a positive voltage–current characteristic, i.e., they dissipate energy. Therefore, if a tunnel diode is connected to properly dimensioned resistors and capacitors a simple oscillator can be built which does not lose energy because the net resistance is zero. Those devices can oscillate at frequencies up to 10^{11} cycles per second.

8.7.9. Transistors

An *n*–*p*–*n* transistor may be considered to be an *n*–*p* diode back-to-back with a *p*–*n* diode. A schematic band diagram for an unbiased *n*–*p*–*n* transistor is shown in Fig. 8.25. The three connections of the transistor are called emitter (E), base (B) and collector (C).

If the transistor is used for the amplification of a signal, the "diode" consisting of emitter and base is forward biased, whereas the base–collector "diode" is strongly reverse biased (Fig. 8.26(a)). The electrons ejected into the emitter, therefore, need to have enough energy to be able to "climb" the potential barrier into the base region. Once there, the electrons diffuse through the base area until they have reached the depletion region between base and collector. Here, the electrons are accelerated in the strong electric field produced by the collector voltage (Fig. 8.26(b)). This acceleration causes amplification of the input a.c. signal.

One may consider this amplification from another point of view. The forward biased emitter–base diode has a small resistance (approximately 10^{-5} Ω cm), whereas the reverse biased base–collector diode has a much larger resistance (about 10^{-1} Ω cm). Since the current flowing through the device is

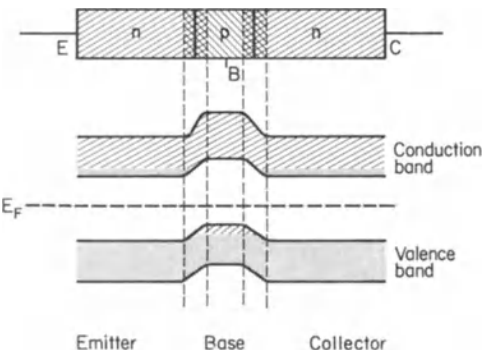

Figure 8.25. Schematic band diagram of an unbiased *n*–*p*–*n* transistor.

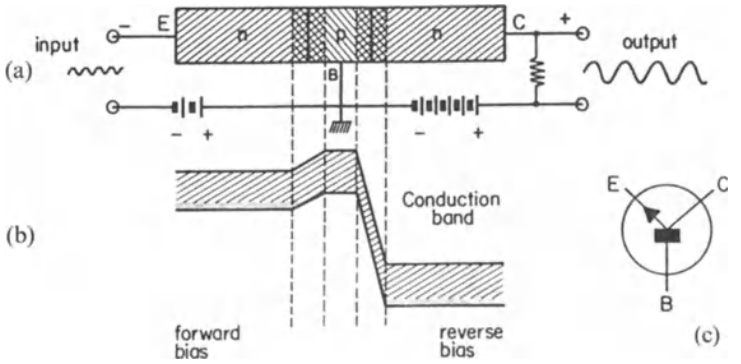

Figure 8.26. (a) Biasing of an n–p–n transistor. (b) Schematic band diagram (partial) of a biased n–p–n transistor. (c) Symbol used for an n–p–n transistor.

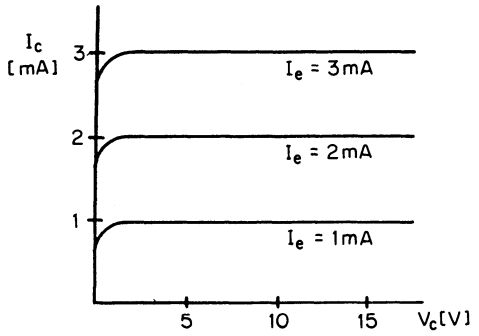

Figure 8.27. Schematic collector voltage–current characteristics of a transistor for various emitter currents.

practically identical in both parts, the power ($N = I^2R$) is larger at the collector side. This results in a power ratio larger than one, i.e., into a power gain.

Some details need to be added about technical features of transistors. In order to obtain a large electron density in the emitter, this area is heavily doped.

In the p-doped base area, the drifting electrons are subject to recombination with holes. Therefore, the number of holes there has to be kept at a minimum, which is accomplished by light doping. Recombination is further decreased by making the base region extremely thin, i.e., 10^{-5} to 10^{-7} m. A narrow base region also has a beneficial side effect: it increases the frequency response. The doping rate of the collector area is in general not critical. Usually, the doping is light to reduce the capacitance of the device.

The voltage–current characteristics for a transistor are shown in Fig. 8.27.

In *p–n–p* transistors, the majority carriers are holes. The function and features of a *p–n–p* transistor are similar to an *n–p–n* transistor.

8.7.10. Semiconductor Device Fabrication

At the end of our discussion about semiconductor devices, a few words should be said about device fabrication. Modern technology has come a long way since the *point contact transistor* which was invented in 1947 by Bardeen and Brattain at Bell Laboratories. The development went via the *junction transistor* (Shockley, 1947), the *planar transistor* (Fairchild, 1962), and the *planar epitaxial transistor* (Texas Instruments, 1963) to the *large scale integration* of today. Figure 8.28 shows the basic components which constitute electronic circuits. It also depicts how the active parts are arranged on one common substrate, called the *wafer*. Repetitions and interconnections of these individual elements on a microscopic scale compose the well known *chips* which can be inexpensively mass-fabricated and are relatively reliable.

The starting material for the wafers is sand (SiO_2) which is electromet reduced to 98% silicon. This raw silicon is reacted with hydrogen chloride to form trichlorosilane ($Si + 3\,HCl \rightarrow Si\,HCl_3 + H_2$) which is then distilled for purification and reduced with hydrogen to polycrystalline silicon. Single crystals are then grown by using either the crucible pulling method introduced by Czochralski, the float zone, or the ribbon technique (Fig. 8.29). The five-inch diameter rods or ribbons obtained in this way are sliced, lapped, etched, and polished to obtain the wafers.

The different *n*- and *p*-regions (see Fig. 8.28) are then introduced by diffusing phosphorous or boron through *windows* into the substrate. These windows are etched through a SiO_2 layer with the aid of masks and a photoresist technique. The individual steps are shown in Fig. 8.30.

The reader who is interested in a more detailed treatment of semiconductor devices and fabrication is referred to specialized books, some of which are listed at the end of Part II.

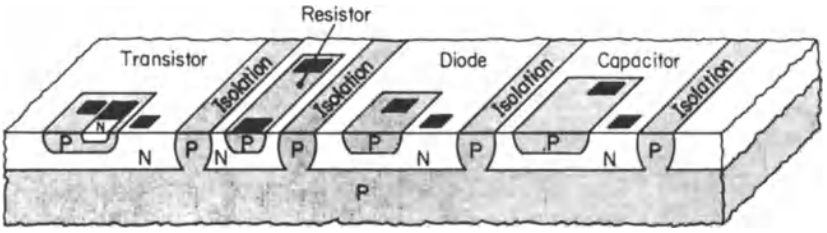

Figure 8.28. Basic components of integrated circuits (bipolar). The dark areas are the contact pads.

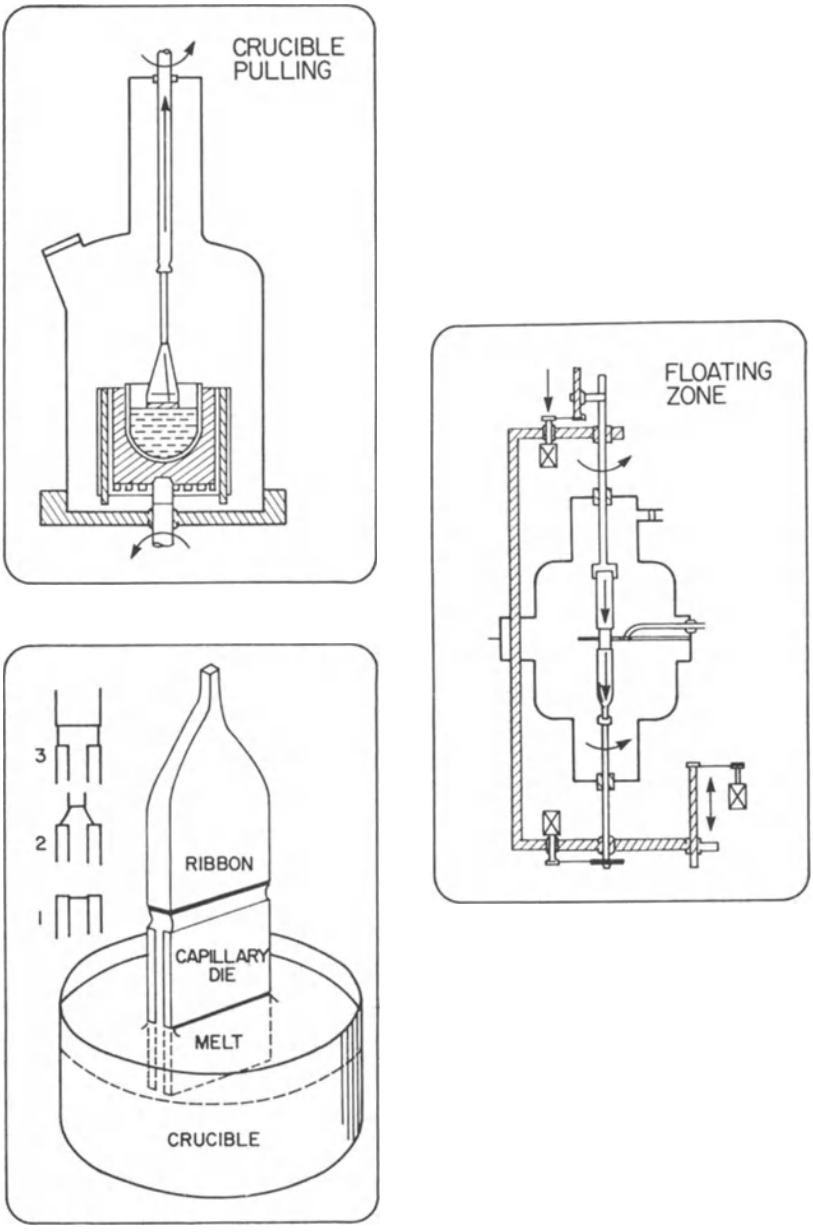

Figure 8.29. Methods for silicon single-crystal growth.

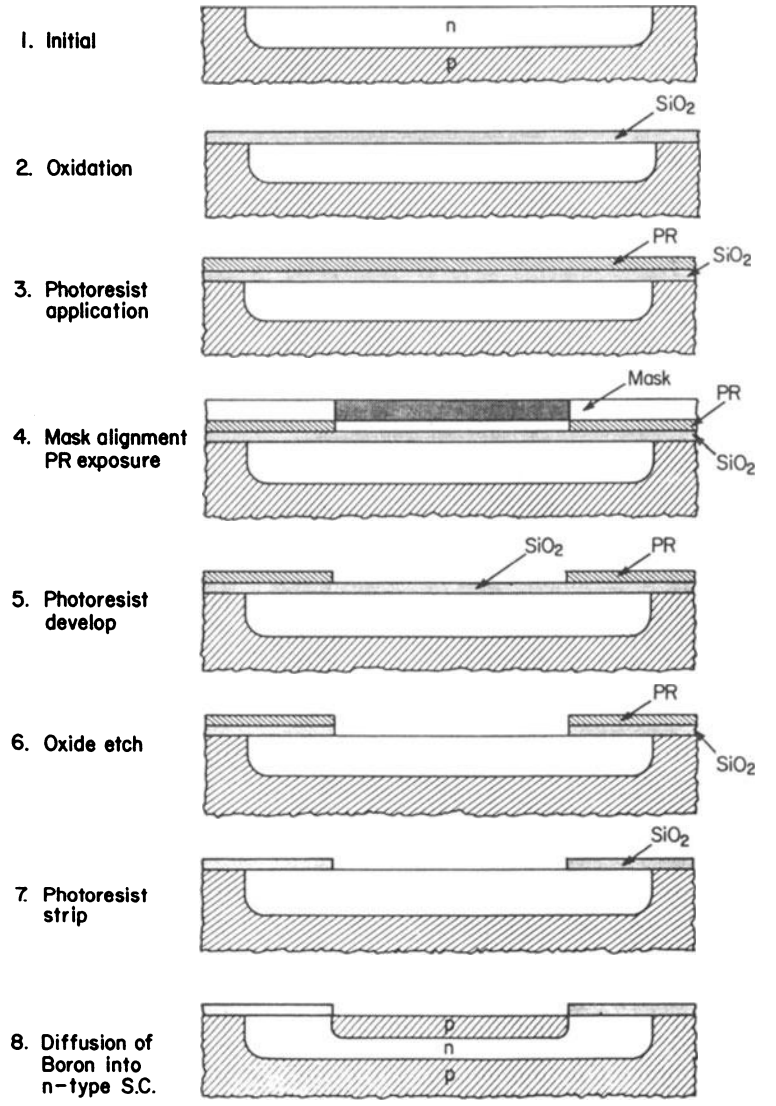

Figure 8.30. Photoresist (PR) masking sequence to obtain a p–n–p transistor.

Problems

Intrinsic Semiconductors

1. Why do we find a narrow *band gap* in semiconducting materials?
2. Would germanium still be a semiconductor if the band gap was 4 eV wide? Explain!
3. Calculate the Fermi energy of an intrinsic semiconductor at $T \neq 0$ K. (*Hint*: Give a mathematical expression for the fact that the probability of finding an electron at the top of the valence band plus the probability of finding an electron at the bottom of the conduction band must be 1.)
4. Calculate the number of electrons in the conduction band for silicon at $T =$ 300 K.
5. The outer electron configuration of neutral germanium in its ground state is listed in a textbook $4s^2 4p^2$. Is this information correct? Someone argues against this configuration that the p-states hold 6 electrons. Therefore, the p-states in germanium and therefore the valence band are only partially filled. Who is right?
6. In the figure below, σ is plotted as a function of the reciprocal temperature for an intrinsic semiconductor. Calculate the gap energy.

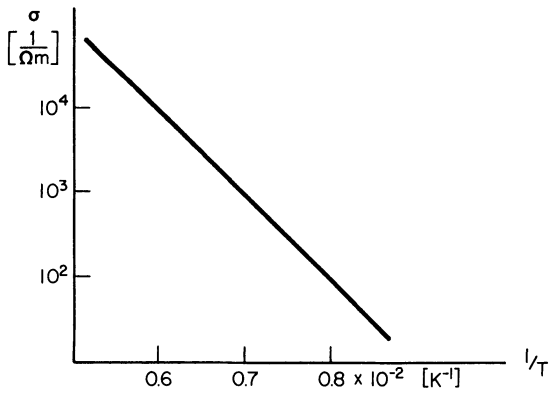

Extrinsic Semiconductors

7. Calculate the Fermi energy and the conductivity at room temperature for germanium containing 5×10^{22} arsenic atoms per m^3.
8. Consider a silicon crystal containing 10^{18} phosphorous atoms per cubic meter. Is the conductivity increasing or decreasing when the temperature is raised from 300° C to 350° C? Explain.

9. Consider a semiconductor with 10^{19} donors/m^3 having an ionization energy of 10 meV and an effective mass of 0.1 m_0. a) What type of impurity atoms (donors or acceptors) could this semiconductor have? b) Calculate the concentration of conduction electrons at $4K$. c) Assuming a gap energy of 1 eV, what is the concentration of conduction electrons at $300K$ ($m^* \equiv m_0$)? d) Which contribution is larger?

10. The binding energy of a donor electron can be calculated by assuming that the extra electron moves in a hydrogen-like orbit. Estimate the donor binding energy of an n-type impurity in a semiconductor by applying the modified equation (4.18a):

$$E = \frac{m^* e^4}{2\hbar^2 \varepsilon_r^2},$$

where $\varepsilon_r = 16$ is the dielectric constant of the semiconductor. Assume $m^* = 0.8\ m_0$. Compare your result with experimental values listed in Appendix 4.

11. What happens when a semiconductor contains both, donor and acceptor impurities? What happens with the acceptor level in the case of a predominance of donor impurities?

Semiconductor Devices

12. You are given a p-type doped silicon crystal and are asked to make an ohmic contact. What material would you use?

13. Describe the band diagram and function of a p–n–p transistor.

14. Can you make a solar cell from metals only? Explain!

*15. A cadmium sulfide photodetector is irradiated over a receiving area of 4×10^{-6} m^2 by light of wavelength 0.4×10^{-6} m and intensity of 20 watts m^{-2}. a) If the energy gap of cadmium sulfide is 2.4 eV, confirm that electron–hole pairs will be generated. b) Assuming each quantum generates an electron–hole pair, calculate the number of pairs generated per second.

16. Calculate the room temperature saturation current and the forward current at 0.3 V for a silver/n-doped silicon Schottky-type diode. Take for the active area 10^{-8} m^2 and for $C = 10^{25}\ A/m^2K^2$.

CHAPTER 9

Electrical Conduction in Polymers, Ceramics, and Amorphous Materials

9.1. Conducting Polymers

Materials which are electrical (and thermal) insulators are of great technical importance and are, therefore, used in large quantities in the electronics industry, for example as handles for a variety of tools, as coatings of wires, or for casings of electrical equipment. Most polymeric materials have the required insulating properties and have been used for decades for this purpose. It came, therefore, as a surprise when it was discovered that some polymers and organic substances may have electrical properties which resemble those of conventional semiconductors, metals, or even superconductors. We shall focus our attention mainly on these materials. This does not imply that conducting polymers are of technical importance at this time. Indeed, they are not. This is due to the fact that presently known conducting polymers seem to not be stable in air, nor are they stable much above room temperature. In addition, many dopants used to impart a greater conductivity are highly toxic and doping often makes the polymers brittle. These problems might be overcome, however, as more conducting polymers are synthesized.

We now attempt to discuss conducting polymers in the light of solid state physics. Conventional solid state physics deals preferably with the properties of well defined regular arrays of atoms. We have learned in Chapter 7 that a periodic array of lattice atoms is imperative for coherent scattering of electron waves and thus for a high conductivity. Further, the periodic arrangement of atoms in a crystal and the strong interactions between these atoms causes, as we know, a widening of energy levels into energy bands (see Section 4.4).

We know that highly conducting materials such as metals are characterized by partially filled bands, which allow a free motion of the conduction electrons in an electric field. Insulators and semiconductors, on the other hand, possess (at least at 0 K) completely filled valence bands, and empty conduction bands.

(a) (b)

Figure 9.1. (a) Polyethylene. (b) Polyvinylchloride. (The dashed enclosures mark the repeat unit.)

The difference in band structure between crystalline insulators and semiconductors is a matter of degree rather than of kind: insulators have wide gaps between valence and conduction bands whereas the energy gaps for semiconductors are narrow. Thus, in the case of semiconductors the thermal energy is large enough to excite some electrons across the gap into the conduction band. The conductivity in pure semiconductors is known to *increase* (exponentially) with increasing temperature and decreasing gap energy (equation (8.14)), whereas the conductivity in metals *decreases* with increasing temperature (Fig. 7.7). Interestingly enough, conducting polymers have a temperature dependence of the conductivity similar to that of semiconductors. This suggests that certain aspects of semiconductor theory may be applied to conducting polymers. The situation in polymers cannot be described, however, without certain modifications to the band model brought forward in the previous chapters. This is due to the fact that polymeric materials may exist in amorphous as well as in crystalline form or, more commonly, as a mixture of both. This needs to be discussed in some detail.

Polymers consist of molecules which are long and chainlike. The atoms which partake in such a chain (or macromolecule) are regularly arranged along the chain. Several atoms combine and form a specific building block, called a monomer, and thousands of monomers combine to a polymer. As an example, we depict polyethylene which consists of monomers of one carbon atom and two hydrogen atoms, Fig. 9.1(a). If one hydrogen atom in ethylene is replaced by a chlorine atom, polyvinylchloride (PVC) is formed (Fig. 9.1(b)). In polystyrene, some hydrogen atoms are replaced by benzene rings. More complicated macromolecules may contain side chains which are attached to the main link. They are appropriately named "branched polymers." Macromolecules whose backbones consist of carbon atoms, as in Fig. 9.1, are called "organic" polymers.

The binding forces which hold the individual atoms in polymers together are usually covalent and sometimes ionic in nature. Covalent forces are much stronger than the binding forces in metals. They are based on the same interactions which are responsible for forming a hydrogen molecule from two hydrogen atoms. Quantum mechanics explains covalent bonds by showing that a lower energy state is achieved when two equal atomic systems are closely coupled and in this way exchange their energy (see Section 16.2). In

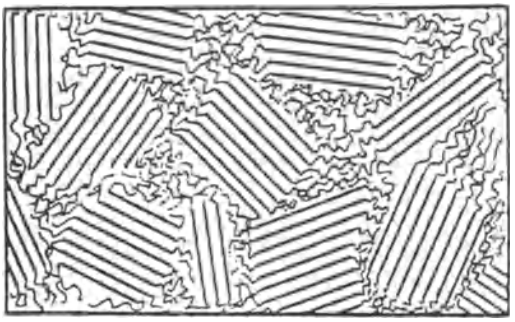

Figure 9.2. Simplified representation of a semicrystalline polymer. (Fringed micell structure.) Reprinted with permission from Flory (1953) *Principles of Polymer Chemistry*, Cornell Univ. Press, Ithaca, N.Y.

organic polymers each carbon atom is often bound to four atoms (see Fig. 9.1) because carbon has four valencies.

In contrast to the strong binding forces between the atoms within a polymeric chain, the interactions between the individual macromolecules are weak. The latter are of the van der Waals type, that is, they are based on forces which induce dipole moments in the molecules. (Similar weak interactions exist between the atoms in rare gases such as argon, neon, etc.).

In order to better understand the electronic properties of polymers by means of the electron theory and the band structure concept, one needs to know the degree of order or the degree of periodicity of the atoms because only ordered and strongly interacting atoms or molecules lead, as we know, to distinct and wide electron bands. Now, it has been observed that the degree of order in polymers depends on the length of the molecules and on the simplicity of the molecular structure. Certain heat treatments may influence some structural parameters. For example, if a simple polymer is slowly cooled below its melting point, one might observe that some macromolecules align parallel to each other. The individual chains are separated by regions of supercooled liquid, that is, of amorphous material (Fig. 9.2). Actually, slow cooling yields, for certain polymers, a highly crystalline structure.

In other polymers, the cooling procedure might cause the entire material to go into a supercooled-liquid state. In this state the molecules can be considered to be randomly arranged. After further cooling, below a *glassy* temperature, the polymer might transform itself into an amorphous solid which is strong, brittle and insulating. As stated before, we shall concern ourselves, however, mainly with polymers which have a high degree of crystallinity. Amorphous materials will be discussed in Section 9.3.

A high degree of crystallinity and a relatively high conductivity have been found in polyacetylene which is the simplest *conjugated* organic polymer. It is considered to be the prototype of a conducting polymer. A conjugated polymer has alternating single and double bonds between the carbons (see Fig. 9.3

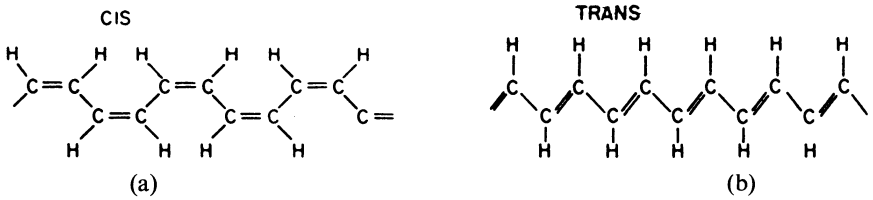

Figure 9.3. Theoretical isomers of polyacetylene (a) cis-transoidal isomer, (b) trans-transoidal isomer. Polyacetylene is synthesized as cis-$(CH)_x$ and is then isomerized into the trans-configuration by heating it at 150°C for a few minutes.

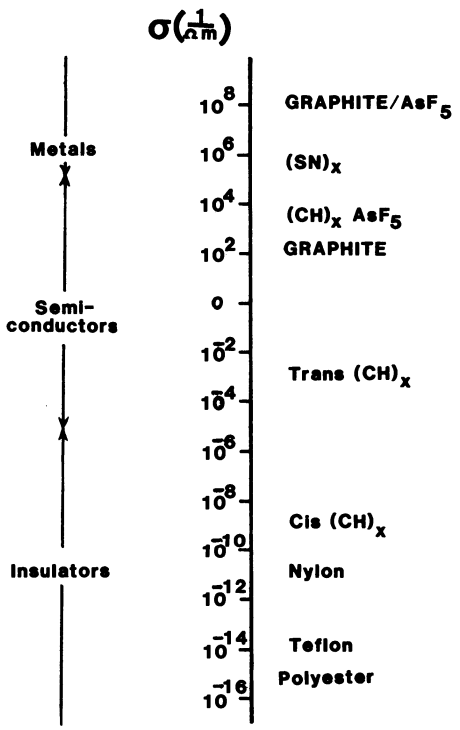

Figure 9.4. Conductivities of polymers in Ω^{-1} m^{-1}. (Compare to Fig. 7.1.)

which should be compared to Fig. 9.1(a)). Two principle isomers are important: in the *trans* form, the hydrogen atoms are alternately bound to opposite sides of the carbons (Fig. 9.3(b)) whereas in the *cis* form the hydrogen atoms are situated on the same side of the double-bond carbons (Fig. 9.3(a)). This causes the hydrogen atoms in the cis form to be relatively close to each other. Trans-polyacetylene is obtained as a silvery, flexible film which has a conductivity comparable to that of silicon (Fig. 9.4).

Figure 9.5 shows three band structures for trans-$(CH)_x$ assuming different

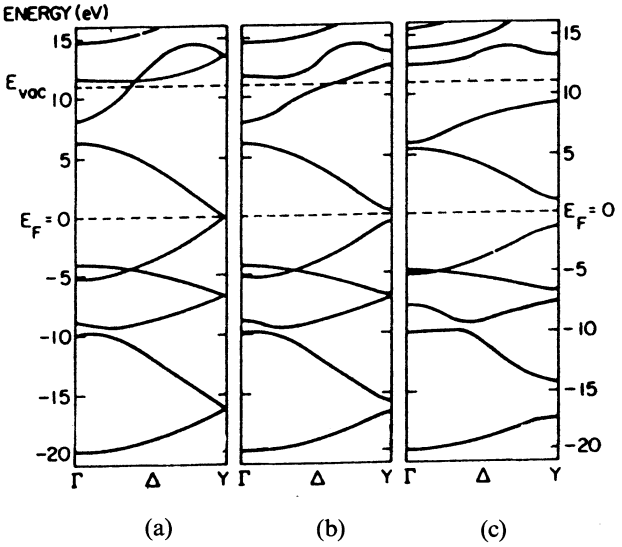

Figure 9.5. Band structure of trans-$(CH)_x$ for different carbon–carbon bond lengths: (a) uniform (1.39 Å); (b) weakly alternating C=C 1.36 Å, C—C 1.43 Å); and (c) strongly alternating (C=C 1.34 Å, C—C 1.54 Å). Note the band gaps at Y as bond alternation occurs. Reprinted with permission from Grant, P.M., and Batra I.P. (1979) *Solid State Comm.* **29**, 225, Pergamon Press, Ltd.

distances between the carbon atoms. In Fig. 9.5(a) all carbon bond lengths are taken to be equal. The resulting band structure is found to be characteristic for a metal, that is, one obtains distinct bands, the highest of which is *partially* filled by electrons. Where are the free electrons in the conduction band coming from? We realize that one of the electrons in the double bond of a conjugated polymer can be considered to be only loosely bound to the neighboring carbon atoms. Thus, this electron is easily disassociated from its carbon atom by a relatively small energy, which may be provided by thermal energy. The delocalized electrons may be accelerated as usual in an electric field.

In reality, however, a uniform bond length between the carbon atoms does not exist in polyacetylene. Instead, the distances between the carbon atoms alternate because of the alternating single and double bonds. Band structure calculations for this case show, interestingly enough, some gaps between the individual energy bands. The resulting band structure is typical for a semiconductor (or an insulator)! The width of the band gap near the Fermi level depends mainly on the degree of alternating bond lengths (Fig. 9.5(b) and (c)).

It has been shown that the band structure in Fig. 9.5(b) best represents the experimental observations. Specifically, one finds a band gap of about 1.5 eV and a total width of the conduction band of 10–14 eV. The effective mass m^* is $0.6m_0$ at $k = 0$ and $0.1m_0$ at $k = \pi/a$. Assuming $\tau \to 10^{-14}$ s, the free carrier mobility, μ, along a chain is calculated to be about 200 cm^2/V s. The

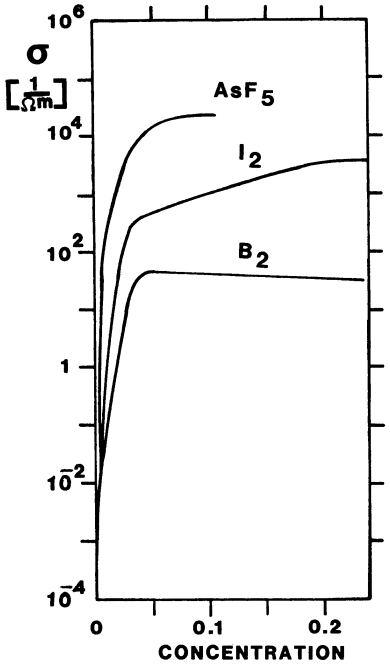

Figure 9.6. Conductivity change of polyacetylene as a result of doping.

latter quantity is, however, hard to measure since the actual drift mobility in the entire solid is reduced by the trapping of the carriers which occurs during the "hopping" of the electrons between the individual macromolecules.

Polyacetylene, as discussed so far, should be compared to conventional intrinsic semiconductors. Now, we know from Section 8.3 that the conductivity of semiconductors can be substantially increased by doping. The same is true for polymer-based semiconductors. Indeed, arsenic-pentafluoride-doped polyacetylene has a conductivity which is about seven orders of magnitude larger than undoped $(CH)_x$. Thus, σ approaches the conductivity of metals, as can be seen in Figs. 9.4 and 9.6. Iodine or AsF_5 provide *p*-type semiconductors, whereas alkali metals are *n*-type dopants. The doping is achieved through the vapor phase or by electrochemical methods. The dopant molecules diffuse between the $(CH)_x$ chains and provide a charge transfer between the polymer and the dopant. The dopant ends up as an anion in the case of acceptor and as a cation in the case of donor dopants.

A refinement in the description of the conduction mechanism in polyacetylene can be provided by introducting the concept of *solitons*. A soliton is a structural distortion in a conjugated polymer and is generated when a single bond meets another single bond, as shown in Fig. 9.7. At the distortion point a localized nonbonding electron state is generated, similar to an *n*-type impurity state in a silicon semiconductor. The result is a localized

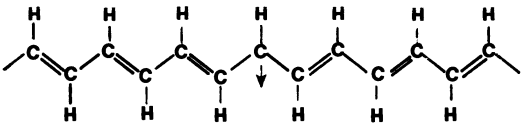

Figure 9.7. A broken symmetry in polyacetylene creates a domain wall or a *soliton*. (An *antisoliton* is the mirror image of a soliton.)

level in the center of the forbidden band. It is believed that when an electron is excited from the valence band into the conduction band (leaving a hole in the valence band) this electron–hole pair decays in about 10^{-12} seconds into a more stable soliton–antisoliton pair.

Near the center of a soliton, the bond lengths are equal. We recall that uniform bond lengths constitute a metal. Thus, when many solitons have been formed and their spheres of influence overlap, a metal-like conductor would result.

It is also conceivable that one of the double bonds next to a soliton switches over to a single bond. If this switching occurs consecutively in one direction, a soliton wave results. This can be compared to a moving electron.

Up to now, we discussed mainly the properties of polyacetylene. However, several additional conductive polymers have been discovered. The chains in inorganic poly(sulfur nitride) consist of alternating sulfur and nitrogen atoms. Because of the different valencies of the S^{2-} and N^{3-} ions, $(SN)_x$ is an electron deficient material with an alternating bond structure. The bond length alternation is not severe, so that $(SN)_x$ has a room temperature conductivity of about 10^5 ohm^{-1}m^{-1} along the chain direction. The conductivity increases with a reduction in temperature. At temperatures close to 0 K, poly (sulfur nitride) becomes superconducting. In brominated $(SN)_x$ the Br_3^- and Br_2 ions are aligned along the chain axis, giving rise to a one-dimensional superlattice.

In graphite, an individual "molecule" consists of a "sheet" of carbon atoms. The conductivity is found to be nearly metallic, at least parallel to the layers (Fig. 9.4). AsF_5-doped graphite has an even higher conductivity. The conduction is increased by producing a mixture of easily ionized electron donors and electron acceptors. The charge is then shared between the donors and acceptors. These materials are called charge transfer complexes.

9.2. Ionic Conduction

In ionic crystals (such as the alkali halides), the individual lattice atoms transfer electrons between each other to form positively charged cations and negatively charged anions. The binding forces between the ions are electrostatic in nature and are thus very strong. The room temperature conductivity

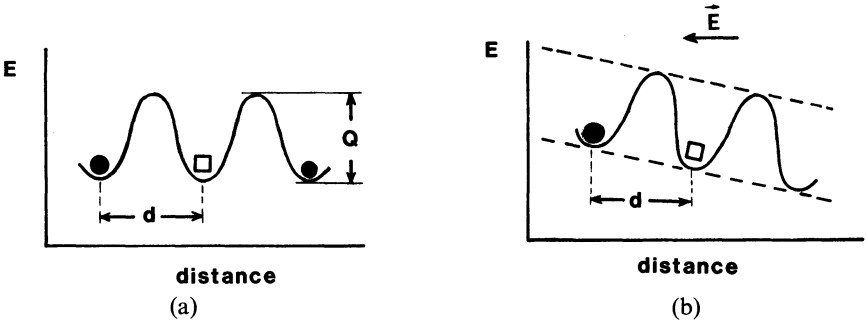

Figure 9.8. Schematic representation of a potential barrier which a lattice atom (●) has to overcome to exchange its site with a vacancy (□) (a) without an external electric field; (b) with external electric field. d = distance between two adjacent lattice sites; Q = activation energy.

of ionic crystals is about 22 orders of magnitude smaller than the conductivity of typical metallic conductors (Fig. 7.1). This large difference in σ can be understood by realizing that the wide band gap in insulators allows only extremely few electrons to be excited from the valence into the conduction band.

The main contribution to the electrical conduction in ionic crystals (as little as it may be) is, however, due to a mechanism which we have not yet discussed, namely to ionic conduction. Ionic conduction is caused by the movement of some negatively (or positively) charged ions which *hop* from lattice site to lattice site under the influence of an electric field. (This type of conduction is similar to that which is known to occur in aqueous electrolytes). The ionic conductivity

$$\sigma_{\text{ion}} = N_{\text{ion}} e \mu_{\text{ion}} \tag{9.1}$$

is like the semiconductor conductivity (8.13), the product of three quantities. In the present case, N_{ion} is the number of ions which can change their position under the influence of an electric field and μ_{ion} is the mobility of these ions.

In order for ions to move through a crystalline solid, they must have sufficient energy to pass over an *energy barrier* (Fig. 9.8). Further, a lattice site next to a given atom must be empty in order for an ion to be able to change its position. Thus, N_{ion} in (9.1) depends on the vacancy concentration in the crystal (that is, on the number of *Schottky defects*). In short, the theory of ionic conduction contains essential elements of diffusion theory, with which the reader might be familiar.

Diffusion theory links the mobility of the ions, which is contained in (9.1), with the diffusion coefficient D, through the Einstein relation:

$$\mu_{\text{ion}} = \frac{De}{k_B T}. \tag{9.2}$$

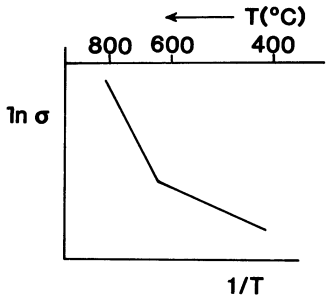

Figure 9.9. Schematic representation of $\ln\sigma$ versus $1/T$ for Na^+ ions in sodium chloride. (Arrhenius plot.)

The diffusion coefficient varies with temperature; this dependence is commonly expressed by an Arrhenius equation,

$$D = D_0 \exp\left[-\left(\frac{Q}{k_B T}\right)\right], \tag{9.3}$$

where Q is the activation energy for the process under consideration (Fig. 9.8) and D_0 is a preexponential factor which depends on the vibrational frequency of the atoms and some structural parameters. Combining equations (9.1) through (9.3) yields:

$$\sigma_{ion} = \frac{N_{ion} e^2 D_0}{k_B T} \exp\left[-\left(\frac{Q}{k_B T}\right)\right]. \tag{9.4}$$

Equation (9.4) is shortened by combining the preexponential constants into σ_0:

$$\sigma_{ion} = \sigma_0 \exp\left[-\left(\frac{Q}{k_B T}\right)\right]. \tag{9.5}$$

Figure 9.9 depicts schematically a plot of $\ln\sigma$ versus $1/T$ as experimentally found for alkali halides. The linear $\ln\sigma$ versus $1/T$ relationship indicates that Fig. 9.9 is an actual representation of (9.5). The slopes of the straight lines in Arrhenius plots are utilized to calculate the activation energy of the processes under consideration. We notice in Fig. 9.9 two temperature regions representing two different activation energies: at low temperatures, the activation energy is small, that is, the thermal energy is just sufficient to allow the hopping of ions into already existing vacancy sites. This temperature range is commonly called the *extrinsic* region. On the other hand, at high temperatures, the thermal energy is large enough to create additional vacancies. The related activation energy is thus the sum of the activation energies for vacancy creation and ion movement. This temperature range is called the *intrinsic* region.

So far, we have not been very specific in describing the circumstances of

vacancy formation in an ionic crystal. Now, we have to realize that whenever vancant lattice sites are created, an overall charge neutrality needs to be maintained. The latter is the case when both a cation and an anion are removed from a lattice. Another permissible mechanism is the formation of a vacancy-interstitial pair (*Frenkel defect*). More often, however, vacancies are created as a consequence of introducing differently charged impurity atoms into an ionic lattice, that is, by substituting, say, a monovalent metal atom with a divalent atom. In order to maintain charge neutrality in this case, a positively charged vacancy needs to be introduced. For example, if a divalent Mg^{2+}-ion substitutes for a monovalent Na^+-ion one extra Na^+-ion has to be removed to restore charge neutrality. Or, if Zirconia (ZrO_2) is treated with CaO (to produce the technically important calcia-stabilized zirconia), the Ca^{2+}-ions substitute for Zr^{4+}-ions and an anion vacancy needs to be created to maintain charge neutrality. Nonstoichiometric compounds contain a high amount of vacancies even at low temperatures, whereas in stoichiometric compounds vacancies need to be formed by elevating the temperature.

In conclusion, we note that in principle, both cations and anions are capable of moving simultaneously under the influence of an electric field. It turns out, however, that in most alkali halides the majority carriers are provided by the metal ions, whereas in other materials, such as the lead halides, the conduction is predominantly performed by the halide ions.

9.3. Amorphous Materials (Metallic Glasses)

Before we discuss electrical conduction in amorphous materials, we need to clarify what the term *amorphous* means in the present context. Strictly speaking *amorphous* implies the random arrangement of atoms, that is, the absence of any periodic symmetry, or the absence of any crystalline structure. One could compare the random distribution of atoms with the situation in a gas, as seen in an instantaneous picture. Now, such a completely random arrangement of atoms is seldom found even in liquids, much less in solids. In actuality, the relative positions of nearest neighbors surrounding a given atom in an amorphous solid are almost identical to the positions in crystalline solids because of the ever-present binding forces between the atoms. In short, the atomic order in amorphous materials is restricted to the nearest neighbors. Amorphous materials exhibit, therefore, only *short-range order*. In contrast to this, the exact positions of the atoms which are farther apart from a given central atom cannot be predicted. This is particularly the case when various kinds of stacking orders, that is, if polymorphic modifications are possible. As a consequence one observes atomic disorder at long range. The term *amorphous solid* should therefore be used *cum grano salis*. We empirically define materials to be amorphous when their diffraction patterns consist of diffuse rings, rather than sharply defined Bragg rings, as characteristic for polycrystalline solids.

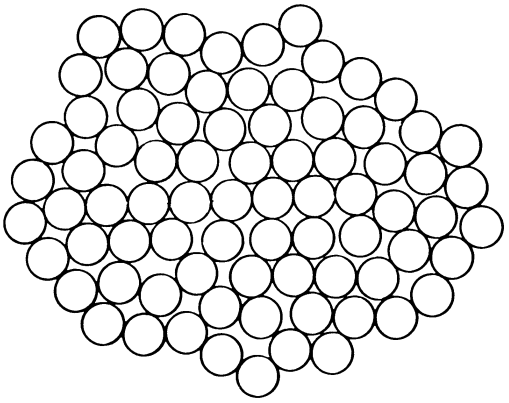

Figure 9.10. Two-dimensional schematic representation of a dense random packing of hard spheres (Bernal model).

So far we have discussed positional disorder only as it might be found in pure materials. If more than one component is present in a material, a second type of disorder is possible: The individual species might be randomly distributed over the lattice sites; that is, the species may not be alternately positioned as is the case for, say, sodium and chlorine atoms in NaCl. This random distribution of species is called *compositional disorder.*

The best-known representative of an amorphous solid is window glass, whose major components are silicon and oxygen. Glass is usually described as a supercooled liquid.

Interestingly enough, many elements and compounds which are generally known to be crystalline under equilibrium conditions can also be obtained in the nonequilibrium amorphous state by applying rapid solidification techniques, i.e., by utilizing cooling rates of about 10^5 K/s. These cooling rates can be achieved by fast quenching, melt spinning, vapor deposition, sputtering, radiation damage, filamentary casting in continuous operation, etc. The degree of amorphousness (or, the degree of short range order) may be varied by the severity of the quench. The resulting *metalic glasses*, or *glassy metals*, have unusual electrical, mechanical, optical, magnetic and corrosion properties and are therefore of considerable interest. Amorphous semiconductors (consisting for example of Ge, Si, GeTe, etc.) have also received substantial attention because they are relatively inexpensive to manufacture, have unusual switching properties, and have found applications in inexpensive photovoltaic cells.

We turn now to the atomic structure of amorphous metals and alloys. They have essentially nondirectional bonds. Thus, the short-range order does not extend beyond the nearest neighbors. The atoms must be packed together tightly, however, in order to achieve the observed density. There are only a limited number of ways of close packing. One way of arranging the atoms in amorphous metals is depicted by the *dense random packing of hard spheres*

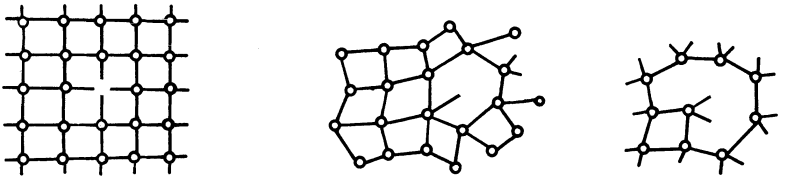

Figure 9.11. Defects in crystalline and amorphous silicon. (a) Monovacancy in a crystalline semiconductor; (b) one and (c) two dangling bonds in a continuous random network of an amorphous semiconductor. (Note the deviations in the interatomic distances and of the bond angles.)

model (Fig. 9.10). This *Bernal* model is considered as the ideal amorphous state. No significant regions of crystalline order are present. In transition metal-metalloid compounds (such as Ni–P) it is thought that the small metalloid atoms occupy the holes which occur as a consequence of this packing (*Bernal–Polk model*).

The atoms in amorphous semiconductors on the other hand do not arrange themselves in a close-packed manner. Atoms of Group IV elements are, as we know, covalently bound. They are often arranged in a *continuous random network* with correlations in ordering up to the third or fourth nearest neighbors (Fig. 9.11(b) and (c)). Amorphous pure silicon contains numerous *dangling bonds* similarly to those found in crystalline silicon in the presence of vacancies (Fig. 9.11(a)).

Since amorphous solids have no long-range crystal symmetry, we can no longer apply the Bloch theorem, which led us in Chapter 4.4 from the distinct energy levels for isolated atoms to the broad quasicontinuous bands for crystalline solids. Thus, the calculation of electronic structures for amorphous metals and alloys has to use alternate techniques, for example the *cluster model* approach. This method has been utilized to calculate the electronic structure of amorphous Zr–Cu (which is a representative of a noble metal-transition metal metallic glass). A series of clusters were assumed which exhibit the symmetry of the close-packed lattices fcc (as for Cu) and hcp[13] (as for Zr). The energy level diagram depicted in Fig. 9.12 shows two distinct "bands" of levels. The lower band consists primarily of copper *d*-levels, while the upper band consists mainly of zirconium *d*-levels. A sort of a gap separates the two bands of levels. Even though the concept of quasicontinuous energy bands is no longer meaningful for amorphous solids, the density of states concept still is as can be seen in Fig. 9.12. We notice that the Fermi energy is located in the upper part of the zirconium levels. Further, we observe partially filled electron states. This has two interesting consequences. First, we expect *metal-like* conduction. Secondly, $Z(E)$ near E_F is small which suggests relatively small values for the conductivity (see (7.26)). Indeed, σ for Cu–Zr is

[13] Hexagonal close-packed.

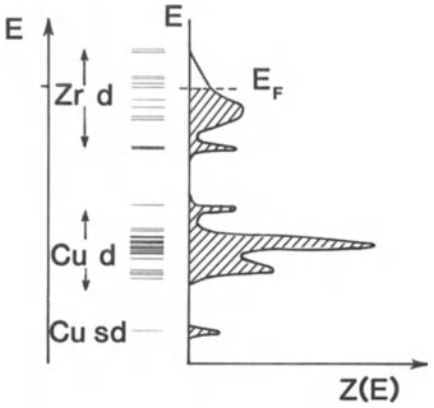

Figure 9.12. Schematic representation of the molecular orbital energy level diagram and the density of states curves for Zr–Cu clusters. The calculated density of states curves agree reasonably well with photoemission experiments.

comparable to that of poor metallic conductors (that is approximately 5×10^5 1/Ωm).

The electrical resistivity of many metallic glasses (such as $Pd_{80}Si_{20}$ or $Fe_{32}Ni_{36}Cr_{14}P_{12}B_6$[14]) stays constant over a fairly wide temperature range up to the temperature which marks the irreversible transition from the amorphous into the crystalline state. This makes these alloys attractive as resistance standards. The mean free path for electrons in metallic glasses is estimated to be about 10 Å.

The energy level diagrams and the density of states curves for amorphous semiconductors are somewhat different from those for amorphous metals. Because of the stronger binding forces which exist between the atoms in covalently bound materials, the valence electrons are tightly bound, or *localized.* As a consequence the density of states for the localized states extend into the "band gap" (Fig. 9.13). This may be compared to the localized impurity states in doped crystalline semiconductors which are also located in the band gap. Thus, we observe density of states *tails.* These tails might extend for some materials so far into the gap that they partially overlap. In general, however, the density of electron and hole states for the localized levels is very small.

The electrical conductivity for amorphous semiconductors σ_A depends, as usual (equation (8.13)), on the number of carriers N_A and the mobility of these carriers, μ_A:

$$\sigma_A = N_A e \mu_A. \tag{9.6}$$

The number of carriers in amorphous semiconductors is extremely small because all electrons are, as said before, strongly bound (localized) to their respective nuclei. Likewise, the mobility of the carriers is small because the

[14] METGLAS 2826A, trademark of Allied Chemical.

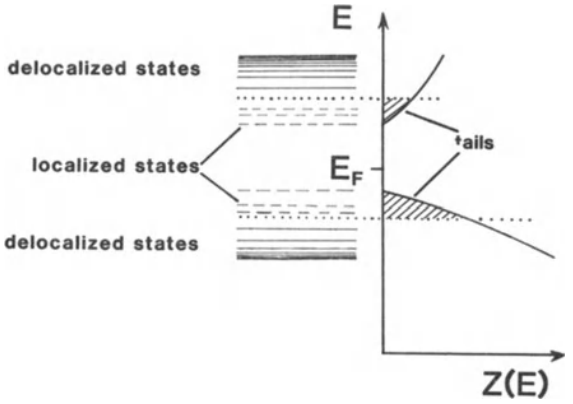

Figure 9.13. Localized and delocalized states and density of states $Z(E)$ for amorphous semiconductors. Note the band tails which are caused by the localized states.

absence of a periodic lattice causes substantial incoherent scattering. As a consequence, the room temperature conductivity in amorphous semiconductors is generally very low (about 10^{-5} 1/Ωm).

Some of the localized electrons might occasionally acquire sufficient thermal energy to overcome barriers which are caused by potential wells of variable depth and hop to a neighboring site. Thus, the conduction process in amorphous semiconductors involves a (temperature dependent) activation energy, Q_A, which leads to an equation similar to (9.5) describing a so-called variable range hopping:

$$\sigma_A = \sigma_0 \exp - \left(\frac{Q_A(T)}{k_B T} \right). \tag{9.7}$$

Equation (9.7), states that the conductivity in amorphous semiconductors increases exponentially with increasing temperature because any increase in thermal energy provides additional free carriers.

The understanding of amorphous metals, alloys, and semiconductors is still in its infancy. Future developments in this field should be followed with a great deal of anticipation because of the potentially significant applications which might arise in the years to come.

Problems

1. Calculate the mobility of the oxygen ions in UO_2 at 700 K. The diffusion coefficient of O^{2-} at this temperature is 10^{-13} cm^2/s. Compare this mobility with electron or hole mobilities in semiconductors (see Appendix 4). Discuss the difference!

2. Calculate the number of vacancy sites in an ionic conductor in which the metal ions are the predominant charge carriers. Assume the room temperature ionic conductivity to be 10^{-15} 1/Ωm and an ionic mobility of 10^{-17} m$^2/V$ s. Does the

calculated result make sense? Discuss how the vacancies might have been introduced into the crystal.

3. Calculate the activation energy for ionic conduction for a metal ion in an ionic crystal at 300 K. Take $D_0 = 10^{-3}$ m^2/s and $D = 10^{-17}$ m^2/s.

4. Calculate the ionic conductivity at 300 K for an ionic crystal. Assume 6×10^{20} Schottky defects per m^3, an activation energy of 0.8 eV and $D_0 = 10^{-3}$ m^2/s.

Suggestions for Further Reading (Part II)

N.W. Ashcroft and N.D. Mermin, *Solid State Physics* Holt, Rinehart and Winston, New York (1976)

A.R. Blythe, *Electrical Properties of Polymers*, Cambridge Univ. Press, Cambridge (1979)

M.H. Brodsky, ed., *Amorphous Semiconductors*, Springer–Verlag Berlin, Heidelberg, New York (1979)

R.H. Bube, *Electronic Properties of Crystalline Solids*, Academic Press, New York (1974)

S.K. Ghandi, *The Theory and Practice of Microelectronics*, J. Wiley, New York (1968)

N.J. Grant and B.C. Giessen eds., *Rapidly Quenched Metals*, Second Int. Conf. The Massachusetts Inst. of Techn., Boston, MA (1976)

B.H. Kear, B.C. Giessen, and K.M. Cohen eds., *Rapidly Solidified Amorphous and Crystalline Alloys*, North Holland Publ. Comp., New York, Amsterdam, Oxford (1982)

C. Kittel, *Introduction to Solid State Physics*, 5th ed., John Wiley and Sons Inc., New York (1976)

J. Mort and G. Pfister, eds., *Electronic Properties of Polymers*, J. Wiley and Sons, New York (1982)

M.A. Omar, *Elementary Solid State Physics*, Addison-Wesley Publ. Corp., Reading, MA (1978)

D.A. Seanov ed., *Electrical Properties of Polymers*, Academic Press, New York, London (1982)

B.G. Streetman, *Solid State Electronic Devices*, 2nd ed., Prentice-Hall, Englewood-Cliffs, NJ (1980)

S.M. Sze, *Physics of Semiconductor Devices*, 2nd ed., J. Wiley and Sons, New York (1981)

H.E. Talley and D.G. Daugherty, *Physical Principles of Semiconductor Devices*, Iowa University Press, Ames, IA (1976)

L.H. Van Vlack, *Physical Ceramics for Engineers*, Addison-Wesley Publ. Comp., Reading, MA (1964)

C.A. Wert and R.M. Thomson, *Physics of Solids*, 2nd ed., McGraw-Hill, New York (1970)

PART III

OPTICAL PROPERTIES OF MATERIALS

CHAPTER 10

The Optical Constants

10.1. Introduction

The most apparent properties of metals, their luster and their color, have been known to mankind since metals are known. Because of these properties, metals were already used in ancient times for mirrors and jewelry. The color was utilized 4000 years ago by the ancient Chinese as a guide to determine the composition of the melt of copper alloys: the hue of a preliminary cast indicated whether the melt, from which bells or mirrors were to be made, already had the right tin content.

The German poet Goethe was probably the first one who explicitly spelled out 200 years ago in his *Treatise on Color* that *color* is not an absolute, that is, measurable, property of matter (such as the resistivity) but requires a living being for its perception and description. Applying Goethe's findings, it was possible to explain qualitatively the color of, say, gold in simple terms. Goethe wrote: "If the color *blue* is removed from the spectrum, then blue, violet, and green are missing and red and yellow remain." Thin gold films are bluish-green when viewed in transmission. These colors are missing in reflection. Consequently, gold appears reddish-yellow.

This chapter treats the optical properties from a completely different point of view. Measurable quantities such as the index of refraction or the reflectivity and their spectral variations are used to characterize materials. In doing so, the term "color" will almost completely disappear from our vocabulary. Instead, it will be postulated that the interactions of the light with the valance electrons of a material are responsible for the optical properties. As in previous chapters, where an understanding of the electrical properties was attempted, an atomistic model and later a quantum mechanical treatment

will be employed. Thus, the electron theory of metals, as introduced in the first six chapters, will serve as a foundation.

It should be added in passing that the study of the interaction of light with matter laid the foundation for modern quantum theory at the beginning of this century. In recent years, optical methods have again become one of the most important tools for the study of the electronic structure of matter.

Before we start we need to define the optical constants. We make use of some elements of physics.

10.2. Index of Refraction, n

When light passes from an optically "thin" into an optically dense medium, one observes that in the dense medium, the angle of refraction β (that is, the angle between the refracted light beam and a line perpendicular to the surface) is smaller than the angle of incidence, α. This well-known phenomenon is used for the definition of the refractive power of a material and is called Snell's law:

$$\frac{\sin\alpha}{\sin\beta} = \frac{n_{\text{med}}}{n_{\text{vac}}} = n. \tag{10.1}$$

Commonly, the index of refraction for vacuum n_{vac} is arbitrarily set to be unity. The refraction is caused by the different velocities, c, of the light in the two media:

$$\frac{\sin\alpha}{\sin\beta} = \frac{c_{\text{vac}}}{c_{\text{med}}}. \tag{10.2}$$

Thus, if light passes from vacuum into a medium, we find

$$n = \frac{c_{\text{vac}}}{c_{\text{med}}} = \frac{c}{v}. \tag{10.3}$$

The magnitude of the refractive index depends on the wavelength of the incident light. This property is called dispersion. In metals, the index of refraction varies in addition with the angle of incidence. This is particularly true for small values of n.

10.3. Damping Constant, k

Metals damp the intensity of light in a relatively short distance. Thus, for characterizing the optical properties of metals, an additional material constant is needed.

We make use of the electromagnetic wave equation which mathematically describes the propagation of light in a medium. The derivation of this wave

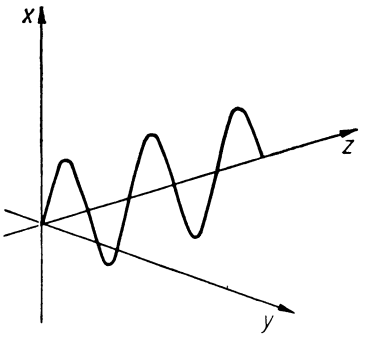

Figure 10.1. Plane polarized wave which propagates in the positive z-direction and vibrates in the x-direction.

equation from the well-known Maxwell equations does not further our understanding of the optical properties. (The interested reader can find the derivation in specialized texts.[1])

For simplification, we consider a plane polarized wave which propagates along the positive z-axis and, which vibrates in the x-direction (Fig. 10.1). We neglect possible magnetic properties. For this special case the electromagnetic wave equation reads

$$c^2 \frac{\partial^2 \mathscr{E}_x}{\partial z^2} = \varepsilon \ddot{\mathscr{E}}_x + 4\pi\sigma \dot{\mathscr{E}}_x, \tag{10.4}$$

where $\mathscr{E}_x$ is the x-component of the electric field strength,[2] ε the dielectric constant, and σ the (a.c.) conductivity. The solution to (10.4) is commonly achieved by using the following trial solution:

$$\mathscr{E}_x = \mathscr{E}_0 \exp\left[i\omega \left(t - \frac{zn}{c} \right) \right], \tag{10.5}$$

where $\mathscr{E}_0$ is the maximal value of the electric field strength (amplitude), and $\omega = 2\pi\nu$ is the angular frequency. Differentiating (10.5) once with respect to time, and twice with respect to time *and* z, and inserting these values into (10.4) yields

$$\hat{n}^2 = \varepsilon - \frac{4\pi\sigma}{\omega} i = \varepsilon - \frac{2\sigma}{\nu} i. \tag{10.6}$$

Equation (10.6) leads to an important result: The index of refraction is generally a complex quantity as inspection of the right-hand side of (10.6) indicates. We denote for clarity the complex index of refraction by $\hat{n}$. As is true

[1] For example, R.E. Hummel, *Optische Eigenschaften von Metallen und Legierungen*, Springer-Verlag, Berlin (1971).

[2] We use for the electric field strength $\mathscr{E}$ to distinguish it from the energy.

for all complex quantities, the complex index of refraction consists of a real and an imaginary part

$$\hat{n} = n_1 - in_2. \tag{10.7}$$

In the literature, the imaginary part of the index of refraction n_2 is often denoted by "k" and (10.7) is then written as

$$\hat{n} = n - ik. \tag{10.8}$$

We will call n_2 or k the *damping constant*. (In some books n_2 or k is named the *absorption constant*. We will not follow this practice because the latter term is extremely misleading. Other authors call k the *attenuation index* or the *extinction coefficient*.)

Squaring (10.8) yields together with (10.6)

$$\hat{n}^2 = n^2 - k^2 - 2nik = \varepsilon - \frac{2\sigma}{\nu} i. \tag{10.9}$$

Equating individually the real and imaginary parts of (10.9) yields two important relations between electrical and optical constants:

$$\varepsilon = n^2 - k^2 \tag{10.10}$$

$$\sigma = nk\nu. \tag{10.11}$$

Let us return to (10.9). The right-hand side is the difference between two dielectric constants (a real and an imaginary one). Thus, the left side must be a dielectric constant too and (10.9) may be rewritten as

$$\hat{n}^2 = n^2 - k^2 - 2nik \equiv \hat{\varepsilon} = \varepsilon_1 - i\varepsilon_2. \tag{10.12}$$

Equating individually the real and imaginary parts in (10.12) yields

$$\varepsilon_1 = n^2 - k^2 \tag{10.13}$$

and

$$\varepsilon_2 = 2nk. \tag{10.14}$$

Similarly as above, ε_1 and ε_2 are called the real and the imaginary parts of the complex dielectric constant $\hat{\varepsilon}$, respectively. (ε_1 in (10.13) is identical with ε in (10.10).) ε_2 is often called the *absorption product*, or briefly the *absorption*.

We consider a special case: For insulators ($\sigma \approx 0$ it follows from (10.11) that $k = 0$ (see also Table 10.1). Then (10.10) reduces to $\varepsilon = n^2$ (*Maxwell relation*).

From (10.10), (10.11), (10.13), and (10.14) one obtains:

$$n^2 = \frac{1}{2}\left(\sqrt{\varepsilon^2 + \left(\frac{2\sigma}{\nu}\right)^2} + \varepsilon\right) = \frac{1}{2}\left(\sqrt{\varepsilon_1^2 + \varepsilon_2^2} + \varepsilon_1\right) \tag{10.15}$$

$$k^2 = \frac{1}{2}\left(\sqrt{\varepsilon^2 + \left(\frac{2\sigma}{\nu}\right)^2} - \varepsilon\right) = \frac{1}{2}\left(\sqrt{\varepsilon_1^2 + \varepsilon_2^2} - \varepsilon_1\right) \tag{10.16}$$

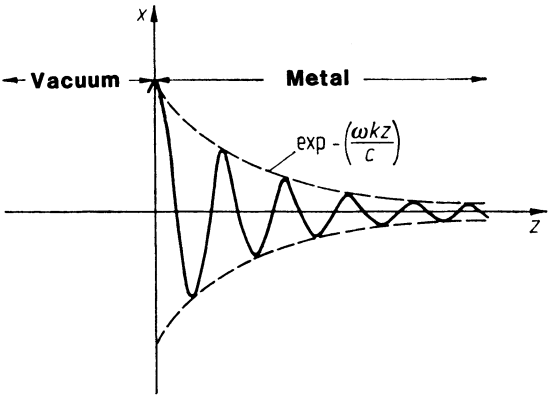

Figure 10.2. Modulated light wave. The amplitude decreases exponentially.

It should be emphasized that (10.10)–(10.16) are only valid if ε, σ, n and k are measured at the same wavelength, because these "constants" are wavelength dependent. For small frequencies, however, the d.c. values for ε and σ can be used with good approximation, as it will be shown later. Finally, it should be noted that the above equations are only valid for optically isotropic media; otherwise ε becomes a tensor.

We return now to (10.5) in which we replace the index of refraction by the general expression (10.8). This yields:

$$\mathscr{E}_x = \mathscr{E}_0 \exp\left[i\omega\left(t - \frac{z(n - ik)}{c}\right)\right] \tag{10.17}$$

which may be rewritten to read:

$$\mathscr{E}_x = \underbrace{\mathscr{E}_0 \exp\left[-\frac{\omega k}{c} z\right]}_{\text{Damped amplitude}} \cdot \underbrace{\exp\left[i\omega\left(t - \frac{zn}{c}\right)\right]}_{\text{Undamped wave}}. \tag{10.18}$$

Equation (10.18) is now the complete solution of the wave equation (10.4). It represents a damped wave and expresses that in matter the amplitude decreases exponentially with increasing z (Fig. 10.2). The constant k determines how much the amplitude decreases, that is, k expresses the degree of damping of the light wave. We understand now why k is termed the *damping constant*.

The result which we just obtained is well-known to electrical engineers. They observe that at high frequencies, the electromagnetic waves are conducted only on the outer surface of a wire. They call this phenomenon the (*normal*) *skin effect*.

Table 10.1. Characteristic Penetration Depth, W, and Damping Constant, k, for Some Materials

Material	Water	Flint glass	Graphite	Gold
W (cm)	32	29	6×10^{-6}	1.5×10^{-6}
k	1.4×10^{-7}	1.5×10^{-7}	0.8	3.2

10.4. Characteristic Penetration Depth, W

The field strength $\mathscr{E}$ is hard to measure. Thus, the intensity, I, which can be measured effortlessly with light sensitive devices (such as a photomultiplier tube) is commonly used. The intensity equals the square of the field strength. Thus, the damping term in (10.18) may be written as

$$I = \mathscr{E}^2 = I_0 \exp\left(-\frac{2\omega k}{c} z\right). \tag{10.19}$$

We define a characteristic penetration depth, W, as that distance at which the intensity of the light wave which travels through a material has decreased to $1/e$ or 37% of its original value, that is, when

$$\frac{I}{I_0} = \frac{1}{e} = e^{-1}. \tag{10.20}$$

This definition yields in conjunction with (10.19)

$$z = W = \frac{c}{2\omega k} = \frac{c}{4\pi\nu k} = \frac{\lambda}{4\pi k}. \tag{10.21}$$

Table 10.1 presents values for k and W for some materials obtained by using sodium vapor light ($\lambda = 589.3$ nm).

10.5. Reflectivity, R

Metals are characterized by a large reflectivity. This stems from the fact that light penetrates a metal only a short distance, as shown in Fig. 10.2 and Table 10.1. Thus, only a small part of the impinging energy is converted into heat. The major part of the energy is reflected. (In some cases close to 99%, see Table 10.2) In contrast to this, visible light penetrates into glass much farther than into metals, that is, approximately seven orders of magnitude more, see Table 10.1. As a consequence, very little light is reflected by glass. Nevertheless, a piece of glass about one or two meters thick eventually dissipates a substantial part of the impinging light into heat. (In practical applications, one does not observe this large reduction in light intensity because windows are as a rule only a few millimeters thick.) It should be noted that typical window panes reflect the light on the front as well as on the back side.

Table 10.2. Optical Constants of Some Metals ($\lambda = 600$ nm)

Metal	n	k	R [%]
Copper	0.14	3.35	95.6
Silver	0.05	4.09	98.9
Gold	0.21	3.24	92.9
Aluminum	0.97	6.0	90.3

The ratio between reflected intensity I_R and incoming intensity I_0 of the light serves as a definition for the reflectivity:

$$R = \frac{I_R}{I_0}. \tag{10.22}$$

Experiments have shown that for insulators, R depends solely on the index of refraction. For perpendicular incidence one finds

$$R = \frac{(n-1)^2}{(n+1)^2}. \tag{10.23}$$

This equation can be derived from Maxwell's equations.

We know already that n is generally a complex quantity. By definition, however, R has to remain real. Thus, the modulus of R becomes

$$R = \left|\frac{\hat{n}-1}{\hat{n}+1}\right|^2 \tag{10.24}$$

which yields

$$R = \frac{(n-ik-1)}{(n-ik+1)} \cdot \frac{(n+ik-1)}{(n+ik+1)} = \frac{(n-1)^2+k^2}{(n+1)^2+k^2} \tag{10.25}$$

(*Beer's equation*). The reflectivity is a unitless material constant and is often given in percent of the incoming light (see Table 10.2). R is, like the index of refraction, a function of the wavelength of the light.

The reflectivity is a function of ε_1 and ε_2. We shall derive this relationship by performing a few transformations. Equation (10.25) is rewritten as

$$R = \frac{n^2+k^2+1-2n}{n^2+k^2+1+2n} \tag{10.26}$$

(1) $$n^2+k^2 = \sqrt{(n^2+k^2)^2} = \sqrt{n^4+2n^2k^2+k^4}$$
$$= \sqrt{n^4-2n^2k^2+k^4+4n^2k^2} = \sqrt{(n^2-k^2)^2+4n^2k^2}$$
$$= \sqrt{\varepsilon_1^2+\varepsilon_2^2}, \tag{10.27}$$

(2) $$2n = \sqrt{4n^2} = \sqrt{2(n^2+k^2+n^2-k^2)} = \sqrt{2(\sqrt{\varepsilon_1^2+\varepsilon_2^2}+\varepsilon_1)}. \tag{10.28}$$

Inserting (10.27) and (10.28) into (10.26) provides

$$R = \frac{\sqrt{\varepsilon_1^2 + \varepsilon_2^2} + 1 - \sqrt{2(\sqrt{\varepsilon_1^2 + \varepsilon_2^2} + \varepsilon_1)}}{\sqrt{\varepsilon_1^2 + \varepsilon_2^2} + 1 + \sqrt{2(\sqrt{\varepsilon_1^2 + \varepsilon_2^2} + \varepsilon_1)}}. \tag{10.29}$$

10.6. Hagen–Rubens Relation

Our next task is to find a relationship between reflectivity and conductivity: For small frequencies, (i.e., $\nu < 10^{13}$ sec^{-1}) the ratio σ/ν for metals is very large (d.c. conductivity $\sigma_0 \approx 10^{17}$ sec^{-1}, $\varepsilon \approx 10$). Thus, we obtain

$$\frac{\sigma}{\nu} \approx \frac{10^{17}}{10^{13}} \gg \varepsilon. \tag{10.30}$$

Then, (10.15) and (10.16) reduce to

$$n^2 \approx \frac{\sigma}{\nu} \approx k^2. \tag{10.31}$$

The reflectivity may now be rewritten by combining (10.25) with (10.31) to read

$$R = \frac{n^2 + 2n + 1 + k^2 - 4n}{n^2 + 2n + 1 + k^2} = 1 - \frac{4n}{2n^2 + 2n + 1}. \tag{10.32}$$

If $2n + 1$ is neglected as small compared to $2n^2$ (which can be only done for small frequencies for which n is much larger than 1), then (10.32) reduces by using (10.31) to

$$R = 1 - \frac{2}{n} = 1 - 2\sqrt{\frac{\nu}{\sigma}}. \tag{10.33}$$

Finally, we set $\sigma = \sigma_0$ which is again only permissible for small frequencies, that is, in the infrared region of the spectrum. This yields the Hagen–Rubens equation:

$$\boxed{R = 1 - 2\sqrt{\frac{\nu}{\sigma_0}}} \tag{10.34}$$

which states that in the infrared (IR) region metals with large electrical conductivity are good reflectors. This equation was found empirically by Hagen and Rubens from reflectivity measurements in the IR and was derived theoretically by Drude. As stated above, the Hagen–Rubens relation is only valid at frequencies below 10^{13} sec^{-1}, or equivalently at wavelengths larger than about 30 μm.

Problems

1. Complete the intermediate steps between (10.5) and (10.6).
2. Calculate the conductivity from the index of refraction and the damping constant for copper (0.14 and 3.35, respectively; measurement at room temperature and $\lambda = 0.6\ \mu$m). Compare your result with the conductivity of copper which you may find in a handbook. You will notice a difference between these conductivities by several orders of magnitude. Why? (Compare only same units!)
3. Express n and k in terms of ε and σ (or ε_1 and ε_2) by using $\varepsilon = n^2 - k^2$ and $\sigma = nkv$. (Compare to (10.15) and (10.16).)
4. The intensity of Na-light passing through a gold film was measured to be about 15% of the incoming light. What is the thickness of the gold film? ($\lambda = 589$ nm; $k = 3.2$. *Note*: $I = \mathscr{E}^2$.)
5. Calculate the reflectivity of silver ($\lambda = 0.6\ \mu$m) and compare it with the reflectivity of flint glass ($n = 1.59$).
6. Calculate the characteristic penetration depth in aluminum for Na-light ($\lambda = 589$ nm; $k = 6$).
7. Derive the Hagen–Rubens relation from (10.29). (*Hint:* In the IR region $\varepsilon_2^2 \gg \varepsilon_1^2$ can be used. Justify this approximation.)
8. The transmissivity of a piece of glass of thickness $d = 1$ cm was measured at $\lambda = 589$ nm to be 89%. What would the transmissivity of this glass be if the thickness would be reduced to 0.5 cm?

CHAPTER 11

Atomistic Theory of the Optical Properties

11.1. Survey

In the preceding chapter, the optical constants and their relationship to electrical constants were introduced by employing the "continuum theory." The continuum theory considers only macroscopic quantities and interrelates experimental data. No assumptions are made about the structure of matter when formulating equations. Thus, the conclusions which have been drawn from the empirical laws in Chapter 10 should have general validity as long as nothing is neglected in a given calculation. The derivation of the Hagen–Rubens equation has served as an illustrative example for this.

The validity of equations derived from continuum theory is, however, often limited to frequencies for which the atomistic structure of metals does not play a major role. Experience shows that the atomistic structure needs not to be considered in the far infrared region. Thus, the Hagen–Rubens equation reproduces the experimental results in the far IR quite well. It has been found, however, that proceeding to higher frequencies (i.e., in the near IR and visible spectrum), the experimentally observed reflectivity decreases faster than predicted by the Hagen–Rubens equation (Fig. 11.1). For the visible and near IR an atomistic model needs to be considered to explain the optical behavior of metals. Drude did this important step at the turn of last century. He postulated that some electrons in a metal can be considered to be free, that is, they can be separated from their respective nuclei. He further assumed that the free electrons can be accelerated by an external electric field. This preliminary Drude model was refined by considering that the moving electrons collide with certain metal atoms in a nonideal lattice.

The free electrons are thought to perform periodic motions in the alternating electric field of the light. These vibrations are restrained by the above-

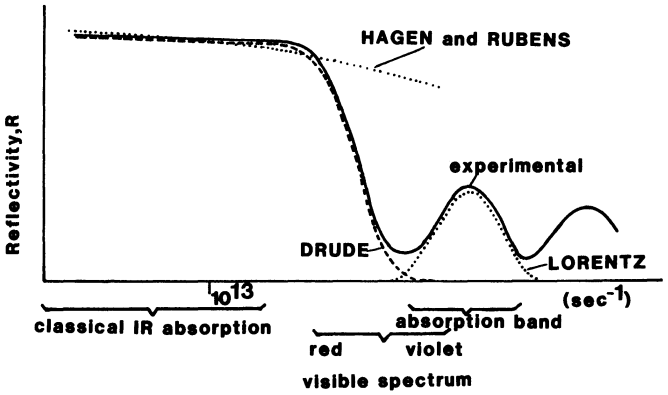

Figure 11.1. Schematic frequency dependence of the reflectivity of metals, experimentally (solid line) and according to three models.

mentioned interactions of the electrons with the atoms of a nonideal lattice. Thus, a *friction force* is introduced which takes this interaction into consideration. The calculation of the frequency dependence of the optical constants is accomplished by using the well-known equations for vibrations, whereby the interactions of electrons with atoms are taken into account by a damping term which is assumed to be proportional to the velocity of the electrons. The free electron theory describes, to a certain degree, the dispersion of the optical constants quite well. This is schematically shown in Fig. 11.1, in which the spectral dependence of the reflectivity is plotted for a specific case. The Hagen–Rubens relation reproduces the experimental findings only up to 10^{13} sec^{-1}. In contrast to this, the Drude theory correctly reproduces the spectral dependence of R even in the visible spectrum. Proceeding to yet higher frequencies, however, the experimentally found reflectivity eventually rises and then decreases again. Such an *absorption band* cannot be explained by the Drude theory. For its interpretation, a new concept needs to be applied.

Lorentz postulated that the electrons should be considered to be bound to their nuclei and that an external electric field displaces the positive charge of an atomic nucleus against the negative charge of its electron cloud. In other words, he represented each atom as an electric dipole. Retracting forces were thought to occur which try to eliminate the displacement of charges. Lorentz postulated further that the centers of gravity of the electric charges are identical if no external forces are present. However, if one shines light onto a solid, that is, if one applies an alternating electric field to the atoms, then the dipoles are thought to perform forced vibrations. Thus, a dipole is considered to behave similarly as a mass which is suspended on a spring, that is, the equations for a harmonic oscillator may be applied. An oscillator is known to absorb a maximal amount of energy when excited near its resonance frequency (Fig. 11.2). The absorbed energy is thought to be mainly dissipated

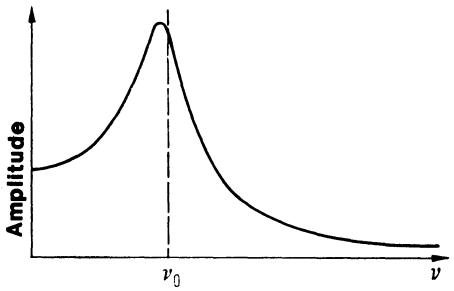

Figure 11.2. Frequency dependence of the amplitude of a harmonic oscillator which was excited to perform forced vibrations, assuming weak damping. ν_0 is the resonance frequency.

by diffuse radiation. Fig. 11.2 resembles an absorption band as shown in Fig. 11.1.

Thirty or forty years ago, many scientists considered the electrons in metals to behave at low frequencies as if they were free and at higher frequencies as if they were bound. In other words, electrons in a metal under the influence of light were described to behave as a series of classical free electrons and a series of classical harmonic oscillators. Insulators, on the other hand, were described by harmonic oscillators only.

We shall now treat the optical constants of materials by applying the above-discussed theories.

11.2. Free Electrons Without Damping

We consider the simplest case at first and assume that the free electrons are excited to perform forced but undamped vibrations under the influence of an external alternating field, i.e., under the influence of light. As explained in Section 11.1, the damping of the electrons is thought to be caused by collisions between electrons and atoms of a nonideal lattice. Thus, we neglect in this section the influence of lattice defects. For simplicity, we treat the one dimensional case because the result obtained this way does not differ from the general case. Thus, we consider the interaction of plane polarized light upon the electrons. The momentary value of the field strength of a plane polarized light wave is given by

$$\mathscr{E} = \mathscr{E}_0 \exp(i\omega t), \tag{11.1}$$

where $\omega = 2\pi\nu$ is the angular frequency, t the time, and $\mathscr{E}_0$ the maximal value of the field strength. The equation describing the motion of an electron which is excited to perform forced, harmonic vibrations under the influence of light is (see Appendix 1 and (7.6))

$$m\frac{d^2x}{dt^2} = e\mathscr{E}, \tag{11.2}$$

where e is the electron charge, m the electron mass, and $e \cdot \mathscr{E}$ the excitation force. The stationary solution of this vibrational equation is obtained by forming the second derivative of the trial solution $x = x_0 \exp(i\omega t)$ and inserting it into (11.2). This yields:

$$x = -\frac{e\mathscr{E}}{m4\pi^2\nu^2}. \tag{11.3}$$

The vibrating electons carry an electric dipole momentum which is the product of electron charge e and displacement x. The polarization P is defined to be the sum of the dipole moments of all N_f free electrons:

$$P = exN_f. \tag{11.4}$$

It is known from electrodynamics that the dielectric constant may be calculated from polarization and electric field strength as follows:

$$\varepsilon = 1 + 4\pi\frac{P}{\mathscr{E}}. \tag{11.5}$$

Inserting (11.3) and (11.4) into (11.5) yields

$$\hat{\varepsilon} = 1 - \frac{e^2N_f}{\pi m\nu^2}. \tag{11.6}$$

(It is appropriate to use in the present case the *complex* dielectric constant, see below.) The dielectric constant equals the square of the index of refraction n (see (10.12)). Equation (11.6) thus becomes

$$\hat{n}^2 = 1 - \frac{e^2N_f}{\pi m\nu^2}. \tag{11.7}$$

We consider two special cases:

(a) For small frequencies, the term $e^2N_f/\pi m\nu^2$ becomes larger than one. Then $\hat{n}^2$ is negative and $\hat{n}$ imaginary. An imaginary $\hat{n}$ means that the real part of $\hat{n}$ disappears. Thus, the reflectivity becomes 100% (see Section 10.5, Fig. 11.3, and Problem 1).

(b) For large frequencies (UV light), the term $e^2N_f/\pi m\nu^2$ becomes smaller than one. Thus, $\hat{n}^2$ is positive and $\hat{n} \equiv n$ real (but smaller than one). The material is transparent for these wavelengths (and perpendicular incidence) and behaves optically like an insulator, see Fig. 11.3.

We define a characteristic frequency ν_1, often called the *plasma frequency*, which separates the reflective from the transparent region (Fig. 11.3). The plasma frequency is defined by setting $e^2N_f/\pi m\nu_1^2$ equal to unity which yields

$$\nu_1^2 = \frac{e^2N_f}{\pi m}. \tag{11.8}$$

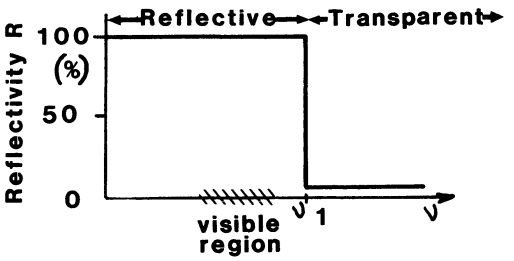

Figure 11.3. Schematic frequency dependence of an alkali metal according to the free electron theory without damping. ν_1 is the plasma frequency.

Table 11.1

Metal	Li	Na	K	Rb	Cs
$\nu_1 \cdot 10^{-14}$ s^{-1}, observed	14.6	14.3	9.52	8.33	6.81
$\nu_1 \cdot 10^{-14}$ s^{-1}, calculated	19.4	14.3	10.34	9.37	8.33
λ_1 *nm* ($= c/\nu_1$), observed	150	210	290	320	360
N_{eff}[free electrons/atom]	0.57	1.0	0.8	0.79	0.67

We conclude from (11.6) that the dielectric constant becomes zero at the plasma frequency because of $e^2 N_f/\pi m \nu_1^2 = 1$. $\hat{\varepsilon} = 0$ is the condition for a *plasma oscillation*, that is, a fluidlike oscillation of the entire electron gas. We will discuss this phenomenon in detail in Section 13.2.2.

The alkali metals behave essentially as shown in Fig. 11.3. They are transparent in the near UV and reflect the light in the visible region. This result indicates that the *s*-electrons[3] of the outer shell of the alkali metals can be considered to be free.

Table 11.1 contains some measured as well as some calculated plasma frequencies. For the calculations, applying (11.8), *one* free electron per atom was assumed. This means that N_f was set equal to the number of atoms per volume N_a. (The latter quantity is obtained by using

$$N_a = \frac{N_0 \cdot \delta}{W} \tag{11.9}$$

where N_0 is the Avogadro constant, δ = density and W = atomic weight.)

We note in Table 11.1 that the calculated and the observed values for ν_1 are only identical for sodium. This may be interpreted to mean that only in sodium exactly *one* free electron per atom is contributing to the electron gas. For other metals an "effective number of free electrons" is commonly introduced which is defined to be the ratio between observed and calculated ν_1^2 values:

[3] See Appendix 3.

$$\frac{\nu_1^2 \text{ (Observed)}}{\nu_1^2 \text{ (Calculated)}} = N_{\text{eff}}. \tag{11.10}$$

The effective number of free electrons is a parameter which is of great interest because it is contained in a number of nonoptical equations (such as Hall constant, electrotransport, superconductivity, etc.). Since for most metals the plasma frequency, ν_1, cannot be measured as readily as for the alkalis, another avenue for determining N_{eff} has to be found. For reasons which will become clear later, N_{eff} can be obtained by measuring n and k in the red or IR spectrum (that is, in a frequency range without absorption bands, Fig. 11.1) and by applying

$$N_{\text{eff}} = \frac{(1 - n^2 + k^2)\nu^2 \pi m}{e^2}. \tag{11.10a}$$

Equation (11.10a) follows by combining (11.6) with (10.10) and replacing N_f by N_{eff}.

11.3. Free Electrons with Damping (Classical Free Electron Theory of Metals)

The simple reflectivity spectrum as depicted in Fig. 11.3 is seldom found for metals. We need to refine our model. We postulate that the motion of electrons in metals is damped. More specifically, we postulate that the velocity is reduced by collisions of the electrons with atoms of a nonideal lattice. Lattice defects may be introduced into a solid by interstitial atoms, vacancies, impurity atoms, dislocations, grain boundaries, or thermal motion of the atoms.

To take account of the damping, we add to the vibration equation (11.2) a damping term $\gamma(dx/dt)$ which is proportional to the velocity (See Appendix 1 and (7.7))

$$m\frac{d^2x}{dt^2} + \gamma\frac{dx}{dt} = e\mathscr{E} = e\mathscr{E}_0 \exp(i\omega t). \tag{11.11}$$

We determine at first the damping factor γ. For this we write a particular solution of (11.11) which is obtained by assuming that the electrons drift with a velocity $v' = \text{const}$ through the crystal. (The drift velocity of the electrons, which is caused by an external field is superimposed on the random motion of the electrons.) The damping is depicted to be a friction force which counteracts the electron motion. $v' = \text{const}$ yields

$$\frac{d^2x}{dt^2} = 0. \tag{11.12}$$

By using (11.12), equation (11.11) becomes

$$\frac{e\mathscr{E}}{\gamma} = \frac{dx}{dt} = v'. \tag{11.13}$$

The drift velocity is

$$v' = \frac{j}{eN_f} \tag{11.14}$$

(see (7.4)), where j is the current density (i.e., that current which passes in one second through an area of one m^2). N_f is the number of free electrons per m^3. The current density is connected with the d.c. conductivity σ_0 and the field strength $\mathscr{E}$ by Ohm's law (7.2)

$$j = \sigma_0 \mathscr{E}. \tag{11.15}$$

Inserting (11.14) and (11.15) into (11.13) yields

$$\gamma = \frac{N_f e^2}{\sigma_0}. \tag{11.16}$$

Thus, (11.11) becomes

$$m\frac{d^2x}{dt^2} + \frac{N_f e^2}{\sigma_0}\frac{dx}{dt} = e\mathscr{E} = e\mathscr{E}_0 \exp(i\omega t). \tag{11.17}$$

We note that the damping term in (11.17) is inversely proportional to the conductivity, that is, proportional to the resistivity. This result makes sense.

The stationary solution of (11.17) is obtained, similarly as in Section 11.2 by differentiating the trial solution $x = x_0 \exp(i\omega t)$ by the time, and inserting first and second derivatives into (11.17) which yields

$$-m\omega^2 x + \frac{N_f e^2}{\sigma_0} x\omega i = \mathscr{E} e. \tag{11.18}$$

Rearranging (11.18) provides

$$x = \frac{\mathscr{E}}{\frac{N_f e\omega}{\sigma_0} i - \frac{m\omega^2}{e}}. \tag{11.19}$$

Inserting (11.19) into (11.4) yields the polarization

$$P = \frac{eN_f \mathscr{E}}{\frac{N_f e\omega}{\sigma_0} i - \frac{m\omega^2}{e}}. \tag{11.20}$$

With (11.20) and (11.5) the complex dielectric constant becomes

$$\hat{\varepsilon} = 1 + 4\pi\frac{P}{\mathscr{E}} = 1 + \frac{1}{\frac{\nu}{2\sigma_0} i - \frac{m\pi}{N_f e^2}\nu^2}. \tag{11.21}$$

Table 11.2

Metal	Li	Na	K	Rb	Cs	Cu	Ag	Au
$\rho_0 \cdot 10^8\ \Omega m^a$	8.55	4.2	6.15	12.5	20	1.67	1.59	2.35
$\sigma_0 \cdot 10^{-17}\ s^{-1}$	1.05	2.14	1.46	0.72	0.45	5.37	5.66	3.83
$\nu_2 \cdot 10^{-12}\ s^{-1}$	10.1	4.8	3.1	4.82	5.15	4.7	4.35	5.9

[a] Handbook of Chemistry and Physics, 1977; room temperature values.

The term $N_f e^2/m\pi$ is set, as in (11.8), equal to ν_1^2, which reduces (11.21) to

$$\hat{\varepsilon} = 1 + \frac{1}{\frac{\nu}{2\sigma_0} i - \frac{\nu^2}{\nu_1^2}} = 1 + \frac{\nu_1^2}{i\nu\frac{\nu_1^2}{2\sigma_0} - \nu^2}. \tag{11.22}$$

The term $\nu_1^2/2\sigma_0$ in (11.22) has the unit of a frequency. Thus, for abbreviation we define a *damping frequency*:

$$\nu_2 = \frac{\nu_1^2}{2\sigma_0}. \tag{11.23}$$

(Table 11.2 lists values for ν_2 which were calculated using experimental σ_0 and ν_1 values.) Now (11.22) becomes:

$$\hat{\varepsilon} = 1 + \frac{\nu_1^2}{i\nu\nu_2 - \nu^2}, \tag{11.24}$$

where $\hat{\varepsilon}$ is, as usual, identical to $\hat{n}^2$:

$$(\hat{n})^2 = n^2 - 2nki - k^2 = 1 - \frac{\nu_1^2}{\nu^2 - \nu\nu_2 i}. \tag{11.25}$$

Multiplying numerator and denominator of the fraction in (11.25) by the complex conjugate of the denominator ($\nu^2 + \nu\nu_2 i$) allows us to individually equate real and imaginary parts. This provides the Drude equations for the optical constants:

$$\boxed{n^2 - k^2 = \varepsilon_1 = 1 - \frac{\nu_1^2}{\nu^2 + \nu_2^2}} \tag{11.26}$$

and

$$\boxed{2nk = \varepsilon_2 = \frac{2\sigma}{\nu} = \frac{\nu_2}{\nu}\frac{\nu_1^2}{\nu^2 + \nu_2^2},} \tag{11.27}$$

with the characteristic frequencies

$$\nu_1 = \sqrt{\frac{e^2 N_f}{\pi m}} \tag{11.8}$$

and

$$\nu_2 = \frac{\nu_1^2}{2\sigma_0}. \tag{11.23}$$

It is noted that the conductivity σ_0 (in cgs units) has the unit $\sec^{-1}$ as can be easily seen from (11.23). The conversion factor from practical units into cgs units is given in Appendix 4. σ and ε_1 in (11.26) and (11.27) need to be measured at the same frequency as n and k. They are *not* identical with the d.c. conductivity σ_0 and the d.c. dielectric constant ε_0.

11.4. Discussion of the Drude Equations

11.4.1. Absorption

We discuss (11.27) for the UV, visible and near IR region, at which the frequency varies between 10^{14} and 10^{15} s^{-1}. The average damping frequency ν_2 is 5×10^{12} s^{-1} (Table 11.2). Thus $\nu^2 \gg \nu_2^2$. Equation (11.27) becomes, therefore,

$$\varepsilon_2 = \frac{\nu_2}{\nu}\frac{\nu_1^2}{\nu^2}. \tag{11.28}$$

With $\nu \approx \nu_1$ (Table 11.1) we obtain

$$\varepsilon_2 = \frac{\nu_2}{\nu}. \tag{11.29}$$

Thus, ε_2 plotted versus the frequency yields a hyperbola with ν_2 as parameter (Fig. 11.4).

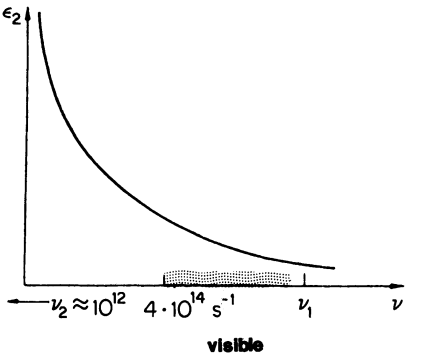

Figure 11.4. The absorption $\varepsilon_2 = 2nk$ versus frequency ν according to the free electron theory (schematic).

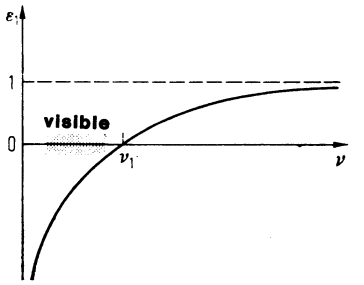

Figure 11.5. The polarization $\varepsilon_1 = n^2 - k^2$ as a function of frequency according to the Drude theory (schematic).

11.4.2. Polarization

We insert in (11.26) three specific frequencies:

a) $\nu = 0$, yields $\varepsilon_1 = 1 - (\nu_1^2/\nu_2^2) \approx -10^6$ (large negative value);
b) $\nu \to \infty$, yields $\varepsilon_1 \to 1$;
c) $\varepsilon_1 = 0$, yields $\nu = \sqrt{\nu_1^2 - \nu_2^2} \approx \nu_1 \approx 10^{15}\ \mathrm{s}^{-1}$.

ε_1 is schematically depicted in Fig. 11.5 as a function of frequency.

11.4.3. Small Frequencies (Far IR)

For very small frequencies ($\nu^2 \ll \nu_2^2$) we may neglect ν^2 in the denominator of (11.27). This yields with (11.23):

$$nk\nu = \sigma = \frac{1}{2}\frac{\nu_1^2}{\nu_2} = \sigma_0. \tag{11.30}$$

Thus, in the far IR the a.c. conductivity σ and the d.c. conductivity σ_0 may be considered to be identical. We already made use of this condition in Section 10.6.

11.5. Reflectivity

The reflectivity of metals is calculated using *Beer's equation* (10.25) or equation (10.29). The calculation of R from (10.29) in conjunction with (11.26) and (11.27) is relatively cumbersome. Thus, a few approximations have been derived which have the advantage that a quick survey of the reflection spectra can be obtained (Table 11.3). These approximations are, of course, valid only in the frequency range, at which the Drude equations are valid, i.e., as long as

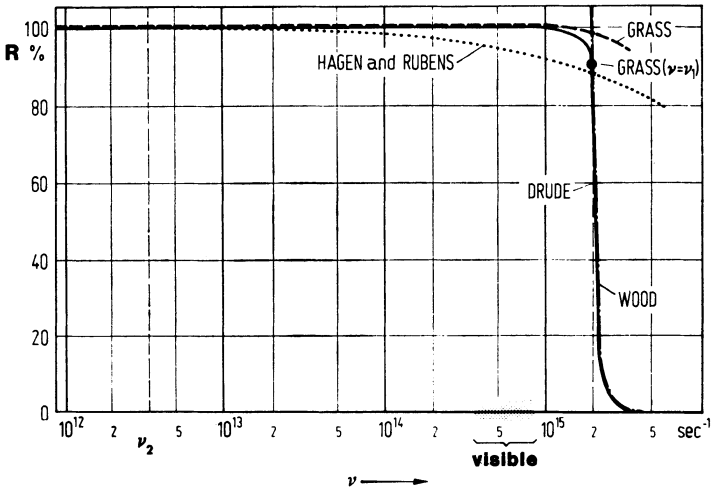

Figure 11.6. Calculated spectral reflectivity using the exact Drude equation (solid line) and the approximations of Table 11.3 using $\nu_1 = 2 \times 10^{15}\ s^{-1}$ and $\nu_2 = 3.5 \times 10^{12}\ s^{-1}$.

Table 11.3

Frequency range	Reflectivity	Reference
$\nu < 10^{13}\ s^{-1}$	$R = 1 - 2\sqrt{\frac{\nu}{\sigma_0}}$	Hagen–Rubens
$\nu_2 < \nu \ll \nu_1$	$R = 1 - \frac{\nu_1^2}{\sigma_0 \nu \sqrt{\frac{\nu_1^2}{\nu^2} - 1}}$	Grass[a]
	$R = 1 - \frac{2\nu_2}{\nu_1} = 1 - \frac{\nu_1}{\sigma_0}$	Försterling
$\nu > \nu_1$	$R = \frac{\delta + 1 - 2\sqrt{\delta}}{\delta + 1 + 2\sqrt{\delta}}$, where $\delta = 1 - \frac{\nu_1^2}{\nu^2}$	Wood[b]
$\nu = \nu_1$	$R = \frac{\alpha - 1}{\alpha + 1}$, where $\alpha = \sqrt{\frac{\nu_1}{2\nu_2}}$	Grass[a]

[a] Grass, G., *Z. Phys.* **139**, 358 (1954).
[b] Wood, R.W., *Physical Optics*, Macmillan Company, New York (1933).

no absorption bands are present. The *Hagen–Rubens equation* is one of these approximations which follows from (10.29) for small frequencies. Figure 11.6 depicts the calculated reflectivity spectra using the exact equation (10.29) and the approximations listed in Table 11.3, for a special case.

11.6. Bound Electrons (Classical Electron Theory of Dielectric Materials)

The preceding sections have shown that the optical properties of metals can be described and calculated quite well in the low frequency range by applying the free electron theory. We mentioned already that this theory has its limits at higher frequencies at which we observe that light is absorbed by metals as well as nonmetals in a narrow frequency band. To interpret these absorption bands, Lorentz postulated that the electrons are bound to their respective nuclei. He assumed that under the influence of an external electric field, the positively charged nucleus and negatively charged electron cloud are displaced with respect to each other (Fig. 11.7). An electrostatic force tries to counteract this displacement. For simplicity we describe the negative charge of the electrons to be united in one point. Thus, we describe the atom in an electric field as consisting of a positively charged core which is bound quasi-elastically to *one* electron (electric dipole, Fig. 11.8). A bound electron, thus, may be compared to a mass which is suspended from a spring. Under the influence of an alternating electric field (that is, by light), the electron is thought to perform forced vibrations. For the description of these vibrations,

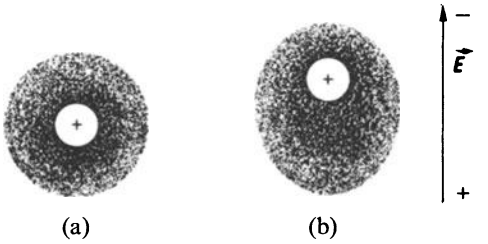

Figure 11.7. An atom is represented by a positively charged core and a surrounding, negatively charged electron cloud (a) in equilibrium (b) in an external electric field.

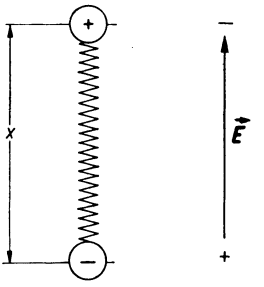

Figure 11.8. Quasielastic bound electron in an external electric field (harmonic oscillator).

the well-known equations of mechanics dealing with a harmonic oscillator may be applied. This will be done now.

We consider at first an isolated atom, that is, we neglect the influence of the surrounding atoms upon the electron. An external electric field with force

$$e\mathscr{E} = e\mathscr{E}_0 \exp(i\omega t) \tag{11.31}$$

displaces an electron from its rest position by a distance x. This displacement is counteracted by a restoring force $\kappa \cdot x$ which is proportional to the displacement x. Then, the vibration equation becomes (see Appendix 1)

$$m\frac{d^2x}{dt^2} + \gamma'\frac{dx}{dt} + \kappa x = e\mathscr{E}_0 \exp(i\omega t). \tag{11.32}$$

The factor κ is the *spring constant* which determines the binding strength between atom and electron. Each vibrating dipole (e.g., an antenna) loses energy by radiation. Thus, $\gamma'(dx/dt)$ represents the damping of the oscillator by radiation (γ' = damping constant). The stationary solution to (11.32) for weak damping is (see Appendix 1)

$$x = \frac{e\mathscr{E}_0}{\sqrt{m^2(\omega_0^2 - \omega^2)^2 + \gamma'^2\omega^2}} \exp i(\omega t - \phi), \tag{11.33}$$

where

$$\omega_0 = 2\pi\nu_0 = \sqrt{\frac{\kappa}{m}} \tag{11.34}$$

is called the resonance frequency of the oscillator, i.e., that frequency at which the electron vibrates freely without an external force. ϕ is the phase difference between forced vibration and the excitation force of the light wave. It is defined to be (see Appendix 1)

$$\tan\phi = \frac{\gamma'\omega}{m(\omega_0^2 - \omega^2)} = \frac{\gamma'\nu}{2\pi m(\nu_0^2 - \nu^2)}. \tag{11.35}$$

As in the previous sections, we calculate the optical constants starting with the polarization P which is the product of the dipole moment $e \cdot x$ of *one* dipole times the number of all dipoles (oscillators) N_a. As before we assumed *one* oscillator per atom. Thus, N_a is identical to the number of atoms per unit volume. We obtain

$$P = exN_a. \tag{11.36}$$

Inserting (11.33) yields

$$P = \frac{e^2N_a\mathscr{E}_0 \exp i(\omega t - \phi)}{\sqrt{m^2(\omega_0^2 - \omega^2)^2 + \gamma'^2\omega^2}}. \tag{11.37}$$

With

$$\exp i(\omega t - \phi) = \exp(i\omega t) \cdot \exp(-i\phi) \tag{11.38}$$

we obtain

$$P = \frac{e^2 N_a \mathscr{E}}{\sqrt{m^2(\omega_0^2 - \omega^2)^2 + \gamma'^2\omega^2}} \exp(-i\phi), \tag{11.39}$$

which yields with (11.5) and (10.12)

$$\hat{\varepsilon} = n^2 - k^2 - 2nki = 1 + \frac{4\pi e^2 N_a}{\sqrt{m^2(\omega_0^2 - \omega^2)^2 + \gamma'^2\omega^2}} \exp(-i\phi). \tag{11.40}$$

Equation (11.40) becomes with[4]

$$\exp(-i\phi) = \cos\phi - i\sin\phi, \tag{11.41}$$

$$\begin{aligned} n^2 - k^2 - 2nki = 1 &+ \frac{4\pi e^2 N_a}{\sqrt{m^2(\omega_0^2 - \omega^2)^2 + \gamma'^2\omega^2}} \cos\phi \\ &- i \frac{4\pi e^2 N_a}{\sqrt{m^2(\omega_0^2 - \omega^2)^2 + \gamma'^2\omega^2}} \sin\phi. \end{aligned} \tag{11.42}$$

The trigonometric terms in (11.42) are replaced, using (11.35), as follows:

$$\cos\phi = \frac{1}{\sqrt{1 + \tan^2\phi}} = \frac{m(\omega_0^2 - \omega^2)}{\sqrt{m^2(\omega_0^2 - \omega^2)^2 + \gamma'^2\omega^2}}, \tag{11.43}$$

$$\sin\phi = \frac{\tan\phi}{\sqrt{1 + \tan^2\phi}} = \frac{\gamma'\omega}{\sqrt{m^2(\omega_0^2 - \omega^2)^2 + \gamma'^2\omega^2}}. \tag{11.44}$$

Separating the real and imaginary parts in (11.42) finally provides the optical constants:

$$\varepsilon_1 = n^2 - k^2 = 1 + \frac{4\pi e^2 m N_a(\omega_0^2 - \omega^2)}{m^2(\omega_0^2 - \omega^2)^2 + \gamma'^2\omega^2},$$

that is,

$$\boxed{\varepsilon_1 = 1 + \frac{4\pi e^2 m N_a(\nu_0^2 - \nu^2)}{4\pi^2 m^2(\nu_0^2 - \nu^2)^2 + \gamma'^2\nu^2},} \tag{11.45}$$

and

$$\varepsilon_2 = 2nk = \frac{4\pi e^2 N_a \gamma'\omega}{m^2(\omega_0^2 - \omega^2)^2 + \gamma'^2\omega^2}$$

or

[4] See Appendix 2.

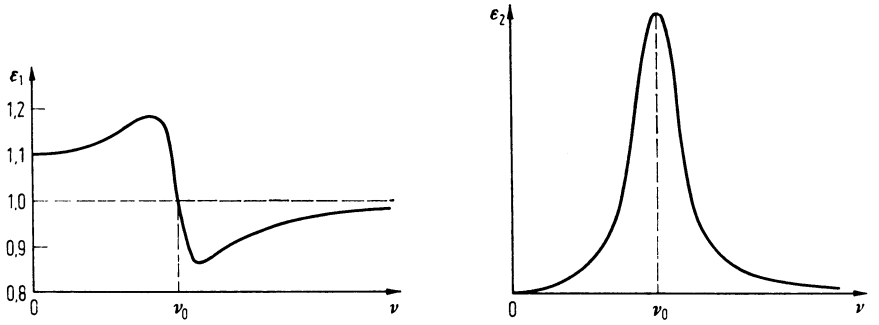

Figures 11.9 and 11.10. Frequency dependence of polarization $\varepsilon_1 = n^2 - k^2$ and absorption $\varepsilon_2 = 2nk$, as calculated with (11.45) and (11.46), respectively, using characteristic values for N_a and γ'.

$$\varepsilon_2 = \frac{2e^2 N_a \gamma' \nu}{4\pi^2 m^2 (\nu_0^2 - \nu^2)^2 + \gamma'^2 \nu^2}. \tag{11.46}$$

The frequency dependencies of ε_1 and ε_2 are plotted in Figs. 11.9 and 11.10. Figure 11.9 resembles the dispersion curve for the index of refraction as it is experimentally obtained for dielectrics. Figure 11.10 depicts the absorption product ε_2 in the vicinity of the resonance frequency ν_0 (absorption band) as experimentally observed for dielectrics. Equations (11.45) and (11.46) reduce to the Drude equations for $\nu_0 \to 0$ (no oscillators).

*11.7. Discussion of the Lorentz Equations for Special Cases

11.7.1. High Frequencies

We observe in Fig. 11.10 that ε_2 approaches zero at very high frequencies and far away from any resonances (absorption bands). In the same frequency region, $\varepsilon_1 = n^2 - k^2$ and thus, essentially n assumes the constant value 1 (Fig. 11.9). This is consistent with experimental observations that X-rays are not refracted and are not absorbed by many materials.

11.7.2. Small Damping

We consider the case for which the radiation induced energy loss of the oscillator is very small. Then, γ' is small. With $\gamma'^2 \nu^2 \ll 4\pi^2 m^2 (\nu_0^2 - \nu^2)^2$ (which is only valid for $\nu \neq \nu_0$), equation (11.45) reduces to

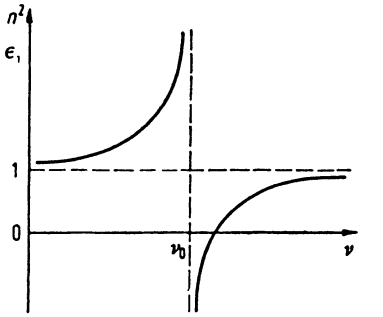

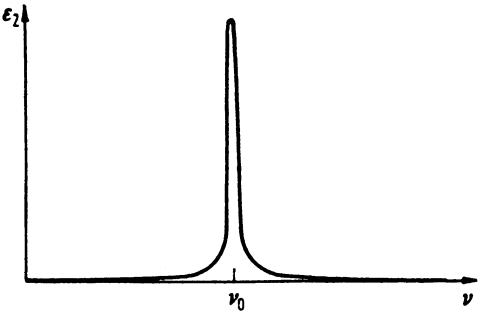

Figures 11.11 and 11.12. The functions $\varepsilon_1(n^2)$ and ε_2, respectively, versus frequency according to the bound electron theory for the special case of small damping.

$$\varepsilon_1 = n^2 - k^2 = 1 + \frac{e^2 N_a}{\pi m(\nu_0^2 - \nu^2)}. \tag{11.47}$$

Figure 11.11 depicts a sketch of (11.47). We observe that for small damping, ε_1 (and thus essentially n^2) approaches infinity near the resonance frequency. A dispersion curve, such as Fig. 11.11, is indeed observed for many dielectrics (glass, etc.).

11.7.3. Absorption Near ν_0

Electrons absorb most energy from light at the resonance frequency, that is, ε_2 has a maximum near ν_0. For small damping, the absorption band becomes an absorption line (see Fig. 11.12). Inserting $\nu = \nu_0$ into (11.46) yields:

$$\varepsilon_2 = \frac{2e^2 N_a}{\gamma' \nu_0} \tag{11.48}$$

which shows that the absorption becomes large for small damping (γ').

11.7.4. More Than One Oscillator

At the beginning of Section 11.6 we assumed that *one* electron is quasielastically bound to a given nucleus; in other words we assumed *one* oscillator per atom. This assumption is certainly a gross simplification, as one can deduce from the occurrence of multiple absorption bands in experimental optical spectra. Thus, each atom has to be associated with a number of i oscillators each having an oscillator strength, f_i. The ith oscillator vibrates with its resonance frequency ν_{0i}. The related damping constant is γ_i'. (This description has its equivalent in the mechanics of a system of mass points having one basic

frequency and higher harmonics.) If all oscillators are taken into account, (11.45) and (11.46) become

$$\varepsilon_1 = n^2 - k^2 = 1 + 4\pi e^2 m N_a \sum_i \frac{f_i(\nu_{0i}^2 - \nu^2)}{4\pi^2 m^2 (\nu_{0i}^2 - \nu^2)^2 + \gamma_i'^2 \nu^2}, \tag{11.49}$$

$$\varepsilon_2 = 2nk = 2e^2 N_a \sum_i \frac{f_i \nu \gamma_i'}{4\pi^2 m^2 (\nu_{0i}^2 - \nu^2)^2 + \gamma_i'^2 \nu^2}. \tag{11.50}$$

Equations (11.49) and (11.50) reduce for weak damping (see above) to:

$$\varepsilon_1 = n^2 - k^2 \approx n^2 = 1 + \frac{e^2 N_a}{\pi m} \sum_i \frac{f_i}{\nu_{0i}^2 - \nu^2}, \tag{11.51}$$

$$\varepsilon_2 = 2nk = \frac{e^2 N_a}{2\pi^2 m^2} \sum_i \frac{f_i \nu \gamma_i'}{(\nu_{0i}^2 - \nu^2)^2}. \tag{11.52}$$

11.8. Contributions of Free Electrons and Harmonic Oscillators to the Optical Constants

In the previous section, we ascribed two different properties to the electrons of a solid. In Section 11.4 we postulated that N_f electrons move freely in metals under the influence of an electric field and that this motion is damped by collisions of the electrons with vibrating lattice atoms and lattice defects. In Section 11.6 we postulated that a certain number of electrons are quasielastically bound to N_a atoms which are excited by light to perform forced vibrations. The energy loss was thought to be by radiation.

The optical properties of metals may be described by postulating a certain number of free electrons and a certain number of harmonic oscillators. Both the free electrons and the oscillators contribute to the polarization. Thus, the equations for the optical constants may be rewritten, by combining (11.26), (11.27), (11.49), and (11.50):

$$\varepsilon_1 = 1 - \frac{\nu_1^2}{\nu^2 + \nu_2^2} + 4\pi e^2 m N_a \sum_i \frac{f_i(\nu_{0i}^2 - \nu^2)}{4\pi^2 m^2 (\nu_{0i}^2 - \nu^2)^2 + \gamma_i'^2 \nu^2}, \tag{11.53}$$

$$\varepsilon_2 = 2nk = \frac{\nu_2}{\nu} \frac{\nu_1^2}{\nu^2 + \nu_2^2} + 2e^2 N_a \sum_i \frac{f_i \nu \gamma_i'}{4\pi^2 m^2 (\nu_{0i}^2 - \nu^2)^2 + \gamma_i'^2 \nu^2}. \tag{11.54}$$

Figures 11.13 and 11.14 depict schematically the frequency dependence of ε_1 and ε_2 as obtained by using (11.53) and (11.54). These figures also show the contributions of free and bound electrons on the optical constants. The experimentally found frequency dependence of ε_1 and ε_2 resembles these calculated spectra quite well. We will elaborate on this in Chapter 13 in which experimental results are presented.

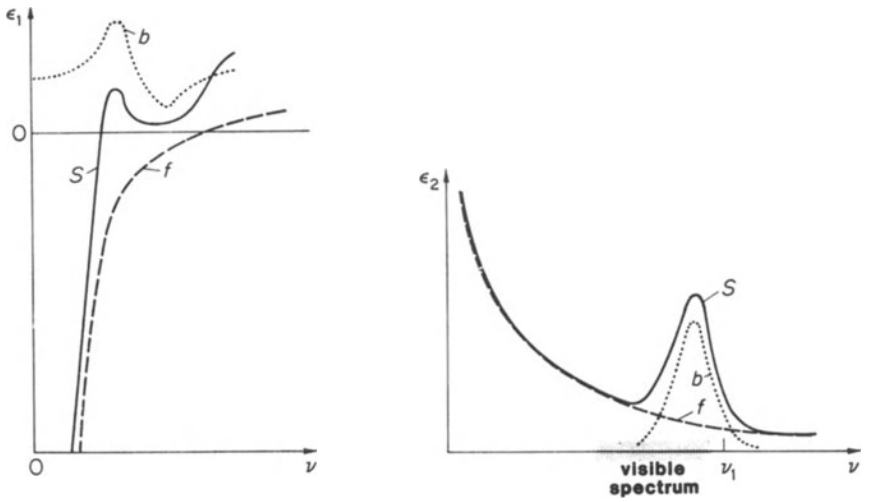

Figures 11.13 and 11.14. Frequency dependence of ε_1 and ε_2 according to (11.53) and (11.54). $(i = 1) \cdot f$ = free electron theory; b = bound electron theory; S = summary curve (schematic).

Problems

1. Calculate the reflectivity of sodium in the frequency ranges $\nu > \nu_1$ and $\nu < \nu_1$ using the theory for free electrons without damping. Sketch R versus frequency.
2. The plasma frequency, ν_1, can be calculated for the alkali metals by assuming *one* free electron per atom, i.e., by substituting N_f by the number of atoms per unit volume (atomic density N_a). Calculate ν_1 for potassium and lithium.
3. Calculate N_{eff} for sodium and potassium. For which of these two metals is the assumption of *one* free electron per atom justified?
4. What is the meaning of the frequencies ν_1 and ν_2? In which frequency ranges are they situated compared to visible light?
5. Calculate the reflectivity of gold at $\nu = 9 \times 10^{12}\ s^{-1}$ from its conductivity. Is the reflectivity increasing or decreasing at this frequency when the temperature is increased? Explain.
6. Calculate ν_1 and ν_2 for silver (0.5×10^{29} free electrons per m^3).
7. The experimentally found dispersion of NaCl is as follows:

$\lambda[\mu m]$	0.3	0.4	0.5	0.7	1	2	5
n	1.607	1.568	1.552	1.539	1.532	1.527	1.519

Plot these results along with calculated values, obtained by using the equations of the "bound electron theory" assuming small damping. Let:

$$\frac{e^2 N_a}{\pi m} = 1.81 \times 10^{30}\ \mathrm{s}^{-2} \quad \text{and} \quad \nu_0 = 1.47 \times 10^{15}\ \mathrm{s}^{-1}.$$

8. The optical properties of an absorbing medium can be characterized by various sets of parameters. One such set is the index of refraction and the damping constant. Explain the physical significance of those parameters, and indicate how they are related to the complex dielectric constant of the medium. What other set of parameters are commonly used to characterize the optical properties? Why are there always "sets" of parameters?

9. Describe the damping mechanisms for free electrons and bound electrons, respectively.

10. Why does it make sense that we assume *one* free electron per atom for the alkali metals?

11. Derive the Drude equations from (11.45) and (11.46) by setting $\nu_0 \to 0$.

CHAPTER 12

Quantum Mechanical Treatment of the Optical Properties

12.1. Introduction

We assumed in the preceding chapter that the electrons behave like particles. This working hypothesis provided us (at least for small frequencies) with equations which reproduce the optical spectra of solids reasonably well. Unfortunately, the treatment had one flaw: For calculation and interpretation of the infrared absorption we used the concept that electrons in metals are free; whereas, the absorption bands in the visible and ultraviolet spectrum could only be explained by postulating harmonic oscillators. From the classical point of view, however, it is not immediately evident why the electrons should behave freely at low frequenices and respond as if they would be bound at higher frequencies. An unconstrained interpretation for this is only possible by applying wave mechanics. This will be done in the present chapter. We make use of the material presented in Chapters 5 and 6.

12.2. Absorption of Light by Interband and Intraband Transitions

When light (photons) having sufficiently large energy impinges on a solid, the electrons in this crystal are thought to be excited into a higher energy level, provided that unoccupied higher energy levels are available. For these transitions the total momentum of electrons and photons must remain constant (conservation of momentum). For optical frequencies, the momentum of a photon, and thus its wave vector $\mathbf{k} = p/h$ (see (4.8)) is much smaller than that

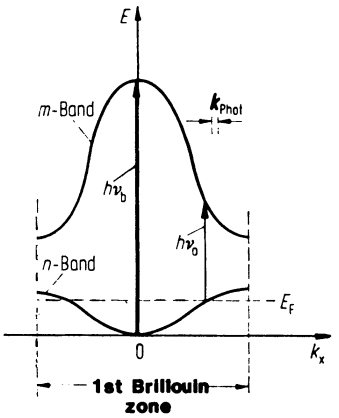

Figure 12.1. Electron bands and direct interband transitions in a reduced zone. (Compare to Fig. 5.4.)

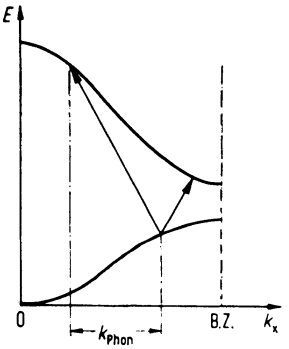

Figure 12.2. Indirect interband transitions. (The properties of phonons are explained in Chapter 20.)

of an electron. Thus, $\mathbf{k}_{phot}$ is much smaller than the diameter of Brillouin zone (Fig. 12.1). Electron transitions at which $\mathbf{k}$ remains constant (vertical transitions) are called "direct interband transitions." Optical spectra for metals are dominated by direct interband transitions.

It should be noted in passing that to a certain extent interband transitions are possible which involve the absorption of a light quantum under participation of a *phonon* (lattice vibration quantum, see Chapter 20). To better understand these "indirect interband transitions" (Fig. 12.2) we have to know that a phonon can only absorb very small energies, but is able to absorb a momentum which is large and comparable to that of an electron. During an indirect interband transition, the excess momentum (i.e., wave number vector) is transfered to the lattice (or is absorbed from the lattice). In other words, a phonon is exchanged with the lattice. Indirect interband transition may be

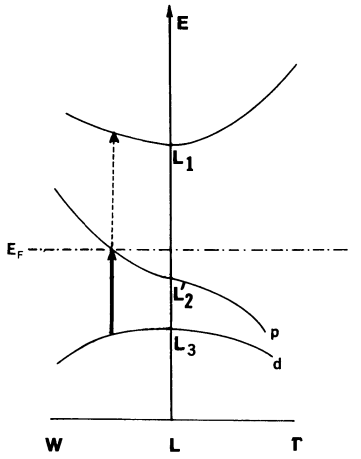

Figure 12.3. Section of the band diagram for copper (schematic). Two pertinent interband transitions are shown with arrows. The smallest possible interband transition occurs from a filled *d*-state to an unfilled state just above the Fermi energy.

disregarded for the interpretation of metal spectra because they are generally weaker than direct transitions by two or three orders of magnitude. They are only observed in the absence of direct transitions. In the case of semiconductors, however, and for the interpretation of photoemission, indirect interband transitions play an important role.

We now make use of the simplified model depicted in Fig. 12.1 and consider direct interband transitions from the n to the m band. The smallest photon energy in this model is absorbed by those electrons whose energy equals the Fermi energy E_F, that is, by electrons which already possess the highest possible energy at $T = 0$ K. This energy is marked in Fig. 12.1 by $h\nu_a$. Similarly, $h\nu_b$ is the *largest* energy, which leads to an interband transition from the n to the m band. In the present case a variety of interband transitions may take place between the energy interval $h\nu_a$ and $h\nu_b$.

Interband transitions are also possible by skipping one or more bands, which occur by involving electrons with even larger energies. Thus, a multitude of absorption bands are possible. These bands may partially overlap.

As an example for interband transitions in an actual case, we consider now the band diagram for copper. In Fig. 12.3, a portion of Fig. 5.21 is shown, that is, the pertinent bands around the L-symmetry point are depicted. The interband transition having the smallest possible energy difference is shown to occur between the upper *d*-band and the Fermi energy. This smallest energy is called the "threshold energy for interband transitions" (or the "fundamental edge") and is marked in Fig. 12.3 by a solid arrow. We mention in passing that this transition, which can be stimulated by a photon energy of 2.2 eV, is responsible for the red color of copper. At slightly higher photon energies, a second transition takes place, which originates *from* the Fermi energy. It is

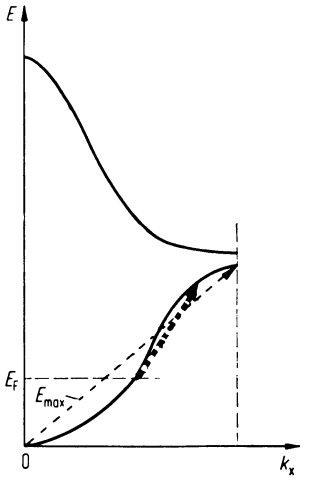

Figure 12.4. Intraband transitions. The largest energy which can be absorbed by intraband transitions is obtained by projecting the arrow marked "E_{max}" onto the energy axis.

marked in Fig. 12.3 by a dashed arrow. Needless to say, many more transitions are possible. They can take place over a wide range in the Brillouin zone. This will become clearer when we shall return to the optical spectra of materials and their interpretation in Chapter 13.

We turn now to another photon-induced absorption mechanism. Under certain conditions photons having only small energies may excite electrons into a higher energy level *within the same band.* This occurs with participation of a phonon. We call such a transition appropriately *intra*band transition (Fig. 12.4). *Intra*band transitions are equivalent to the behavior of *free* electrons in classical physics, that is, to the "classical infrared absorption." It should be kept in mind, however, that because of the Pauli principle, electrons can only be excited into empty states. Thus, intraband transitions can only be observed in metals because only metals have unfilled electron bands. In other words, insulators and semiconductors have no classical infrared absorption. This explains why some insulators (such as glass) are transparent in the visible spectrum or more precisely why they are transparent in the absence of interband transitions. The largest photon energy, E_{max}, which can be absorbed by means of an intraband transition, corresponds to an excitation from the lower to the upper band edge, see Fig. 12.4. All energies which are smaller than E_{max} are absorbed continuously.

In summary, at low photon energies, intraband transitions (if possible) are the prevailing absorption mechanism. Intraband transitions are not quantized and occur in metals only. Above a critical light frequency *inter*band transitions set in. Only certain energies or energy intervals are absorbed in this case. The onset of this absorption mechanism depends on the energy difference between the bands in question. *Interband* transitions occur in metals as

well as in insulators or semiconductors. They are analogous to optical excitations in solids with *bound* electrons. In an intermediate frequency range interband as well as intraband transitions may take place.

*12.3. Dispersion

For calculating the behavior of electrons in a periodic lattice we used in Section 4.4 the periodic potential shown in Fig. 4.9. We implied at this time that the potential does not vary with time. This proposition needs to be dropped when the interaction of light with a solid is considered. The alternating electric field of the light which impinges on the solid perturbs the potential field of the lattice periodically. Thus, we need to add to the potential energy a correction term, the so-called perturbation potential V':

$$V = V_0 + V' \tag{12.1}$$

(V_0 = unperturbed potential energy). It goes without saying that this perturbation potential oscillates with the frequency ν of the light.

We consider, as always, plane polarized light. The momentary value of the field strength $\mathscr{E}$ is

$$\mathscr{E} = A \cos \omega t, \tag{12.2}$$

where A is the maximal value of the field strength. Then, the perturbation potential (potential energy of the perturbation, or force times displacement x) is

$$V' = e\mathscr{E}x = eA \cos(\omega t) \cdot x. \tag{12.3}$$

Since the potential varies now with time, we need to make use of the time dependent Schrödinger equation (3.8)

$$\nabla^2 \Psi - \frac{2m}{\hbar^2} V \Psi - \frac{2im}{\hbar} \frac{\partial \Psi}{\partial t} = 0, \tag{12.4}$$

which reads with (12.1) and (12.3)

$$\nabla^2 \Psi - \frac{2m}{\hbar^2}(V_0 + eAx \cos \omega t)\Psi - \frac{2im}{\hbar} \frac{\partial \Psi}{\partial t} = 0. \tag{12.5}$$

Our goal is to calculate the optical constants from the polarization, in a similar way as it was done in Sections 11.2, 11.3, and 11.6. We have to note, however, the following: In wave mechanics, the electron is not considered to be a point, but instead is thought to be "smeared" about the space $d\tau$. The locus of the electron in classical mechanics is thus replaced by the probability $\Psi\Psi^*$ of finding an electron in space (see (2.10)). The classical polarization

$$P = Nex$$

(11.4) is replaced in wave mechanics by

$$P = Ne \int x\Psi\Psi^* \, d\tau. \tag{12.6}$$

We seek to find a solution Ψ of the *perturbed Schrödinger equation* (12.5) and calculate from that the *norm* $\Psi\Psi^*$; then by using (12.6) we can calculate the polarization P. The equation for the optical constants thus obtained is given in (12.31).

The detailed calculation of this approach will be given below. The first step is to transform the space *and* time dependent Schrödinger equation into a Schrödinger equation which is only space dependent. The perturbed Schrödinger equation (12.5) is rewritten, using the Euler equation[5] $\cos\rho = \frac{1}{2}(e^{i\rho} + e^{-i\rho})$, as

$$\nabla^2\Psi - \frac{2m}{\hbar^2} V_0\Psi - \frac{2im}{\hbar}\frac{\partial\Psi}{\partial t} = \frac{2m}{\hbar^2} eAx\frac{1}{2}[e^{i\omega t} + e^{-i\omega t}]\Psi. \tag{12.7}$$

Now, the left side of (12.7) has the form of the unperturbed Schrödinger equation (12.4). We assume that the perturbation is very small. Then, we can insert in the perturbation term (right side of (12.7)) the expression (3.4), and get

$$\Psi_i^0(x, y, z, t) = \psi_i^0(x, y, z)e^{i\omega_i t} \tag{12.8}$$

for the unperturbed ith eigen function. This yields:

$$\nabla^2\Psi - \frac{2m}{\hbar^2} V_0\Psi - \frac{2im}{\hbar}\frac{\partial\Psi}{\partial t} = \frac{m}{\hbar^2} eAx\psi_i^0[e^{i(\omega_i+\omega)t} + e^{i(\omega_i-\omega)t}]. \tag{12.9}$$

The right hand side shall be contracted to simplify the calculation:

$$\nabla^2\Psi - \frac{2m}{\hbar^2} V_0\Psi - \frac{2im}{\hbar}\frac{\partial\Psi}{\partial t} = \frac{m}{\hbar^2} eAx\psi_i^0 e^{i(\omega_i\pm\omega)t}. \tag{12.10}$$

To solve (12.10), we seek a trial solution which consists of an unperturbed solution and two terms with the angular frequencies $(\omega_i + \omega)$ and $(\omega_i - \omega)$:

$$\Psi = \Psi_i^0 + \psi_+ e^{i(\omega_i+\omega)t} + \psi_- e^{i(\omega_i-\omega)t}. \tag{12.11}$$

This trial solution is condensed as before:

$$\Psi = \Psi_i^0 + \psi_\pm e^{i(\omega_i\pm\omega)t}. \tag{12.12}$$

Equation (12.12) is differentiated twice with respect to space and once with respect to time, and the results are inserted into (12.10). This yields

$$\begin{aligned} &\underline{\nabla^2\Psi_i^0} + \nabla^2\psi_\pm e^{i(\omega_i\pm\omega)t} - \underline{\frac{2m}{\hbar^2} V_0\Psi_i^0} - \frac{2m}{\hbar^2} V_0\psi_\pm e^{i(\omega_i\pm\omega)t} \\ &- \underline{\frac{2im}{\hbar}\frac{\partial\Psi_i^0}{\partial t}} + \frac{2m}{\hbar}(\omega_i \pm \omega)\psi_\pm e^{i(\omega_i\pm\omega)t} = \frac{m}{\hbar^2} eAx\psi_i^0 e^{i(\omega_i\pm\omega)t}. \end{aligned} \tag{12.13}$$

[5] See Appendix 2.

The underlined terms in (12.13) vanish according to (12.4) if Ψ_i^0 is the solution to the unperturbed Schrödinger equation. In the remaining terms, the exponential factors can be cancelled, which yields with $\hbar\omega = h\nu = E$,

$$\nabla^2\psi_\pm + \frac{2m}{\hbar^2}\Psi_\pm(E_i \pm h\nu - V_0) = \frac{m}{\hbar^2}eAx\psi_i^0. \tag{12.14}$$

In writing (12.14) we have reached our first goal, that is, to obtain a time independent, perturbed Schrödinger equation. We solve this equation with a procedure which is common in perturbation theory. We develop the function $x\psi_i^0$ (the right side of (12.14)) in a series of eigen functions

$$x\psi_i^0 = a_{1i}\psi_1^0 + a_{2i}\psi_2^0 + \cdots + a_{ni}\psi_n^0 + \cdots = \sum a_{ni}\psi_n^0, \tag{12.15}$$

multiply (12.15) by ψ_n^{0*}, and integrate over the entire space $d\tau$. Then, due to $\int \psi\psi^* d\tau = 1$ (3.15) and $\int \psi_m\psi_n^* d\tau = 0$ (for $m \neq n$), we obtain

$$\int x\psi_i^0\psi_n^{0*}\,d\tau = a_{1i}\underbrace{\int \psi_1^0\psi_n^{0*}\,d\tau}_{0} + \cdots + a_{ni}\underbrace{\int \psi_n^0\psi_n^{0*}\,d\tau}_{1} + \cdots = a_{ni}. \tag{12.16}$$

Similarly, we develop the function $\psi_\pm$ in a series of eigen functions

$$\psi_\pm = \sum b_{\pm n}\psi_n^0. \tag{12.17}$$

Inserting (12.15) and (12.17) into (12.14) yields

$$\begin{aligned}\sum b_{\pm n}\left(\underline{\nabla^2\psi_n^0} + \frac{2m}{\hbar^2}E_i\psi_n^0 \pm \frac{2m}{\hbar^2}h\nu\psi_n^0 - \underline{\frac{2m}{\hbar^2}V_0\psi_n^0}\right)\\ = \frac{m}{\hbar^2}eA\sum a_{ni}\psi_n^0.\end{aligned} \tag{12.18}$$

Rewriting the unperturbed time independent Schrödinger equation (3.1) yields

$$\nabla^2\psi_n^0 - \frac{2m}{\hbar^2}V_0\psi_n^0 = -\frac{2m}{\hbar^2}E_n\psi_n^0. \tag{12.19}$$

Equation (12.19) shows that the underlined terms in (12.18) may be equated to the right side of (12.19). Thus, (12.18) may be rewritten as

$$\frac{2m}{\hbar^2}\sum \psi_n^0 b_{\pm n}(E_i - E_n \pm h\nu) = \frac{2m}{\hbar^2}\frac{eA}{2}\sum \psi_n^0 a_{ni}. \tag{12.20}$$

Comparing the coefficients in (12.20) yields with

$$E_i - E_n = E_{ni} = h\nu_{ni} \tag{12.21}$$

the following expression:

$$b_{\pm n} = \frac{eAa_{ni}}{2(E_i - E_n \pm h\nu)} = \frac{eAa_{ni}}{2h(\nu_{ni} \pm \nu)}. \tag{12.22}$$

Now, we are able to determine the functions ψ_+ and ψ_- by using (12.22) and (12.17). We insert these functions together with (3.4) in the trial solution (12.11) and obtain a solution for the time dependent, perturbed Schrödinger equation (12.5)

$$\Psi = \psi_i^0 e^{i\omega_i t} + \frac{1}{2h}\sum eAa_{ni}\psi_n^0\left[\frac{e^{i(\omega_i+\omega)t}}{\nu_{ni}+\nu} + \frac{e^{i(\omega_i-\omega)t}}{\nu_{ni}-\nu}\right] \tag{12.23}$$

and thus

$$\Psi^* = \psi_i^{0*} e^{-i\omega_i t} + \frac{1}{2h}\sum eAa_{ni}^*\psi_n^{0*}\left[\frac{e^{-i(\omega_i+\omega)t}}{\nu_{ni}+\nu} + \frac{e^{-i(\omega_i-\omega)t}}{\nu_{ni}-\nu}\right]. \tag{12.24}$$

In order to write the polarization (12.6) we have to form the product $\Psi\Psi^*$. As can be seen from (12.23) and (12.24) this calculation yields time dependent as well as time independent terms. The latter ones need not be considered here since they provided only an additive constant to the polarization (light scattering). The time dependent part of the norm $\Psi\Psi^*$ is

$$\begin{aligned}\Psi\Psi^* = \frac{eA}{2h}\Bigg[\sum a_{ni}^*\psi_n^{0*}\psi_i^0\underbrace{\left(\frac{e^{-i\omega t}}{\nu_{ni}+\nu} + \frac{e^{i\omega t}}{\nu_{ni}-\nu}\right)}_{Q} \\ + \sum a_{ni}\psi_n^0\psi_i^{0*}\underbrace{\left(\frac{e^{i\omega t}}{\nu_{ni}+\nu} + \frac{e^{-i\omega t}}{\nu_{ni}-\nu}\right)}_{R}\Bigg].\end{aligned} \tag{12.25}$$

To simplify, we abbreviate the terms in parenthesis by Q and R respectively. The polarization (12.6) is then

$$P = \frac{Ne^2A}{2h}\Bigg[\sum a_{ni}^* Q\underbrace{\int x\psi_n^{0*}\psi_i^0\,d\tau}_{a_{ni}} + \sum a_{ni}R\underbrace{\int x\psi_n^0\psi_i^{0*}\,d\tau}_{a_{ni}^*}\Bigg], \tag{12.26}$$

which reduces with (12.16)

$$\int x\psi_i^0\psi_n^{0*}\,d\tau = a_{ni}$$

and

$$a_{ni}\cdot a_{ni}^* = |a_{ni}|^2 \equiv a_{ni}^2 \tag{12.27}$$

to

$$P = \frac{Ne^2 A}{2h} \sum a_{ni}^2 (Q + R). \tag{12.28}$$

A numerical calculation applying the above quoted Euler equation yields

$$Q + R = \frac{2\nu_{ni} e^{-i\omega t}}{\nu_{ni}^2 - \nu^2} + \frac{2\nu_{ni} e^{i\omega t}}{\nu_{ni}^2 - \nu^2} = \frac{4\nu_{ni} \cos \omega t}{\nu_{ni}^2 - \nu^2}, \tag{12.29}$$

which gives with (12.2)

$$P = \frac{Ne^2 \mathscr{E}}{\pi \hbar} \sum a_{ni}^2 \frac{\nu_{ni}}{\nu_{ni}^2 - \nu^2}. \tag{12.30}$$

Finally, we make use of (10.13) and (11.5) and obtain with (12.30)

$$\boxed{\varepsilon_1 = n^2 - k^2 = 1 + \frac{4Ne^2}{\hbar} \sum a_{ni}^2 \frac{\nu_{ni}}{\nu_{ni}^2 - \nu^2}.} \tag{12.31}$$

Equation (12.31) is the sought after relation for the optical properties of solids, obtained by wave mechanics. It is similar in form to the classical dispersion equation (11.51). A comparison of classical and quantum mechanical results might be helpful to better understand the meaning of the empirically introduced oscillator strength f_i. We obtain

$$\boxed{f_i = \frac{4\pi m}{\hbar} a_{ni}^2 \nu_{ni}.} \tag{12.32}$$

We know that $h\nu_{ni}$ is that energy which an electron absorbs when it is excited from the n-band into the i-band (e.g., the m-band). Thus, the resonance frequency ν_{0i} of the ith oscillator introduced in Section 11.6 is replaced in wave mechanics by a frequency ν_{ni} which corresponds to an allowed electron transition from the nth into the ith band. Furthermore, we see from (12.16) that a_{ni} is proportional to the probability of an electron transition from the nth into the ith band.

Problems

1. What information can it be gained from the quantum mechanical treatment of the optical properties of metals which cannot be obtained by the classical treatment?
2. What can we conclude from the fact that the spectral reflectivity of a metal (for example, copper) has "structure?"

3. Below, the reflection spectra for two materials A and B are given.
   a) What type of material belongs to reflection spectrum A, what type to B? (Justify.) Note the scale difference!
   b) For which colors are these (bulk) materials transparent?
   c) What is the approximate threshold energy for interband transitions for these materials?
   d) For which of the materials would you expect intraband transitions in the IR region? (Justify.)
   e) Why do these intraband transitions occur in this region?

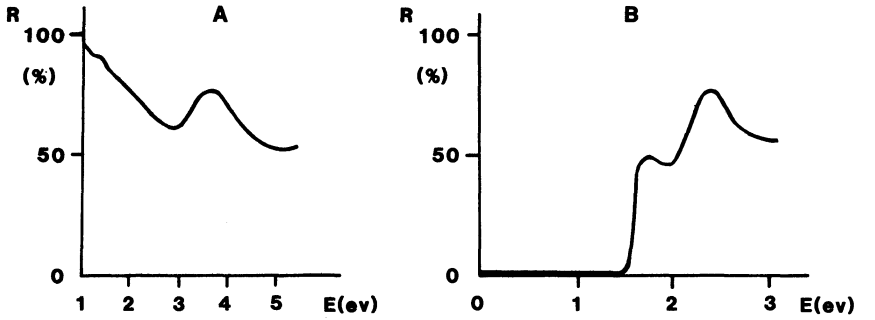

4. What is the smallest possible energy for interband transitions for aluminum? (*Hint*: Consult the band diagram in Fig. 5.22.)

5. Are intraband transitions possible in semiconductors at high temperatures?

CHAPTER 13

Applications

Optical spectra are the principal means to experimentally obtain the band gaps and energies for interband transitions. For isolated atoms and ions the absorption and emission spectra are known to be extremely sharp. Thus, absorption and emission energies for atoms can be determined with great accuracy. The same is basically true for molecular spectra. In contrast to this, the optical spectra of solids are rather broad. This stems from the high particle density in solids and from the interatomic interactions which split the atomic levels into quasicontinuous bands. The latter extend through the three-dimensional momentum space of a Brillouin zone.

A further factor has to be considered too. Plain reflection spectra of solids are in general not too useful for the deduction of transition energies, mainly because R is a rather involved function of ε_1 and ε_2 (see (10.29)). Thus, ε_2 (that is, absorption) spectra are often utilized. The characteristic features in the ε_2-spectra of solids stem from discontinuities in the energy profile of the density of states. However, relatively sharp features in ε_2 spectra are superimposed on noncharacteristic transitions from other parts of the Brillouin zone. In other words the ε_2-spectra derive their shape from a summation over extended rather than localized regions in the Brillouin zone. Modulated optical spectra (see below) separate the small contributions stemming from points of high symmetry (such as centers and edges of a Brillouin zone) from the general, much larger background. This will become clearer once we proceed in this chapter.

13.1. Measurement of the Optical Properties

The measurement of the optical properties of solids is simple in principle but can be involved in practice. This is so because many bulk solids (particularly metals) are opaque so that the measurements have to be taken in reflection.

Now, light penetrates about 10 nm into a metal (see Table 10.1). As a consequence, the optical properties are basically measured near the surface which is susceptible to oxidation, deformation (polishing), or contamination by adsorbed layers. One tries to alleviate the associated problems by utilizing ultrahigh vacuum, vapor deposition, sputtering, etc. Needless to say, the method by which a given sample was prepared may have an effect on the numerical value of its optical properties.

Let us assume that the surface problems have been resolved. Then, still another problem remains. The most relevant optical properties, namely n, k, ε_1, ε_2, and the energies for interband transitions cannot be easily deduced by simply measuring the reflectivity, that is, the ratio between reflected and incident intensity. Thus, a wide range of techniques have been developed in the past century to obtain the above-mentioned parameters. Only three methods will be briefly discussed here. It should be mentioned, however, that thirty or forty other techniques could be easily presented. They all have certain advantages for some specific applications and disadvantages for others.

*13.1.1. Kramers–Kronig Analysis (Dispersion Relations)

This method was very popular in the 1960s and involves the measurement of the reflectivity over a wide spectral range. A relationship exists between real and imaginary terms of any complex function which enables one to calculate *one* component of a complex quantity if the other one is known. In the present case, one calculates the phase jump δ' (between reflected and incident ray) from the reflectivity which was measured at a given frequency ν. This is accomplished by the Kramers–Kronig relation:

$$\delta'(\nu_x) = \frac{1}{\pi}\int_0^\infty \frac{d\ln\rho}{d\nu}\ln\left|\frac{\nu+\nu_x}{\nu-\nu_x}\right| d\nu, \tag{13.1}$$

where

$$\rho = \sqrt{R} = \sqrt{\frac{I_R}{I_0}} \tag{13.2}$$

is obtained from the reflected intensity I_R and the incident intensity I_0 of the light. The optical constants are calculated by applying

$$n = \frac{1-\rho^2}{1+\rho^2+2\rho\cos\delta'} \tag{13.3}$$

and

$$k = \frac{2\rho\sin\delta'}{1+\rho^2+2\rho\cos\delta'}. \tag{13.4}$$

Equation (13.1) shows that the reflectivity should be known in the entire

frequency range (i.e., between $\nu = 0$ and $\nu = \infty$). Since measured values can hardly be obtained for such a large frequency range, one usually extrapolates the reflectivity beyond the experimental region using theoretical or phenomenological considerations. Such an extrapolation would not cause a substantial error if one could assume that no interband transitions exist beyond the measured spectral range. This assumption is probably valid only in rare occasions. (For details, see specialized books listed at the end of Part III.)

*13.1.2. Spectroscopic Ellipsometry

This technique was developed in its original form at the turn of the century. The underlying idea is as follows: If plane polarized light impinges under an angle α on a metal, the reflected light is generally elliptically polarized. The analysis of this elliptically polarized light yields two parameters, the *azimuth* and the *phase difference* from which the optical properties are calculated.

We consider plane polarized light whose vibrational plane is inclined by 45° towards the plane of incidence (Fig. 13.1). This angle is called azimuth ψ_e in contrast to the azimuth of the reflected light ψ_r which is defined as

$$\tan \psi_r = \frac{\mathscr{E}_{Rp}}{\mathscr{E}_{Rs}}, \tag{13.5}$$

see Fig. 13.1, where $\mathscr{E}_{Rp}$ and $\mathscr{E}_{Rs}$ are parallel and perpendicular components of the reflected electric field strength $|\mathscr{E}|$, that is, the amplitudes of the reflected light wave.

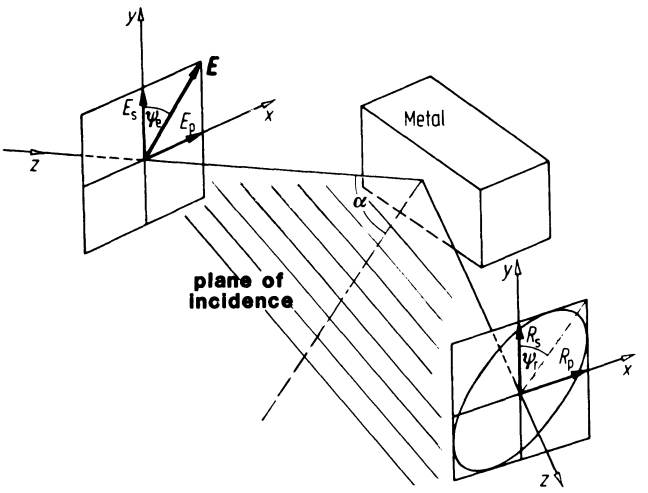

Figure 13.1. Reflection of plane polarized light on a metal surface. (Note: in the figure $\mathscr{E}_{Rp} \equiv R_p$ and $\mathscr{E}_{Rs} = R_s$.)

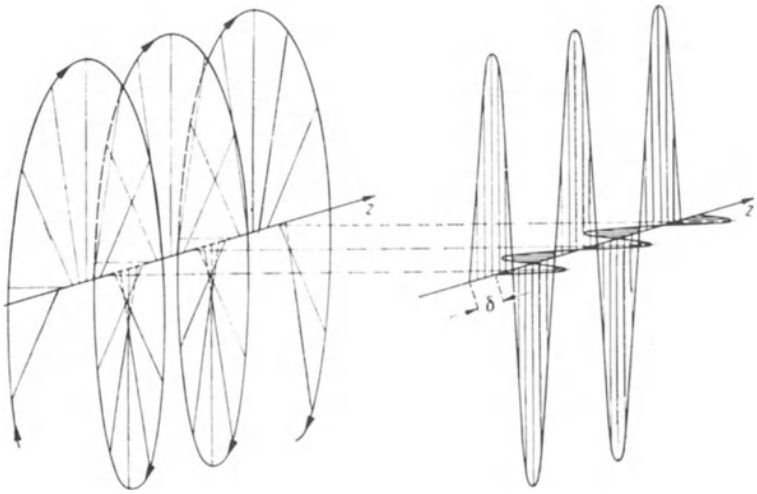

(a) (b)

Figure 13.2. (a) Elliptically polarized light and (b) decomposition of elliptically polarized light into two mutually perpendicular plane polarized waves with phase difference δ. Adapted from Pohl, R. W. (1958) *Optik und Atomphysik*. Springer-Verlag, Berlin, Heidelberg, New York, Tokyo.

In elliptically polarized light the length and direction of the light vector is altered periodically. The tip of the light vector moves along a continuous screw, having the direction of propagation as an axis (Fig. 13.2(a)). The projection of this screw onto the x–y plane is an ellipse (Fig. 13.1). Elliptically polarized light can be thought to be composed of two mutually perpendicular, plane polarized waves, having a phase difference δ in between them (expressed in fractions of 2π) (see Fig. 13.2(b)).

For the actual measurement of ψ_r and δ, one needs two polarizers (consisting of a birefringent material which allows only plane polarized light to pass), and a compensator (also consisting of birefringent material which allows one to measure the phase difference δ; see Fig. 13.3). In Fig. 13.4, the light reflected from a metal is represented by two light vectors pointing into the x- and the y-direction, respectively. They have a phase difference δ between them. By varying the thickness of the birefringent materials in the compensator, one accomplishes eventually that the light which leaves the compensator is plane polarized (i.e., $\delta = 0°$). The resulting vector R_{res} is then tilted by an angle ψ_r against the normal to the plane of incidence. One determines ψ_r by turning the analyzer to a position at which its axis is perpendicular to R_{res}. In short, δ and ψ_r are measured by simultaneously alternating the thickness of the compensator and turning the analyzer until no light leaves the analyzer. It is evident that this method is cumbersome and time consuming, particularly in cases in which an entire spectrum needs to be measured point by point.

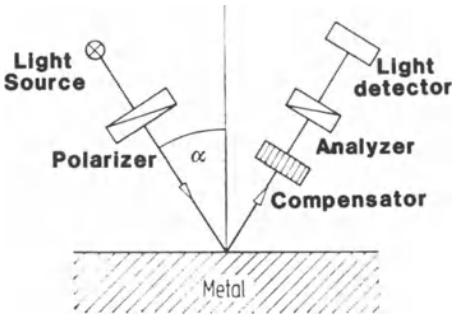

Figure 13.3. Schematic of an ellipsometer (polarizer and analyzer are identical devices).

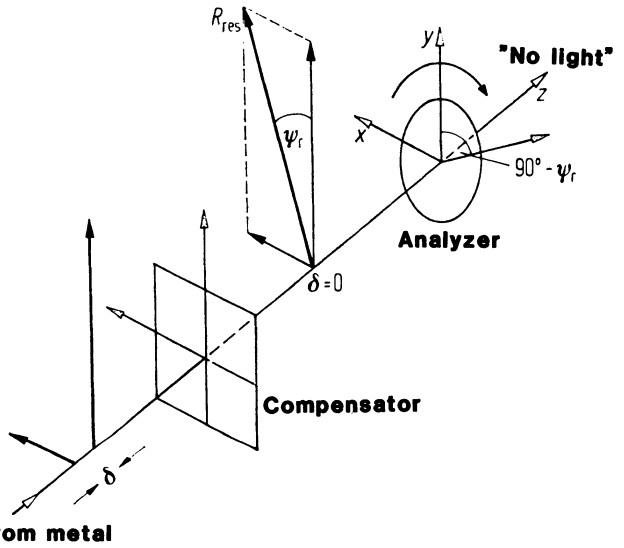

Figure 13.4. Vector diagram of light reflected from a metal surface. The vectors having solid arrow heads give vibrational direction and magnitude of the light.

Thus, in recent years it was attempted to automate and computerize the ellipsometer.

The optical constants are calculated using

$$n^2 = \tfrac{1}{2}[\sqrt{(a^2 - b^2 + \sin^2\alpha)^2 + 4a^2b^2} + a^2 - b^2 + \sin^2\alpha] \quad (13.6)$$

$$k^2 = \tfrac{1}{2}[\sqrt{(a^2 - b^2 + \sin^2\alpha)^2 + 4a^2b^2} - (a^2 - b^2 + \sin^2\alpha)] \quad (13.7)$$

with

$$a = \frac{\sin\alpha \tan\alpha \cos 2\psi_r}{1 - \cos\delta \sin 2\psi_r} \quad (13.8)$$

and

$$b = -a \sin\delta \tan 2\psi_r. \tag{13.9}$$

Alternately, one obtains for the polarization ε_1 and absorption ε_2

$$\varepsilon_1 = n^2 - k^2 = \sin^2\alpha\left[1 + \frac{\tan^2\alpha(\cos^2 2\psi_r - \sin^2 2\psi_r \sin^2\delta)}{(1 - \sin 2\psi_r \cos\delta)^2}\right], \tag{13.10}$$

$$\varepsilon_2 = 2nk = -\frac{\sin 4\psi_r \sin\delta \tan^2\alpha \sin^2\alpha}{(1 - \sin 2\psi_r \cos\delta)^2}. \tag{13.11}$$

*13.1.3. Differential Reflectometry

The information gained by differential reflectometry is somewhat different from that obtained by the aforementioned techniques. A "differential reflectogram" allows the direct measurement of the energies which the electrons absorb from photons as they are raised into higher allowed energy states. The differential reflectometer measures the normalized difference between the reflectivities of two similar specimens which are mounted side by side (Fig. 13.5). For example, one specimen might be pure copper and the other copper with, say, one percent zinc. Unpolarized light coming from a monochromator is alternately deflected under near normal incidence to one or the other sample by means of a vibrating mirror. The reflected light is electronically processed

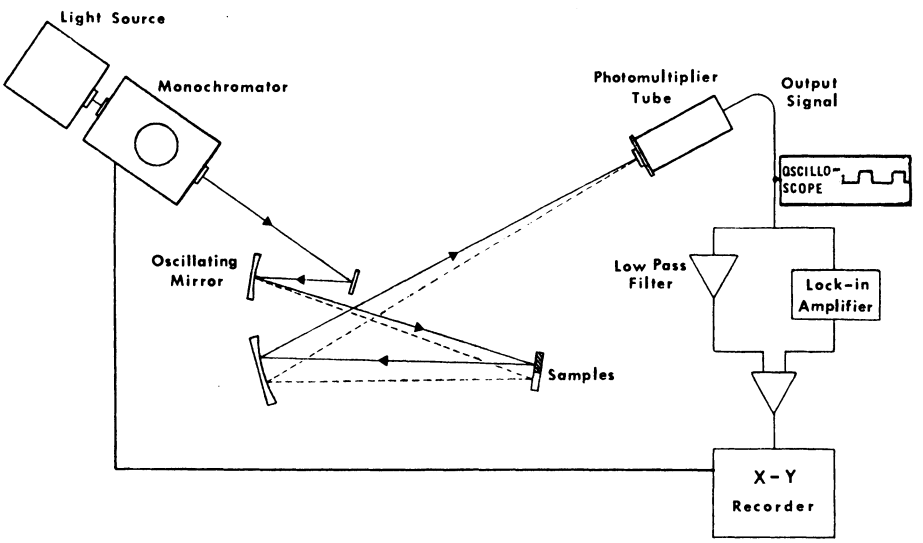

Figure 13.5. Schematic diagram of the differential reflectometer. (For clarity the angle of incidence of the light beam impinging on the samples is drawn larger than it is in reality.) From Hummel, R. E. (1983) *Phys. Stat. Sol.* (a) **76**.

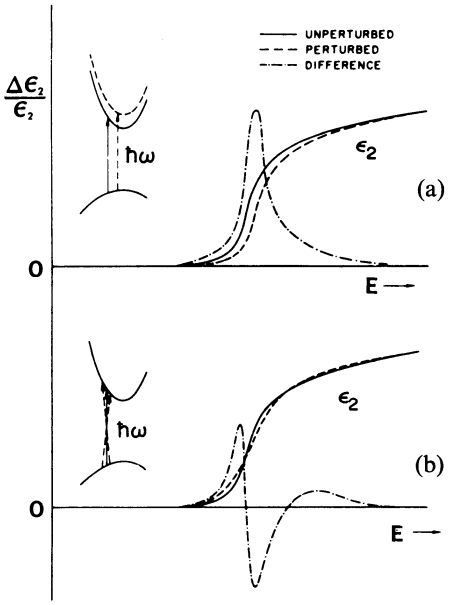

Figure 13.6. Schematic representation of (a) first derivative and (b) third derivative of an ε_2 spectrum. The equivalent interband transitions at a so-called M_0 symmetry point are shown in the inserts. Adapted from Aspnes, D. E. (1973) *Surface Science* **37**, 418.

to yield $\Delta R/\bar{R} = 2(R_1 - R_2)/(R_1 + R_2)$. A complete differential reflectogram, i.e., a scan from the near IR through the visible into the near UV, is generated automatically and takes about two minutes. The main advantage of differential reflectometry over conventional optical techniques lies in its ability to eliminate any undesirable influences of oxides, deformations, windows, electrolytes (for corrosion studies), or instrumental parameters upon a differential reflectogram, owing to the differential nature of the technique. No vacuum is needed. Thus, the formation of a surface layer due to environmental interactions can be studied *in situ*. Finally, the data can be taken under near normal incidence.

Differential reflectometry belongs to a family of techniques, called *modulation spectroscopy*, in which the derivative of the unperturbed reflectivity (or ε_2) with respect to an external parameter is measured. Modulation techniques restrict the action to so-called *critical points* in the band structure, that is, they emphasize special electron transitions from an essentially featureless background. This background is caused by the allowed transitions at practically all points in the Brillouin zone. Most modulation techniques, such as differential reflectometry, wavelength modulation, thermoreflectance, or piezoreflectance, are *first-derivative* techniques (Fig. 13.6(a)). In semiconductor research (Section 13.6) another modulation technique, called electroreflectance, is often used, which provides the third derivative of R or ε_2. (It utilizes an

alternating electric field which is applied to the semiconducting material during the reflection measurement.) The third derivative provides sharper and more richly structured spectra than the first derivative techniques (Fig. 13.6(b)). In a first derivative modulation spectrum, the lattice periodicity is retained, the optical transitions remain vertical and the interband transition energy changes with the perturbation (see insert of Fig. 13.6(a)). In electromodulation, the formerly sharp vertical transitions are spread over a finite range of initial and final momenta (see insert of Fig. 13.6(b)). A relatively involved line-shape analysis of electroreflectance spectra yields eventually the interband transition energies.

We shall make use of reflection, absorption, first, and third derivative spectra in the sections to come.

13.2. Optical Spectra of Pure Metals

13.2.1. Reflection Spectra

The spectral dependence of the optical properties of metals was described and calculated in Chapter 11 by postulating that light interacts with a certain number of *free electrons* and a certain number of *classical harmonic oscillators*, or equivalently, by *intraband* and *interband* transitions. In the present section we shall inspect experimental reflection data and see which conclusions can be drawn from these results with respect to the electron band structure.

Figure 13.7 depicts the spectral reflectivity for silver. From this diagram,

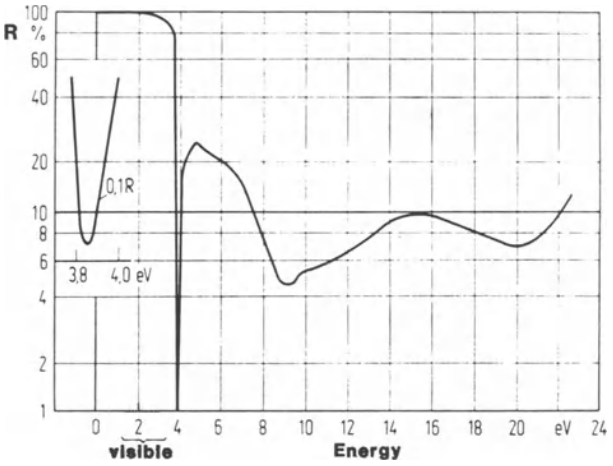

Figure 13.7. Reflectivity spectrum for silver. Adapted from Ehrenreich, H., et al., *IEEE Spectrum* **2**, 162. © 1965 IEEE.

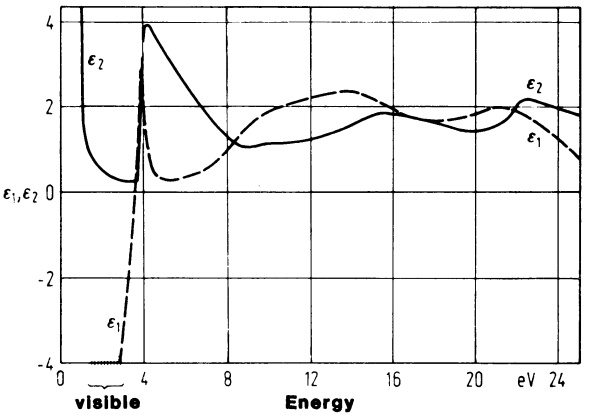

Figure 13.8. Spectral dependence of ε_1 and ε_2 for silver. ε_1 and ε_2 were obtained from Fig. 13.7 by a Kramers–Kronig analysis. Adapted from Ehrenreich, H., et al., *IEEE Spectrum* **2**, 162. © 1965 IEEE.

the optical constants (that is, the real and imaginary parts of the complex dielectric constant, $\varepsilon_1 = n^2 - k^2$ and $\varepsilon_2 = 2nk$) have been calculated by means of a Kramers–Kronig analysis (Section 13.1.1). Comparing Fig. 13.8 with Fig. 11.5 shows that for small photon energies, i.e., for $E < 3.8$ eV, the spectral dependences of ε_1 and ε_2 have the characteristic curve shapes for free electrons. In other words, the optical properties of silver can be described in this region by the concept of free electrons. Beyond 3.8 eV, however, the spectral dependence of ε_1 and ε_2 deviates considerably from the free-electron behavior. In this range, classical oscillators, or equivalently, interband transitions need to be considered.

Now, it is possible to separate the contributions of free and bound electrons in ε_1 and ε_2 spectra. For this, one *fits* the theoretical ε_2 to the experimental ε_2 curves in the low-energy region. The theoretical spectral dependence of ε_2 is obtained by the Drude equation (11.27). An "effective mass" and the damping frequency ν_2 are used as adjustable parameters. With these parameters, the free electron part of ε_1 (denoted by ε_1^f) is calculated in the *entire* spectral range by using (11.26). Next, ε_1^f is subtracted from the experimental ε_1, which yields the bound electron contribution ε_1^b. Fig. 13.9 depicts an absorption band thus obtained which resembles a calculated absorption band quite well (Fig. 11.9).

We turn now to the optical spectra for copper (Figs. 13.10 and 13.11). We notice immediately one important feature: Copper possesses an absorption band in the *visible* spectrum which is, as already mentioned, responsible for the characteristic color of copper. We defined above a threshold energy at which interband transitions set in. In copper the threshold energy is about 2.2 eV (Fig. 13.11) which is assigned to the *d*-band $\rightarrow E_F$ transition near the *L*-symmetry point. (This is marked by an arrow in Fig. 5.21.) A further peak is observed at slightly above 4 eV which is ascribed to interband transitions

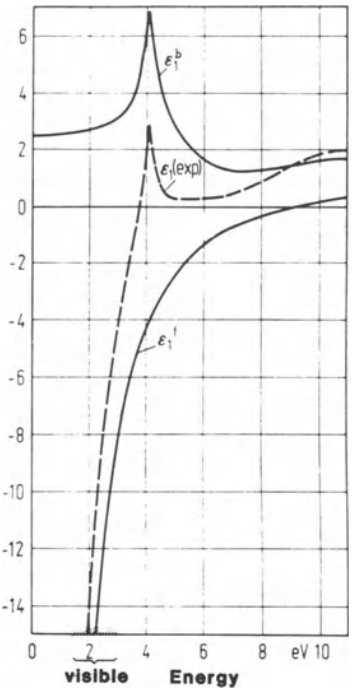

Figure 13.9. Separation of ε_1 for silver in ε_1^f (free electrons) and ε_1^b (bound electrons). Adapted from Ehrenreich, H., et al., *IEEE Spectrum* **2**, 162. © 1965 IEEE.

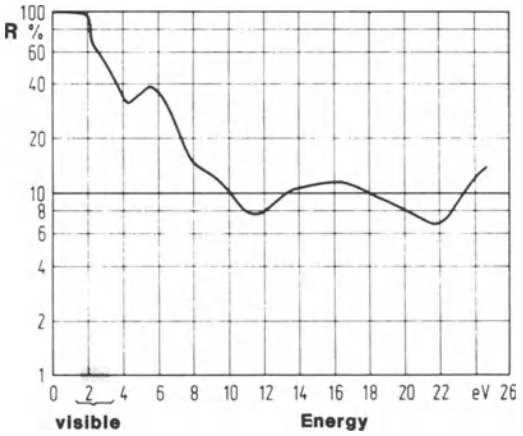

Figure 13.10. Reflectivity spectrum for copper. Adapted from Ehrenreich, H. et al., *IEEE Spectrum* **2**, 162. © 1965 IEEE.

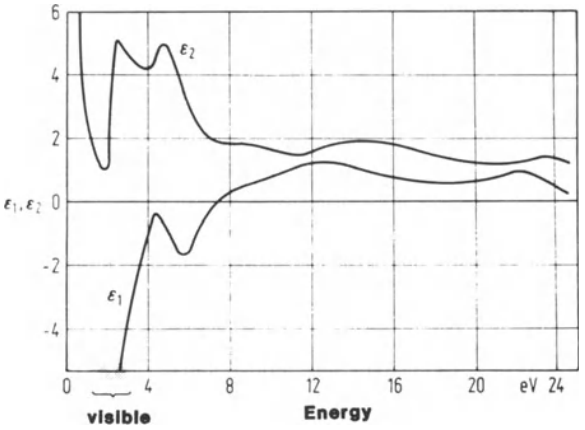

Figure 13.11. Spectral dependence of ε_1 and ε_2 for copper. ε_1 and ε_2 were obtained from Fig. 13.10 by a Kramers–Kronig analysis. Adapted from Ehrenreich, H., et al., *IEEE Spectrum* **2**, 162. © 1965 IEEE.

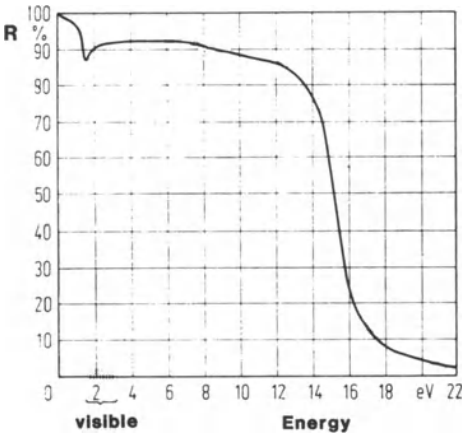

Figure 13.12. Reflection spectrum for aluminum. Adapted from Ehrenreich, H., et al., *IEEE Spectrum* **2**, 162. © 1965 IEEE.

from the Fermi energy near the *L*-symmetry point, as depicted in Figs. 12.3 and 5.21.

As a final example, we inspect the reflection spectrum of aluminum. Figures 13.12 and 13.13 show that the spectral dependences of ε_1 and ε_2 resemble those shown in Fig. 11.5 except in the small energy region around 1.5 eV. Thus, the behavior of aluminum may be described essentially by the free electron theory. This free electron-like behavior of aluminum can also be deduced from its band structure (Fig. 5.22) which has essential characteristics of free electron bands

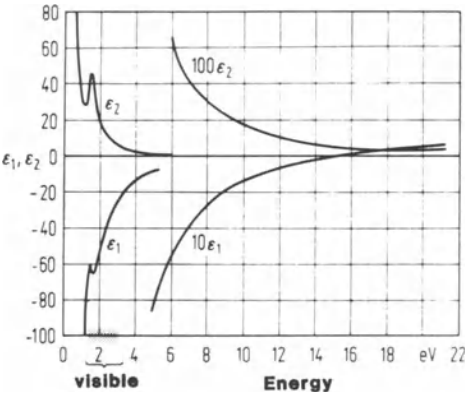

Figure 13.13. Spectral dependence of ε_1 and ε_2 for aluminum. Adapted from Ehrenreich, H., et al., *IEEE Spectrum* **2**, 162. © 1965 IEEE.

for fcc metals (Fig. 5.20). Interband transitions which contribute to the ε_2-peak near 1.5 eV occur between the W_2' and W_1 symmetry points and the closely spaced and almost parallel Σ_3 and Σ_1 bands. A small contribution stems from the $W_3 \rightarrow W_1$ transition near 2 eV.

*13.2.2. Plasma Oscillations

We postulate now that the free electrons of a metal interact electrostatically, thus forming an electron "plasma" which can be excited by light of proper photon energy to collectively perform fluidlike oscillations. This plasma possesses, just as an oscillator, a resonance frequency, often called the plasma frequency. We already introduced in Section 11.2 the plasma frequency ν_1 and noted that the dielectric constant $\hat{\varepsilon}$ becomes zero at ν_1. Thus, (10.12) reduces to

$$\hat{\varepsilon} = \varepsilon_1 - i\varepsilon_2 = 0, \tag{13.12}$$

from which we conclude that at the plasma frequency ε_1 as well as ε_2 must be zero. Experience shows that oscillations of the electron plasma occur already when ε_1 and ε_2 are close to zero.

The frequency dependence of the imaginary part of the reciprocal dielectric constant peaks at the plasma frequency, as we will see momentarily. We write

$$\frac{1}{\hat{\varepsilon}} = \frac{1}{\varepsilon_1 - i\varepsilon_2} = \frac{\varepsilon_1 + i\varepsilon_2}{\varepsilon_1^2 + \varepsilon_2^2} = \frac{\varepsilon_1}{\varepsilon_1^2 + \varepsilon_2^2} + i\frac{\varepsilon_2}{\varepsilon_1^2 + \varepsilon_2^2}. \tag{13.13}$$

The imaginary part of the dielectric constant, that is,

$$\operatorname{Im}\frac{1}{\hat{\varepsilon}} = \frac{\varepsilon_2}{\varepsilon_1^2 + \varepsilon_2^2}, \tag{13.14}$$

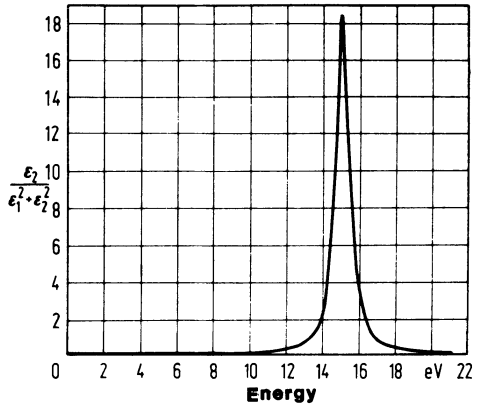

Figure 13.14. Energy loss function for aluminum. Adapted from Ehrenreich, H., et al., *IEEE Spectrum* **2**, 162. © 1965 IEEE.

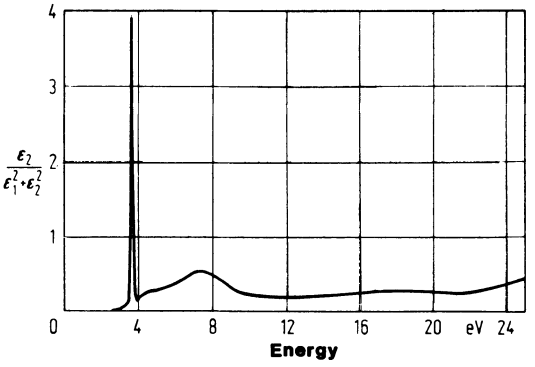

Figure 13.15. Energy loss function for silver. Adapted from Ehrenreich, H., et al., *IEEE Spectrum* **2**, 162. © 1965 IEEE.

is called the "energy loss function" which is large for $\varepsilon_1 \to 0$ and $\varepsilon_2 < 1$, that is, at the plasma frequency. We shall inspect now the energy loss functions for some metals. We begin with aluminum because its behavior may well be interpreted by the free electron theory. We observe in Fig. 13.14 a pronounced maximum of Im $(1/\hat{\varepsilon})$ near 15.2 eV. The real part of the dielectric constant (ε_1) is zero at this frequency and ε_2 is small (see Fig. 13.13). Thus, we conclude that aluminum has a plasma resonance at 15.2 eV.

Things are slightly more complicated for silver. Here, the energy loss function has a steep maximum near 4 eV (Fig. 13.15) which cannot be completely attributed to free electrons, since ε_1^f is only zero at 9.2 eV (see Fig. 13.9). The plasma resonance near 4 eV originates by cooperation of the *d*- as

well as the conduction electrons. The loss function for silver has another but much weaker resonance near 7.5 eV. This maximum is essentially caused by the conduction electrons, but is perturbed by interband transitions which occur at higher energies.

The reflection spectrum for silver (Fig. 13.7) can now be completely interpreted. The sharp decrease in R near 4 eV by almost 99% within a fraction of an electron volt is caused by a weakly damped plasma resonance. The sudden increase, only 0.1 eV above the plasma resonance takes place because of interband transitions which commence at this energy. Such a dramatic change in optical constants is unparalleled.

13.3. Optical Spectra of Alloys

It was demonstrated in the previous sections that knowledge of the spectral dependence of the optical properties contributes to the understanding of the electronic structure of metals. We shall now extend our discussion to alloys. Several decades ago, N. F. Mott suggested that when a small amount of metal A is added to a metal B, the Fermi energy would simply assume an average value, while leaving the electron bands of the solvent intact. It was eventually recognized, however, that this "rigid band model" needed some modification and that the electron bands are somewhat changed for an alloy. We use copper–zinc as an example. Figure 13.16 shows a series of differential reflectograms (see Section 13.1.3) from which the energies for interband transitions, E_T, can be taken. Peak A represents the threshold energy for interband transitions which can be seen to shift to higher energies with increasing zinc content. E_T is plotted in Fig. 13.17 as a function of zinc content (X). Essentially, a linear increase in E_T with increasing X is observed. The threshold energy for copper has been identified in Section 12.2 to be associated with electron transitions from the upper d-band to the conduction band, just above the Fermi surface (see Fig. 12.3). The rise in energy difference between upper d-band and Fermi level, caused by solute additions, can be explained in a first approximation by suggesting a rise in the Fermi energy which results when extra electrons are introduced into the copper matrix from the higher valent solute. Gallium, which has three valence electrons would thus raise the Fermi energy more than zinc, which is indeed observed in Fig. 13.17. The slope of the $E_T = f(X)$ curve in Fig. 13.17 for zinc (as well as for other solutes) is considerably smaller than that predicted by the rigid band model. This suggests that the d-bands are likewise raised with increasing solute content and/or that the Fermi level is shifted up much less than anticipated. Band calculations substantiate this suggestion. They reveal that upon solute additions to copper, the d-bands become narrower (which results from a reduction in Cu–Cu interactions) and that the d-bands are lifted up as a whole. Furthermore, the calculations show that solute additions to copper cause a rise in E_F and a downward

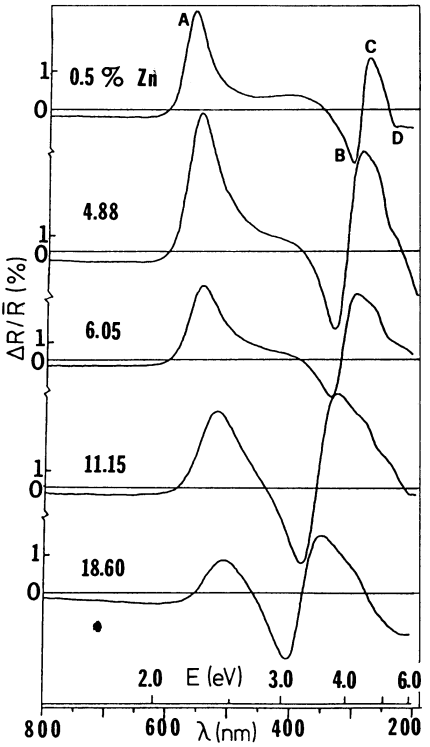

Figure 13.16. Experimental differential reflectograms for various copper–zinc alloys. The parameter on the curves is the average zinc concentration of the two alloys in at %. The curve marked 0.5%, for example, resulted by scanning the light beam between pure copper and a Cu–1% Zn alloy. From Nastasi-Andrews, R. J., and Hummel, R. E. (1977) *Phys. Rev. B* **16**, 4314.

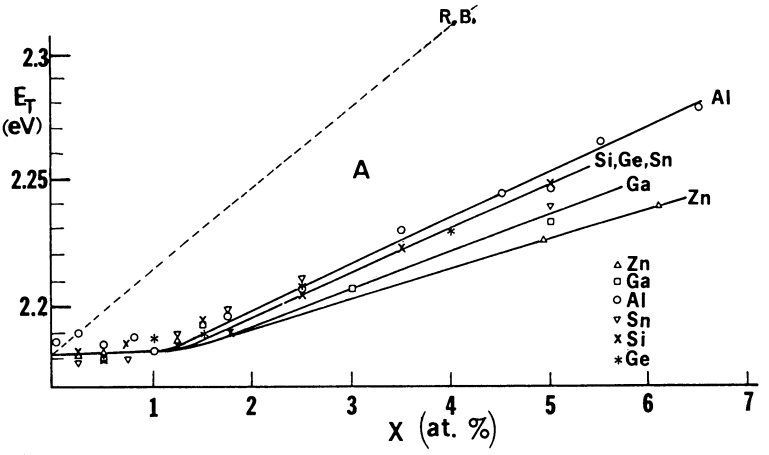

Figure 13.17. Threshold energies E_T for interband transitions for various copper-based alloys as a function of solute content. The E_T-values are taken from differential reflectograms similar to those shown in Fig. 13.16. The rigid band line (R.B.) for Cu–Zn is added for comparison. From Nastasi-Andrews, R. J., and Hummel, R. E. (1977) *Phys. Rev. B* **16**, 4314.

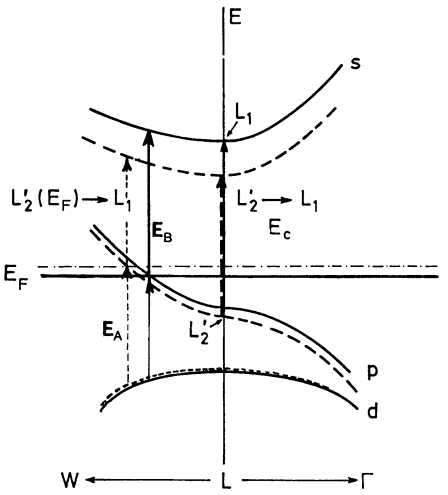

Figure 13.18. Schematic band structure near L for copper (solid lines) and an assumed dilute copper-based alloy (dashed lines). Compare to Figs. 12.3 and 5.21.

shift of the bottom of the s-band. Figure 13.18 reflects these results. Because of the lowering of the bottom of the s-band (Γ_1 in Fig. 5.21), the Fermi energy rises much less than predicted, had $E_{\Gamma 1}$ remained constant.

An unexpected characteristic of all $E_T = f(X)$ curves is that the threshold energy for interband transitions, E_T, does not vary appreciably for solute concentrations up to slightly above 1 at. % (Fig. 13.17). Friedel predicted just this type of behavior and related it to "screening" effects. He argued that for the first few atomic percent solute additions to copper, the additional charge from the higher valent solute is effectively screened and the copper matrix behaves as if the impurities were not present. The matrix remains essentially unperturbed as long as the impurities do not mutually interact.

The differential reflectograms shown in Fig. 13.16 suggest two additional interband transitions, one of which corresponds to feature 'D' near 5 eV and is assigned to electron transitions from the *lower d*-bands to the Fermi surface. An E_T versus X plot for peak 'D' resembles Fig. 13.17.

The third transition in the chosen energy region occurs at about 4 eV and involves the structural features 'B' and 'C'. The associated transition energy is seen to decrease with increasing solute content (Fig. 13.19). Features 'B' and 'C' are ascribed to transitions near the L-symmetry point, originating near the Fermi energy and terminating at the conduction band. It can be seen in Fig. 13.18 that the transition energy just mentioned is smaller for copper-based alloys than for pure copper, quite in agreement with the experimental findings. The reader is asked at this point to compare Figs. 13.10 and 13.11 with Fig. 13.16 and convince himself how different optical techniques complement each other in revealing the electronic structure of solids.

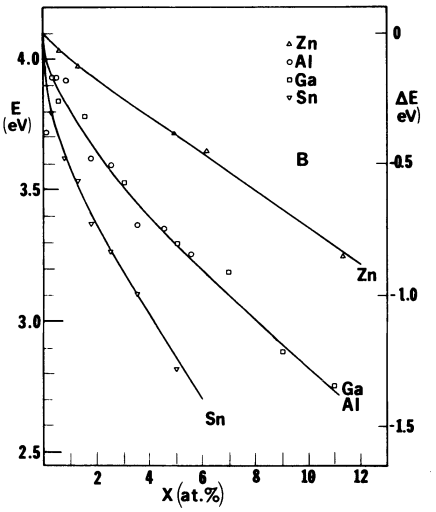

Figure 13.19. Energy of peak B for various dilute copper-based alloys. From Nastasi-Andrews, R. J., and Hummel, R. E. (1977) *Phys. Rev. B* **16**, 4314.

*13.4. Ordering

It was shown in Section 7.5.3 that the resistivity decreases when solute atoms of an alloy are periodically arranged on the regular lattice sites. Thus, we conclude that ordering has an effect on the electronic structure and hence on the optical properties of alloys. The best way to study ordering is to compare two specimens of the same alloy when one of them is ordered, and the other is in the disordered state. This way, peaks occur in a differential optical spectrum whenever the ordered state causes *extra* interband transitions comparable to superlattice lines in X-ray spectroscopy. As an example, Fig. 13.20 depicts an optical spectrum for the intermetallic phase Cu_3Au. We note several transitions, among them an ε_2-type structure with a peak energy at 2.17 eV and an ε_1-type structure with a transition energy around 3.6 eV (median between 3.29 and 3.85 eV, see Fig. 11.9). We shall explain them by referring to Fig. 13.21 which depicts the first Brillouin zone of the disordered fcc lattice in which a simple cubic Brillouin zone, representing the superlattice, is inscribed. The Γ–X direction of the fcc Brillouin zone is bisected by the face of the cubic Brillouin zone at the point $\bar{X}$. The point X is then thought to be folded back to the point Γ. A new transition from the d-bands (e.g., at Γ_{12}) to the point X_4' (unfolded) can now take place (see Fig. 5.21). Folding along Γ–M–K and possibly along other directions explains the other transitions.

Short-range ordering shows comparatively smaller effects than long-range ordering (Fig. 13.22). The reflectivity difference between ordered and disordered alloys is about 3% for long-range ordering compared to 0.5% in the

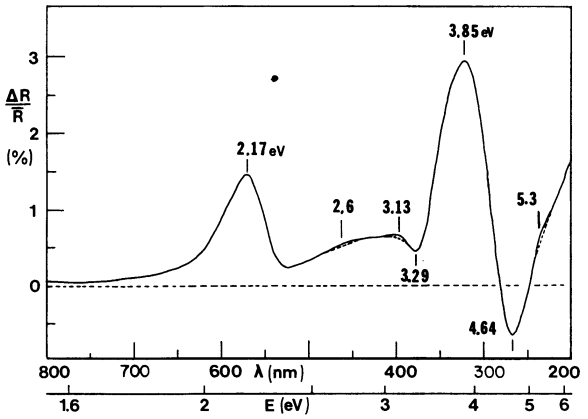

Figure 13.20. Differential reflectogram of (long-range) ordered versus disordered Cu_3Au. From Hummel, R. E., (1983) *Phys. Stat. Sol.* (*a*) **76**, 11.

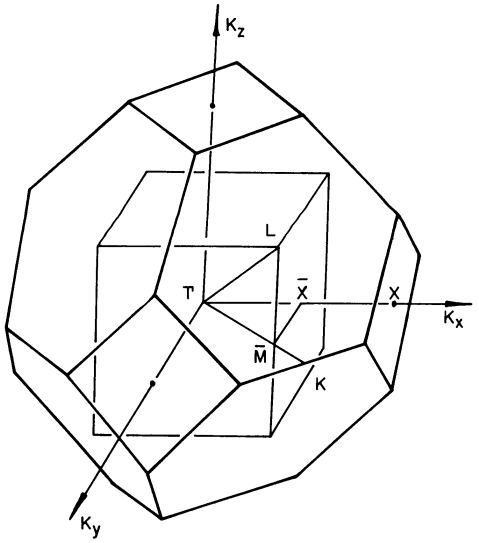

Figure 13.21. First Brillouin zone of an fcc lattice with inscribed Brillouin zone representing a cubic primitive superlattice.

case of short-range ordering. Still, even in the latter case, a superlattice transition is observed, which is attributed to the periodic arrangement of solute atoms in small domains (about 10–20 *Å* in diameter).

Interestingly enough, optical investigations provide a further piece of information which enables us to look upon the short-range ordered state from a different perspective. It has been observed that certain peaks in a differential

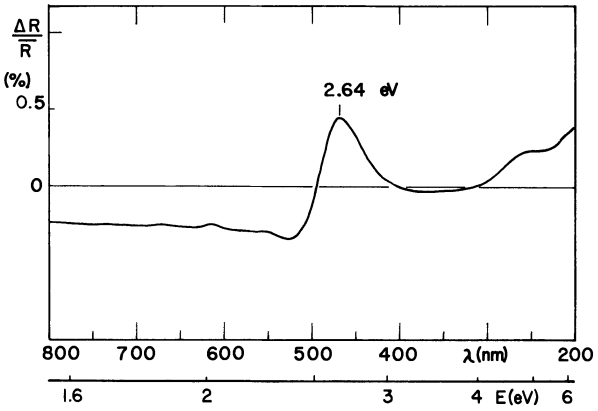

Figure 13.22. Differential reflectogram of (short-range) ordered versus disordered Cu-17 at. % Al. From Andrews, J. B., Andrews, R. J., and Hummel, R. E. (1980) *Phys. Rev B* **22**, 1837.

reflectogram shift due to ordering exactly as they would do when a solute is added to a solvent (see Section 13.3). From this we conclude that in the short-range ordered state, the interaction between dissimilar atoms is slightly larger than that for similar atoms.

*13.5. Corrosion

Studies of the optical properties have been used for many decades for the investigation of environmentally induced changes of surfaces. Optical studies are *nondestructive*, simple, and allow the investigation of oxides during their formation. No vacuum is required in contrast to many other surface techniques. We use as an example the electrochemical corrosion of copper in an aqueous solution. A copper disc is divided into two parts which are electrically insulated from each other by a thin polymer film. One half is held electrically at the protective potential (as reference) and the other at the corrosion potential. No artifacts from the electrolyte, the corrosion cell window, or the metal substrate are experienced since the only difference in the light path of a differential reflectometer is the corrosion film itself. Figure 13.23 depicts a series of differential reflectograms demonstrating the evolution of Cu_2O on a copper substrate. We observe that the peak height near 3.25 eV and thus the corrosion film thickness initially grows rapidly. The growth rate slows down as the film becomes thicker. The growth kinetics has been observed to obey a logarithmic relationship.

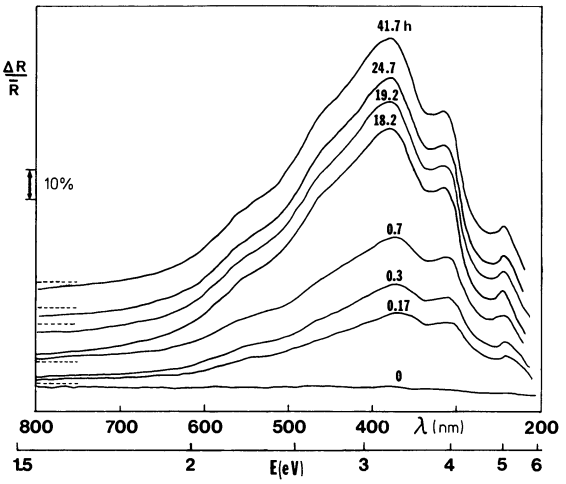

Figure 13.23. Differential reflectograms depicting the *in situ* evolution of Cu_2O on copper substrate in a buffered electrolyte of pH 9. One sample half was held potentiostatically at −200 mV (SCE) for various times, the other at the protective potential (−500 mV (SCE)). From Hummel, R. E. (1983) *Phys. Stat. Sol.* (*a*) **76**, 11.

13.6. Semiconductors

Intrinsic semiconductors have, at low temperatures, a completely filled valence band and an empty conduction band (see Chapter 8). Consequently, no *intra*band transition, or classical infrared absorption, is possible at low temperatures. Thus, the optical behavior of an intrinsic semiconductor is similar to that of an insulator, that is, it is transparent in the low energy (far infrared) region. Once the energy of the photons is increased and it eventually reaches the gap energy, then the electrons are excited from the top of the valence band to the bottom of the conduction band. The semiconductor becomes opaque like a metal. The onset for *inter*band transitions is thus determined by the gap energy, which characteristically has values between 0.5 and 3 eV (see Table 8.1). The corresponding wavelength lies in the near infrared or visible region.

As an example, the ε_2-spectrum for germanium is shown along with its band diagram in Figs. 13.24 and 13.25. The threshold energy for electron excitations across the gap from Γ'_{25} to Γ'_2 can be clearly identified in both figures. Of particular interest are the nearly parallel bands Σ_4 and Σ_1 including the symmetry points X_4 and X_1 which cause a strong peak in ε_2 around 4.5 eV. (This transition is said to occur at an "M_1 critical point".) The designations of some further peaks are marked in Fig. 13.24 and should be compared to the band diagram.

We mentioned already in Section 13.1.3 that electroreflectance spectroscopy can enhance a relatively featureless part of an ε_2-spectrum and gives in

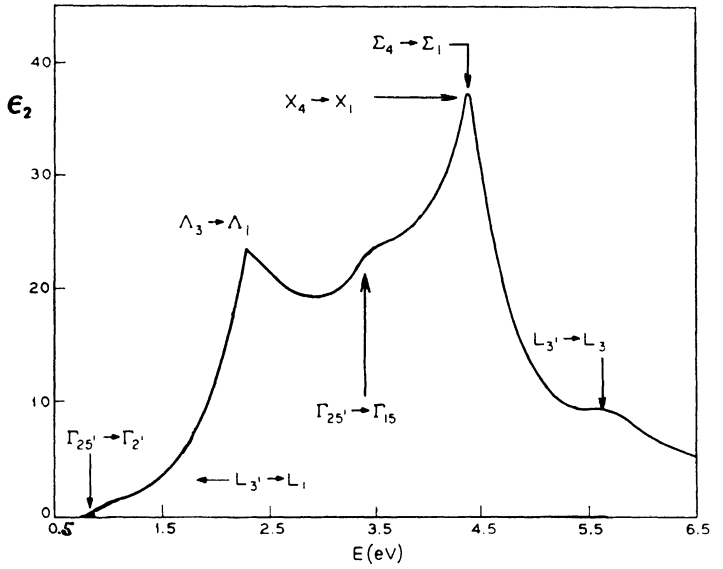

Figure 13.24. Experimental ε_2 spectrum for Ge. Adapted from Phillips, J. C. (1966) *Optical Properties and Electronic Structure of Metals and Alloys* (F. Abelès ed.) North-Holland Publ. Comp., Amsterdam.

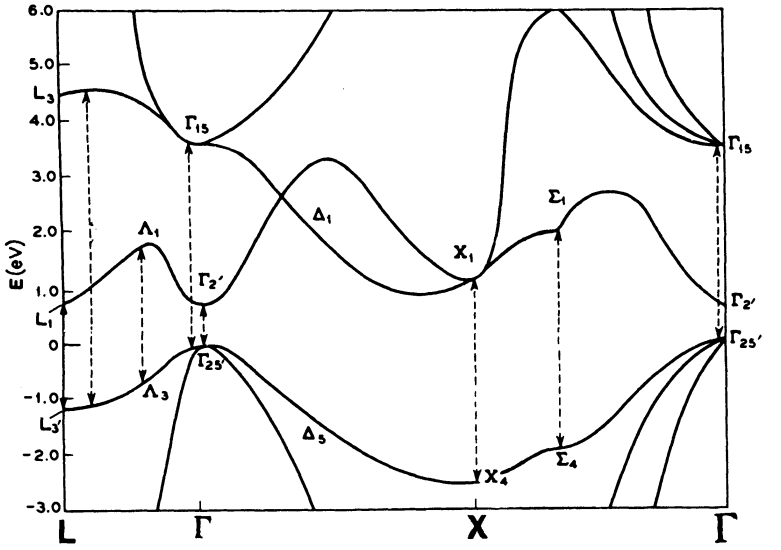

Figure 13.25. Energy band structure of Ge. Some pertinent direct interband transitions are marked. Adapted from Brust, D., *et al.* (1964) *Phys. Rev A* **134**, 1337.

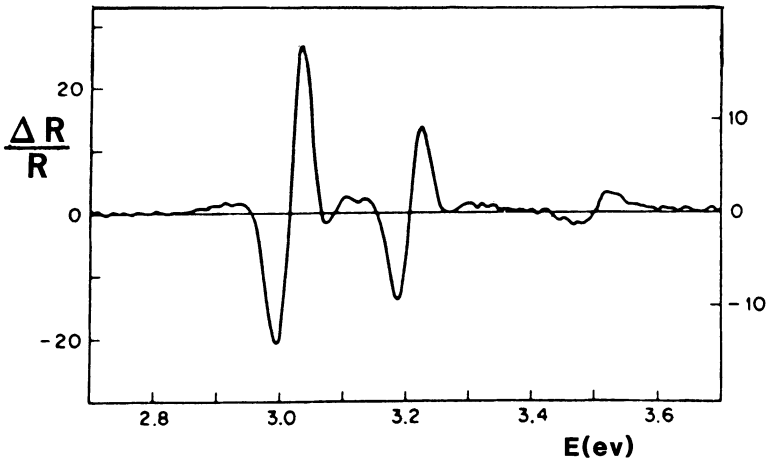

Figure 13.26. Electroreflectance spectrum of germanium at 78K. Compare to Fig. 13.6(b). Adapted from Aspnes, D. E. (1972) *Phys. Rev. Letters* **28**, 913.

addition some information about critical point transitions. Figure 13.26 depicts the electroreflectance spectrum for germanium between 2.8 and 3.6 eV.

The ε_2-spectrum (Fig. 13.24) shows only a shoulder in this region, that is, for the Γ'_{25}–Γ_{15} transition. It should be kept in mind, however, that electroreflectance is a third derivative techniques (Fig. 13.6(b)) which means that a sequence of peaks represent only *one* interband transition.

As a second example we consider silicon. By inspecting its band diagram (see Fig. 5.23 or 8.2) we notice that the maximum of the valence band and the minimum of the conduction band are not at the same point in **k** space. Vertical transitions are thus not permissible at energies below about 3.4 eV ($\Gamma'_{25} \rightarrow \Gamma_{15}$). However, nonvertical transitions between the top of the valence band and the bottom of the conduction band are possible. They involve the band gap energy ($E_g = 1.1$ eV), provided the change in the wave vector **k** (or the momentum) is furnished by a phonon. We discussed phonon-assisted transitions already in Section 12.2 and explained there that indirect interband transitions are particularly observed in the absence of direct transitions.

Our discussion of the optical spectra of semiconductors is not complete by considering only direct or indirect interband transitions. Several other absorption mechanisms may occur. It has been observed, for example, that the absorption spectra for semiconductors show structure for photon energies slightly *below* the gap energy (Fig. 13.27). Frenkel explained this behavior by postulating that a photon may excite an electron so that it remains in the vicinity of its nucleus, thus forming an electron–hole pair, called an *exciton.* Electron and holes are thought to be bound together by electrostatic forces and revolve around their mutual center of mass. The electrons may hop through the crystal and change their respective partner. This motion is called an exciton wave. One depicts the excitons by introducing "exciton levels" into

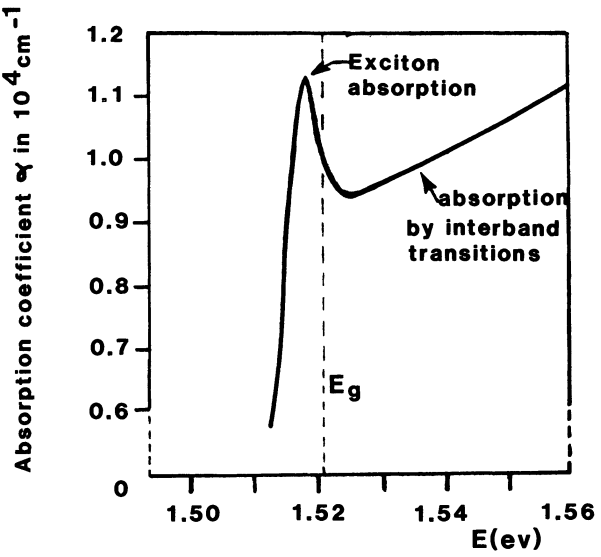

Figure 13.27. Spectral dependence of the absorption coefficient $\alpha = 4\pi k/\lambda$ (10.21)) for gallium arsenide at 21K. Adapted from Sturge, M. D. (1962) *Phys. Rev.* **127**, 768.

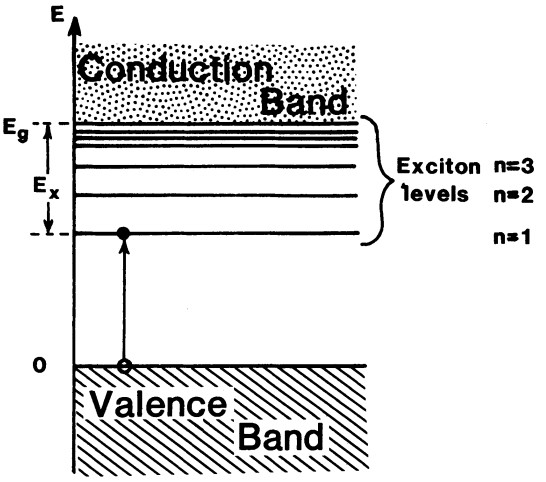

Figure 13.28. Schematic representation of exciton energy levels and an exciton in a semiconductor (or insulator).

the forbidden band (Fig. 13.28). They are separated from the conduction band by the "binding energy" E_x whose position can be calculated by an equation similar to (4.18a):

$$E_x = -\frac{m^* e^4}{2n^2\hbar^2\varepsilon^2}, \tag{13.15}$$

where n is an integer and m^* is the effective mass of the exciton. E_x is characteristically about 0.01 eV. The exciton levels are broadened by interactions with impurities or phonons.

Finally, *extrinsic* semiconductors have, as we know, donor or acceptor states near the conduction or the valence band, respectively (Section 8.3). At sufficiently high temperatures, optical transitions from and to these states can take place which also cause weak absorption peaks below the gap energy.

It should be noted that the temperature slightly influences the absorption characteristics of a semiconductor. The change in gap energy is about -2×10^{-4} eV/K which stems from an apparent broadening of valence and conduction levels with increasing temperature due to transitions with simultaneous emission and absorption of phonons. Another temperature-enhanced effect should be considered too. Once electrons have been excited from the valence into the conduction band (either by photons or thermal excitation), holes are present in the upper part of the valence bands. Then, photons having energies well below E_g can be absorbed by *intra*band transitions. These transitions are, however, relatively weak.

Optical absorption measurements are widely used in semiconductor research since they provide the most accurate way to determine the gap energies and the energies of the localized states. Measurements are normally performed at low temperatures so that the thermal excitations of the electrons do not mask the transitions to be studied.

13.7. Insulators (Dielectric Materials)

As we know, insulators are characterized by completely filled valence bands and empty "conduction" bands. Thus, no *intra*band transitions, that is, no classical infrared absorption takes place. Furthermore, the gap energy for insulators is fairly large (typically 5 eV or larger) so that *inter*band transitions do not occur in the IR and visible spectrum either. They take place, however, in the ultraviolet region. Third, *excitons* may be created which cause absorption peaks somewhat below the gap energy. For example, the lowest energy for an exciton level (and thus for the first exciton absorption peak) for NaCl has been found to be at about 7 eV, that is, in the vacuum UV region. (Other alkali halides have very similar exciton energies.) We suspect, therefore, that insulators are transparent from the far IR throughout the visible up to the UV region. This is indeed essentially observed. However, in the infrared region a new absorption mechanism may take place which we have not yet discussed. It is caused by the light-induced vibrations of the lattice atoms, that is, by the excitation of phonons by photons. We need to explain this in some more detail.

Let us consider at first a monoatomic crystal (one kind of atom). The individual atoms are thought to be excited by light of appropriate frequency to

perform oscillations about their points of rest. Now, the individual atoms are surely not vibrating independently. They interact with their neighbors which causes them to move simultaneously. For simplicity, we model the atoms to be interconnected by elastic springs. Thus, the interaction of light with the lattice can be mathematically represented in quite a similar manner to the one used when we discussed and calculated the classical *electron* theory of dielectric materials. (In Section 11.6 we represented *one* atom in an electric field as consisting of a positively charged core which is bound quasielastically to an electron.) A differential equation similar to (11.32) may be written for the present case:

$$m\frac{d^2x}{dt^2} + \gamma'\frac{dx}{dt} + \kappa x = e\mathscr{E}_0 \exp(i\omega t), \tag{13.16}$$

which represents the oscillations of atoms under the influence of light whose excitation force is $e\mathscr{E}_0 \exp(i\omega t)$. As before, the factor $\kappa \cdot x$ is the restoring force which contains the displacement x and an interatomic force constant κ (i.e., a "spring constant," or a "binding strength" between the atoms). The damping of the oscillations is represented by the second term in (13.16). Damping is thought to be caused by interactions of the phonons with lattice imperfections, or with external surfaces of the crystal, or with other phonons. The oscillators possess a resonance frequency, ω_0, which depends on the mass of the atoms and on the restoring force (see (11.34)). The solution of the differential equation (13.16) yields a spectral dependence of ε_1 and ε_2 which is very similar to that shown in Figs. 11.9–11.12.

The situation becomes slightly more complicated when diatomic solids, such as ionic crystals, are considered. In this case, two differential equations of the type of (13.16) need to be written. They have to be solved simultaneously. Actually, one needs to solve $2N$ coupled differential equations, where N is the number of unit cells in the lattice. The result is, however, qualitatively still the same. The resonance frequency for diatomic crystals is

$$\omega_0 = 2\kappa\left(\frac{1}{m_1} + \frac{1}{m_2}\right), \tag{13.17}$$

where m_1 and m_2 are the masses of the two ion species. Figure 13.29 depicts the spectral reflectivity of NaCl in the IR. Sodium chloride is transmissive between 0.04 and 7 eV. At the upper boundary energy, exciton absorption sets in. Fused quartz is transparent between 0.29 and 6.9 eV.

A word should be added about the opacity of some dielectric materials, such as enamels, opal glasses, glazes, or porcelains, which should be transparent in the visible region according to our discussion above. This opacity is caused by the scattering of the light on small particles which are contained in the matrix. Part of the light is diffusely transmitted and part of it is diffusely reflected. The larger the specular part of the reflected light, the higher is the gloss. Very often, *opacifiers* are purposely added to a dielectric material to

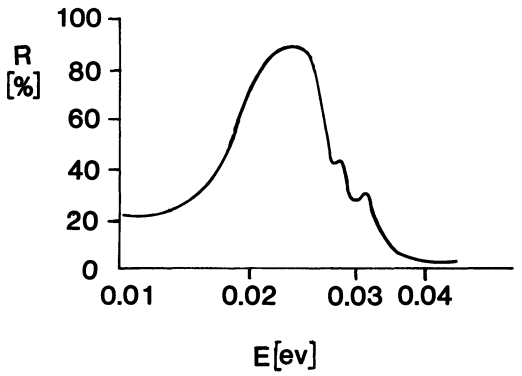

Figure 13.29. Spectral reflectivity of NaCl at room temperature in the far IR region.

cause wanted effects. The particle size should be nearly the same as the wavelength of the light, and the index of refraction should be largely different from that of the material, to obtain maximal scattering.

13.8 Lasers

So far we discussed only the *absorption* of light by matter. We learned that due to the interaction of photons with electrons, the electrons are excited into higher energy states. The present section deals with the *emission* of photons, particularly with stimulated emission. A brief description of the light-emitting diode (LED) will be also given at the end of this section.

An electron, once excited, must eventually revert back into a lower, empty energy state. This occurs, as a rule, spontaneously within a fraction of a second and is accompanied by the emission of a photon and/or the dissipation of heat. This fast luminescence process is called fluorescence. (In some materials, the emission continues for several seconds or even minutes. This slower process is referred to as phosphorescence.) Spontaneous emission possesses none of the characteristic properties of laser light: the radiation is emitted through a wide angular region in space, the light is phase *in*coherent and it often polychromatic.

The situation changes, however, considerably when stimulated emission is induced. Let us consider two energy levels E_1 and E_2 and let us assume for a moment that the higher energy level E_2 contains more electrons than the lower level E_1, that is, let us assume a *population inversion* of electrons (Fig. 13.30(a)). We further assume that by some means (which we shall discuss in a moment) the electrons in E_2 are made to stay there for an appreciable amount of time. Nevertheless, one electron will eventually revert to the lower state. As a consequence a photon with energy $E_{21} = h\nu_{21}$ is emitted (Fig. 13.30(b)). This photon might stimulate a second electron to *descend in step* to E_1, thus

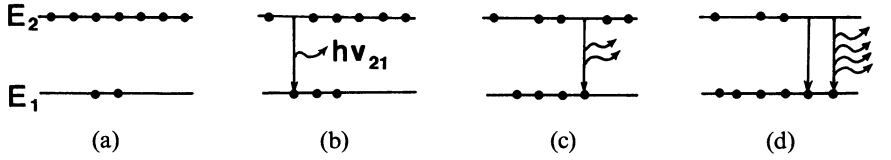

Figure 13.30. Schematic representation of stimulated emission between two energy levels E_2 and E_1. The dots symbolize electrons.

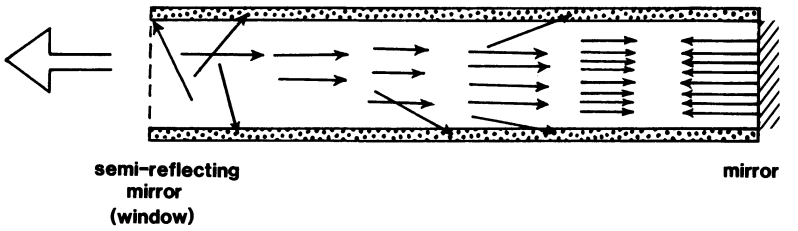

Figure 13.31. Schematic representation of a laser cavity and the buildup of laser oscillations. The stimulated emission eventually dominates over the spontaneous emission. The light leaves the cavity at the left side.

causing the emission of another photon which vibrates in phase with the first one. The two photons are consequently *phase coherent* (Fig. 13.30(c)). They might stimulate two more electrons to descend in step (Fig. 13.30(d)) and so on until an avalanche of photons is created. In short, stimulated emission of light occurs when electrons are forced by incident radiation to add more photons to an incident beam. The acronym LASER can now be understood, it stands for *light amplification by stimulated emission of radiation.*

Laser light is highly monochromatic because it is generated by electron transitions between two narrow energy levels. (As a consequence laser light can be focused to a spot less than 1μm in diameter.) Another outstanding feature of laser light is its strong collimation, that is, the parallel emergence of light from a laser window. (The cross section of a laser beam transmitted to the moon is only 3 km in diameter!) We understand the reason for the collimation best by knowing the physical setup of a laser.

The lasing material is contained in a long narrow container called the cavity; the two faces at opposite ends of this cavity must be absolutely parallel to each other. One of the faces is silvered and acts as a perfect mirror, whereas the other face is partially silvered and thus transmits some of the light (Fig. 13.31). The laser light is reflected back and forth by these mirrors, thus increasing the number of photons during each pass. After the laser has been started, the light is initially emitted in all possible directions (left part of Fig. 13.31). However, only photons which travel strictly parallel to the cavity axis will remain in action whereas the photons travelling at an angle will be eventually absorbed

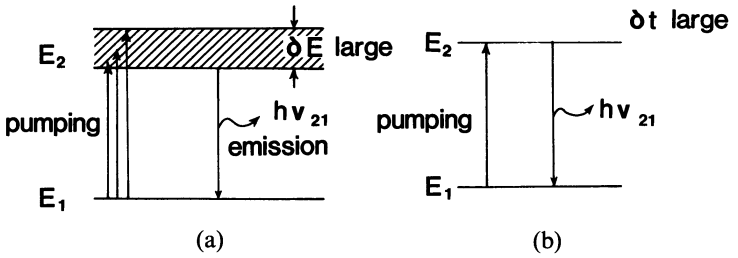

Figure 13.32. Examples of possible energy states in a two level configuration (a) δE large, that is, large pumping efficiency but little or no population inversion. (b) Potentially large population inversion (δt large) but small pumping efficiency. (*Note:* Actual two level lasers do not produce a population inversion because absorption and emission compensate each other.)

by the cavity walls (center part in Fig. 13.31). A fraction of the photons escape through the partially transparent mirror. They constitute the emitted beam.

We need to explain now how the electrons arrive at the higher energy level, that is, we need to discuss how they are *pumped* from E_1 into E_2. One of the methods is, of course, *optical pumping*, that is, the absorption of light stemming from a polychromatic light source. (Xe flashlamps for pulsed lasers or tungsten-iodine lamps for continuously operating lasers are often used for pumping. The lamp is either wrapped in helical form around the cavity, or the lamp is placed in one of the focal axes of a specularly reflecting elliptical cylinder whereas the laser rod is placed along the second focal axis.) Other pumping methods involve collisions in an electric discharge, chemical reactions, nuclear reactions, or external electron beam injection.

The *pumping efficiency* is large if the bandwidth δE of the upper electron state is broad. This way, an entire frequency range (rather than a single wavelength) leads to excited electrons (Fig. 13.32(a)).

Next, we discuss how population inversion can be achieved. For this we need to quote Heisenberg's uncertainty principle

$$\delta E \cdot \delta t \sim h, \tag{13.18}$$

which states that the time span δt, for which an electron remains at the higher energy level E_2, is large when the bandwidth δE of E_2 is narrow. In other words, a sharp energy level (δE small, δt large) supports the population inversion, Fig. 13.32(b)). On the other hand, a large pumping efficiency requires a large δE (Fig. 13.32(a)) which results in a small δt and a small population inversion. Thus, high pumping efficiency and population inversion mutually exclude each other in a two level configuration.

The three level laser (Fig. 13.33) provides improvement over a two level configuration. There, the "pump band" E_3 is broad, which enables a good pumping efficiency. The electrons revert after 10^{-7} s into an intermediate level E_2 via a nonradiative, phonon-assisted process. Since E_2 is sharp, the electrons

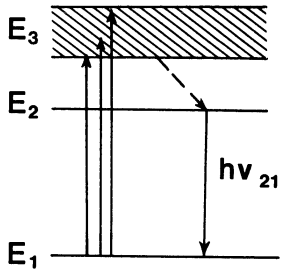

Figure 13.33. Three level laser. The nonradiative, phonon assisted decay is marked by a dashed line. Lasing occurs between levels E_2 and E_1. High pumping efficiency to E_3. High population inversion at E_2.

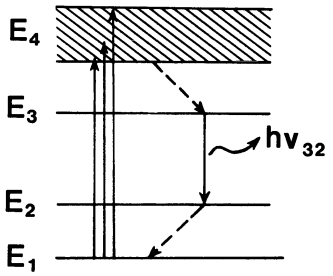

Figure 13.34. Four level laser.

remain much longer, that is, for some milliseconds on this level. This provides the required population inversion.

An even larger population inversion is obtained using a four level laser. In this configuration the energy level E_2 is emptied rapidly by electron transitions into a lower level E_1 (Fig. 13.34). It should be added that some three and four level lasers have several closely spaced pumping bands which, of course, increases the pumping efficiency.

The highest population inversion is achieved by adding *Q-switching*. For this method, the mirror in Fig. 13.31 is turned sideways during the pumping to reduce stimulated emission, that is, to build up a substantial population inversion. After some time the mirror is turned back into its original vertical position which results in a burst of light lasting 10–20 ns.

Laser materials cannot be created at will in, say, three or four level configurations. They can be, however, selected from hundreds of substances to suit a specific purpose. Laser materials include *crystals* (such as ruby), *glasses* (such as neodymium-doped glass), *gases* (such as helium, argon, xenon), *metal vapors* (such as cadmium, zinc or mercury), *molecules* (such as carbon dioxide) or *liquids* (solvents which contain organic dye molecules). Table 13.1 lists the properties of some widely used lasers. We observe that most lasers (except the tunable dye lasers) emit their light in the red or IR spectrum. Lasers can be

Table 13.1

Type of Laser	Wave-length(s) (nm)	Beam Diver-gence (mrad)	Power Output	Comments
Ruby (Cr^{3+}-doped Al_2O_3)	694.3	10	CW[a]: ~5 W pulsed: ~20 KW Q-switched: 10 MW	Optically pumped three level laser. Lasing occurs between Cr^{3+} levels. Low efficiency. Historic device.
Neodymium (Nd^{3+}-doped glass or YAG[b])	1,064	3–8	CW: 150 W pulsed: 10 KW	Optically pumped four level laser. High efficiency.
HeNe	632.8 (1150; 3390)	1	$10^{-3} - 10^{-2}$ W	See Fig. 13.35 and text. Most widely used.
CO_2	10,600 9,600	2	CW: 1–15 KW plused: 10 MW	High efficiency (20%). Lasing occurs between vibrational levels (Fig. 13.36).
GaAs Semi-conductor	840		CW 10^{-2} W	Small size, direct conversion of electrical energy into optical energy. 10% efficiency. See Fig. 13.37.
Dye (organic dyes in solvents)	360–650	3	Average: 100 W	Lasing occurs between vibrational sublevels of molecules. Tunable by Littrow prism (Fig. 13.35(a)).

[a] CW: Continuous wave.

[b] Yttrium aluminum garnet ($Y_3Al_2O_{15}$).

operated in a continuous mode (CW), or with a higher power output, in the pulsed mode. The power output varies over many orders of magnitude (and it can even be increased if Q-switching is applied). A few important laser types need special mention.

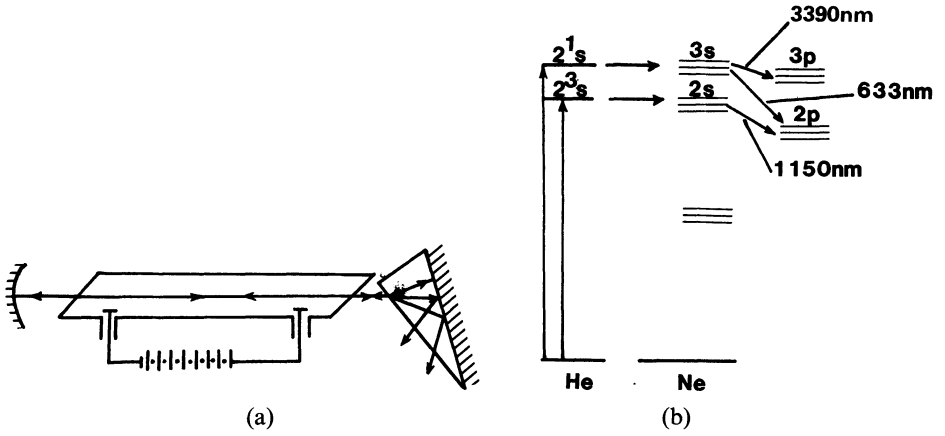

Figure 13.35. Helium–Neon Laser. (a) Schematic diagram of the laser cavity with Littrow prism to obtain preferred oscillation at one wavelength. (The end windows are inclined at the Brewster angle for which plane polarized light suffers no reflection losses.) (b) Energy level diagram for He and Ne. The decay time for the *p*-states is ~ 10 ns, that of the *s*-states 100 ns. The letters on the energy levels represent the angular momentum quantum number; the number in front of the letters gives the value for the principal quantum number; and the superscripts represent the multiplicity (singulette, doublette, etc.), see Appendix 3.

Helium–Neon Laser. A cavity about 2 mm in diameter is filled with 0.1 Torr Ne and 1 Torr He (Fig. 13.35(a)). A current which passes through the gas produces free electrons (and ions). The electrons are accelerated by the electric field and excite the He-gas by electron–atom collisions. Some of the He levels are resonant with Ne levels so that the neon gas also becomes excited by resonant energy transfer (Fig. 13.35(b)). This constitutes a very efficient pumping into the Ne 2*s*- and 3*s*-levels. (Direct electron–Ne collisions also contribute to the pumping). Lasing occurs between the neon *s*- and *p*-levels and produces three characteristic wavelengths. Suppression of two of the wavelengths is accomplished by multilayer dielectric mirrors which provide a maximum reflectivity at the desired wavelength, or by a Littrow prism, as shown in Fig. 13.35(a).

Carbon Dioxide Laser. The CO_2 molecules possesses three fundamental modes of vibration, as shown in Fig. 13.36(a). The lasing occurs between these levels as shown in Fig. 13.36(b). Pumping is accomplished by electron–atom collisions (see above) and by a resonant energy transfer from N_2 molecules which are added to the CO_2. Nitrogen (and helium) greatly improve the pumping efficiency of the CO_2 laser which is one of the most efficient and the most powerful lasers.

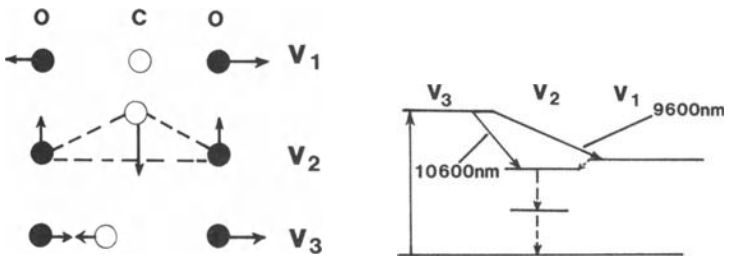

(a) (b)

Figure 13.36. CO_2-laser. (a) Fundamental modes of vibration for a CO_2 molecule; v_1: symmetric stretching mode; v_2: bending mode; v_3: asymmetric stretching mode. (b) Energy level diagram for various vibrational modes.

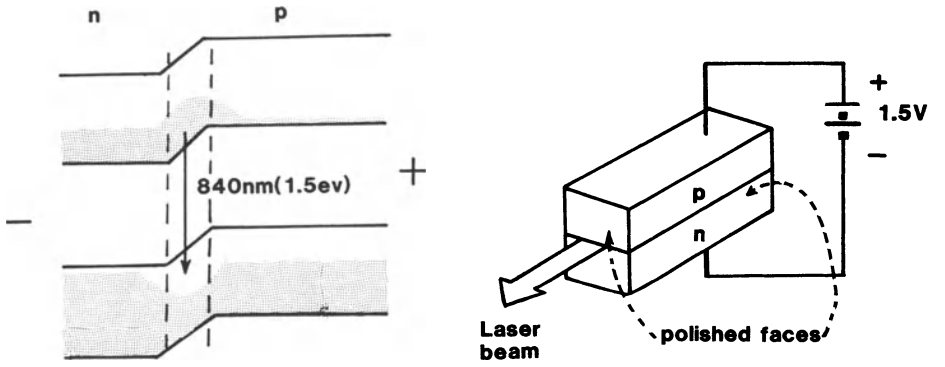

(a) (b)

Figure 13.37. (a) Energy band diagram of a heavily doped, forward biased semiconductor. (b) Schematic setup of a semiconductor laser.

Semiconductor Laser. The "cavity" for this laser consists of heavily doped ($10^{24}m^{-3}$) *n*- and *p*-type semiconductor material such as GaAs. The energy band diagram for a *p–n* junction has been shown in Fig. 8.19 and is redrawn for the case of forward bias in Fig. 13.37(a). We notice a population inversion of electrons in the depletion layer (which is characteristically 0.1 μm wide). Two opposite end faces of this *p–n* junction are made parallel and are polished or cleaved along crystal planes. The other faces are left untreated to suppress lasing in unwanted directions (Fig. 13.37(b)). A reflective coating of the window is usually not necessary since the reflectivity of the semiconductor is already 35%. The pumping occurs by direct injection of electrons and holes into the depletion region. Semiconductor lasers are small and very efficient. The emitted beam can be modulated by electrical modulation of the injection current (optical communication!).

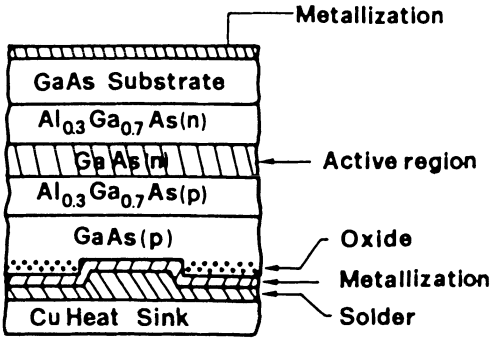

Figure 13.38. Schematic representation of a double heterojunction laser in which the active region consists of an *n*-doped GaAs layer.

Lasers for which the *p*-type and the *n*-type materials are alike (for example GaAs) are called *homojunction* lasers. In these devices the active region, in which the lasing occurs, extends over the depletion region and is about 1 μm thick. Homojunction lasers need to be cooled for continuous operation because of high absorption effects which occur in the *p*- and *n*-part of the active region. This problem is overcome by using a heterojunction laser in which for example *two* junctions are utilized as depicted in Fig. 13.38. If the refractive index of the active region is larger than that of the neighboring areas an optical waveguide structure is effectively achieved (total reflection !) which confines the laser mode within the GaAs layer. This way, virtually no energy is absorbed by the non-active, that is, absorbing *n* and *p* regions which allows the laser to be operated at room temperature.

For optical communication purposes a wide variety of wavelengths need to be generated. For example, lasers which operate at 1.3 or 1.6 μm are desirable. At these values for λ quartz (which is used for optical fibers) has absorption minima. Quaternary alloys for the active region such as $In_{1-x}\,Ga_x\,As_y\,P_{1-y}$ fulfill this requirement, whereas InP is used for the *p* and *n* sides. By varying the composition of the alloys, the output wavelength can be varied between 0.92 and 1.6 μm.

Light-Emitting Diode. A brief description of light-emitting diodes (LED) shall conclude this section. These devices are of great technical importance as an inexpensive, rugged, small, and efficient light source for display purposes. The LED consists, like the semiconductor laser, of a forward biased *p–n* junction. The above-mentioned special facing procedures are, however, omitted during the manufacturing process. Thus, the LED does not operate in the lasing mode. The emitted light is therefore neither phase coherent nor collimated. Semiconductor materials whose photon emission is caused by direct interband transitions are preferred for these devices because indirect transitions dissipate some of the energy into heat (Fig. 12.2). Furthermore, it is, of course, desirable that the light emission occurs in the visible spectrum.

Certain III/V compound semiconductors, such as $Ga_x As_{1-x} P$; GaP, and $Ga_x Al_{1-x} As$ fulfill these requirements. These materials emit light in the red, green, yellow, and orange part of the spectrum. Blue color is possible (SiC) but very expensive. The radiation leaves the device through a window which was etched through the metallic contact of the *n*-doped part (surface emitter).

Suggestions for Further Reading (Part III)

F. Abelès, ed., Optical Properties and Electronic Structure of Metals and Alloys, *Proc. Int. Conf.*, Paris, 13–16 Sept. 1965, North-Holland Publ. Co., Amsterdam (1966).
F. Abelès, ed., *Optical Properties of Solids*, North-Holland Publ. Co., Amsterdam, London (1972).
M. Born and E. Wolf, *Principles of Optics*, 3rd ed., Pergamon Press, Oxford (1965).
M. Cardona, *Modulation Spectroscopy*, *Solid State Physics*, Suppl. 11, Academic Press, New York, London (1969).
M. P. Givens, Optical Properties of Metals, in *Solid State Physics*, Vol. 6, Academic Press, New York, London (1958).
O. S. Heavens, *Optical Properties of Thin Solid Films*, Academic Press, New York, London (1955).
R. E. Hummel, *Optische Eigenschaften von Metallen und Legierungen*, Springer-Verlag Berlin, Heidelberg, New York (1971).
T. S. Moss, *Optical Properties of Semiconductors*, Buttersworth London (1959).
P. O. Nilsson, *Optical Properties of Metals and Alloys*, Solid State Physics, Vol. 29, Academic Press, New York, London (1974).
B. O. Seraphin, ed., *Optical Properties of Solids—New Developments*, North-Holland Publ. Co./American Elsevier, Amsterdam, Oxford, New York (1976).
A. V. Sokolov, *Optical Properties of Metals*, American Elsevier Publ. Co., New York (1967).
O. Svelto, *Principles of Lasers*, 2nd Ed Plenum Press, New York, London (1982).
A. Vašíček, *Optics of Thin Films*, North-Holland Publ. Co., Amsterdam (1960).
F. Wooten, *Optical Properties of Solids*, Academic Press, New York (1972).

PART IV

MAGNETIC PROPERTIES OF MATERIALS

CHAPTER 14

Foundations of Magnetism

14.1. Introduction

The phenomenon of magnetism, that is, the mutual attraction of two pieces of iron or iron ore, was surely known to the antique world. The ancient Greeks have been reported to experiment with this "mysterious" force. The name *magnetism* is said to be derived from a region in Turkey which was known by the name of *Magnesia* and which had plenty of iron ore.

Interestingly enough, a piece of magnetic material such as iron ore does not immediately attract other pieces of the same material. For this, at least one of the pieces has to be *magnetized*, that is, simply said, its internal "elementary magnets" need alignment in order for it to become a permanent magnet. Magnetizing causes no problem in modern days. One merely places iron into an electric coil through which a direct current passes for a short time. (This was discovered by Oersted at the turn of the last century.) But how did the ancients do it? There may have been at least two possibilities: first, a bolt of lightning could have caused a magnetic field large enough to magnetize a piece of iron ore. Once one magnet had been produced and identified, more magnets could have been obtained by rubbing virgin pieces of iron ore with the first magnet. There could have been another possibility: it is known that if a piece of iron is repeatedly hit very hard, the "elementary magnets" will be "shaken loose" and align in the direction of the earth's magnetic field. An iron hammer, for example, is *north-magnetic* on its face of impact in the northern hemisphere. Could it have been that a piece of iron ore was used as a hammer and thus it became a magnet?

Magnetic materials made an important contribution to the development of the consciousness of mankind because they paved the way to discoveries of new continents once the compass had been invented. (A compass needle is a

pivoted bar magnet which positions itself approximately in the north–south direction. We call the tip that points to geographic north, the north-seeking pole, or simply the north pole, and the opposite end the south pole.) The British coined the word *lodestone* for the iron ore Fe_3O_4 which meant to say that this mineral points the way. Our modern technology would be unthinkable without magnetic materials and magnetic properties. Magnetic tapes, television, motors, generators, telephones, and transformers are only a few examples of their applications.

Thus far, we have used the word magnetism very loosely when implying the mutual magnetic attraction of pieces of iron. There are, however, several other classes of magnetic materials that differ in kind and degree in their mutual interaction. We shall distinguish in the following between ferromagnetism (which term we restrict to the classical magnetism in iron and a few other metals and alloys) and para-, dia-, antiferro-, and ferrimagnetism. The oldest known magnetic ore, the magnetite, or lodestone, Fe_3O_4 is actually a *ferri*magnet $(FeO) \cdot Fe_2O_3$ called *iron ferrite*.

In the sections to come, we shall define at first the magnetic constants and then remind the readers of some fundamental equations in magnetism before discussing magnetism by classical and quantum theory. Practical applications of magnetic materials are presented in a final chapter.

14.2. Basic Concepts in Magnetism

The goal of this chapter is to characterize the magnetic properties of materials. At least five different types of magnetic materials exist as mentioned in the Introduction. A qualitative, as well as a quantitative distinction between these different types, can be achieved in a relatively simple way by utilizing a method proposed by Faraday. The magnetic material to be investigated is suspended from one of the arms of a sensitive balance and is allowed to reach into an inhomogeneous magnetic field (Fig. 14.1). Diamagnetic materials are expelled from this field, whereas para-, ferro-, antiferro-, and ferrimagnetic materials are attracted in different degrees. It has been empirically found that the apparent loss or gain in mass, that is, the force F on the sample exerted by the magnetic field is

$$F = V\chi H\frac{dH}{dx}, \tag{14.1}$$

where dH/dx is the change of the "magnetic field strength" $|\mathbf{H}|$ in the x-direction and V is the volume of the sample. The magnetic material can be characterized by a material constant, χ, called the susceptibility which expresses how responsive this material is to an applied magnetic field (see (14.1)). Characteristic values for χ are given in Table 14.1. Frequently, a second material constant, the permeability μ, is used. This constant is related

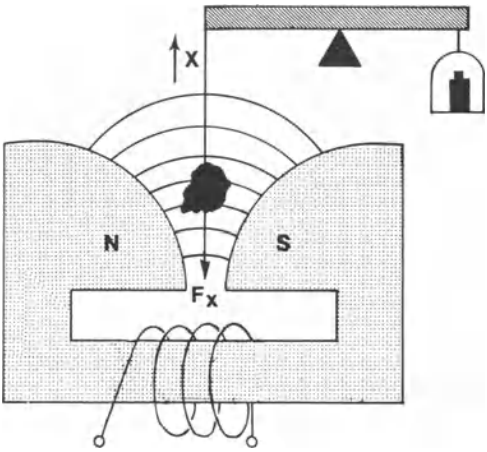

Figure 14.1. Measurement of the magnetic susceptibility in an inhomogeneous magnetic field.

Table 14.1. Magnetic Constants of Some Materials at Room Temperature (Source: Landolt–Börnstein, *Zahlenwerte der Physik*, 6th ed., Springer-Verlag, Berlin (1962), Vol. 11/9).

Material	χ_m [cm^3/g]	χ_v Unitless	μ Unitless	Type of Magnetism
Bi	-1.34×10^{-6}	-13.13×10^{-6}	0.99983	
Be	-1.0×10^{-6}	-1.85×10^{-6}	0.99998	
Ag	-0.192×10^{-6}	-2.016×10^{-6}	0.99997	Diamagnetic
Au	-0.142×10^{-6}	-2.74×10^{-6}	0.99996	
Ge	-0.106×10^{-6}	-0.564×10^{-6}	0.99999	
Cu	-0.086×10^{-6}	-0.77×10^{-6}	0.99999	
Superconductors[a]		$\sim -8 \times 10^{-2}$		
Snβ	$+0.026 \times 10^{-6}$	$+0.19 \times 10^{-6}$	1	
W	$+0.32 \times 10^{-6}$	$+6.18 \times 10^{-6}$	1.00008	
Al	$+0.61 \times 10^{-6}$	$+1.65 \times 10^{-6}$	1.00002	Paramagnetic
Pt	$+0.983 \times 10^{-6}$	$+21.04 \times 10^{-6}$	1.00026	
Mn	$+8.9 \times 10^{-6}$	$+66.13 \times 10^{-6}$	1.00083	
Low Carbon Steel			5×10^3	
Fe–3% Si (grain oriented)			4×10^4	Ferromagnetic
Ni–Fe–Mo			10^6	

[a] See Section 7.6.1

Note: The table lists the mass susceptibility (or specific susceptibility), χ_m, whose unit is cm^3/g and the unitless volume susceptibility, χ_v, which was calculated from χ_m by multiplying χ_m by the density. Other sources may provide mass, atomic, molar, or gram equivalent susceptibilities in cgs or mks units.

to the susceptibility by the definition

$$\mu = 1 + 4\pi\chi. \tag{14.2}$$

For empty space, and for all practical purposes, also for air, χ is zero and thus $\mu = 1$ (see equation (14.2)). For diamagnetic materials one finds χ to be small and negative and thus μ slightly less than 1 (see Table 14.1). For para- and antiferromagnetic materials χ is again small, but positive. Thus, μ is slightly larger than one. Finally, χ and μ are large and positive for ferro- and ferrimagnetic materials. The magnetic constants are temperature dependent, except for diamagnetic materials, as we will see later.

The magnetic field parameters at a given point in space are defined to be the magnetic field strength **H**, which we introduced above, and the magnetic flux density or magnetic induction **B**. In free space **B** and **H** are identical. Inside a magnetic material, the induction **B** consists of the free-space component (**H**), plus a contribution to the magnetic field which is due to the presence of matter:

$$\mathbf{B} = \mathbf{H} + 4\pi\mathbf{M}, \tag{14.3}$$

where **M** is called the "magnetization" of the material. For a material in which the magnetization is thought to be proportional to the applied field strength we define

$$\mathbf{M} = \chi\mathbf{H}. \tag{14.4}$$

Combining (14.2), (14.3), and (14.4) yields

$$\mathbf{B} = \mathbf{H}(1 + 4\pi\chi) = \mu\mathbf{H}. \tag{14.5}$$

Above, we defined **B** to be the magnetic flux density in a material, that is, the magnetic flux per unit area. The magnetic flux ϕ is then defined as the scalar product of **B** and area (represented by a vector **A**), that is,

$$\phi = \mathbf{B} \cdot \mathbf{A}. \tag{14.6}$$

In free space for which $\mathbf{M} = 0$ we obtain, by using (14.3),

$$\phi = \mathbf{H} \cdot \mathbf{A}. \tag{14.7}$$

Finally, we need to define the magnetic moment $\boldsymbol{\mu}_m$ through the following equation:

$$\mathbf{M} = \frac{\boldsymbol{\mu}_m}{V}, \tag{14.8}$$

that is, the magnetization is the magnetic moment per unit volume.

*14.3. Units

It needs to be noted that in magnetic theory several unit systems are commonly in use. The scientific and technical literature on magnetism is still widely written in electromagnetic cgs (emu) units. Thus, we shall use this system here.

Conversion into SI units are given in Appendix four. The magnetic field strength in cgs units is measured in Oersted and the magnetic induction in Gauss. Equation (14.3) reads in SI units

$$B = \mu_0(H + M), \tag{14.9}$$

where $\mu_0 = 4\pi \times 10^{-7}$ (kg · m/C^2) is called the permeability of free space. Writing (14.5) in SI units yields

$$B = \mu_0(1 + \chi)H = \mu_0\mu_r H, \tag{14.10}$$

where

$$\mu_r = (1 + \chi) \tag{14.11}$$

is now called the relative permeability. Comparison between (14.11) and (14.2) explains the difference of 4π in the permeabilities mentioned above. The (relative) permeability in the cgs and SI system is unitless and has the same value. The volume susceptibility is also unitless in both systems but differs by a factor 4π (see Appendix 4).

Problems

1. Show that the unit for 1 Oe is equivalent to [g$^{1/2}$/cm$^{1/2}$ · s] by making use of (14.1).
2. An electromagnet is a helical winding of wire through which an electric current flows. The magnetic field strength of such a solenoid is (in cgs units)

$$|\mathbf{H}| = \frac{4\pi}{10}\frac{In}{l}(\text{Oe}),$$

where I is the current (in A), n the number of turns, and l is the length of the solenoid (in cm). In SI units the field strength is $H = In/l$ (A-turns/m or A/M.) A solenoid of 1000 turns is 10 cm long and is passed through by a current of 2 A. What is the field strength in Oe and A/m?

CHAPTER 15

Magnetic Phenomena and Their Interpretation—Classical Approach

15.1. Overview

We stated in the last chapter that different types of magnetism exist and that they are characterized by the magnitude and the sign of the susceptibility (see Table 14.1).

Since various materials respond so differently in a magnetic field, we suspect that several fundamentally different mechanisms must be responsible for the magnetic properties. In the first part of this chapter we shall attempt to unfold the multiplicity of the magnetic behavior of materials by describing some pertinent experimental findings and giving some brief interpretations. In the sections to follow, we shall treat the atomistic theory of magnetism in more detail.

15.1.1. Diamagnetism

Ampère postulated more than one hundred years ago that *molecular currents* are responsible for the magnetism in a solid. He compared the molecular currents to an electric current in a loop-shaped piece of wire which is known to cause a magnetic moment. Today, we replace Ampère's molecular currents by *orbiting valence electrons.*

For the understanding of diamagnetism, a second aspect needs to be considered. It was found by *Lenz* that a current is induced in a wire loop whenever a bar magnet is moved towards (or from) this loop. The current thus induced causes in turn a magnetic moment which is opposite to the one of the bar magnet (Fig. 15.1). (This has to be so in order for mechanical work to be expended in producing the current; otherwise, a perpetual motion would be

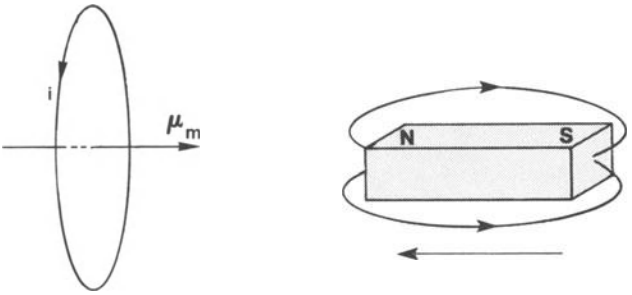

Figure 15.1. Induction of a current in a loop-shaped piece of wire by moving a bar magnet towards (or from) the wire loop. The current in the loop causes a magnetic field which is directed opposite to the magnetic field of the bar magnet (Lenz's law).

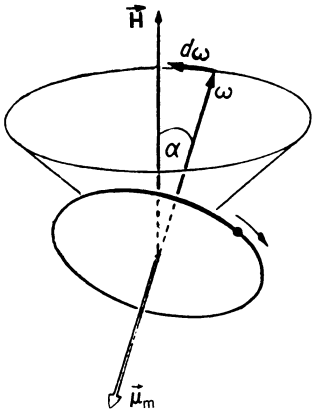

Figure 15.2. Precession of an orbiting electron in an external magnetic field. Precession is the motion which arises as a result of external torque acting on a spinning body (such as a spinning top) or, as here, on an orbiting electron.

created!) Diamagnetism may then be explained by postulating that the external magnetic field induces a change in the magnitude of inner-atomic currents, that is, *the external field accelerates or decelerates the orbiting electrons*, in order that their magnetic moment is in the opposite direction from the external magnetic field. In other words, the responses of the orbiting valence electrons counteract the external field and thus shield the inner electrons from an external magnetic field. A more accurate and quantitative explanation of diamagnetism replaces the induced currents by precessions of the electron orbits about the magnetic field direction (Larmor precession, see Fig. 15.2).

So far, we implicitly considered only electrons which are *bound* to their respective nuclei. Now, metals are known to also have *free electrons*. They are

forced to move in a magnetic field in a circular path. This leads to a second contribution to the diamagnetic moment; specifically, the circulating *free* electrons cause a magnetic moment, similarly as described above.

15.1.2. Paramagnetism

Paramagnetism in *solids* is attributed to a large extent to a magnetic moment that results from electrons which spin around their own axis. We have already introduced the *electron spin* in Section 6.4 and mentioned there that because of the Pauli principle, no two electrons can have the same value and sign for the spin moment. In other words, each electron state can be occupied by two electrons only; one with positive and one with negative spin, or as it is often said, one with spin up and one with spin down. An external magnetic field tries to turn the unfavorably oriented spin moments in the direction of the external field. We shall talk about the quantum mechanical aspect of spin paramagnetism in more detail in Chapter 16. Spin paramagnetism is slightly temperature dependent. It is in general very weak and is observed in some metals and in salts of the transition elements.

Free atoms (dilute gases) as well as rare-earth elements and their salts and oxides possess an additional source of paramagnetism. It stems from the magnetic moment of the orbiting electrons. Without an external magnetic field, these magnetic moments are randomly oriented and thus they mutually cancel one another. As a result, the net magnetization is zero. However, when an external field is applied the individual magnetic vectors tend to turn into the field direction. Thermal agitation counteracts the alignment. Thus, electron-orbit paramagnetism is temperature dependent.

The temperature dependence of many paramagnetic materials is governed by the experimentally found Curie law which states that the susceptibility χ is inversely proportional to the absolute temperature T

$$\chi = \frac{C}{T}, \tag{15.1}$$

where C is called the Curie constant. For many other substances, a more general relationship is observed, which is known as the Curie–Weiss law:

$$\chi = \frac{C}{T - \theta}, \tag{15.2}$$

where θ is another constant which has the same unit as the temperature and may have positive as well as negative values (see Fig. 15.3). We shall explain the meaning of the constants C and θ in Section 15.3.

Metals, with a few exceptions, do *not* obey the Curie–Weiss law, as we shall see in Chapter 16. However, Ni, the rare earth elements, and salts of the transition elements (for example, the carbonates, chlorides, or sulfates of Fe, Co, Cr, Mn) obey the Curie–Weiss law quite well.

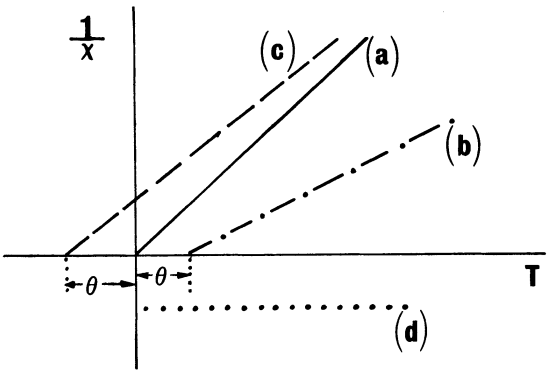

Figure 15.3. Schematic representation of the Curie law (a) and the Curie–Weiss law (b) and (c). The diamagnetic behavior is also shown for comparison (d).

We have just mentioned that in most solids, only spin paramagnetism is observed. This is believed to be due to the fact that in crystals, the electron orbits are essentially coupled to the lattice which prevents the orbital magnetic moments from turning into the field direction. One says in this case that the orbital moments are "quenched." Exceptions are the rare earth elements and their derivatives, which have "deep lying" 4*f*-electrons.[1] The latter ones are shielded by the outer electrons from the crystalline field of the neighboring ions. Thus, the orbital magnetic moments of the *f*-electrons may turn into the external field direction and contribute to electron-orbit paramagnetism. The fraction of the total magnetic moment contributed by orbital motion versus by spin is defined as the "*g*-factor."

It is now possible to make some general statements about whether para- or diamagnetism might be expected in certain materials. For paramagnetic materials, the magnetic moment of the electrons is thought to point *in* the direction of the external field, that is, the magnetic moment enhances the external field. Diamagnetism counteracts an external field, as we have seen in Section 15.1.1. Thus, para- and diamagnetism oppose each other. Solids, which have both orbital as well as spin paramagnetism, are clearly paramagnetic. Rare earth metals with unfilled 4*f*-electron-bands are an example for this. In most other solids, however, the orbital paramagnetism is "quenched," as we said above. Yet, they still might have spin paramagnetism. The presence of a net spin-paramagnetic moment depends upon whether or not the magnetic moments of the individual spins cancel each other. More specifically, if a solid has *completely filled electron bands*, we anticipate (because of the Pauli principle) the same number of electrons with spins up as well as with spins down. For example, a completely filled *d*-band contains 5N electrons with spins up and 5N electrons with spins down. This results in a cancellation of the

[1] See Appendix 3.

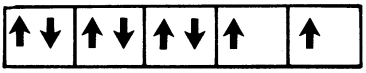

Figure 15.4. Schematic representation of the spin alignment in a *d*-band which is partially filled with eight electrons (Hund's rule).

spin moments and no net spin paramagnetism is expected. These materials are thus diamagnetic (no orbital and no spin paramagnetic moment). We mention as examples for filled bands, intrinsic semiconductors, insulators, and ionic crystals such as NaCl. (In the latter case, an electron transfer occurs between cations and anions which causes closed electron shells, that is, filled bands.)

In materials with partially filled bands, the electron spins are arranged, according to "Hund's rule" in such a manner that the total spin moment is maximized. This condition is energetically more favorable, as quantum mechanics shows. For example, in an atom with eight valence *d*-electrons, five of the spins align, say, up, and three spins point down which results in a net total of 2 spins up (Fig. 15.4). The atom is then expected to have two units of magnetism.

The smallest unit (or quantum) of the magnetic moment is called one Bohr magneton

$$\mu_B = \frac{eh}{4\pi m} = 0.927 \times 10^{-20} \left(\frac{\text{erg}}{\text{Oe}}\right). \tag{15.3}$$

(The symbols have the usual meaning.) We shall return to the Bohr magneton in Chapter 16. In the above example, the metal is said to have 2 Bohr magnetons per atom.

One word of caution should be added about applying the above general principles too rigidly. Some important exceptions do exist. They must be explained by considering additional information (see Chapter 16). For example, copper which has one *s*-electron in its valence band should be paramagnetic according to our considerations brought forward so far. In reality, copper is diamagnetic. Other examples are superconductors which are perfect diamagnetics below a transition temperature; they repel the magnetic flux lines from their interior, as we explained in Section 7.6.1.

15.1.3. Ferromagnetism

We turn now to ferromagnetics and commence with the experimentally found magnetization curve for these materials. A newly cast piece of iron (often called *virgin iron*) is inserted into a ring-shaped solenoid (Fig. 15.5). (The ring shape is used to contain the magnetic field within the coil.) If the external field strength is increased (by increasing the current in the primary winding), then the magnetization (measured in a secondary winding with a flux meter) rises at first slowly and then more rapidly (Fig. 15.6). Finally, M levels off and reaches

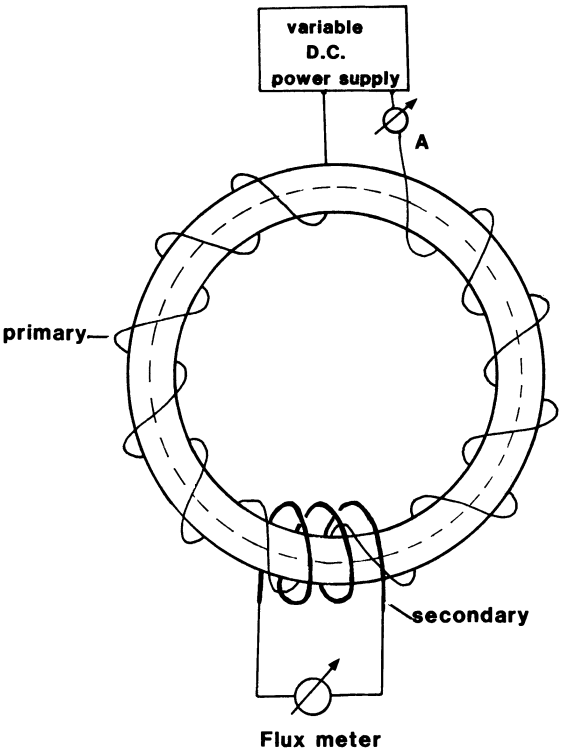

Figure 15.5. A ring-shaped solenoid with primary and secondary windings. Note the dashed flux lines.

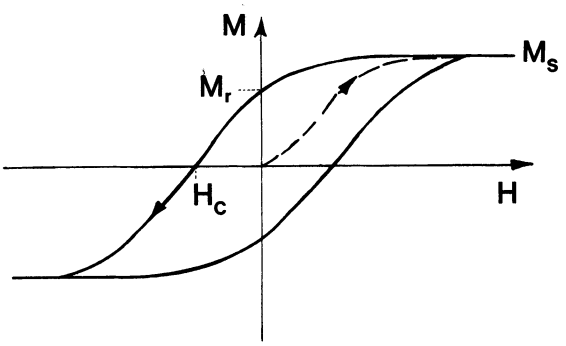

Figure 15.6. Schematic representation of a hysteresis loop of a ferromagnetic material. The dashed curve is for virgin material.

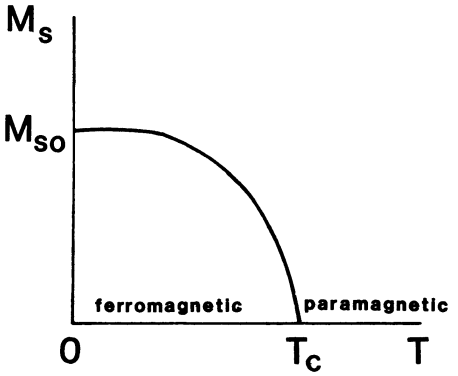

Figure 15.7. Temperature dependence of the saturation magnetization of ferromagnetic materials. See also the enlarged area near T_C in Fig. 15.8.

Table 15.1. Saturation Magnetization at 0 K and Curie Temperature (T_C) for Some Ferromagnetic Materials

Metal	$4\pi M_{s0}$ (Maxwells/cm^2)	$T_C(K)$
Fe	2.20×10^4	1043
Co	1.82×10^4	1404
Ni	0.64×10^4	631
Gd	7.11×10^4	289

a constant value, called the saturation magnetization M_s. When H is reduced to zero, the magnetization retains a positive value, called the remanent magnetization or remanence M_r. It is this retained magnetization which is utilized in permanent magnets. The remanent magnetization can be removed by reversing the magnetic field strength to a value H_c, called the coercive field. Solids having a large combination of M_r and H_c are called *hard magnetic materials* (in contrast to *soft* magnetic materials for which the area inside the loop of Fig. 15.6 is very small). A complete cycle through positive and negative H-values, as shown in Fig. 15.6, is called a *hysteresis loop*. It should be noted that a second type of hysteresis curve is often used, *in which B* (instead of M) is plotted versus H. No saturation value for B is observed. (The residual induction B_r at $H = 0$ is called the retentivity. Removal of B_r requires a field which is called *coercivity*. However, remanence and retentivity, as well as coercive field, coercive force, and coercivity are often used interchangeably.)

The saturation magnetization is temperature dependent (Fig. 15.7). Above the Curie temperature, T_C, ferromagnetics become paramagnetic. Table 15.1 lists saturation magnetizations and Curie temperatures of some elements.

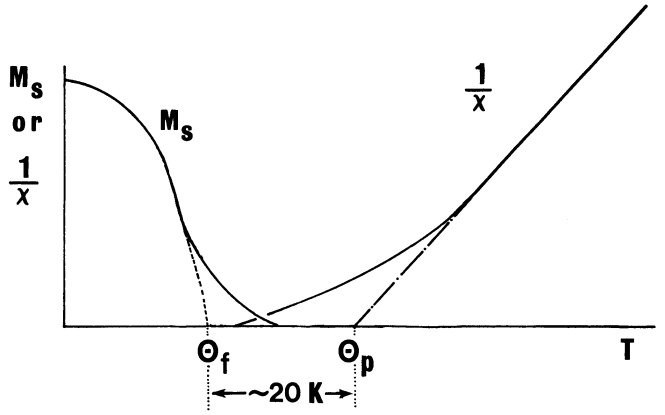

Figure 15.8. Enlarged area near the Curie temperature, showing the paramagnetic Curie point θ_p (which is identical with the θ in the Curie–Weiss law) and the ferromagnetic Curie point θ_f (which is identical with T_C).

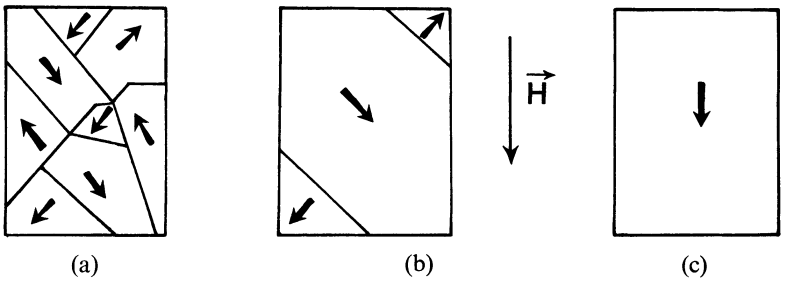

Figure 15.9. (a) Domain walls and spontaneous magnetization of a virgin piece of ferromagnetic material below T_C. (b) Growth of domains in a magnetic field. (c) Single magnetic domain with spin alignment in the external field direction. The domain boundaries (Bloch walls) are *not* identical with the grain boundaries.

For ferromagnetics the Curie temperature T_C and the constant θ in the Curie–Weiss law are nearly identical. A small difference exists, however, because the transition from ferromagnetism to paramagnetism is gradual, as can be seen in Fig. 15.8.

A few preliminary words should be said to explain the above mentioned observations. In ferromagnetic materials, the spins of unfilled *d*-bands spontaneously align parallel below T_C, that is, they align within small domains without the presence of an external magnetic field (Fig. 15.9). Specifically, the individual domains are magnetized to saturation. The spin direction in each domain is, however, different (see Fig. 15.9(a)) so that the individual magnetic moments for the material as a whole cancel each other and the net magnetization is zero. An external magnetic field causes those domains whose spins are

parallel or nearly parallel to the external field to grow at the expense of the unfavorably aligned domains (Fig. 15.9(b) and (c)). An increase in temperature progressively destroys the spontaneous alignment. The gradual transition from ferromagnetism to paramagnetism is believed to be due to the fact that slightly above T_C, small clusters of spins are still aligned parallel to each other, a phenomenon which is called magnetic short-range order. We shall return to ferromagnetism in Section 15.4 and Chapter 16.

15.1.4. Antiferromagnetism

Antiferromagnetic materials exhibit, just as ferromagnetics, a spontaneous alignment of moments below a critical temperature. However, the responsible neighboring atoms in antiferromagnetics are aligned in an antiparallel fashion (Fig. 15.10). Actually, one may consider an antiferromagnetic crystal to be divided into two interpenetrating sublattices A and B, each of which has a spontaneous parallel alignment of spins. Figure 15.10 depicts the spin alignments for two manganese compounds. (Only the spins of the manganese ions contribute to the antiferromagnetic behavior.) Figure 15.10(a) shows that the ions in a given (111) plane possess parallel spin alignment, whereas ions in the adjacent plane have antiparallel spins with respect to the first plane. Thus, the magnetic moments of the solid cancel each other and the material as a whole has no net magnetic moment.

Antiferromagnetic materials are paramagnetic above the *Néel temperature* T_N, that is, they obey there a linear $T = f(1/\chi)$ law (see Fig. 15.11). Below T_N, however, the inverse susceptibility may rise with decreasing temperature. The extrapolation of the paramagnetic line to $1/\chi = 0$ yields a negative θ. Thus, the

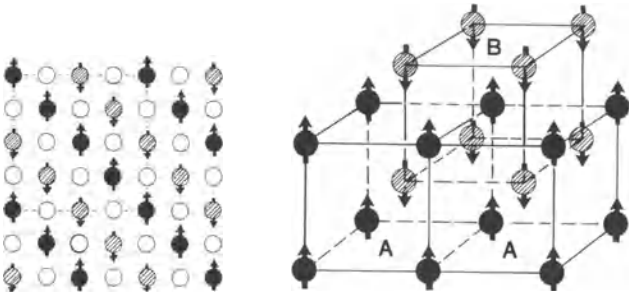

(a) (b)

Figure 15.10. Schematic representation of spin alignments for antiferromagnetics at 0 K: (a) Two-dimensional representation of MnO. The oxygen ions (open circles) do not contribute to the antiferromagnetic behavior. MnO has a NaCl structure. (b) Three-dimensional representation of the spin alignment of manganese ions in MnF_2. (The fluorine ions are not shown.) This figure demonstrates the interpenetration of two manganese sublattices A and B having antiparallel aligned moments.

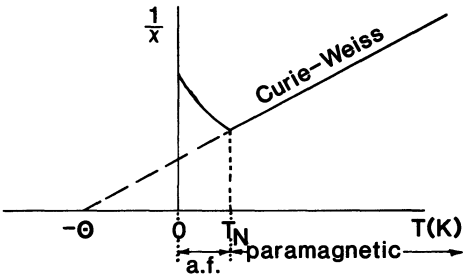

Figure 15.11. Schematic representation of the temperature dependence of a polycrystalline antiferromagnetic (a.f.) material.

Table 15.2. Characteristic Data for Some Antiferromagnetic Materials

Substance	$T_N(K)$	$-\theta(K)$
MnO	116	610
MnF_2	67	82
α-Mn	100	?
FeO	198	570
NiO	523	~2000
CoO	293	330
Cr	310	?

Curie–Weiss law (15.2) needs to be modified for antiferromagnetics to read

$$\chi = \frac{C}{T-(-\theta)} = \frac{C}{T+\theta}. \tag{15.4}$$

The Néel temperature is often below room temperature (Table 15.2). Most antiferromagnetics are found among ionic compounds. They are insulators or semiconductors. No practical application for antiferromagnetism is known at this time.

15.1.5. Ferrimagnetism

Ferrimagnetic materials are of great technical importance because they exhibit a spontaneous magnetic moment below a Curie temperature just as iron, cobalt, or nickel and they are poor electrical conductors. A large resistivity is often desired for high frequency applications (e.g., to prevent eddy currents in cores of coils, see Chapter 17).

To explain the spontaneous magnetization in ferrimagnetics, Néel proposed that two sublattices should exist in these materials (just as in antifer-

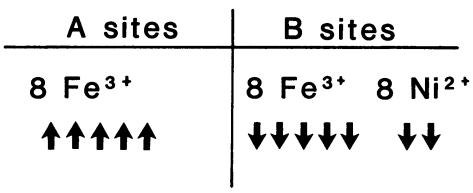

Figure 15.12. Distribution of spins upon A and B sites for the inverse spinel $NiO \cdot Fe_2O_3$. The spins within one site are arranged considering Hund's rule (Fig. 15.4). The iron ions are equally distributed among the A and B sites. The Ni ions are only situated on B sites. The relevance of the number of ions per unit cell is explained later on in the text.

Table 15.3. Calculated and Measured Number of Bohr Magnetons for Some Ferrites

Ferrite	Mn	Fe	Co	Ni	Cu
Calculated μ_B	5	4	3	2	1
Measured μ_B	4.6	4.1	3.7	2.3	1.3

romagnetics) each of which contains ions whose spins are aligned parallel to each other. The crucial point is that each of the sublattices contain a *different* amount of magnetic ions. This causes some of the magnetic moments to remain uncancelled. As a consequence, a net magnetic moment results. Ferrimagnetic materials can thus be described as *imperfect antiferromagnetics*. The crystallography of ferrites is rather complex. We defer its discussion until later. For the time being it suffices to know that there are two types of lattice sites which are available to be occupied by the metal ions. They are called A sites and B sites. (As before, oxygen ions do not contribute to the magnetic moments).

We will now discuss as an example nickel ferrite, $NiO \cdot Fe_2O_3$. The Fe^{3+} ions are equally distributed between A and B sites (Fig. 15.12) and since ions on A and B sites exhibit spontaneous magnetization in opposite directions, we expect overall cancellation of spins for these ions. Specifically, atomic iron possesses six $3d$-electrons and two $4s$-electrons ($3d^6 4s^2$, see Appendix 3). The Fe^{3+} ions are deprived of three electrons, so that five d-electrons, or five spin moments per atom remain in its outermost shell. This is indicated in Fig. 15.12.

The electron configuration of nickel in its atomic state is $3d^8 4s^2$. Two electrons are stripped in the Ni^{2+}-ion so that eight d-electrons per atom remain. They are arranged, according to Hund's rule (Fig. 15.4), to yield two net magnetic moments (Fig. 15.12). All nickel ions are accommodated on the B sites. Nickel ferrite is thus expected to have two uncancelled spins, that is, 2 Bohr magnetons (per formula unit), which is essentially observed (see Table 15.3).

The small discrepancy between experiment and calculation is believed to

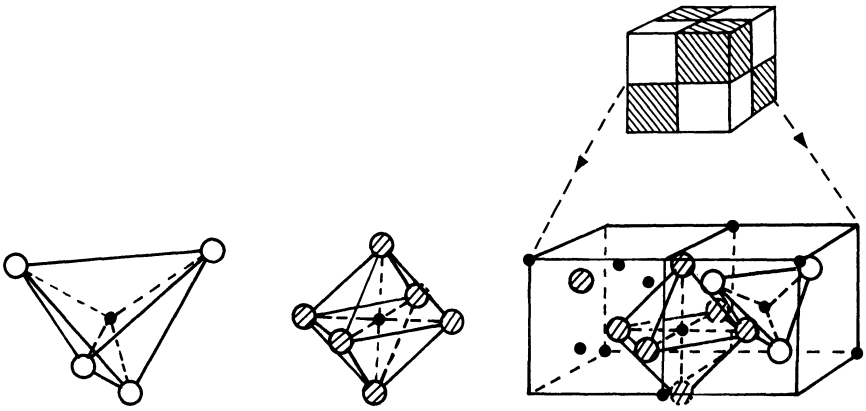

Figure 15.13. Crystal structure of cubic ferrites. The small, filled circles represent metal ions, the large open or shaded circles represent oxygen ions; (a) tetrahedral or A sites; (b) octahedral or B sites; (c) one fourth of the unit cell of a cubic ferrite. A tetrahedron and an octahedron are marked. Adapted from Smit, J., and Wijn, H.P.J. (1959) *Ferrites*, John Wiley & Sons, Inc., New York.

be caused by some contributions of orbital effects to the overall magnetic moment, and by a slight deviation of the distribution of metal ions on the A and B sites from that shown in Fig. 15.12.

The unit cell of cubic ferrites contains a total of 56 ions. Some of the metal ions are situated inside a *tetrahedron formed by the oxygen ions*. These are the above mentioned A sites (Fig. 15.13(a)). Other metal ions are arranged in the center of an *octahedron* and are said to be on the B sites (Fig. 15.13(b)). The A and B sites are nestled inside a unit cell (Fig. 15.13(c)). Now, only 8 tetrahedral sites and 16 octahedral sites are occupied by metal ions. In $NiO \cdot Fe_2O_3$ twice as many iron ions as nickel ions are present. Eight of the Fe^{3+}-ions per unit cell occupy the A sites, eight of them occupy some of the B sites and the eight Ni^{2+} ions fill the remaining B sites (Fig. 15.12). This distribution is called an *inverse spinel structure* (in contrast to a *normal spinel* such as for $ZnO \cdot Fe_2O_3$ in which *all* Fe^{3+} ions occupy the B sites).

The temperature dependence of most ferrimagnetics is very similar to ferromagnetics (Fig. 15.14): The saturation magnetization decreases with increasing temperature until it vanishes at a Curie temperature T_C. Above T_C, ferrimagnetics behave paramagnetically, having a nonlinear $1/\chi$ versus T relationship.

In conclusion, this section described in a mostly qualitative way the difference between dia-, para-, ferro-, antiferro-, and ferrimagnetism. In the sections to come, we shall again pick up the different forms of magnetism and deepen our understanding of these phenomena by following essentially the train of thought brought forward by Langevin, Weiss, and Néel.

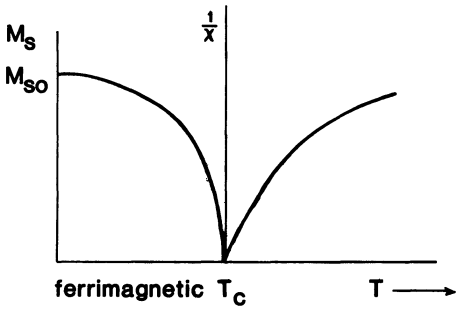

Figure 15.14. Schematic representation of the temperature dependence of the saturation magnetization M_s and the reciprocal susceptibility for ferrites.

15.2. Langevin Theory of Diamagnetism

We shall develop now the classical theory of diamagnetism in a quantitative way as put forward by Langevin at the turn of this century.

We stated before that the orbital motion of an electron about its nucleus induces a magnetic moment μ_m. We compared the latter with a magnetic moment which is created by a current passing through a loop-shaped wire. This magnetic moment is naturally larger, the larger the current I, and the larger the area A, of the orbit or loop:

$$\mu_m = I \cdot A = \frac{q}{t} A = \frac{q}{s/v} A = \frac{ev\pi r^2}{2\pi r} = \frac{evr}{2} \tag{15.5}$$

(q is the charge in general, e the electron charge, and r the radius of the orbit).

We know that an external magnetic field accelerates (or decelerates) the orbiting electrons, which results in a change in magnetic moment. We shall now calculate this change in μ_m.

The external magnetic field induces an electric field (Section 15.1.1) which, in turn, exerts an electrostatic force $|\mathbf{F}|$ on the orbiting electron which is:

$$F = ma = \mathscr{E}e, \tag{15.6}$$

where $|\mathscr{E}|$ is the electric field strength and m is the mass of the electron. From this equation we obtain the acceleration of the electron

$$a = \frac{dv}{dt} = \frac{\mathscr{E}e}{m}. \tag{15.7}$$

To calculate the acceleration we need to know the electric field strength $\mathscr{E}$. It is defined as the ratio of the induced voltage (or emf) V_e per orbit length L (see Section 7.1), that is

$$\mathscr{E} = \frac{V_e}{L}. \tag{15.8}$$

As we said earlier, a change in an external magnetic flux ϕ induces in a loop-shaped wire an emf which opposes, according to Lenz's law, the change in flux:

$$V_e = -\frac{d\phi}{dt} = -\frac{d(HA)}{dt} \tag{15.9}$$

(see (14.7.)). Thus, the acceleration of the electron becomes, by combining (15.7)–(15.9),

$$\frac{dv}{dt} = \frac{\mathscr{E}e}{m} = \frac{V_e e}{Lm} = -\frac{eA}{Lm}\frac{dH}{dt} = -\frac{e\pi r^2}{2\pi rm}\frac{dH}{dt} = -\frac{er}{2m}\frac{dH}{dt}. \tag{15.10}$$

A change in the magnetic field strength from 0 to H yields a change in the velocity of the electrons:

$$\int_{v_1}^{v_2} dv = -\frac{er}{2m}\int_0^H dH \tag{15.11}$$

or

$$\Delta v = -\frac{erH}{2m}. \tag{15.12}$$

This change in electron velocity yields in turn a change in magnetic moment, as we see by combining (15.5) with (15.12):

$$\Delta\mu_m = \frac{e\Delta vr}{2} = -\frac{e^2r^2H}{4m}. \tag{15.13}$$

So far we implicitly assumed that the magnetic field is perpendicular to the plane of the orbiting electron. In reality, however, the orbit plane varies constantly in direction with respect to the external field. Thus, we have to find an average value for $\Delta\mu_m$ which we expect to be slightly smaller than that given in (15.13) since $\Delta\mu_m$ approaches zero when the field direction and the orbit plane become parallel. A simple calculation (see Problem 2) yields

$$\overline{\Delta\mu_m} = -\frac{e^2\bar{r}^2H}{6m}. \tag{15.14}$$

One further consideration needs to be made. Up to now, we treated only *one* electron. If we take all Z electrons in the outermost orbit into account (Section 15.1.1), then the *average change in magnetic moment per atom* is

$$\overline{\Delta\mu_m} = -\frac{e^2Z\bar{r}^2H}{6m}. \tag{15.15}$$

The *magnetization, caused by this change of magnetic moment* is, according to (14.8),

$$M = \frac{\mu_m}{V} \equiv -\frac{e^2Z\bar{r}^2H}{6mV}. \tag{15.16}$$

This, finally, yields together with (14.4) the susceptibility:

$$\boxed{\chi = \frac{M}{H} = -\frac{e^2 Z \bar{r}^2}{6mV} = -\frac{e^2 Z \bar{r}^2}{6m} \frac{N_0 \delta}{W},} \tag{15.17}$$

where $N_0\delta/W$ is the number of atoms per unit volume (with N_0 = Avogadro constant, δ = density, and W = atomic weight. Since we are working in electromagnetic cgs units, H is given in Oe, μ_m in erg/Oe, and e in abcoul.) Inserting specific numbers into (15.17) yields susceptibilities between -10^{-5} and -10^{-7}, quite in agreement with the experimental values listed in Table 14.1 (see Problem 1).

The quantities in (15.17) are essentially temperature-independent which is in agreement with the experimental observation that χ does not vary much with temperature for diamagnetic materials.

*15.3. Langevin Theory of (Electron Orbit) Paramagnetism

We turn now to the atomistic theory of paramagnetism as brought forward by Langevin. This theory should explain the observations made by Curie and Weiss, that is, it should explain the temperature dependence of the susceptibility, as shown in Fig. 15.3. The Langevin theory does *not* treat spin paramagnetism which is, as we said before, responsible for the paramagnetic behavior of many *solids* and which is only *slightly* temperature dependent.

Langevin postulated that the magnetic moments of the electrons are responsible for paramagnetism. The magnetic moments of the electrons in a crystal are thought to point in random directions. An external magnetic field tries to align the individual magnetic moments parallel to the field direction. Once aligned, the magnetic moments have a potential energy E_p which is naturally greater the larger the field strength $\mathbf{H}$ and the larger $\boldsymbol{\mu}_m$. As a matter of fact, the maximum potential energy is reached when the magnetic moments are completely aligned, that is, when $\mathbf{H}$ is parallel to $\boldsymbol{\mu}_m$. In general, the potential energy is

$$E_p = -\mu_m H \cos\alpha, \tag{15.18}$$

where α is the angle between field direction and $\boldsymbol{\mu}_m$ (see Fig. 15.15). The sign in (15.18) defines the direction in which $\boldsymbol{\mu}_m$ points to with respect to $\mathbf{H}$.

As we explained earlier, thermal agitation tends to counteract the alignment caused by the external magnetic field. The randomizing effect obeys, as usual, the laws of Boltzmann statistics. The probability of an electron to have the energy E_p is thus proportional to $\exp(-E_p/k_B T)$, where k_B is the Boltzmann constant and T the absolute temperature.

Let us assume the electrons to be situated at the center of a sphere. The

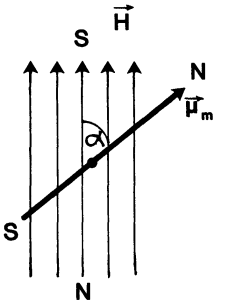

Figure 15.15. Schematic representation of the magnetic moment of an electron which has been partially aligned by an external magnetic field.

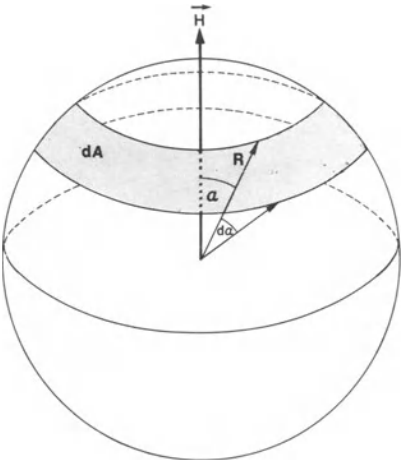

Figure 15.16. Schematic representation of a unit sphere in whose center the electrons are thought to be located.

vectors, representing their magnetic moments, may point in all possible directions. Let us consider at present a small number, dn, of these vectors only. They are thought to point in the direction interval $d\alpha$ and thus penetrate an area, dA, situated at the surface of the unit sphere; see Fig. 15.16. This infinitesimal number dn of magnetic moments which have the energy E_p is

$$dn = \text{const.}\, dA \exp(-E_p/k_B T). \tag{15.19}$$

We relate the area dA to the angle interval $d\alpha$ which yields, because of trigonometric considerations (see Problem 2),

$$dA = 2\pi R^2 \sin\alpha \, d\alpha, \tag{15.20}$$

where $R = 1$ is the radius of the unit sphere. Combining (15.18)–(15.20) gives:

$$dn = \text{const.}\, 2\pi \sin\alpha\, d\alpha \exp\left(\frac{\mu_m H}{k_B T}\cos\alpha\right). \tag{15.21}$$

We use for abbreviation

$$\xi = \frac{\mu_m H}{k_B T}. \tag{15.22}$$

Integrating (15.21) provides:

$$n = 2\pi\,\text{const.} \int_0^\pi \sin\alpha \exp(\xi\cos\alpha)\, d\alpha \tag{15.23}$$

which yields:

$$\text{const.} = \frac{n}{2\pi \int_0^\pi \sin\alpha \exp(\xi\cos\alpha)\, d\alpha}. \tag{15.24}$$

Now, the magnetization M is, according to (14.8), the magnetic moment μ_m per unit volume. In our case, the total magnetization must be the sum of all individual magnetic moments. And if we consider the magnetic moments in the field direction, then the magnetization per unit volume is

$$M = \int_0^n \mu_m \cos\alpha\, dn \tag{15.25}$$

which yields with (15.21)

$$M = \text{const.}\, 2\pi\mu_m \int_0^\pi \cos\alpha \sin\alpha \exp(\xi\cos\alpha)\, d\alpha \tag{15.26}$$

and with (15.24)

$$M = \frac{n\mu_m \int_0^\pi \cos\alpha \sin\alpha \exp(\xi\cos\alpha)\, d\alpha}{\int_0^\pi \sin\alpha \exp(\xi\cos\alpha)\, d\alpha}. \tag{15.27}$$

This function can be brought into a standard form by setting $x = \cos\alpha$ and $dx = -\sin\alpha\, d\alpha$ (see Problem 5) which yields:

$$M = n\mu_m\left(\coth\xi - \frac{1}{\xi}\right) = n\mu_m\left(\frac{\xi}{3} - \frac{\xi^3}{45} + \frac{2\xi^5}{945} - \cdots\right). \tag{15.28}$$

The term $\xi = \mu_m H/k_B T$ is usually much smaller than one (Problem 6), so that (15.28) reduces to

$$M = n\mu_m \frac{\xi}{3} = \frac{n\mu_m{}^2 H}{3k_B T}, \tag{15.29}$$

which yields for the susceptibility (14.4)

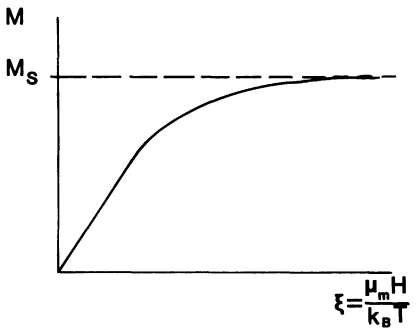

Figure 15.17. Schematic representation of the Langevin function $L(\xi) = \coth \xi - 1/\xi$.

$$\boxed{\chi_{\text{para}} = \frac{M}{H} = \frac{n\mu_m^2}{3k_B}\frac{1}{T} \equiv C \cdot \frac{1}{T}.} \tag{15.30}$$

This is Curie's law (15.1) which expresses that the susceptibility is inversely proportional to the temperature. The Curie constant is thus

$$C = \frac{n\mu_m^2}{3k_B}. \tag{15.31}$$

Let us now discuss the results of the Langevin theory for paramagnetism. If we insert actual values in (15.30), we obtain susceptibilities which are small and positive, which is quite in agreement with experimental findings (see Table 14.1 and Problem 7).

The Langevin theory for paramagnetism yields that for a given temperature and for small values of the field strength the magnetization is a linear function of H (Fig. 15.17 and equation (15.29)). For large field strengths the magnetization eventually reaches a saturation value M_s. (This behavior is quite similar to the one observed for virgin iron or other ferromagnetics.) It indicates that eventually a limit is reached at which all magnetic moments are aligned to their maximum value. The Langevin model yields a temperature dependence of the susceptibility as found experimentally by Curie for many substances. The $1/\chi$ dependence of T is characteristic for electron-orbital paramagnetism.

One can refine the Langevin result by applying quantum theory. This was done by Brillouin who took into account that not all values for the magnetic moment (or the angular moment) are allowed, that is, that the angular moments are quantized in an external magnetic field (Appendix 3). This restriction is termed *space quantization*. The calculation leads to the *Brillouin function* which improves the quantitative agreement between theory and experiment.

Finally, we know from Section 15.1.2 that the temperature dependence of the susceptibility for many solids does not always obey the Curie (or the Curie–Weiss) law. Actually, the susceptibility for most metals and alloys

varies only very little with temperature. We have learned that in these solids the spin-paramagnetism is predominant, which is not considered in the atomistic Langevin model. Quantum theory can explain the relative temperature insensitivity of spin paramagnetism, as we shall see in Section 16.1.

*15.4. Molecular Field Theory

So far, we implied that the magnetic field, which tries to align the magnetic moments, stems from an external source only. This assumption seems to be not always correct. Weiss observed that some materials obey a somewhat modified Curie law, as shown in Fig. 15.3(b) and (c). He postulated, therefore, that the magnetic moments of the individual electrons (or atoms) interact with each other. In this case, the total magnetic field, H_t, acting on a magnetic moment, is thought to be composed of two parts, namely the external field H_e and the *molecular field* H_m:

$$H_t = H_e + H_m, \tag{15.32}$$

where

$$H_m = \gamma M \tag{15.33}$$

contains the molecular field constant γ. The susceptibility is calculated by using (15.30), (15.32), and (15.33)

$$\chi = \frac{M}{H_t} = \frac{M}{H_e + \gamma M} = \frac{C}{T}. \tag{15.34}$$

Solving (15.34) for M yields

$$M = \frac{H_e C}{T - \gamma C}. \tag{15.35}$$

Finally, we obtain

$$\chi = \frac{M}{H_e} = \frac{C}{T - \gamma C} = \frac{C}{T - \theta}, \tag{15.36}$$

which is the experimentally observed Curie–Weiss law (15.2). If θ is found to be positive then the interactions of the individual magnetic moments reinforce each other, that is, the magnetic moments align parallel. In this case, the susceptibility becomes larger, as can be deduced from (15.36).

We now attempt to interpret *ferromagnetism* by making use of the molecular field theory. We know already from Section 15.1.3 that in ferromagnetic materials, the neighboring magnetic moments interact with each other, which leads, below T_C, to a spontaneous magnetization in small domains. Weiss postulated that the above-introduced internal or molecular field is responsible

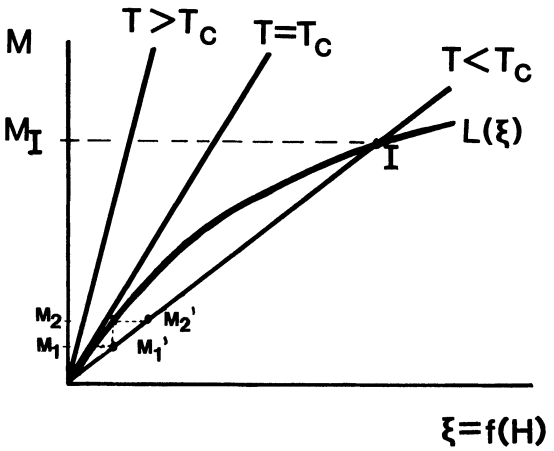

Figure 15.18. Langevin function $L(\xi)$, i.e., (15.28) and plot of (15.38) for three temperatures.

for this parallel alignment of spins and considered ferromagnetics to be essentially paramagnetics having a very large molecular field. In essence, he applied the Langevin theory to ferromagnetics. In the light of quantum theory the molecular field is essentially the *exchange force*, as we shall see in Section 16.2.

We follow the train of thought put forward by Weiss. Let us consider the case for no external magnetic field. Then the spins are only subjected to the molecular field H_m. This yields for the Langevin variable ξ (see (15.22)) with (15.33)

$$\xi = \frac{\mu_m H_m}{k_B T} = \frac{\mu_m \gamma M}{k_B T} \tag{15.37}$$

and provides for the magnetization by rearranging (15.37)

$$M = \frac{k_B T}{\mu_m \gamma} \xi. \tag{15.38}$$

We note from (15.38) that for the present case the magnetization is a linear function of ξ with the temperature as a proportionality factor (see Fig. 15.18). The intersection I of a given temperature line with the Langevin function $L(\xi)$ represents the finite spontaneous magnetization, M_I, at this temperature.[2] With increasing temperature, the straight lines in Fig. 15.18 increase in slope, thus decreasing the point of intercept I and therefore the value for the

[2] The intersection at the origin is an unstable state, as can be easily seen: If the ferromagnetic material is exposed to, say, the magnetic field of the earth, its magnetization will be, say, M_1. This causes a molecular field of the same value (M_1') which in turn magnetizes the material to the value M_2 and so on until the point I is reached.

spontaneous magnetization. Finally, at the Curie temperature T_C, no intercept, that is, no spontaneous magnetization is present anymore. The slope $k_B T/\mu_m \gamma$ in (15.38) is then identical with the slope of the Langevin function near the origin which is $n\mu_m/3 = M/3$ according to (15.29) and (14.8). This yields, for T_C:

$$\frac{k_B T_C}{\mu_m \gamma} = \frac{M}{3}. \tag{15.39}$$

A value for the molecular field constant γ can then be calculated by measuring the Curie temperature and inserting T_C into the rearranged equation (15.39)

$$\gamma = \frac{3k_B T_C}{\mu_m M}. \tag{15.40}$$

This yields for the molecular magnetic field strength (15.33):

$$H_m = \gamma M = \frac{3k_B T_C}{\mu_m}. \tag{15.41}$$

Numerical values for the molecular field are around 10^7 Oe (see Problem 10). This hypothetical field is several orders of magnitude larger than any steady magnetic field which can be produced in a laboratory. We should note that even though the molecular field theory gives some explanation of ferromagnetism, it cannot predict which solids are ferromagnetic. Quantum theory extends considerably our understanding of this matter.

We mention in closing that the molecular field theory can be also applied to antiferromagnetics and to ferrimagnetic materials. As we know from Section 15.1.4 we need to consider in this case two interpenetrating sublattices A and B, each having mutually antiparallel aligned spins. This means that we have to consider now a molecular field H_{mA} acting on the A ions which stems from the magnetization M_B of the B ions. Since the magnetization of A and B ions point in opposite directions, the molecular field from an adjacent ion is now negative. The calculations, which follow similar lines as shown above, yield equation (15.4), that is, the Curie–Weiss law for antiferromagnetics.

Problems

1. Calculate the diamagnetic susceptibility of germanium. Take for r the atomic radius (1.37 Å). *Note*: Check your units! Does χ come out unitless? Have you inserted e in abcoul? Compare your result with that listed in Table 14.1.

2. In the text, we introduced an average value for the magnetic moment which we said is somewhat smaller than the maximal value for $\boldsymbol{\mu}_m \| \mathbf{H}$. Calculate this $\Delta\mu_m$. (*Hint*: Consider all orbits projected on a plane perpendicular to the field direction and calculate thus an average value for the square of the orbit radius. Refer to the figure on the next page. Show at first that $dA = 2\pi R^2 \sin\alpha \, d\alpha$.)

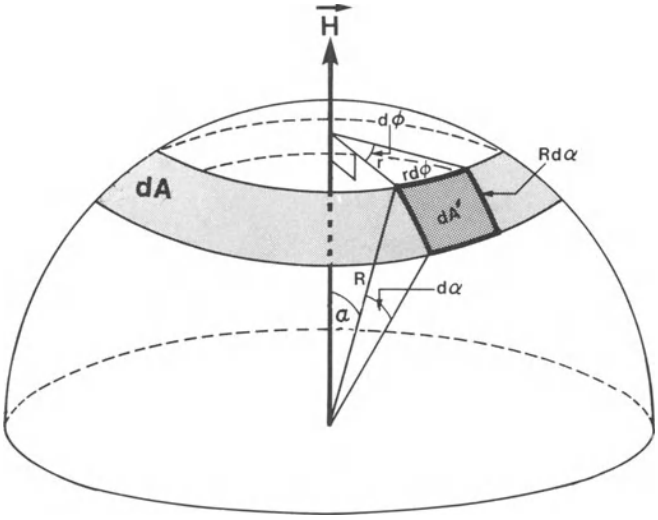

3. Convince yourself that the units in equations (15.15), (15.16), (15.17), and (15.5) are consistent with the electromagnetic cgs system.

4. Confirm the numerical value of the Bohr magneton listed in (15.3) and confirm the unit given there.

5. Evaluate the function

$$\frac{\int_0^{\pi} \cos\alpha \sin\alpha \exp(\xi \cos\alpha)\, d\alpha}{\int_0^{\pi} \sin\alpha \exp(\xi \cos\alpha)\, d\alpha}$$

by substituting $x = \cos\alpha$ and $dx = -\sin\alpha\, d\alpha$. Compare your result with (15.28).

6. Calculate a value for ξ in the Langevin function assuming $\mu_m = 3\mu_B$, $H = 10$ KOe, and room temperature.

7. Calculate the susceptibility for a paramagnetic substance at room temperature, assuming $\mu_m = \mu_B$ and 10^{23} magnetic moments per cm^3. Compare your result with Table 14.1. What is the implication of $n = 10^{23}$ magnetic moments per cm^3?

8. Estimate the number of Bohr magnetons for iron and cobalt ferrite from their electron configuration, as done in the text. Compare your results with those listed in Table 15.3. Explain the discrepancy between experiment and calculation. Give the chemical formula for these ferrites.

9. Explain the term "mixed ferrites." Explain also why the *lodestone* Fe_3O_4 is a ferrimagnetic material. Give its chemical formula.

10. Calculate the molecular field for iron ($\mu_m = 2.22\ \mu_B$, $T_C = 1043$ K).

CHAPTER 16

Quantum Mechanical Considerations

We have seen in the previous chapter that the classical electromagnetic theory is quite capable of explaining the essentials of the magnetic properties of materials. Some discrepancies between theory and experiment have come to light, however, which need to be explained. Therefore, we now refine and deepen our understanding by considering the contributions which quantum mechanics provides to magnetism. We shall see in the following that quantum mechanics yields answers to some basic questions. We shall discuss why certain metals that we expect to be paramagnetic are in reality diamagnetic; why the paramagnetic susceptibility is relatively small for most metals; and why most metals do not obey the Curie–Weiss law. We shall also see that ferromagnetism can be better understood by applying elements of quantum mechanics.

16.1. Paramagnetism and Diamagnetism

We mentioned at the beginning of the previous chapter that for most solids, the dominant contribution to paramagnetism stems from the magnetic moment of the *spinning electrons*. We recall from Chapter 6 that each electron state may be occupied by a maximum of two electrons, one having positive and one having negative spin (shortly called spin up and spin down). To visualize the distribution of spins, we consider an electron band to be divided into two halves, each of which is thought to be occupied under normal conditions by an identical amount of electrons of opposite spin, as shown in Fig. 16.1(a). Now, if we apply an external magnetic field to a free electron solid, some of the electrons having unfavorably oriented spins tend to change

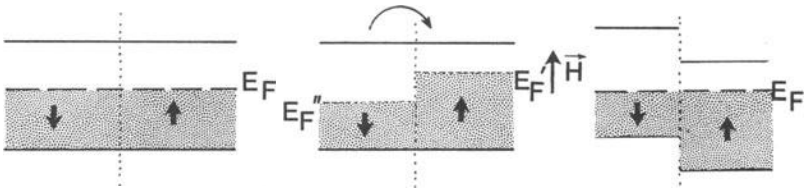

Figure 16.1. Schematic representation of the effect of an external magnetic field on the electron distribution in a partially filled electron band (a), without magnetic field (b), and (c) with magnetic field.

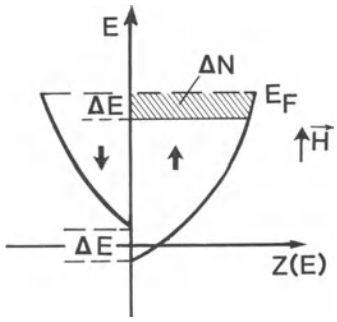

Figure 16.2. Schematic representation of the density of states $Z(E)$ in two half bands. The shift of the two half bands occurs as a result of an external magnetic field. Free electron case. (See also Fig. 16.1(c).) The area ΔN equals $\Delta E \cdot Z(E)$.

their field direction. This can only be achieved, however, when the affected electrons assume an energy which is higher than the Fermi energy E_F, since all lower electron states of opposite spin direction are already occupied (Fig. 16.1(b)). Thus, theoretically, the transfer of electrons from one half band into the other would cause two individual Fermi energies (E_F' and E_F'') to occur. This is, of course, not possible. In reality the two band halves shift relatively to each other until equilibrium, that is, a common Fermi energy is reached (Fig. 16.1(c)).

Now, we recall from Chapter 6 that the electron distribution within a band is not uniform. We rather observe a parabolic distribution of energy states, as shown in Fig. 6.4. Thus, we refine our treatment by replacing Fig. 16.1(c) by Fig. 16.2 which depicts the density of states of the two half bands. We observe a relatively large $Z(E)$ near E_F. Thus, a small change in energy (provided by the external magnetic field) may cause a large number of electrons to switch into the opposite spin direction.

We calculate now the susceptibility from this change in energy ΔE. It is evident that ΔE is larger the larger the external magnetic field strength $|\mathbf{H}|$ and the larger the magnetic moment of the spinning electrons $|\boldsymbol{\mu}_{ms}|$, that is

$$\Delta E = H\mu_{ms}. \tag{16.1}$$

As mentioned already, the number of electrons ΔN transferred from spin down into spin up direction depends on the density of states at the Fermi energy, $Z(E_F)$, and the energy difference ΔE (Fig. 16.2), that is

$$\Delta N = \Delta E Z(E_F) = H\mu_{ms} Z(E_F). \tag{16.2}$$

The magnetization $|\mathbf{M}|$ of a solid, caused by an external magnetic field is, according to (14.8),

$$M = \frac{\mu_m}{V}. \tag{16.3}$$

The magnetization is, of course, larger the more electrons are transferred from spin down into spin up. We thus obtain for the present case

$$M = \frac{\mu_{ms}}{V}\Delta N = \frac{\mu_{ms}^2 H Z(E_F)}{V} \tag{16.4}$$

which yields for the susceptibility

$$\chi = \frac{M}{H} = \frac{\mu_{ms}^2 Z(E_F)}{V}. \tag{16.5}$$

The spin magnetic moment of one electron equals one Bohr magneton μ_B (see below). Thus, (16.5) becomes finally

$$\boxed{\chi_{para}^{spin} = \frac{\mu_B^2 Z(E_F)}{V}}. \tag{16.6}$$

The susceptibilities for paramagnetic metals calculated with this equation agree fairly well with those listed in Table 14.1 (see Problem 1). Thus, (16.6) substantiates, in essence, that only the electrons close to the Fermi energy are capable of realigning in the magnetic field direction. If we would postulate instead that *all* valence electrons would contribute to χ_{para} we would wrongfully calculate a susceptibility which is two or even three orders of magnitude larger than that obtained by (16.6).

It is important to realize that the ever-present diamagnetism makes a sizable contribution to the overall susceptibility so that χ for metals might be positive or negative depending on which of the two components predominates. This shall be elucidated now in a few examples.

To begin with, we discuss beryllium which is a bivalent metal having a filled $2s$-shell in its atomic state (see Appendix 3). However, in the crystalline state, we observe band-overlapping (see Chapter 6) which causes some of the $2s$-electrons to spill over into the $2p$-band. They populate the very bottom of this band (see Fig. 16.3). Thus, the density of states at the Fermi level and consequently, χ_{para} is very small. In effect, the diamagnetic susceptibility predominates which makes Be diamagnetic.

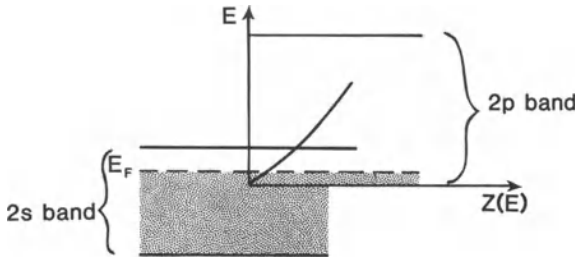

Figure 16.3. Overlapping of 2*s*- and 2*p*-bands in Be and density of states curve for the 2*p*-band.

In order to understand why copper is diamagnetic, we need to remember that for this metal the Fermi energy is close to the band edge (Fig. 5.21). Thus, the density of states near E_F and the paramagnetic susceptibility (16.6) are relatively small. Furthermore, we have to recall that the diamagnetic susceptibility (15.17)

$$\boxed{\chi_{dia} = -\frac{e^2 Z \bar{r}^2}{6mV}} \tag{16.7}$$

is proportional to the square of the average orbit radius $\bar{r}$, and proportional to the total number of electrons, Z, in a given orbit. Copper has about ten 3*d*-electrons which makes $Z \approx 10$. Further, the radius of *d*-shells is fairly large. Thus, for copper, χ_{dia} is large because of two contributions. The diamagnetic contribution predominates over the paramagnetic one. As a result, Cu is diamagnetic. The same is true for Ag and Au and the elements which follow copper in the periodic chart such as Zn and Ga.

Intrinsic semiconductors which have filled valence bands and whose density of states at the top of the valence band is zero (Fig. 6.6) have, according to (16.6), no paramagnetic susceptibility and are therefore, diamagnetic. However, a small paramagnetic contribution might be expected for highly doped *extrinsic* semiconductors which have at high enough temperatures a considerable amount of electrons in the conduction band (see Chapter 8).

We turn now to the temperature dependence of the susceptibility of metals. The relevant terms in both (16.6) as well as (16.7) do not vary much with temperature. Thus, it is conceivable that the susceptibility of diamagnetic metals is not temperature dependent and that the susceptibility of paramagnetic metals often does *not* obey the Curie–Weiss law. In fact, the temperature dependence of the susceptibility for different paramagnetic *metals* has been observed to decrease, to increase, or it remains essentially constant (Fig. 16.4). However, nickel (above T_C) and rare earth metals obey the Curie–Weiss law, reasonably well.

At the end of this section we remind the reader that in dilute gases (and also in rare earth metals and their salts) a second component contributes to

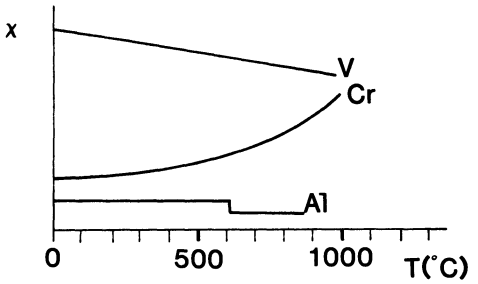

Figure 16.4. Temperature dependence of the paramagnetic susceptibility for V, Cr, and Al in arbitrary units. From Landolt–Börnstein, *Zahlenwerte der Physik*, 6th ed., Vol. II/9, (1962) Springer-Verlag, Berlin, Heidelberg, New York, Tokyo.

paramagnetism. It stems from a magnetic moment which is caused by the angular momentum of the orbiting electrons. We mentioned already in Section 15.1 that this contribution is said to be "quenched" (that is, nonexistent) in most solids. The magnetic moment μ_m of an orbiting electron was calculated in Section 15.2 to be

$$\mu_m = \frac{evr}{2}. \tag{16.8}$$

Now, quantum theory postulates that the angular momentum mvr of an electron is not continuously variable but that it rather changes in discrete amounts of integer multiples of $\hbar$ only, that is

$$mvr = n\hbar = \frac{nh}{2\pi}. \tag{16.9}$$

If one combines (16.8) with (16.9) one obtains

$$\mu_m = \frac{enh}{4\pi m}. \tag{16.10}$$

Using $n = 1$ for the first electron orbit yields for the magnetic moment of an orbiting electron

$$\mu_m = \frac{eh}{4\pi m}. \tag{16.11}$$

It was found experimentally and theoretically that the magnetic moment of an electron due to orbital motion, as well as the magnetic moment of the spinning electron, are identical and given by (16.11). This is the Bohr magneton

$$\mu_B = \frac{eh}{4\pi m} = 0.927 \times 10^{-20}(\text{erg/Oe}) \tag{16.12}$$

which we already introduced without further explanation in (15.3).

16.2. Ferromagnetism and Antiferromagnetism

The ferromagnetic metals, iron, cobalt, and nickel are characterized by unfilled *d*-bands (see Appendix 3). These *d*-bands overlap the next higher *s*-band, in a similar manner to the one shown in the band structure of Fig. 5.21. The density of states for a *d*-band is relatively large because of its potential to accommodate up to ten electrons. This is schematically shown in Fig. 16.5, along with the Fermi energies for Fe, Co, Ni and Cu. Since the density of states for, say, Ni is comparatively large at the Fermi energy, one needs only a relatively small amount of energy to transfer a considerable amount of electrons from spin down into spin up configurations, that is, from one half band into the other. We have already discussed in the previous section this transfer of electrons under the influence of an external magnetic field (Fig. 16.1). Now, there is an important difference between paramagnetics and ferromagnetics. In the former case an external energy (that is, the magnetic field) is needed to accomplish the flip in spin alignment whereas for ferromagnetic materials the parallel alignment of spins occurs spontaneously in small domains of about 1–100 μm diameter. Any theory of ferromagnetism must be capable of satisfactorily explaining the origin of this energy which transfers electrons into a higher energy state.

The energy in question was found to be the *exchange energy*. It is "set free" when equal atomic systems are closely coupled, and in this way exchange their energy. This needs some further explanation.

We digress for a moment and compare two ferromagnetic atoms with two identical pendula which are interconnected by a spring. (The spring represents the interactions of the electrical and magnetic fields.) If one of the pendula is

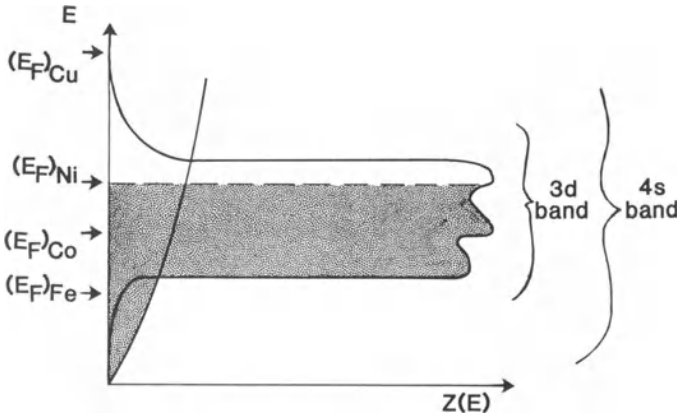

Figure 16.5. Schematic representation of the density of states for 4*s*- and 3*d*-bands and the Fermi energies for Fe, Co, Ni and Cu. The population of the bands by the ten nickel ($3d + 4s$) electrons is indicated by the shaded area.

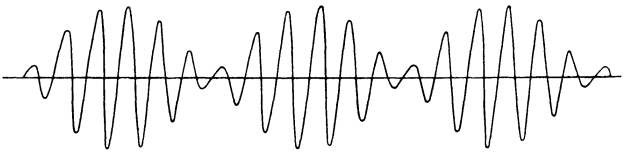

Figure 16.6. Amplitude modulation resulting from coupling of two pendula. The vibrational pattern shows *beats* similarly as known from two oscillators which have almost identical pitch.

deflected, its amplitude slowly decreases until all energy has been transferred to the second pendulum, which then in turn transfers its energy back to the first one and so on. Thus, the amplitudes decrease and increase periodically with time as shown in Fig. 16.6. The resulting vibrational pattern is similar to that of two violin strings tuned at almost equal pitch. A mathematical expression for this pattern is obtained by adding the equations for two oscillators having similar frequencies ω_1 and ω_2

$$X_1 = b \sin \omega_1 t \tag{16.13}$$

$$X_2 = b \sin \omega_2 t, \tag{16.14}$$

which yields:

$$X_1 + X_2 = X = 2b \cos \frac{\omega_1 - \omega_2}{2} t \cdot \sin \frac{\omega_1 + \omega_2}{2} t. \tag{16.15}$$

Equation (16.15) provides two frequencies, $(\omega_1 - \omega_2)/2$ and $(\omega_1 + \omega_2)/2$ which can be identified in Fig. 16.6. The difference between the resulting frequencies is larger the stronger the coupling. If the two pendula vibrate in a parallel fashion, the "pull" on the spring, that is, the restoring force κ is small. As a consequence, the frequency

$$\nu_0 = \frac{1}{2\pi} \sqrt{\frac{\kappa}{m}} \tag{16.16}$$

(see Appendix 1) is likewise small and is smaller than for independent vibrations. (On the other hand, antisymmetric vibrations cause large values of κ and ν_0.) This classical example demonstrates that two coupled and symmetrically vibrating systems may have a lower energy than two individually vibrating systems would have.

Quantum mechanics treats ferromagnetism in a similar way. The exact calculation involving many atoms is, however, not a trivial task. Thus, one simplifies the problem by solving the appropriate Schrödinger equation for two atoms only. The potential energy in the Schrödinger equation contains then the exchange forces between the nuclei a and b, the forces between two electrons 1 and 2, and the interactions between the nuclei and their neighboring electrons. This simplification seems to be justified because the exchange forces decrease rapidly with distance.

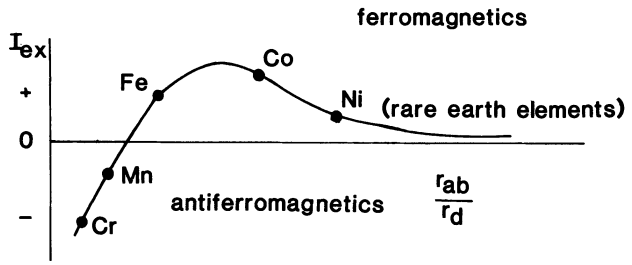

Figure 16.7. Exchange integral I_{ex} versus ratio of interatomic distance r_{ab} and radius of unfilled d-shell. The position of the rare earth elements (which have unfilled f-shells) are also shown for completeness.

The calculation first performed by Slater and Bethe leads to an *exchange integral*

$$I_{ex} = \int \psi_a(1)\psi_b(2)\psi_a(2)\psi_b(1)\left[\frac{1}{r_{ab}} - \frac{1}{r_{a2}} - \frac{1}{r_{b1}} + \frac{1}{r_{12}}\right] d\tau. \qquad (16.17)$$

A positive value for I_{ex} means that parallel spins are energetically more favorable than antiparallel spins (and vice versa). We see immediately from (16.17) that I_{ex} becomes positive for a small distance r_{12} between the electrons, that is, a small radius of the d-orbit, r_d. Similarly, I_{ex} becomes positive for a large distance between nuclei and neighboring electrons r_{a2} and r_{b1}.

I_{ex} is plotted in Fig. 16.7 versus the ratio r_{ab}/r_d. The curve correctly separates the ferromagnetics from manganese which is not ferromagnetic. Figure 16.7 suggests that if the interatomic distance r_{ab} in manganese would be increased (for example, by inserting nitrogen atoms into the Mn lattice), the crystal thus obtained should become ferromagnetic. This is indeed observed. The ferromagnetic alloys named after Heusler, such as Cu_2MnAl or Cu_2MnSn, are particularly interesting in this context because they contain constituents which are not ferromagnetic; but all contain Mn.

The Bethe–Slater curve (Fig. 16.7) suggests that Co should have the highest and Ni (and the rare earth elements) the lowest Curie temperature among the ferromagnetics because of the magnitude of their I_{ex} values. This is indeed observed (Table 15.1). Overall, quantum theory is capable of explaining some ferromagnetic properties which cannot be understood with classical electromagnetic theory.

We turn now to a discussion on the number of Bohr magnetons in ferromagnetic metals as listed in Table 16.1. Let us consider nickel as an example and reinspect in this context Fig. 16.5. We notice that because of band overlapping the combined ten $(3d + 4s)$-electrons occupy the lower s-band and fill almost completely the $3d$-band. It comes thus as no surprise that nickel behaves experimentally as if the $3d$-band would be filled by 9.4 electrons. To estimate μ_B we need to apply Hund's rule (Fig. 15.4) which states that the electrons in a solid occupy the available electron states in a manner which

Table 16.1. Magnetic Moment μ_m at 0 K for Ferromagnetic Metals

Metal	μ_m
Fe	2.22 μ_B
Co	1.72 μ_B
Ni	0.60 μ_B
Gd	7.12 μ_B

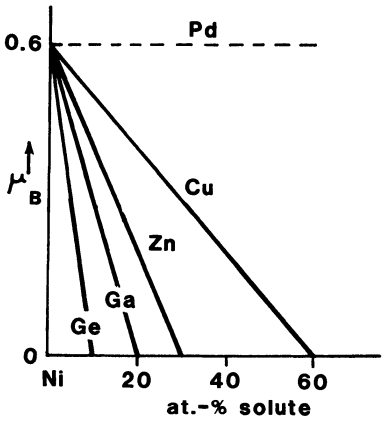

Figure 16.8. Magnetic moment per nickel atom as a function of solute concentration.

maximizes the imbalance of spin moments. For the present case this rule would suggest 5 electrons with, say, spin up and an average of 4.4 electrons with spin down, that is, we obtain a spin imbalance of 0.6 spin moments or 0.6 Bohr magnetons per atom (see Table 16.1). The average number of Bohr magnetons may also be calculated from experimental values of the saturation magnetization M_{s0} (see Table 15.1). Similar considerations can be made for the remaining ferromagnetics as listed in Table 16.1.

We proceed now one step further and discuss the magnetic behavior of certain nickel-based alloys. We use Ni–Cu alloys as an example. Copper has one valence electron more than nickel. If Cu is alloyed to Ni the extra copper electrons progressively fill the *d*-band and therefore compensate some of the unsaturated spins of nickel. Thus, the magnetic moment per atom of the alloy (and also its Curie temperature) is reduced. Ni lacks about 0.6 electrons per atom for complete spin saturation. Thus, about 60% Cu atoms are needed until the magnetic moment (and μ_B) of Ni have reached a zero value (Fig. 16.8). Cu–Ni alloys, having a copper concentration of more than about 60% are consequently no longer ferromagnetic—they are paramagnetic.

Zinc contributes about two extra valence electrons to the electron gas when alloyed to nickel. Thus, we expect a zero magnetization at about 30 at % Zn, etc. Palladium, on the other hand, has the same number of valence electrons as nickel and thus does not change the magnetization of the nickel atoms when alloyed to nickel. (The total magnetization of the alloy is, of course, diluted by the nonmagnetic palladium. The same is also true for the other alloys.)

We conclude our discussion by adding a few interesting details. The rare earth elements are weakly ferromagnetic. They are characterized by unfilled *f*-shells. Thus, their electronic structure and their density of states has several features in common with Fe, Co and Ni. They have a positive I_{ex} (see Fig. 16.7).

Copper has one more valence electron than nickel which locates its Fermi energy slightly above the *d*-band (Fig. 16.5). Thus, the condition for ferromagnetism, that is, an unfilled *d*- or *f*-band is not fulfilled for Cu. The same is true for the following elements such as Zn or Ga.

We noted already that Mn is characterized by a negative value of the exchange integral. The distance between the Mn atoms is so small that their electron spins assume an antiparallel alignment. Thus, manganese and many Mn compounds are antiferromagnetic (see Fig. 15.10). Chromium has also a negative I_{ex} and thus is likewise antiferromagnetic (see Table 15.2).

Problems

1. The density of states near the Fermi surface of 1 cm^3 of a paramagnetic metal at $T = 0$ K is approximately 5×10^{41} energy states per Joule. Calculate the volume susceptibility. Compare your value with those of Table 14.1. What metal could this value represent? Explain possible discrepancies between experiment and calculation.

2. Derive (16.15) by adding (16.13) and (16.14).

3. Compare the experimental saturation magnetization M_{s0} (Table 15.1) with the magnetic moment μ_m at 0 K for ferromagnetic metals (Table 16.1). What do you notice? Estimate the degree of *d*-band filling for Fe and Co.

4. From the results obtained in Problem 3 above, calculate the number of Bohr magnetons for crystalline (solid) Fe and Co and compare your results with those listed in Table 16.1. What is the number of Bohr magnetons for an iron *atom* and a Co-atom? What is μ_B for iron and cobalt ferrite?

5. Refer to Figure 15.1(b). Why are two different Fermi energies not possible within the same metal?

CHAPTER 17

Applications

17.1. Introduction

The production and consumption of ferro- and ferrimagnetic materials is a large scale operation, measured in quantity as well as in currency. (This is in contrast to the products of the computer industry where the price of the material which goes into a chip is a minute fraction of the device fabrication cost.) As an example, the annual sales of so-called electrical steel used for electromotors and similar devices reaches the millions of tons and their market values are in the hundreds of millions of dollars. Other large scale production items are permanent magnets for loudspeakers, etc., or magnetic recording tapes. The following sections will give some impression about the technology (that is, mostly materials science) which has been developed to improve the properties of magnetic materials.

17.2. Electrical Steels

Electrical steel is used to multiply the magnetic flux in the cores of electromagnetic coils. These materials are therefore widely incorporated in many electrical machines of daily use. Among their applications are cores of transformers, electromotors, generators, or electromagnets.

In order to make these devices most energy efficient and economical, one needs to find magnetic materials which have the highest possible permeability (at the lowest possible price). Furthermore, magnetic core materials should be capable of being easily magnetized or demagnetized. In other words, the area within the hysteresis loop (or the coercive force H_c) should be as small as

possible (Fig. 15.6). We remember that materials whose hysteresis loop is narrow are called *soft* magnetic materials.

Electrical steels are classified by some of their properties, for example, by the amount of their core losses, by their composition, by their susceptibility, and whether or not they are *grain oriented.* We shall discuss these different properties now in detail.

17.2.1. Core Losses

The core loss is the energy which is dissipated in the form of heat within the core of electromagnetic devices when the core is subjected to an alternating magnetic field. Several types of losses are known, among which the eddy current loss and the hysteresis loss contribute the most. Typical core losses are between 0.3 and 3 watts per Kg of core material (Table 17.1).

Let us discuss at first the eddy current. Consider a transformer whose primary and secondary coils are wound around the legs of a rectangular iron yoke (Fig. 17.1(a)). An alternating electric current in the primary coil causes an alternating magnetic flux in the core which in turn induces in the secondary coil an alternating electromotive force V_e proportional to $d\phi/dt$, see equations (14.6) and (15.9)

$$V_e = -\frac{d\phi}{dt} = -A\frac{dB}{dt}. \tag{17.1}$$

Concurrently, an alternating emf is induced within the core itself as shown in Fig. 17.1a. This emf gives rise to the eddy current I_e. The eddy current is larger the larger the permeability μ (because $B = \mu \cdot H$), the larger the conductivity σ of the core material, the higher the applied frequency, and the larger the cross-sectional area A of the core. (A is perpendicular to the magnetic flux ϕ, see Fig.

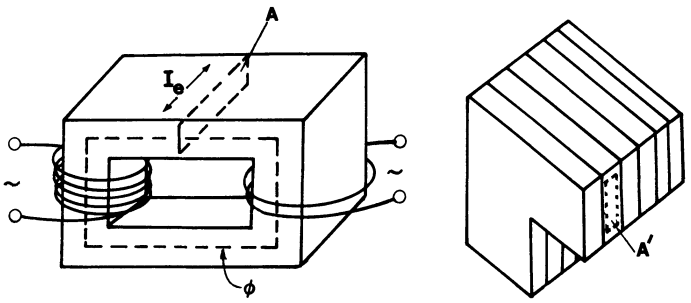

Figure 17.1. (a) Solid transformer core with eddy current I_e in a cross-sectional area A. Note the magnetic flux lines ϕ. (b) Cross section of a laminated transformer core. The area A' is smaller than area A in (a).

17.1(a).) We note in passing that particularly at high frequencies the eddy current shields the interior of the core from the magnetic field so that only a thin exterior layer of the core contributes to the flux multiplication (skin effect).

In order to decrease the eddy current, several remedies are possible. First, the core can be made of an insulator in order to decrease σ. Ferrites are thus an effective but expensive way to build magnetic cores (see Section 15.1). They are indeed used for high frequency applications. Second, the core can be manufactured out of pressed iron powder whereby each particle (which is about 50 to 100 μ in diameter) is covered by an insulating coating. However, the decrease in σ, in this case, is at the expense of a large decrease in μ. Third, the most widely applied method to reduce eddy currents is the utilization of cores made out of thin sheets which are electrically insulated from each other (Fig. 17.1(b)). This way the cross-sectional area A is reduced, which in turn decreases V_e (17.1), and additionally reduces losses due to the skin effect. Despite the lamination, a residual eddy current loss still exists which is caused by current losses within the individual laminations and due to interlaminar losses that may arise if laminations are not sufficiently insulated from each other. These losses are, however, less than 1% of the total energy transferred.

Hysteresis losses are encountered when the magnetic core is subjected to a complete hysteresis cycle (Fig. 15.6). The work thus dissipated into heat is proportional to the area enclosed by a B, H loop. Proper materials selection, heat treatment, and rolling of the materials greatly reduces the area of a hysteresis loop (see below).

17.2.2. Grain Orientation

The permeability of electrical steel can be substantially increased and the hysteresis losses decreased by making use of favorable grain orientations in the material. This needs some explanation. The magnetic properties of crystalline ferromagnetic materials depend on the crystallographic direction in which an external field is applied, an effect which is called magnetic anisotropy. Let us use iron as an example. Figure 17.2(a) shows magnetization curves for three crystallographic directions. We observe that if the external field is applied in the $\langle 100 \rangle$ direction, the saturation is achieved with the smallest possible field strength. The $\langle 100 \rangle$ direction is thus called the "easy direction."

This experimental finding gives us, incidentally, some clues about the spontaneous orientation of the spin magnetic moments in the demagnetized state. Specifically, in virgin iron the spins are aligned along the easy directions. Suppose now that an external field is applied parallel to an easy direction. Then, the domains already having favorable alignment grow without effort at the expense of other domains until eventually the crystal contains one single domain (Fig. 15.9). The energy which is consumed during this process (which

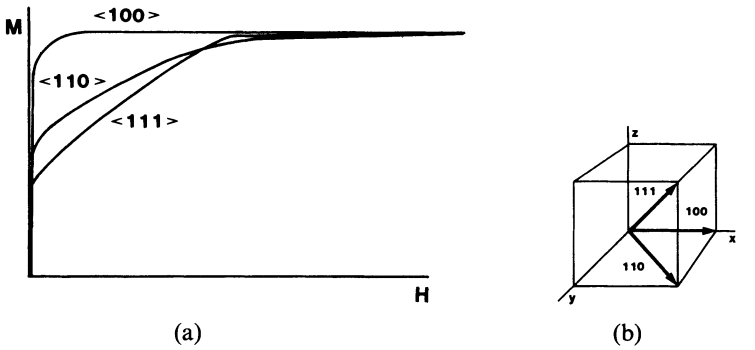

(a) (b)

Figure 17.2. (a) Schematic magnetization curves for an iron single crystal. The magnetic field was applied in three different crystallographic directions (b) Reminder of the Miller indices.

is proportional to the area within the hysteresis loop) is used to move the domain walls through the crystal.

A second piece of information needs to be considered too. Metal sheets, which have been manufactured by rolling, often possess a "texture," that is, they have a preferred orientation of the grains. It just happens that in iron and iron alloys the ⟨100⟩ direction is parallel to the rolling direction. This property is exploited when utilizing electrical steel.

Grain-oriented electrical steel is produced by initial hot rolling the alloy followed by two stages of cold reduction with intervening anneals. During the rolling, the grains are elongated and their orientation is altered as described above. Finally, the sheets are recrystallized whereby some crystals grow in size at the expense of others (occupying the entire sheet thickness).

In summary, the magnetic properties of grain-oriented steels are best in the direction parallel to the direction of rolling. Electrical machines having core material of grain-oriented steel need less iron and are therefore smaller; the price increase due to the more elaborate fabrication procedure is often compensated by the savings in material.

17.2.3. Composition of Core Materials

The least expensive core material is commercial, low carbon steel (0.05% C). It possesses a relatively small permeability and has about ten times higher core losses than grain-oriented iron alloys (Table 17.1). Low carbon steel is used where low cost is more important than the efficient operation of a device. Purification of iron increases the permeability but increases also conductivity (eddy current!) and price.

Iron–silicon alloys containing between 1.4 and 3.5% Si and very little carbon have a higher permeability and a lower conductivity than low carbon

Table 17.1. Properties of Some Magnetic Materials

Name	Composition (weight %)	Permeability μ_{max} (unitless)	Coercivity H_c (Oe)	Saturation Induction[a] B_s (kG)	Resistivity $\rho(\mu\Omega \cdot cm)$	Core Loss at 15 KG (W/kg)
Low carbon steel	Fe–0.05% C	5×10^3	1.0	21.5	10	2.8
Nonoriented silicon iron	Fe–3% Si 0.005% C, 0.15% Mn	7×10^3	0.5	19.7	60	0.9
Grain-oriented silicon iron	Fe–3% Si 0.003% C, 0.07% Mn	4×10^4	0.1	20	47	0.3
78 Permalloy	Ni–22% Fe	10^5	0.05	10.8	16	
Mumetal	77% Ni; 16% Fe 5% Cu, 2% Cr	10^5	0.05	6.5	62	
Supermalloy	79% Ni; 16% Fe, 5% Mo	10^6	0.002	7.9	60	
Supermendur	49% Fe, 49% Co 2% V	6×10^4	0.2	24	27	

[a] Above B_s the magnetization is constant and dB/dH is unity.

steel (see Table 17.1). Furthermore, because of special features in the phase diagram ("γ-loop"), heat treatments of these alloys can be performed at much higher temperatures without interference from phase changes during cooling. The core losses decrease with increasing silicon content. However, for silicon concentrations above 4 or 5 weight % the material becomes too brittle to allow rolling. Grain orientation in silicon alloys (see above) further increases the permeability and decreases the hysteresis losses. Other constituents in iron–silicon alloys are aluminum and manganese in amounts less than 1 %. They are added mainly for metallurgical reasons because of their favorable influence on the grain structure and their tendency to reduce hysteresis losses. Grain-oriented silicon "steel" is the favored commercial product for highly efficient–high flux multiplying core applications.

The highest permeability is achieved for certain multicomponent Ni-based alloys such as Permalloy, Supermalloy, or Mumetal (Table 17.1). The latter can be rolled into thin sheets and is used to shield electronic equipment from stray magnetic fields.

17.3. Permanent Magnets

Permanent magnets are devices which retain their magnetic field indefinitely. They are characterized by a large remanence B_r (or M_r), a relatively large coercivity H_c, and a large area within the hysteresis loop. They are called *hard magnetic materials* (see Section 15.1.3).

The best means to visualize the properties of permanent magnets is to inspect their *demagnetization curve* (Fig. 17.3) which is a part of a hysteresis loop as shown in Fig. 15.6. Another parameter which is used to characterize magnetic materials is the *maximum amount of the energy product*, $(BH)_{max}$, which is related to the area within the hysteresis loop. We see immediately from Fig. 17.3 that B times H is zero at the intercepts of the demagnetization curve with the coordinate axes, and that the energy product peaks somewhere between these extreme values depending on the shape and size of the hysteresis curve. The values for B_r, H_c, and $(BH)_{max}$ for some materials which are used as permanent magnets are listed in Table 17.2.

The remanence B_r shown in Fig. 17.3 or listed in Table 17.2 is the maximal residual induction which can be obtained in a circular, close-loop magnet inserted in a coil. However, all magnets need to have exposed poles in order to be useful. The necessary *air gap* between north and south poles reduces the remanence because the exposed poles create a *demagnetizing field* H_d which acts in the opposite direction to the B lines. We understand intuitively that the demagnetizing field depends on the shape, the size, and the gap length of a magnet. Thus, a reduced value for the residual induction, termed B_d, is obtained as shown in Fig. 17.3. Another effect which reduces the useful magnetic field is *fringing* near the air gap and *leakage* from the sides of a magnet (Fig. 17.4).

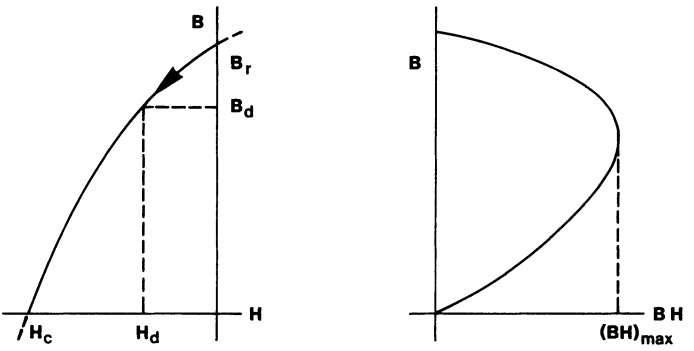

Figure 17.3. (a) Demagnetization curve for a ferromagnetic material. (Second quadrant in a B–H diagram.) (b) Energy product BH as a function of induction B.

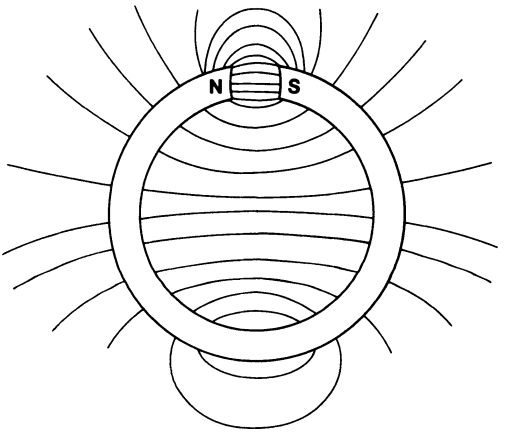

Figure 17.4. Fringing and leakage of a permanent magnet.

We turn now to the properties of some common hard magnetic materials. Today, many permanent magnets are made of Alnico alloys which contain various amounts of aluminum, nickel, cobalt, and iron, along with some minor constituents such as copper and titanium (Table 17.2). Their properties are improved by heat treatments (homogenization at 1250°C, fast cooling, and tempering at 600°C, Alnico 2). Further improvement is accomplished by cooling the alloys in a magnetic field (Alnico 5). The best properties are achieved when the grains are made to have a preferred orientation. This is obtained by cooling the bottom of the crucible after melting, thus forming long columnar grains with a preferred ⟨100⟩ axis in the direction of heat flow. A magnetic field parallel to the ⟨100⟩ axis yields Alnico 5-DG (directional grain).

Table 17.2. Properties of Materials Used for Permanent Magnets

Material	Composition (weight %)	Remanence B_r (kG)	Coercivity H_c (Oe)	Maximum Energy Product $(BH)_{max}$ (MGOe)
Steel	Fe–1% C	9	51	0.2
36 Co steel	36 Co, 3.75 W 5.75 Cr, 0.8 C	9.6	228	0.93
Alnico 2	12 Al, 26 Ni, 3 Cu, 63 Fe	7	650	1.7
Alnico 5	8 Al, 15 Ni, 24 Co 3 Cu, 50 Fe	12	720	5.0
Alnico 5 DG	same as above	13.1	700	6.5
Ba-ferrite (Ceramic 5)	$BaO \cdot 6Fe_2O_3$	3.95	2400	3.5
PtCo	77 Pt, 24 Co	6.45	4300	9.5
Remalloy	12 Co, 17 Mo, 71 Fe	10	230	1.1
Vicalloy 2	13 V, 52 Co, 35 Fe	10	450	3.0
Samarium–Cobalt	$SmCo_5$	9	8700	20
Neodymium–Boron–Iron	$Nd_2F_{14}B_1$	13	14000	40

The superior properties of heat-treated Alnico stems from the fact that during cooling and tempering of these alloys, rod-shaped iron and cobalt-rich α-precipitates are formed which are parallel to the $\langle 100 \rangle$ directions (shape anisotropy). These strongly magnetic precipitates are single domain particles and are imbedded in a weakly magnetic Ni and Al matrix (α). Alnico alloys are mechanically hard and brittle and can, therefore, only be shaped by casting or by pressing and sintering of metal powders. The newest hard magnetic materials are made of neodymium–boron–iron, see Table 17.2.

Ceramic ferrite magnets, such as barium or strontium ferrite ($BaO \cdot 6Fe_2O_3$ or $SrO \cdot 6Fe_2O_3$), are brittle and relatively inexpensive. They crystallize in the form of plates with the hexagonal c-axis (which is the easy axis) perpendicular to the plates. Some preferred orientation is observed because the flat plates arrange parallel to each other during pressing and sintering. Ferrite powder is often imbedded in plastic materials which yields flexible magnets. They are used, for example, in the gaskets of refrigerator doors.

High carbon steel magnets with or without Co, W, or Cr are only of historic interest. Their properties are inferior to other magnets. It is believed that the permanent magnetization of quenched steel stems from the martensite-induced internal stress which impedes the domain walls from moving through the crystal.

17.4. Magnetic Recording

Magnetic recording tapes consist of small, needlelike oxide particles about 0.1×10.5 μm in size which are imbedded in a flexible, nonmagnetic binder. The particles are too small to sustain a domain wall. They consist therefore of a single magnetic domain which is magnetized to saturation along the major axis (shape anisotropy). The elongated particles are aligned by a field during manufacturing so that their long axes are parallel with the length of the tape. The most popular magnetic material has been ferrimagnetic γ-Fe_2O_3. The coercivity for these tapes is 250–350 Oe. More recently, ferromagnetic chromium dioxide has been used having a coercivity between 450–550 Oe and a particle size of 0.2–1.5 μm. Other tapes use cobalt-doped-γ-Fe_2O_3 which has a higher Curie temperature than chromium dioxide. Most recently, iron particles have been utilized.

The recording head of a tape machine consists of a laminated electromagnet made of permalloy or ferrite (Table 17.1) which has an air gap about 1.5 μm wide (Fig. 17.5). The tape is passed along this electromagnet whose fringing field redirects the spin moments of the particles in a certain pattern proportional to the current which is applied to the recording head. This leaves a permanent record of the signal. In the playback mode, the moving tape induces an alternating emf in the coil of the same head. The emf is amplified, filtered and fed to a loudspeaker.

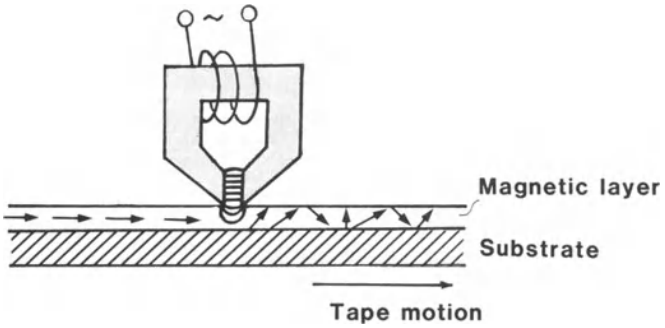

Figure 17.5. Schematic arrangement of recording (playback) head and magnetic tape. The gap width is exaggerated. (Recording mode.)

17.5. Ferrite Core Memories

Ferrite core memories used to be the dominant devices for random access storage in computers. The principle is simple: a donut-shaped piece of ferrimagnetic material, having a nearly square-shaped hysteresis loop, is threaded with a wire (Fig. 17.6(a)). If a sufficiently high current pulse is sent through this wire then the core becomes magnetically saturated. Now, suppose the flux lines point clockwise. An opposite directed current of sufficient strength magnetizes the ferrite core counterclockwise. These two magnetization directions constitute the two possible values (0 and 1) in a binary system.

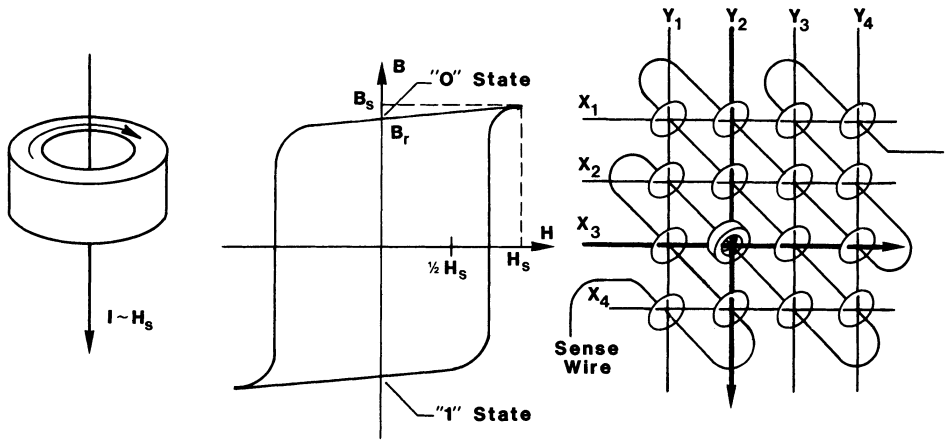

Figure 17.6. (a) Single ferrite core which is magnetized by a current-induced magnetic field; (b) square-shaped hysteresis loop of a ferrite memory core; (c) one plane of a "coincident-current core memory device."

A toroid-shaped memory core is used because a close-flux structure reacts efficiently to currents from a center wire but is not disturbed by external stray fields.

The actual configuration of a complete memory system consists of a stack of identical memory planes, each of which contains a set of wires in the x- as well as in the y-directions. The toroids are placed at the intersections (Fig. 17.6(c)). In order to switch the, say, X_3/Y_2 core from *zero* to *one* a current proportional to half the saturation field ($H_s/2$) is sent through each of the X_3 and the Y_2 wires (Fig. 17.6(b)). This provides only the X_3/Y_2 core with the necessary field for switching—the other cores stay at their present state. The information thus permanently stored can be read by again sending a current pulse proportional to $H_s/2$ through the X_3/Y_2 wires. A third wire, the sensing wire, which passes through all the cores of a given plane, senses whether or not the core was switched during the reading process. Since the reading process destroys the stored information, a special circuit is needed to rewrite the information back into the core.

Problems

1. Calculate the energy expended during one full hysteresis cycle of a magnetic material having a rectangular hysteresis loop. Assume $H_c = 0.5$ Oe, $B_s = 20$ kG, and $V = 0.5$ cm^3. What units can be used?
2. Which core material should be utilized to supply a large scale and constant magnetic field in a synchrotron? Justify your choice.
3. Pick an actual motor of your choice and find out (by analysis, by means of a data sheet, or by writing to the manufacturer) which type of electrical steel was used as core material. Also, find out the core loss (often given in watts/lb).
4. Find from a manufacturer's data sheet the price of several qualities of electrical steel.
5. Inspect the magnets contained in a gasket of a modern refrigerator. How does the magnet work? Where are the south and the north poles?
6. It was said in the text that transformers suffer eddy current as well as hysteresis losses. What other types of losses can be expected in a transformer? How can those losses be reduced?

Suggestions for Further Reading (Part IV)

R.M. Bozorth, *Ferromagnetism*, D. Van Nostrand Company, New York (1951).
S. Chikazumi, *Physics of Magnetism*, John Wiley, New York (1964).
B.D. Cullity, *Introduction to Magnetic Materials*, Addison-Wesley Publishing Company, Reading MA (1972).

J.D. Jackson, *Classical Electrodynamics*, John Wiley, New York (1962).
E. Kneller, *Ferromagnetismus*, Springer-Verlag, Berlin, Heidelberg (1962).
F.W. Sears, *Electricity and Magnetism*, Addison-Wesley, Reading, MA (1953).
T. Smit and H.P.T. Wijn, *Ferrites*, John Wiley, New York (1959).
R.S. Tebble, D. J. Craik, *Magnetic Materials*, Wiley Interscience, London, New York (1969).
J.K. Watson, *Applications of Magnetism*, Wiley Interscience, New York (1980).

PART V

THERMAL PROPERTIES OF MATERIALS

CHAPTER 18

Introduction

Heat was considered to be an invisible fluid, called *caloric* until late into the eighteenth century. It was believed that a hot piece of material contained more caloric than a cold one and that an object would become warmer by transferring caloric into it. At the mid 1800s, Mayer, Helmholtz, and Joule discovered independently that heat is simply a form of energy. They realized that when two bodies have different temperatures, thermal energy is transferred from the hotter to the colder one when brought into contact. Count Rumford discovered, by observing the boring of cannons, that mechanical work, expended in the boring process, was responsible for the creation of heat. He concluded that mechanical energy could be transformed into heat energy. This observation lead eventually to the concept of a *mechanical heat equivalent*.

The thermal properties of materials are important whenever heating and cooling devices are designed. Thermally induced expansion of materials has to be taken into account in the construction industry as well as in the design of precision instruments. Heat conduction plays a large role in thermal insulation, for example, in homes, industry, and spacecraft. Some materials such as copper or silver conduct heat very well; other materials, like wood or rubber, are poor heat conductors. Good electrical conductors are generally also good heat conductors. This was discovered in the middle of the last century by Wiedemann and Franz who found that the ratio between heat conductivity and electrical conductivity (divided by the temperature) is essentially constant for all metals.

The thermal conductivity of materials only varies within four orders of magnitude (Fig. 18.1). This is in sharp contrast with the variation in electrical conductivity, which spans about twenty-five orders of magnitude (Fig. 7.1).

The thermal conductivity of metals and alloys can be readily interpreted by making use of the electron theory which was developed in Part I of this book.

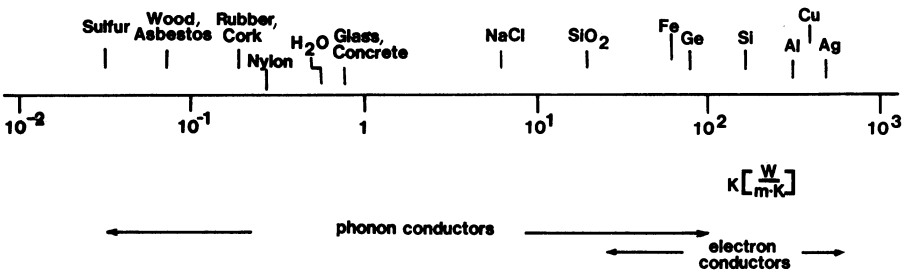

Figure 18.1. Room temperature thermal conductivities for some materials.

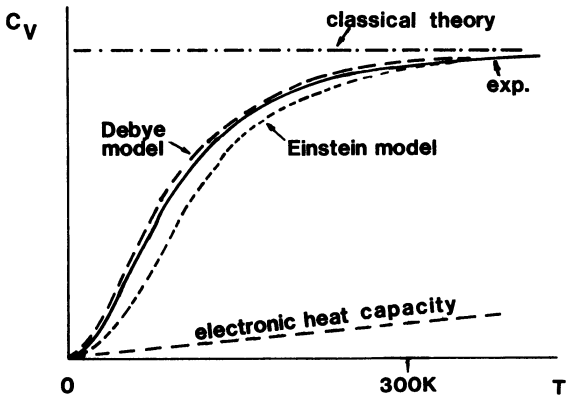

Figure 18.2. Schematic representation of the temperature dependence of the molar heat capacity, experimental and according to four models.

The electron theory postulates that free electrons in the hot part of a metal bar pick up energy by interactions with the vibrating lattice atoms. This thermal energy is eventually transmitted to the cold end of the bar by a mechanism which we will treat in Chapter 21.

In electrical insulators, in which no *free* electrons exist, the conduction of thermal energy must occur by a different mechanism. This new mechanism was found by Einstein at the beginning of the century. He postulated the existence of *phonons* or lattice vibration quanta which are thought to be created in large numbers in the hot part of a solid and partially eliminated in the cold part. Transferral of heat in dielectric solids is thus linked to a flow of phonons from hot to cold.

Figure 18.1 indicates that in a transition region both electrons as well as phonons may contribute to thermal conduction.

Another thermal property which will receive considerable attention in the following chapters is the specific heat, as well as a related property, the molar heat capacity. Their importance can best be appreciated by the following experimental observations: Two substances with the same mass but different

values for the specific heat require different amounts of thermal energy to reach the same temperature. Aluminum, for example, which has a relatively high specific heat needs more thermal energy to reach a given temperature than, say, copper or lead of the same mass.

The molar heat capacity is the product of the specific heat and the molecular weight. Its experimentally observed temperature dependence, as shown in Fig. 18.2, has stimulated various theories, among them the phonon model. Figure 18.2 shows schematically how the various theories for the interpretation of the heat capacity compare with the experimental findings. We shall discuss these models in the chapters to come.

CHAPTER 19

Fundamentals of Thermal Properties

Before we discuss the atomistic and quantum mechanical theories of the thermal properties of materials, we need to remind the reader of some relevant fundamental concepts and definitions which the reader might have been exposed to before in courses of physics and thermodynamics.

19.1. Heat Energy, Q

When two bodies of different temperature are brought in contact with each other, heat energy Q flows from the hotter to the colder substance. (The heat energy is sometimes called thermal energy or just *heat*.) Units of heat energy are the calorie, or in SI units the Joule. The calorie used to be defined as that heat which is needed to raise the temperature of one gram of water from 14.5° C to 15.5° C. The new thermomechanical calorie is defined as

$$1 \text{ cal} = 4.184 \text{ J} \tag{19.1}$$

which yields

$$1 \text{ J} = 0.239 \text{ cal.} \tag{19.2}$$

The conversion factor which links Joules and calories is obtained through a measurement which was proposed by Joule in 1850. The experiment involves rotating paddles which raise the temperature of a given amount of water by means of friction. The paddles are driven by the mechanical work provided by descending weights.

19.2. Heat Capacity, C

Different substances need different amounts of heat energy to raise their temperature by a given temperature interval. For example, it takes 1 calorie to raise 1 g water by 1 K. But the same heat energy raises the temperature of 1 g copper by about 11 K. In other words, water has a large heat capacity compared to copper. (The large heat capacity of water is incidentally the reason for the balanced climate in coastal regions and the heating of North European countries by the Gulf Stream.)

The heat capacity C is the amount of heat energy dQ which needs to be transferred to a substance in order to raise its temperature by a certain temperature interval. Possible units for the heat capacity are (cal/K) or (J/K).

The heat capacity is not defined uniquely, that is, one needs to specify the conditions under which the heat energy is added to the system. Even though several choices for the heat capacities are possible, one is generally interested in only two: the *heat capacity at constant volume* C_v and the heat capacity at constant pressure C_p. The former one is the most useful quantity because C_v is obtained immediately from the energy of the system. The heat capacity at constant volume is defined as:

$$C_v = \left(\frac{\partial E}{\partial T}\right)_v = \left(\frac{dQ}{dT}\right)_v. \tag{19.3}$$

On the other hand, it is much easier to measure the heat capacity of a solid at constant pressure than at constant volume. Fortunately, the difference between C_p and C_v *for solids* vanishes at low temperatures and is only about 5% at room temperature. C_v can be calculated from C_p if the volume expansion coefficient α and the compressibility κ of a material are known, by applying

$$C_v = C_p - \frac{\alpha^2 TV}{\kappa}, \tag{19.4}$$

where V is the volume of the solid. Equation (19.4) is derived in textbooks on thermodynamics.

19.3. Specific Heat, c

The specific heat is the heat capacity *per unit mass*:

$$c = \frac{C}{m} = \frac{\Delta Q}{m\Delta T}. \tag{19.5}$$

It is a material constant and it is temperature dependent. Characteristic values for the specific heat are given in Table 19.1. The unit of the specific heat is

Table 19.1. Experimental Thermal Parameters of Various Substances at Room Temperature and Ambient Pressure

Substance	Specific Heat (c_p) $\left(\frac{\text{cal}}{\text{g}\cdot\text{K}}\right)$	$\left(\frac{\text{J}}{\text{g}\cdot\text{K}}\right)$	Molecular (Atomic) Wt. $\left(\frac{\text{g}}{\text{mol}}\right)$	Molar Heat Capacity C_p $\left(\frac{\text{cal}}{\text{mol}\cdot\text{K}}\right)$	$\left(\frac{\text{J}}{\text{mol}\cdot\text{K}}\right)$	C_v $\frac{\text{cal}}{\text{mol}\cdot\text{K}}$
Al	0.215	0.899	27.0	5.80	24.3	5.5
Fe	0.110	0.460	55.9	6.15	25.7	5.9
Ni	0.109	0.456	58.9	6.42	26.8	5.9
Cu	0.092	0.385	63.5	5.84	24.4	5.6
Pb	0.031	0.130	207.0	6.42	26.9	5.9
Ag	0.056	0.236	108	6.05	25.5	5.8
C (graphite)	0.216	0.904	12.0	2.60	10.9	2.2
Water	1.000	4.184	18	18	75.3	

(cal/g · K) or (J/g · K). We note from Table 19.1 that values for the specific heat of solids are considerably smaller than the specific heat of water.

Rearranging (19.5) yields

$$\Delta Q = mc\Delta T, \tag{19.6}$$

which expresses that the heat energy ΔQ which is transferred to a body equals the product of body mass m, increase in temperature, and specific heat.

19.4. Molar Heat Capacity, C_v

A further useful material constant is the heat capacity *per mole* of a substance (rather than mass). It compares materials that contain the same number of molecules. The molar heat capacity is obtained by multiplying the specific heat c_v (or c_p) by the molecular weight W (see Table 19.1):

$$C_v \text{ (per mole)} = c_v \cdot W = \frac{\Delta Q}{\Delta T m} W. \tag{19.7}$$

The units are (cal/mol · K) or (J/mol · K). One mole contains $N_0 = 6.022 \times 10^{23}$ of elementary entities. (The gram molecular weight of a substance is the number of grams per mole of that substance.)

We see from Table 19.1 that the room temperature molar heat capacity at constant volume is approximately 6 cal/mol · K for most solids. This was experimentally discovered in 1819 by Dulong and Petit. We shall attempt to interpret this interesting result in a later section.

The experimental molar heat capacities for some materials are depicted in Fig. 19.1 as a function of temperature. We notice that some materials, such as carbon, reach the Dulong–Petit value of 6 cal/mol · K only at high tempera-

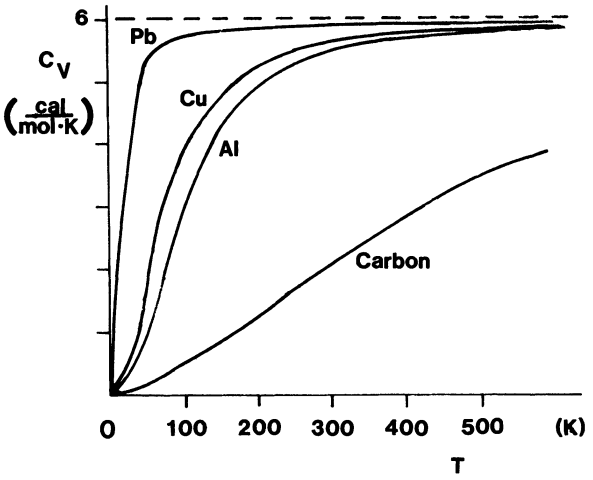

Figure 19.1. Temperature dependence of the molar heat capacity C_v for some materials.

Table 19.2. Debye Temperatures of Some Materials

Substance	θ_D(K)
Pb	95
Au	170
Ag	230
W	270
Cu	340
Fe	360
Al	375
Si	650
C	1850

tures. Some other materials such as lead reach 6 cal/mol · K at relatively low temperatures.

All molar heat capacities are zero at $T = 0$ K. The C_v-values near $T = 0$ K climb in proportion to T^3 and reach 96% of their final value at a temperature θ_D which is defined to be the Debye temperature. We shall see later that θ_D is an approximate dividing point between a high temperature region, where classical models can be used for the interpretation of C_v, and a low temperature region, where quantum theory needs to be applied. Selected Debye temperatures are listed in Table 19.2.

Table 19.3. Thermal Conductivities at Room Temperature[a]

Substance	$K\left(\frac{W}{m \cdot K}\right) \equiv \left(\frac{J}{s \cdot m \cdot K}\right)$	$K\left(\frac{cal}{s \cdot m \cdot K}\right)$
Silver	4.1×10^2	9.7×10^1
Copper	3.9×10^2	9.3×10^1
Aluminum	2.0×10^2	4.8×10^1
Silicon	1.5×10^2	3.6×10^1
Brass	1.1×10^2	2.6×10^1
Iron	6.7×10^1	1.6×10^1
Ni–Silver[b]	3.3×10^1	7.9
Water	6.3×10^{-1}	1.5×10^{-1}
Glass	8.0×10^{-1}	1.9×10^{-1}
Wood	8.0×10^{-2}	1.9×10^{-2}
Sulfur	2.0×10^{-2}	4.7×10^{-3}
Air	2.3×10^{-4}	5.5×10^{-5}

[a] See also Fig. 18.1.
[b] 62% Cu, 15% Ni, 22% Zn.

19.5. Thermal Conductivity, K

Heat conduction is the transfer of thermal energy from a hot body to a cold body when both bodies are brought into contact. For best visualization we consider a bar of a material of length x whose ends are held at different temperatures. The amount of thermal energy Q which crosses a unit area of this bar per unit time (i.e., the heat flux J_Q) is proportional to the temperature gradient dT/dx. The proportionality constant is called the thermal conductivity K. We thus write

$$J_Q = -K\frac{dT}{dx}. \tag{19.8}$$

The negative sign indicates that the heat flows from the hot to the cold end. Possible units for the heat conductivity are (cal/m · s · K), or (J/m · s · K), or (W/m · K). The heat flux J_Q is measured in (cal/m² · s) or (J/m² · s). Table 19.3 gives some characteristic values for K. The thermal conductivity decreases slightly with increasing temperature. For example, K for copper decreases by 20% within a temperature span of 1000° C. In the same temperature region K for iron decreases by 10%.

19.6. The Ideal Gas Equation

Free electrons in metals and alloys can often be considered to behave like an ideal gas. An ideal gas is an abstraction which is frequently used in thermody-

namics. It is usually defined to be a gas whose density is low enough in order for it to obey the equation

$$PV = nRT, \tag{19.9}$$

where P is the pressure of the gas, V its volume, n the number of moles, T the absolute temperature, and R the universal gas constant

$$\begin{aligned} R &= k_B N_0 = 8.314 \text{ (J/mol} \cdot \text{K)} \\ &= 1.986 \text{ (cal/mol} \cdot \text{K)}. \end{aligned} \tag{19.10}$$

Equation (19.9) is a combination of two experimentally obtained thermodynamics laws: One, discovered by Boyle and Mariotte (PV = const, at constant T) and the other, discovered by Gay-Lussac ($V \sim T$, at constant P). The reader who has taken classes in physics or thermodynamics is undoubtedly familiar with these equations.

19.7. Kinetic Energy of Gases

In the chapters to come, we need to know the kinetic energy of atoms, molecules or electrons at a given temperature from a classical point of view. The calculation which is summarized below is usually contained in textbooks on thermodynamics.

We commence by quoting the number of molecules in a gas which interact in the unit time with the end face of unit area of a bar which has the length dx. We assume that, because of thermal agitation, 1/3 of the electrons move in the x-directions, that is, 1/6 in the positive x-direction. The unit volume, shown in Fig. 19.2, is

$$dV = A\,dx = Av\,dt, \tag{19.11}$$

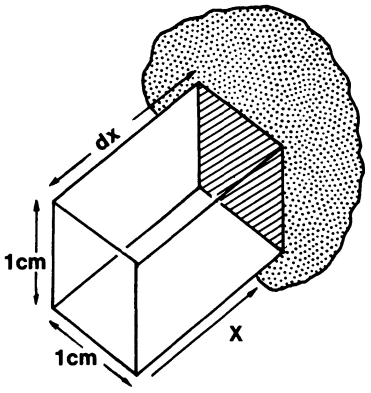

Figure 19.2. Diagram for the derivation of the kinetic energy of gases.

where A is the unit area and v the velocity of the particles which fly in the x-direction. The number of particles reaching the end face is naturally proportional to the number of particles n_v in the given volume, that is,

$$z' = \tfrac{1}{6} n_v \cdot dV = \tfrac{1}{6} n_v A v \, dt.$$

The number of particles per unit time and unit area which hit the end face is consequently:

$$z = \tfrac{1}{6} n_v v, \tag{19.12}$$

where

$$n_v = \frac{N}{V} \tag{19.13}$$

is the *number of particles per unit volume*. Each particle transfers the momentum $2mv$ during its collision with the wall and subsequent reflection. The *momentum per unit time and unit area* is then

$$p = z 2mv = \frac{1}{6} n_v v 2mv = \frac{1}{3} \frac{N}{V} mv^2. \tag{19.14}$$

This yields for the pressure

$$P = \frac{F}{A} = \frac{ma}{A} = \frac{d(mv)/dt}{A} = \frac{dp/dt}{A} = \frac{1}{3} \frac{N}{V} mv^2. \tag{19.15}$$

With

$$PV = nRT = nk_B N_0 T = Nk_B T \tag{19.16}$$

(see (19.9) and (19.10)), we obtain from (19.15)

$$PV = \tfrac{1}{3} Nmv^2 = k_B NT. \tag{19.17}$$

Inserting

$$E_{kin} = \tfrac{1}{2} mv^2 \tag{19.18}$$

into (19.17) yields

$$k_B NT = \tfrac{1}{3} N 2 \tfrac{1}{2} mv^2 = \tfrac{2}{3} NE_{kin} \tag{19.19}$$

which finally yields for the kinetic energy of a particle

$$E_{kin} = \tfrac{3}{2} k_B T. \tag{19.20}$$

A more precise calculation which considers the mutual collisions of the particles, and thus a velocity distribution, replaces the kinetic energy in (19.20) by an average kinetic energy.

Problems

Note: The problems in this chapter contain engineering applications in order to make the student aware of the importance of thermal properties in daily life.

1. Calculate the number of gas molecules which are left in an ultrahigh vacuum of 10^{-9} Pa ($\sim 7.5 \times 10^{-12}$ Torr) at room temperature.
2. Calculate the rate of heat loss in a 5 mm thick window glass when the exterior temperature is 0° C and the room temperature is 20° C. Compare your result with the heat loss in an aluminum and a wood frame of 10 mm thickness. How can you decrease the heat loss through the window?
3. A block of copper, whose mass is 50 g, is quenched directly from an annealing furnace into a 200 g glass container which holds 500 g of water. What is the temperature of the furnace when the water temperature rises from 0° to 15° C? ($c_{\text{glass}} = 0.12$ cal/g · K)
4. Explain in simple terms why wood has a smaller heat conductivity than copper.
5. What are the implications for the semiconductor industry that silicon has a relatively good heat conductivity?
6. Why is the fiberglass insulation used for buildings, etc. loose rather than compact? (*Hint*: Compare K for glass and air. Discuss also heat convection.)
7. Find in a handbook the relationship between cal/g · K and BTU/lb. ° F.

CHAPTER 20

Heat Capacity

20.1. Classical (Atomistic) Theory of Heat Capacity

This section attempts to interpret the thermal properties of materials using atomistic concepts. In particular, an interpretation of the experimentally observed molar heat capacity at high temperatures, that is, $C_v = 6$ (cal/mol · K) is of interest.

We postulate that each atom in a crystal is bound to its site by a harmonic force. A given atom is thought to be capable to absorb thermal energy, and in doing so it starts to vibrate about its point of rest. The amplitude of the oscillation is restricted by electrostatic repulsion forces of the nearest neighbors. The extent of this thermal vibration is therefore not more than 5 or 10% of the interatomic spacing, depending on the temperature. In short, we compare an atom with a sphere which is held at its site by two springs (Fig. 20.1(a)). The thermal energy which a harmonic oscillator of this kind can absorb is proportional to the absolute temperature of the environment. The proportionality factor has been found to be the Boltzmann constant k_B (see below). The average energy of the oscillator is then

$$E = k_B T. \tag{20.1}$$

Now, solids are three-dimensional. Thus, a given atom in a cubic crystal also responds to the harmonic forces of lattice atoms in the two other directions. In other words, it is postulated that each atom in a cubic crystal represents three oscillators (Fig. 20.1(b)), each of which absorbs the thermal energy $k_B T$. Therefore, the *average energy per atom* is

$$E = 3k_B T. \tag{20.2}$$

We note in passing that the same result is obtained by using the kinetic theory

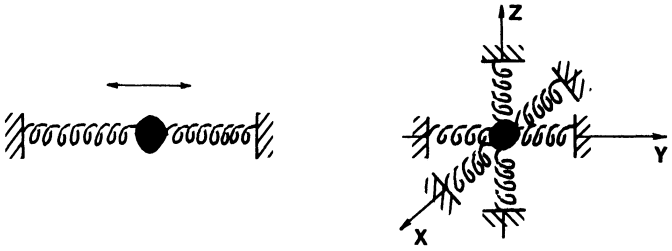

(a) (b)

Figure 20.1. (a) One-dimensional harmonic oscillator; (b) three-dimensional harmonic oscillator.

of gases. It was shown in (19.20) that the average kinetic energy of a particle (or in the present case an atom) is

$$E_{\text{kin}} = \tfrac{3}{2} k_{\text{B}} T. \tag{20.3}$$

Now, each elastic vibration in a solid involves not only kinetic energy, but also potential energy which has the same average energy as the kinetic energy. The total energy of a vibrating lattice atom is thus

$$E = 2 \cdot \tfrac{3}{2} k_{\text{B}} T \tag{20.4}$$

which is the result of (20.2).

We consider now all N_0 atoms per mole. Then the *total internal energy per mole* is

$$E = 3 N_0 k_{\text{B}} T. \tag{20.5}$$

Finally, the molar heat capacity is given by combining (19.3) with (20.5) which yields

$$\boxed{C_v = \left(\frac{dE}{dT}\right)_v = 3 N_0 k_{\text{B}}.} \tag{20.6}$$

Inserting the numerical values for N_0 and k_{B} into (20.6) yields

$$C_v = 25 \text{ J/mol} \cdot \text{K} \quad \text{or} \quad 5.98 \text{ cal/mol} \cdot \text{K},$$

quite in agreement with the experimental findings at high temperatures (Fig. 18.2).

It is satisfying to see that a simple model involving three harmonic oscillators per atom can explain readily the experimentally observed heat capacity. However, one shortcoming is immediately evident: the calculated molar heat capacity turned out to be temperature independent, according to (20.6), and also independent on the material. This discrepancy with the observed behavior (see Fig. 18.2) was puzzling to scientists at the turn of this century and had to await quantum theory to be properly explained.

20.2. Quantum Mechanical Considerations—The Phonon

20.2.1. Einstein Model

Einstein postulated in 1903 that the energies of the above mentioned classical oscillators should be quantized, that is, he postulated that only certain vibrational modes should be allowed, quite in analogy to the allowed energy states of electrons. These lattice vibration quanta were called *phonons*.

The term *phonon* stresses an analogy with *electrons* or *photons*. As we know from Chapter 2, photons are quanta of electromagnetic radiation, that is, photons describe (in the appropriate frequency range) classical light. Phonons, on the other hand, are quanta of the ionic displacement field which (in the appropriate frequency range) describe classical sound.

The phonon describes the *particle* nature of an oscillator. A phonon has, in analogy to the de Broglie relation (2.3), the momentum $p = \hbar/\lambda$.

Furthermore, Einstein postulated a particle–wave duality. This suggests *phonon waves* which propagate through the crystal with the speed of sound. Phonon waves are *not* electromagnetic waves: they are *elastic waves*, vibrating in a longitudinal and/or in a transversal mode.

In analogy to the electron case shown in Part I of this book, one can describe the properties of phonons in terms of band diagrams, Brillouin zones, or density of states curves. Small differences exist however. For example, the energy in the band diagram of an electron is replaced in a phonon band diagram by the vibrational frequency ω of the phonon. The branches in the phonon band diagram are sinusoidal in nature (compared to parabolic in the free electron case). The individual phonon bands are no longer called valence or conduction bands, but more appropriately *acoustic bands* and *optical bands*, mainly because the frequencies in which the branches are situated are in the acoustical and optical ranges, respectively. The density of states, or better the *density of vibrational modes* $D(\omega)$ for the phonon case is defined so that $D(\omega) \cdot d\omega$ is the number of modes whose frequencies lie in the interval ω and $\omega + d\omega$. For a continuous medium the density of modes is

$$D(\omega) = \frac{3V}{2\pi^2} \frac{\omega^2}{v_s^3}, \tag{20.7}$$

where v_s is the sound velocity. This equation can be derived quite similarly as demonstrated in Section 6.3.

The allowed energies of a single oscillator are

$$E_n = n\hbar\omega, \tag{20.8}$$

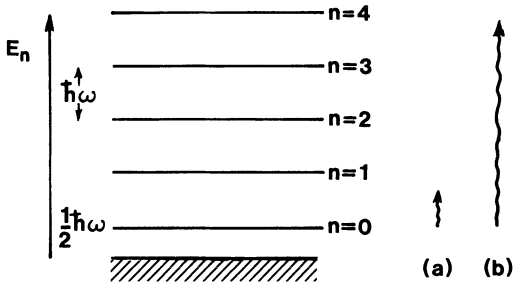

Figure 20.2. Allowed energy levels of a phonon: (a) average thermal energy at low temperatures; (b) average thermal energy at high temperatures.

similarly as in Section 4.2, where n is an integer.[1] A schematic energy level diagram for the allowed phonon energies is shown in Fig. 20.2.

One important difference between phonons and electrons needs to be emphasized. Phonons are created by raising the temperature, and eliminated by lowering it, that is, the number of phonons is *not* conserved as we shall show momentarily. (In contrast to this, the number of electrons is constant.) Einstein postulated that with increasing temperature more and more phonons are created, each of which has the same energy $\hbar\omega$ or the same frequency of vibration ω. The average number of phonons $\bar{N}_{\text{ph}}$ at a given temperature was found by Bose and Einstein to obey a special type of statistics:

$$\bar{N}_{\text{ph}} = \frac{1}{\exp\left(\dfrac{\hbar\omega}{k_B T}\right) - 1}. \tag{20.10}$$

This equation is similar in form to the Fermi distribution function (6.1).

We note in passing that for high phonon energies $\hbar\omega$, the exponential term in (20.10) becomes large when compared to unity so that the number of phonons can be approximated by Boltzmann statistics, that is, by the laws of classical thermodynamics:

$$\bar{N}_{\text{ph}} \approx e^{-\hbar\omega/k_B T}. \tag{20.11}$$

We already made a similar statement in Section 6.2. We see also from (20.10) that the number of phonons decreases rapidly when the temperature approaches 0 K.

The average energy of an isolated oscillator is then the average number of phonons, times the energy of a phonon:

---

[1] Since the ground state ($n = 0$) has still a zero point energy of $\frac{1}{2}\hbar\omega$ we should more appropriately write

$$E_n = n\hbar\omega + \tfrac{1}{2}\hbar\omega = (n + \tfrac{1}{2})\hbar\omega. \tag{20.9}$$

The zero point energy is, however, of no importance for the present considerations.

$$E_{\text{osc}} = \hbar\omega \bar{N}_{\text{ph}} = \frac{\hbar\omega}{\exp\left(\frac{\hbar\omega}{k_B T}\right) - 1}. \tag{20.12}$$

The *thermal energy of a solid* can now be calculated by taking into account (as in Section 20.1) that a mole of a substance contains $3N_0$ oscillators. This yields for the thermal energy per mole

$$E = 3N_0 \frac{\hbar\omega}{\exp\left(\frac{\hbar\omega}{k_B T}\right) - 1}. \tag{20.13}$$

The molar heat capacity is finally

$$\boxed{C_v = \left(\frac{dE}{dT}\right)_v = 3N_0 k_B \left(\frac{\hbar\omega}{k_B T}\right)^2 \frac{\exp\left(\frac{\hbar\omega}{k_B T}\right)}{\left(\exp\left(\frac{\hbar\omega}{k_B T}\right) - 1\right)^2}.} \tag{20.14}$$

We discuss C_v for two special temperature regions. For large temperatures the approximation $e^x \simeq 1 + x$ can be applied, which yields $C_v \simeq 3N_0 k_B$ (see Problem 5) in agreement with (20.6), that is, we obtain the classical Dulong–Petit value. For $T \to 0$, C_v approaches zero, again in agreement with experimental observations. Thus, the temperature dependence of C_v is now in qualitative accord with the experimental findings. One minor discrepancy has to be noted however: At very small temperatures the experimental C_v decreases by T^3, as stated in Section 19.4. The Einstein theory predicts instead an exponential reduction. The Debye theory which we shall discuss below alleviates this discrepancy by postulations that the individual oscillators interact with each other.

By inspecting (20.14) we observe that this relation contains only one adjustable parameter, namely the angular frequency, which we shall redesignate for this particular case by ω_E. By fitting (20.14) to experimental curves, the frequency of the phonon waves can be obtained. For copper the angular frequency ω_E has been found this way to be $2.5 \times 10^{13}\ \text{s}^{-1}$, which yields $\nu_E = 4 \times 10^{12}\ \text{s}^{-1}$. It is customary to call frequencies up to $10^5\ \text{s}^{-1}$ sound waves, frequencies between 10^5 and $10^9\ \text{s}^{-1}$ ultrasonics, and frequencies above $10^9\ \text{s}^{-1}$ thermal waves. The Einstein frequency is thus situated very appropriately in the thermal wave region.

Occasionally, the *Einstein temperature* θ_E is quoted, which is defined by equating the phonon energy

$$\hbar\omega_E = k_B \theta_E, \tag{20.15}$$

which yields

$$\theta_E = \frac{\hbar\omega_E}{k_B}. \tag{20.16}$$

Characteristic values for θ_E are between 200 and 300 K. From the above-quoted ω_E value for copper, θ_E^{Cu} can be calculated to be 240 K.

20.2.2. Debye Model

We refine now the Einstein model by taking into account that the atoms in a crystal interact with each other. Consequently, the oscillators are thought to vibrate interdependently. We recall that the Einstein model considered only *one* frequency of vibration, ω_E. When interactions between the atoms occur, many more frequencies are thought to exist which range from about the Einstein frequency down to frequencies of the acoustical modes of oscillation. We postulate that these vibrational modes are quantized (Fig. 20.2). The total displacement of a given atom in a crystal during the oscillation is found by summing up all vibrational modes. This has been done by Debye who modified the Einstein equation (20.13) by replacing the $3N_0$ oscillators of a single frequency by the number of modes in a frequency interval $d\omega$ and by summing up over all allowed frequencies. The total energy of vibration for the solid is then

$$E = \int E_{osc} D(\omega)\, d\omega, \tag{20.17}$$

where E_{osc} is the energy of one oscillator given in (20.12), and $D(\omega)$ is the density of modes given in (20.7). Inserting (20.7) and (20.12) into (20.17) yields

$$E = \frac{3V}{2\pi^2 v_s^3} \int_0^{\omega_D} \frac{\hbar\omega^3}{\exp\left(\frac{\hbar\omega}{k_B T}\right) - 1} d\omega. \tag{20.18}$$

The integration is performed between $\omega = 0$ and the Debye frequency ω_D, because above the Debye frequency the oscillators are defined to behave in a classical manner, see Section 19.5.

The molar heat capacity C_v is obtained, as usual, by performing the derivative of (20.18) with respect to temperature. This yields:

$$C_v = \frac{3V\hbar^2}{2\pi^2 v_s^3 k_B T^2} \int_0^{\omega_D} \frac{\omega^4 \exp\left(\frac{\hbar\omega}{k_B T}\right)}{\left(\exp\left(\frac{\hbar\omega}{k_B T}\right) - 1\right)^2} d\omega \tag{20.19}$$

or

$$C_v = 9k_B N_0 \left(\frac{T}{\theta_D}\right)^3 \int_0^{\theta_D/T} \frac{x^4 e^x}{(e^x - 1)^2} dx, \tag{20.20}$$

where

$$x = \frac{\hbar\omega}{k_B T} \tag{20.21}$$

varies with the angular frequency ω, and

$$\theta_D = \frac{\hbar\omega_D}{k_B} \tag{20.22}$$

is called the Debye temperature. Values for θ_D can be obtained again by curve-fitting, particularly at low temperatures. They have been listed in Table 19.2. For low temperatures, that is, for $T < \theta_D$ the upper limit of the integral in (20.20) can be approximated by infinity. Then (20.20) can be evaluated and it becomes

$$C_v = \frac{12\pi^4}{5} N_0 k_B \left(\frac{T}{\theta_D}\right)^3. \tag{20.23}$$

From both equations, (20.20) as well as (20.23), it can be seen that C_v decreases proportionally to T^3 at low temperatures, which is quite in agreement with the experimental observations.

In summary, the main difference between the two theories is that the Debye model takes the low frequency modes into account whereas the Einstein model does not. We have to realize, however, that the excitation of oscillators at low temperatures occurs only with a small probability because at low temperatures only a few oscillators can be raised to the next higher level. This is a consequence of the fact that the energy difference between levels is comparatively large for the available small thermal energies, as schematically illustrated in Fig. 20.2.

It should be noted that even (20.20) is only an approximation, because the underlying model does not take into consideration the periodicity of the atoms in a crystal lattice. Thus, a refinement of the Debye model needs to utilize the actual density of modes function $D(\omega)$ for a given material. This has been done by scientists with good success. Equation (20.20) is, however, a fairly good approximation (see Fig. 18.2).

20.3. Electronic Contribution to the Heat Capacity

In the previous sections we have digressed considerably from the principal theme of this book, namely the description of the *electronic* properties of materials. We return now to our main topic by discussing the contributions

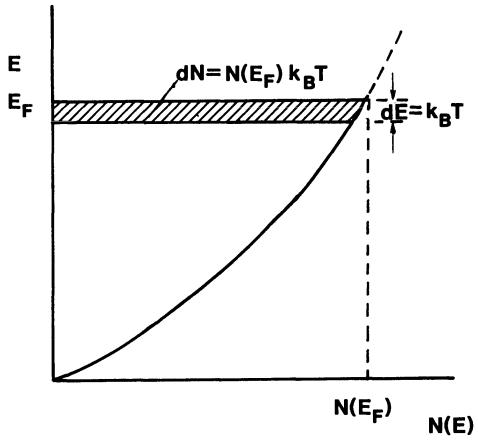

Figure 20.3. Population density as a function of energy for a metal. The electrons within the shaded area below E_F can be excited by a thermal energy $k_B T$.

which the electrons provide to the specific heat. We shall see quickly that this contribution is relatively small compared to that of the phonons.

At first, we need to remember that only the kinetic energy of the *free* electrons can be raised with increasing temperature. Consequently, our present discussion is restricted to metals and alloys which have, as we know, partially filled bands and thus free electrons. Secondly, we need to remember that only those electrons which lie within an energy interval $k_B T$ of the Fermi energy can be excited into higher states because only these electrons find empty energy states after their excitation. We know that the number dN of these excitable electrons depends on the population density of the metal under consideration (Section 6.4). In other words dN is the product of population density at the Fermi level, $N(E_F)$, and energy interval $k_B T$, as indicated by the shaded area in Fig. 20.3.

We postulate that the electrons which are excited by thermal energy behave like a monatomic gas. We have already shown in (19.20) that the mean kinetic energy of gas molecules, or in the present case, the mean kinetic energy of the electrons above the Fermi energy is $\frac{3}{2}k_B T$. Thus, the thermal energy at a given temperature is

$$E_{kin} = \tfrac{3}{2}k_B T\, dN = \tfrac{3}{2}k_B T N(E_F) k_B T. \tag{20.24}$$

The heat capacity of the electrons is then, as usual:

$$C_v^{el} = \left(\frac{dE}{dT}\right)_v = 3k_B^2 T N(E_F). \tag{20.25}$$

We need now an expression for $N(E_F)$. We obtain this by combining (6.8) and (6.11) for $E < E_F$ (see Fig. 20.3 and Problem 9), which yields:

$$N(E_F) = \frac{3N^*}{2E_F}\left(\frac{\text{electrons}}{\text{J}}\right), \tag{20.26}$$

where N^* is the number of electrons which have an energy equal to or smaller than E_F (Section 6.4). Inserting (20.26) into (20.25) yields

$$C_v^{el} = \frac{9}{2}\frac{N^* k_B^2 T}{E_F}\left(\frac{\text{J}}{\text{K}}\right). \tag{20.27}$$

So far we assumed that the thermally excited electrons behave like a classical gas. In reality, the excited electrons must obey the Pauli principle. If this is taken into consideration properly, (20.27) changes slightly and reads:

$$\boxed{C_v^{el} = \frac{\pi^2}{2}\frac{N^* k_B^2 T}{E_F} = \frac{\pi^2}{2} N^* k_B \frac{T}{T_F}.} \tag{20.28}$$

Let us assume now a monovalent metal in which we can reasonably assume one free electron per atom (see Part I). Then, N^* can be equated to the number of atoms per mole N_0, and (20.28) becomes the heat capacity per mole

$$\boxed{C_v^{el} = \frac{\pi^2}{2}\frac{N_0 k_B^2 T}{E_F} = \frac{\pi^2}{2} N_0 k_B \frac{T}{T_F}\left(\frac{\text{J}}{\text{K}\cdot\text{mol}}\right).} \tag{20.29}$$

We see from (20.29) that C_v^{el} is a linear function of temperature and is zero at $T = 0$ K, quite in agreement with the experimental observations, see Fig. 18.2. The room temperature contribution of the electronic specific heat to the total specific heat is less than 1% (see Problem 3). There are, however, two temperature regions where the electronic specific heat plays an appreciable role. This is at very low temperatures, that is, at $T < 5$ K (see Fig. 18.2). Secondly, we have learned in the previous sections that the lattice heat capacity levels off above the Debye temperature. Thus, the electron heat capacity can give at high temperatures a small contribution to the Dulong–Petit value.

An interesting aspect is added: Equation (20.25) may be rewritten in the following form:

$$C_v^{el} = \gamma T, \tag{20.30}$$

where

$$\gamma = 3k_B^2 N(E_F). \tag{20.31}$$

Furthermore, (20.20) can be rewritten as

$$C_v^{ph} = \beta T^3. \tag{20.32}$$

Below the Debye temperature, the heat capacity of metals is the sum of electron and phonon contributions, that is,

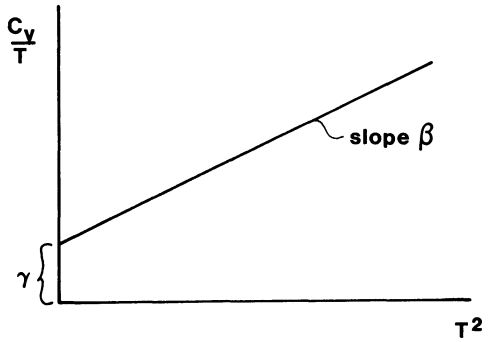

Figure 20.4. Schematic representation of an experimental plot of C_v/T versus T^2.

Table 20.1.

Substance	γ, observed		γ, calculated		$\frac{m^*_{th}}{m_0}$
	$\left(\frac{\text{cal}}{\text{mol}\cdot\text{K}^2}\right)$	$\left(\frac{\text{J}}{\text{mol}\cdot\text{K}^2}\right)$	$\left(\frac{\text{cal}}{\text{mol}\cdot\text{K}^2}\right)$	$\left(\frac{\text{J}}{\text{mol}\cdot\text{K}^2}\right)$	
Ag	1.54×10^{-4}	0.646×10^{-3}	1.54×10^{-4}	0.645×10^{-3}	1.0
Al	3.22×10^{-4}	1.35×10^{-3}	2.18×10^{-4}	0.912×10^{-3}	1.48
Au	1.74×10^{-4}	0.729×10^{-3}	1.53×10^{-4}	0.642×10^{-3}	1.14
Na	3.11×10^{-4}	1.3×10^{-3}	2.37×10^{-4}	0.992×10^{-3}	1.31
Fe	1.19×10^{-3}	4.98×10^{-3}			
Ni	1.68×10^{-3}	7.02×10^{-3}			

$$C_v^{\text{tot}} = C_v^{\text{el}} + C_v^{\text{ph}} = \gamma T + \beta T^3, \tag{20.33}$$

which yields

$$\frac{C_v^{\text{tot}}}{T} = \gamma + \beta T^2. \tag{20.34}$$

A plot of experimental values for C_v^{tot}/T versus T^2 provides the material constants γ (intercept) and β (slope), see Fig. 20.4. Heat capacity measurements thus serve as a means to obtain the electron population density at the Fermi surface by using (20.31).

Some calculated and observed values for γ are given in Table 20.1. From the slight discrepancy between observed and free-electron γ-values, a *thermal effective mass* can be calculated which is defined as

$$\frac{m^*_{\text{th}}}{m_0} = \frac{\gamma(\text{obs})}{\gamma(\text{calc})}. \tag{20.35}$$

The deviation between the two γ-values is interpreted to stem from neglecting electron–phonon and electron–electron interactions.

Problems

1. How many electrons (in percent of the total number of electrons per mole) lie within $k_B T$ of the Fermi energy? Take $E_F = 5$ eV and $T = 300$ K.
2. Calculate C_v at high temperatures (500 K) by using the quantum mechanical equation derived by Einstein. Assume an Einstein temperature of 250 K, and convince yourself that C_v approaches the classical value at high temperatures.
3. Calculate the electronic specific heat for $E_F = 5$ eV and $T = 300$ K. How does your result compare with the experimental value of 6 (cal/mol K)?
4. Calculate the population density at the Fermi level for a metal whose electronic specific heat at 4 K was measured to be 2×10^{-3} (cal/mol K).
5. Confirm that (20.14) reduces for large temperatures to the Dulong–Petit value.
6. At which temperature does the electronic contribution to C_v of silver become identical with the Dulong–Petit value? *Hint*: Use proper units for the heat capacity! Take $E_F = 5$ eV, $N_f = 10^{28}$ el/m^3.
7. Discuss thermal expansion in materials from an atomistic point of view.
8. Show that for small temperatures, (20.20) reduces to (20.23) and that for large temperatures (20.20) reduces to the Dulong–Petit value.
9. Derive (20.26) for $E < E_F$ as shown in Figure 20.3 by combining (6.8) and (6.11) and eliminating the Planck constant.

CHAPTER 21

Thermal Conduction

We stated in Chapter 19 that heat conduction can be described as the transfer of thermal energy from the hot to the cold part of a piece of material. We shall discuss now the mechanisms which are involved in this transfer of thermal energy.

We postulate that the heat transfer in solids may be provided by *free electrons* as well as by *phonons*. We understand immediately that in insulators, which do not contain any free electrons, the heat must be conducted exclusively by phonons. In metals and alloys, on the other hand, the heat conduction is dominated by electrons because of the large number of free electrons in metals. Thus, the phonon contribution is usually neglected in this case.

One particular point should be clarified right at the beginning. Electrons in metals travel in equal numbers from hot to cold and from cold to hot in order that the charge neutrality be maintained. Now, the electrons in the hot part of a metal possess and transfer a high energy. In contrast to this, the electrons in the cold end possess and transfer a lower energy. The heat transferred from hot to cold is thus proportional to the difference in the energies of the electrons.

The situation is quite different in phonon conductors. We know from Section 20.2.1 that the number of phonons is larger at the hot end than at the cold end. Thermal equilibrium thus involves in this case a net transfer of phonons from the hot into the cold part of a material.

21.1. Thermal Conduction in Metals and Alloys—Classical Approach

We now attempt to calculate the heat conductivity K (see (19.8)). The train of thought is borrowed from the kinetic theory of gases because the same arguments hold true for electrons as for gas molecules.

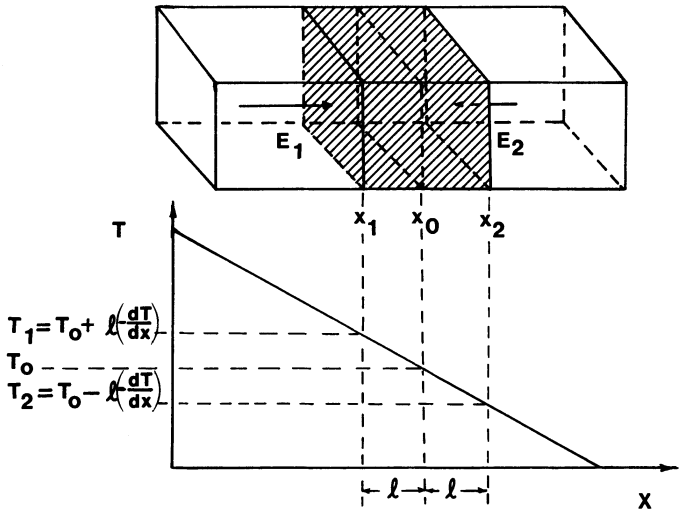

Figure 21.1. For the derivation of the heat conductivity in metals. Note that (dT/dx) is negative for the case shown in the graph.

Consider a bar of metal whose left side is hot and whose right side is cold (Fig. 21.1). Thus, a temperature gradient dT/dx exists in the x-direction of the bar. Consider also a volume at the center of the bar whose faces have the size of a unit area and whose length is $2l$, where l is the mean free path between two consecutive collisions between an electron and lattice atoms. We assume that at the distance l from the center x_0 the average electron has had its last collision and has picked up the energy of this place. We calculate first the energy E_1 per unit time and unit area of the electrons which drift from the left into the above mentioned sample volume. This energy E_1 equals the number of electrons z, times the energy of one of the electrons. The latter is, according to (19.20), $\frac{3}{2}k_B T_1$, where T_1 can be taken from Fig. 21.1, and z is given in (19.12):

$$E_1 = z \cdot \frac{3}{2} k_B \left(T_0 + l\left(-\frac{dT}{dx} \right) \right) = \frac{n_v v}{6} \frac{3}{2} k_B \left(T_0 - l \frac{dT}{dx} \right). \tag{21.1}$$

The same amount of electrons is drifting from right to left through the volume under consideration. These electrons, however, carry a lower energy E_2 because of the lower temperature of the particles at the site of interaction. Thus,

$$E_2 = \frac{n_v v}{6} \cdot \frac{3}{2} k_B \left(T_0 + l \frac{dT}{dx} \right). \tag{21.2}$$

The excess thermal energy transferred per unit time into the unit volume is therefore

$$J_Q = E_1 - E_2 = -\frac{n_v v}{6} \frac{3}{2} k_B \left(2l \frac{dT}{dx} \right) = -\frac{n_v v}{2} k_B l \frac{dT}{dx}. \tag{21.3}$$

We compare (21.3) with (19.8)

$$J_Q = -K\frac{dT}{dx}. \tag{21.4}$$

Then we obtain for the heat conductivity of the electrons

$$\boxed{K = \frac{n_v v k_B l}{2}}. \tag{21.5}$$

The heat conductivity is thus larger the more electrons are involved, the larger their velocity, and the larger the mean free path between two consecutive electron–atom collisions. This result intuitively makes sense.

We seek now a connection between the heat conductivity and C_v^{el}. We know from (19.20) the kinetic energy of all n_v electrons per unit volume:

$$E = n_v \tfrac{3}{2} k_B T. \tag{21.6}$$

From this we obtain the heat capacity *per volume*

$$C_v^{el} = \left(\frac{dE}{dT}\right)_v = n_v \frac{3}{2} k_B. \tag{21.7}$$

Combining (21.5) with (21.7) yields

$$K = \tfrac{1}{3} C_v^{el} v l. \tag{21.8}$$

All three variables contained in (21.8) are temperature dependent, but while C_v^{el} increases with temperature, l and to a small degree also v are decreasing. Thus, K should change very little with temperature, which is indeed experimentally observed. As mentioned in Section 19.5, the thermal conductivity decreases about 10^{-5} W/mK per degree. K also changes at the melting point and when a change in atomic packing occurs.

21.2. Thermal Conduction in Metals and Alloys—Quantum Mechanical Considerations

The question arises, as to what velocity do the electrons (that participate in the heat conduction process) have, and do all the electrons participate in the heat conduction? We have raised a similar question in Section 20.3, see Fig. 20.3. We know from there that only those electrons which have an energy close to the Fermi energy E_F are able to participate in the conduction process. Thus, the velocity in (21.5) and (21.8) is essentially the Fermi velocity v_F which can be calculated with

$$E_F = \tfrac{1}{2} m v_F^2 \tag{21.9}$$

if the Fermi energy is known.

The number of participating electrons contained in (21.5) is determined by the population density at the Fermi energy $N(E_F)$, that is, in first approximation, by the number of free electrons N_f per volume. Inserting the quantum mechanical expression for C_v^{el} (20.28)

$$C_v^{el} = \frac{\pi^2}{2} \frac{N_f k_B^2 T}{E_F} \left(\frac{J}{K \cdot m^3} \right) \tag{21.10}$$

into (21.8) yields

$$K = \frac{\pi^2 N_f k_B^2 T v_F l_F}{6 E_F}, \tag{21.11}$$

which reduces with (21.9) and $l_F = \tau v_F$ (τ = relaxation time) to

$$\boxed{K = \frac{\pi^2 N_f k_B^2 T \tau}{3 m^*}}. \tag{21.12}$$

This is the result we were seeking. Again, the heat conductivity is larger the more *free* electrons are involved and the smaller the (effective) mass of the electrons.

Next we return to a statement which we made in Chapter 18. We pointed out there that Wiedemann and Franz observed that good electrical conductors are also good thermal conductors. We are now in a position to compare the thermal conductivity (21.12) with the electrical conductivity (7.15)

$$\sigma = \frac{N_f e^2 \tau}{m^*}. \tag{21.13}$$

The ratio of K and σ is proportional to a constant called the Lorentz number L which is a function of two universal constants k_B and e

$$\frac{K}{\sigma T} = L = \frac{\pi^2 k_B^2}{3 e^2}. \tag{21.14}$$

The Lorentz number is calculated to be 5.838×10^{-9} ($\Omega \cdot \text{cal}/\text{K}^2 \cdot \text{s}$) or 2.443×10^{-8} ($\text{J} \cdot \Omega/\text{K}^2 \cdot \text{s}$) (see Problem 2). Experiments for most metals confirm this number quite well.

21.3. Thermal Conduction in Dielectric Materials

Heat conduction in dielectric materials occurs by a flow of phonons. The hot end possesses more phonons than the cold end causing a drift of phonons down a concentration gradient.

The thermal conductivity can be calculated similarly as in the previous section, which leads to the same equation as (21.8):

$$K = \tfrac{1}{3} C_v^{ph} v l. \tag{21.15}$$

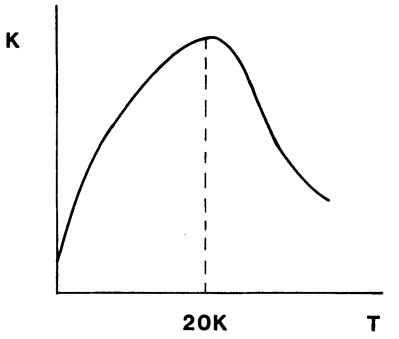

Figure 21.2. Schematic representation of thermal conductivity in dielectrical materials as a function of temperature.

In the present case C_v^{ph} is the (lattice) heat capacity per volume of the phonons, v is the phonon velocity, and l the phonon mean free path. A typical value for v is about 5×10^5 cm/s (sound velocity) with v being relatively temperature independent. In contrast, the mean free path varies over several orders of magnitude, that is, from about 10 nm at room temperature to 10^4 nm near 20 K. The drifting phonons interact on their path with lattice imperfections, with external boundaries, and with other phonons. These interactions constitute a thermal resistivity which is quite analogous to the electrical resistivity. Thus, we may treat the thermal resistance just as we did in Part II, that is, in terms of interactions between particles (here phonons) and matter, or in terms of scattering of phonon waves on lattice imperfections.

At low temperatures, where only few phonons exist, the thermal conductivity depends mainly on the heat capacity C_v^{ph} which increases with the third power of increasing temperature according to (20.20) (see Fig. 21.2). At low temperatures, the phonons possess small energies, that is, long wavelengths which are too long to be scattered by lattice imperfections. The mean free path l becomes thus a constant and it is virtually identical to the dimensions of the material.

More effective are the phonon–phonon interactions which are dominant at higher temperatures since, as we know, the phonon density increases with increasing T. Thus, the mean free path and consequently, the thermal conductivity decreases for temperatures above about 20 K (Fig. 21.2).

Another mechanism which impedes the flow of phonons at higher temperatures has been discovered. We explain this mechanism in quantum mechanical terms. When two phonons collide, a third phonon results in a proper manner to conserve momentum. Now, phonons (just like electrons) can be represented to travel in k-space. The same arguments, as discussed in Chapter 5, may then apply here. We need to consider Brillouin zones which represent the areas in which the phonon interactions occur. In the example of Fig. 21.3, the resultant vector $\mathbf{a}_1 + \mathbf{a}_2 = \mathbf{a}_3$ is shown to be outside the first Brillouin zone. We project this vector back to a corresponding place *inside* the first Brillouin zone by applying a similar vector relationship as in (5.34)

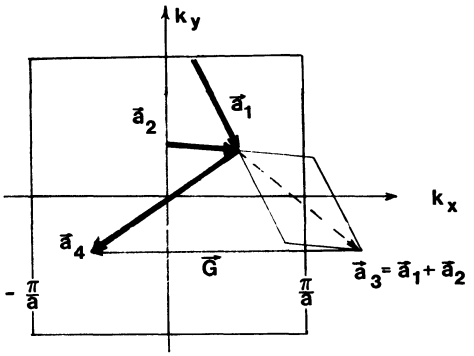

Figure 21.3. First Brillouin zone in a reciprocal square lattice. Two phonons $\mathbf{a}_1$ and $\mathbf{a}_2$ are shown to interact. In the example, the resultant vector $\mathbf{a}_3$ lies outside the first Brillouin zone.

$$\mathbf{a}_1 + \mathbf{a}_2 = \mathbf{a}_3 + \mathbf{G}, \tag{21.16}$$

where $\mathbf{G}$ is again a translational vector which has in the present case the modulus $-2\pi/a$ (see Fig. 21.3). As a consequence, the resultant phonon of vector $\mathbf{a}_4$ proceeds after the collision in a direction which is almost opposite to $\mathbf{a}_2$, which constitutes, of course, a resistance against the flow of phonons. This mechanism is called *umklapp* process (German for "flipping over" process).

Phonon collisions in which $\mathbf{a}_1$ and $\mathbf{a}_2$ are small so that the resultant vector $\mathbf{a}_3$ stays inside the first Brillouin zone (that is, $\mathbf{G} = 0$) are called *normal processes*. A normal process has no effect on the thermal resistance since the resultant phonon proceeds essentially in the same direction.

Problems

1. Calculate the thermal conductivity for a metal assuming $\tau = 3 \times 10^{-14}$ s, $T =$ 300 K, and $N_f = -2.5 \times 10^{28}$ el/m^3.
2. Calculate the Lorentz number from values of e and k_B. Show how you arrived at the correct units!
3. Calculate the mean free path of electrons in a metal, such as silver, at room temperature from heat capacity and heat conduction measurements. Take $E_F =$ 5 eV, $K = 4.1 \times 10^2$ J/s·m·K, and $C_v^{el} = 1\%$ of the lattice heat capacity. *Hint*: Remember that the heat capacity in (21.8) is given per volume!
4. Why is the thermal conduction in dielectric materials two or three orders of magnitude smaller than in metals?
5. Why does the thermal conductivity span only 4 orders of magnitude whereas the electrical conduction spans nearly 25 orders of magnitude?
6. Is there a theoretical possibility for a thermal superconductor?
7. Discuss why the thermal conductivity of alloys is lower than that of the pure constituents.

CHAPTER 22

Thermal Expansion

The length L of a rod increases with increasing temperature. Experiments have shown that in a relatively wide temperature range the linear expansion ΔL is proportional to the increase in temperature ΔT. The proportionality constant is called the coefficient of linear expansion α_L. The observations can be summarized in

$$\frac{\Delta L}{L} = \alpha_L \Delta T. \tag{22.1}$$

Experimentally observed values for α_L are given in Table 22.1.

The expansion coefficient has been found to be proportional to the molar heat capacity C_v, that is, the temperature dependence of α_L is similar to the

Table 22.1. Linear Expansion Coefficients α_L for Some Solids Measured at Room Temperature

Substance	α_L in $10^{-5}[K^{-1}]$
Hard rubber	8.00
Lead	2.73
Aluminum	2.39
Brass	1.80
Copper	1.67
Iron	1.23
Glass (ordinary)	0.90
Glass (pyrex)	0.32
NaCl	0.16
Invar	0.07
Quartz glass	0.05

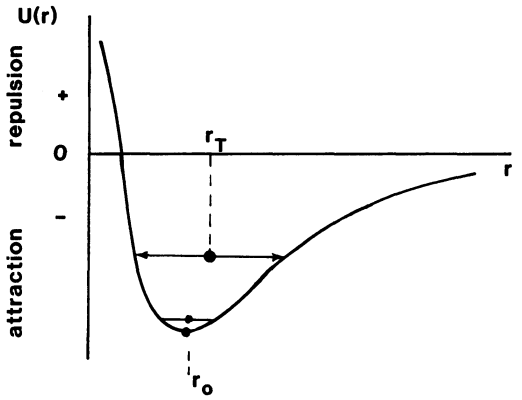

Figure 22.1. Schematic representation of the potential energy, $U(r)$, for two adjacent atoms as a function of internuclear separation, r.

temperature dependence of C_v. As a consequence, the temperature dependence of α for dielectric materials follows closely the $C_v = f(T)$ relationship predicted by Debye and shown in Fig. 18.2. Specifically, α approaches a constant value for $T \gg \theta_D$ and vanishes as T^3 for $T \to 0$. The thermal expansion coefficient for metals, on the other hand, decreases at very small temperatures in proportion to T, and depends, in other temperature regions, on the sum of the heat capacities of phonons and electrons.

We turn now to a discussion of possible mechanisms which may explain thermal expansion from an atomistic point of view. We postulate, as in the previous chapters, that the lattice atoms absorb thermal energy by vibrating about their equilibrium position. In doing so, a given atom responds with increasing temperature and vibrational amplitude to the repulsive forces of the neighboring atoms. Let us consider for a moment two adjacent atoms only and let us inspect their potential energy as a function of internuclear separation (Fig. 22.1). We understand that as two atoms move closer to each other, strong repulsive forces are experienced between them. As a consequence, the potential energy curve rises steeply with decreasing r. On the other hand, we know that two atoms also attract each other somewhat. This results in a slight decrease in $U(r)$ with decreasing r.

Now, for small temperatures, a given atom may rest in its equilibrium position r_0, that is, at the minimum of potential energy. If, however, the temperature is raised, the amplitude of the vibrating atom increases too. Since the amplitudes of the vibrating atom are symmetric about a median position and since the potential curve is not symmetric, a given atom moves further apart from its neighbor, that is, the average position of an atom moves to a larger r, say, r_T, as shown in Fig. 22.1. In other words, the thermal expansion is a direct consequence of the asymmetry of the potential energy curve. The same arguments hold true if all atoms in a solid are considered.

A few substances are known to behave differently from that described

above. They contract during a temperature increase. This happens, however, only within a narrow temperature region. For its explanation, we need to realize that longitudinal as well as transverse vibrational modes may be excited by thermal energy (see Section 20.2). The lattice is expected to contract if transverse modes predominate. Interestingly enough only one known liquid substance, namely water, behaves in a limited temperature range in this manner. Specifically, water has its largest density at 4° C (Furthermore, the density of ice is smaller than the density of water at the freezing point.) As a consequence, water of 4° C sinks to the bottom of a lake during winter, while ice stays on top. This prevents the freezing of a lake at the bottom and thus enables aquatic life to survive during the winter. This exceptional behavior of water suggests that the laws of physics do not just "happen," but rather they were created by a superior being. I want to conclude my book with this thought.

Problems

1. Estimate the force which is exerted by the end of a 1 m long iron rod of 1 cm^2 cross section which was heated by 100° C.
2. Calculate the gap which has to be left between two 10 m long railroad tracks when they are installed at 0° C and if no compression is allowed at 40° C.
3 Explain some engineering applications of thermal expansion such as the bimetal thermal switch, metal thermometer, etc.
4. What happens if a red hot piece of glass is immersed into cold water? What happens if the same experiment is done with quartz glass?

Suggestions for Further Reading (Part V)

A.J. Dekker, *Solid State Physics*, Prentice-Hall, Englewood-Cliffs, NJ (1957).
C. Kittel and H. Kroemer, *Thermal Physics*, 2nd ed., W.H. Freeman & Company, San Francisco, CA (1980).
P.G. Klemens and T.K. Chu, eds., *Thermal Conductivity*, Volumes 1–17, Plenum Press, New York and London.
T.F. Lee, F.W. Sears, and D.L. Turcotte, *Statistical Thermodynamics*, Addison-Wesley Publishing Company, Inc., Reading, MA (1963).
J.M. Ziman, *Electrons and Phonons*, Oxford University Press, Oxford (1960).

APPENDICES

APPENDIX 1

Periodic Motions

A *vibration* is a time dependent *or* space dependent periodic motion. We restrict our discussion to harmonic vibrations. In this case, the space dependence of time is represented by a simple sine or cosine function, or equivalently, because of the Euler equations (see Appendix 2), by an exponential function.

A.1.1. Undamped Vibration

(a) Differential equation for *time dependent periodicity*:

$$m\frac{d^2u}{dt^2} + \kappa u = 0 \tag{A.1}$$

(m = mass, κ = retracting force parameter). A solution is

$$u = Ae^{i\omega t}, \tag{A.2}$$

where

$$\omega = \sqrt{\frac{\kappa}{m}} = 2\pi\nu \tag{A.3}$$

is the angular frequency and A is a constant called maximum amplitude.

(b) Differential equation for *space dependent periodicity* (in one dimension):

$$a\frac{d^2u}{dx^2} + bu = 0. \tag{A.4}$$

Solution:

$$u = Ae^{iax} + Be^{-iax}, \tag{A.5}$$

where A and B are constants, and

$$\alpha = \sqrt{\frac{b}{a}}. \tag{A.6}$$

A.1.2. Damped Vibration

(a) Differential equation for *time dependent periodicity*:

$$m\frac{d^2u}{dt^2} + \gamma\frac{du}{dt} + \kappa u = 0 \tag{A.7}$$

(γ is the damping constant). The solution is

$$u = Ae^{-\beta t} \cdot e^{i(\omega_0 t - \phi)}, \tag{A.8}$$

where

$$\omega_0 = \sqrt{\frac{\kappa}{m} - \beta^2} \tag{A.9}$$

is the resonance frequency,

$$\beta = \frac{\gamma}{2m} \tag{A.10}$$

is the damping factor, and ϕ is the phase (angle) difference. In a damped vibration, the amplitude $Ae^{-\beta t}$ decreases exponentially.

(b) Differential equation for *space dependent periodicity*:

$$\frac{d^2u}{dx^2} + D\frac{du}{dx} + Cu = 0. \tag{A.11}$$

Solution:

$$u = e^{-Dx/2}(Ae^{i\rho x} + Be^{-i\rho x}), \tag{A.12}$$

where

$$\rho = \sqrt{C - \frac{D^2}{4}} \tag{A.13}$$

and A, B, C and D are constants.

A.1.3. Forced Vibration (Damped)

Differential equation for *time dependent periodicity*:

$$m\frac{d^2u}{dt^2} + \gamma\frac{du}{dt} + \kappa u = K_0 e^{i\omega t}. \tag{A.14}$$

The right hand side is the time periodic excitation force. The solution consists of the start-up vibration and a steady-state part. The steady-state solution is

$$u = \frac{K_0}{\sqrt{m^2(\omega_0^2 - \omega^2)^2 + \gamma^2\omega^2}} e^{i(\omega t - \phi)}, \tag{A.15}$$

where

$$\omega_0 = \sqrt{\frac{\kappa}{m}} \tag{A.16}$$

is the resonance frequency of the undamped, free oscillation.

The tangent of the phase difference ϕ between the excitation force and the forced vibration is

$$\tan\phi = \frac{\gamma\omega}{m(\omega_0^2 - \omega^2)}. \tag{A.17}$$

A.1.4. Wave

A wave is a space *and* time dependent periodic motion.

(a) The differential equation for the undamped wave is

$$v^2\nabla^2 u = \frac{\partial^2 u}{\partial t^2}, \tag{A.18}$$

where

$$\nabla^2 = \frac{\partial^2}{\partial x^2} + \frac{\partial^2}{\partial y^2} + \frac{\partial^2}{\partial z^2}. \tag{A.19}$$

The differential equation for the plane wave is

$$v^2\frac{\partial^2 u}{\partial x^2} = \frac{\partial^2 u}{\partial t^2}, \tag{A.20}$$

whose solution is

$$u(t, x) = e^{i\omega t}(Ae^{i\alpha x} + Be^{-i\alpha x}), \tag{A.21}$$

or

$$u(t, x) = Ae^{i(\omega t + \alpha x)} + Be^{i(\omega t - \alpha x)}, \tag{A.22}$$

or

$$u(t, x) = Ae^{i\omega(t + (x/v))} + Be^{i\omega(t - (x/v))}. \tag{A.23}$$

(b) Damped wave:

$$v^2\frac{\partial^2 u}{\partial x^2} = a\frac{\partial u}{\partial t} + b\frac{\partial^2 u}{\partial t^2}. \tag{A.24}$$

The solution is possible by using (A.23). The general wave equation

$$v^2\nabla^2 u = a\frac{\partial u}{\partial t} + b\frac{\partial^2 u}{\partial t^2} \tag{A.25}$$

can be solved with

$$u(t, x, y, z) = Ae^{i(\omega t - \mathbf{k}\cdot v)}, \tag{A.26}$$

where

$$|\mathbf{k}| = \frac{2\pi}{\lambda} \tag{A.27}$$

is the wave number vector. It has the unit of a reciprocal length.

APPENDIX 2

Euler Equations

$$\cos\phi = \frac{1}{2}(e^{i\phi} + e^{-i\phi}) \tag{A.28}$$

$$\sin\phi = \frac{1}{2i}(e^{i\phi} - e^{-i\phi}) \tag{A.29}$$

$$\sinh\phi = \frac{1}{2}(e^{\phi} - e^{-\phi}) = \frac{1}{i}\cdot\sin i\phi \tag{A.30}$$

$$\cosh\phi = \frac{1}{2}(e^{\phi} + e^{-\phi}) = \cos i\phi \tag{A.31}$$

$$e^{i\phi} = \cos\phi + i\sin\phi \tag{A.32}$$

$$e^{-i\phi} = \cos\phi - i\sin\phi. \tag{A.33}$$

APPENDIX 3

Summary of Quantum Number Characteristics

The energy states of electrons are characterized by four quantum numbers. The main quantum number n determines the overall energy of the electrons, that is, essentially the radius of the electron distribution. It can have any integral value. For example, the electron of a hydrogen atom in its ground state has $n = 1$.

The quantum number l is a measure of the angular momentum L of the electrons and is determined by $|\mathbf{L}| = \sqrt{l(l+1)}\hbar$, where l can assume any integral value between 0 and $n - 1$.

It is common to specify a given energy state by a symbol which utilizes the n and l values. States with $l = 0$ are called s-states; with $l = 1$, p-states; and with $l = 2$, d-states, etc. A $4d$-state, for example, is one with $n = 4$ and $l = 2$.

The possible orientations of the angular momentum vector with respect to an external magnetic field are again quantized and given by the magnetic quantum number m. Only m values between $+l$ and $-l$ are permitted.

The electrons of an atom fill the available states starting with the lowest state and obeying the Pauli principle which requires that each state can be filled only with two electrons having opposite spin ($|\mathbf{s}| = \pm 1/2$). Because of the just mentioned multiplicity, the maximal number of electrons in the s-states is 2, in the p-states 6, in the d-states 10, and in the f-states 14.

The electron bands in solids are named by using the same nomenclature as above, that is, a $3d$-level in the atomic state widens to a $3d$-band in a solid. The electron configurations of some isolated atoms are listed on the next page.

Z	Element	K $1s$	L $2s$ $2p$	M $3s$ $3p$ $3d$	N $4s$ $4p$ $4d$ $4f$	O $5s$ $5p$ $5d$ $5f$
1	H	1				
2	He	2				
3	Li	2	1			
4	Be	2	2			
5	B	2	2 1			
6	C	2	2 2			
7	N	2	2 3			
8	O	2	2 4			
9	F	2	2 5			
10	Ne	2	2 6			
11	Na	2	2 6	1		
12	Mg	2	2 6	2		
13	Al	2	2 6	2 1		
14	Si	2	2 6	2 2		
15	P	2	2 6	2 3		
16	S	2	2 6	2 4		
17	Cl	2	2 6	2 5		
18	Ar	2	2 6	2 6		
19	K	2	2 6	2 6	1	
20	Ca	2	2 6	2 6	2	
21	Sc	2	2 6	2 6 1	2	
22	Ti	2	2 6	2 6 2	2	
23	V	2	2 6	2 6 3	2	
24	Cr	2	2 6	2 6 4	1	
25	Mn	2	2 6	2 6 5	2	
26	Fe	2	2 6	2 6 6	2	
27	Co	2	2 6	2 6 7	2	
28	Ni	2	2 6	2 6 8	2	
29	Cu	2	2 6	2 6 10	1	
30	Zn	2	2 6	2 6 10	2	
31	Ga	2	2 6	2 6 10	2 1	
32	Ge	2	2 6	2 6 10	2 2	
33	As	2	2 6	2 6 10	2 3	
34	Se	2	2 6	2 6 10	2 4	
35	Br	2	2 6	2 6 10	2 5	
36	Kr	2	2 6	2 6 10	2 6	
37	Rb	2	2 6	2 6 10	2 6	1
38	Sr	2	2 6	2 6 10	2 6	2
39	Y	2	2 6	2 6 10	2 6 1	2
40	Zr	2	2 6	2 6 10	2 6 2	2
41	Nb	2	2 6	2 6 10	2 6 4	1
42	Mo	2	2 6	2 6 10	2 6 5	1
43	Tc	2	2 6	2 6 10	2 6 5	2

APPENDIX 4

Tables

The International System of Units (SI or mksA System)

In the SI-unit system, essentially four base units, the meter, the kilogram (for the mass), the second, and the ampere are *defined.* Further base units are the Kelvin, the mole (for the amount of substance), and the Candela (for the luminous intensity). All other units are *derived units* as shown in the table below. Even though the use of the SI-unit system is highly recommended, other unit systems are still widely used.

			Expression in terms of	
Quantity	Name	Symbol	Other SI units	SI base units
Force	Newton	N	—	$kg \cdot m/s^2$
Energy, wok	Joule	J	$N \cdot m$	$kg \cdot m^2/s^2$
Pressure	Pascal	Pa	N/m^2	$kg/m \cdot s^2$
El. charge	Coulomb	C	J/V	$A \cdot s$
Power	Watt	W	J/s	$kg \cdot m^2/s^3$
El. potential	Volt	V	W/A	$kg \cdot m^2/A \cdot s^3$
El. resistance	Ohm	Ω	V/A	$kg \cdot m^2/A^2 \cdot s^3$
Magn. flux	Weber	Wb	$V \cdot s$	$kg \cdot m^2/A \cdot s^2$
Magn. field	Tesla	T	Wb/m^2	$kg/A \cdot s^2$
Inductance	Henry	H	Wb/A	$kg \cdot m^2/A^2 \cdot s^2$
Capacitance	Farad	F	C/V	$A^2 \cdot s^4/kg \cdot m^2$

Physical Constants (cgs and SI units)

Mass of electron (Free electron mass)	$m_0 = 9.11 \times 10^{-28}\,(\mathrm{g}) = 9.11 \times 10^{-31}\,(\mathrm{kg})$
Charge of electron	$e = 1.602 \times 10^{-19}\,(\mathrm{C})$
	$= 4.803 \times 10^{-10}\,(\mathrm{statcoul}) \equiv (\mathrm{cm}^{3/2} \cdot \mathrm{g}^{1/2}/\mathrm{s}) \equiv (\mathrm{erg/stat\,V})$
	$= 1.602 \times 10^{-20}\,(\mathrm{abcoul}) \equiv (\mathrm{g}^{1/2} \cdot \mathrm{cm}^{1/2})$
Velocity of light	$c = 2.998 \times 10^{10}\,(\mathrm{cm/s}) = 2.998 \times 10^{8}\,(\mathrm{m/s})$
Planck constant	$h = 6.626 \times 10^{-27}\,(\mathrm{g \cdot cm^2/s}) = 4.136 \times 10^{-15}\,(\mathrm{eV \cdot s})$
	$= 6.625 \times 10^{-34}\,(\mathrm{J \cdot s})$
	$\hbar = 1.054 \times 10^{-27}\,(\mathrm{g \cdot cm^2/s}) = 6.57 \times 10^{-16}\,(\mathrm{eV \cdot s})$
	$= 1.054 \times 10^{-34}\,(\mathrm{J \cdot s})$
Avogadro constant	$N_0 = 6.025 \times 10^{23}\,(\mathrm{atoms/mol})$
Boltzmann constant	$k_B = 1.381 \times 10^{-16}\,(\mathrm{erg/K}) = 8.616 \times 10^{-5}\,(\mathrm{eV/K})$
	$= 1.381 \times 10^{-23}\,(\mathrm{J/K})$
Bohr magneton	$\mu_B = 9.274 \times 10^{-21}\left(\frac{\mathrm{erg}}{\mathrm{Oe}}\right) \equiv (\mathrm{Oe \cdot cm^3}) \equiv (\mathrm{g^{1/2}\,cm^{5/2}/s})$
Gas constant	$\mathrm{R} = 8.314\,(\mathrm{J/mol \cdot K}) = 1.986\,(\mathrm{cal/mol \cdot K})$

Useful Conversions

$1\,(\mathrm{eV}) = 1.602 \times 10^{-12}\,(\mathrm{g \cdot cm^2/s^2}) = 1.602 \times 10^{-19}\,(\mathrm{kg \cdot m^2/s^2})$

$1\,(\mathrm{J}) = 1\left(\frac{\mathrm{kg \cdot m^2}}{\mathrm{s^2}}\right) = 10^{7}\,(\mathrm{erg}) = 10^{7}\left(\frac{\mathrm{g \cdot cm^2}}{\mathrm{s^2}}\right) = 2.39 \times 10^{-1}\,(\mathrm{cal})$

$1\,(\mathrm{Rydberg}) = 13.6\,(\mathrm{eV})$

$1\,(1/\Omega\mathrm{cm}) = 9 \times 10^{11}\,(1/\mathrm{s})$

$1\,(1/\Omega\mathrm{m}) = 9 \times 10^{9}\,(1/\mathrm{s})$

$1\,(\mathrm{C}) = 1\,(\mathrm{A \cdot s}) = 1\,(\mathrm{J/V})$

$1\,(\text{Å}) = 10^{-10}\,(\mathrm{m})$

$1\,(\mathrm{torr}) \equiv 1\,(\mathrm{mm\ Hg}) = 133.3\,(\mathrm{N/m^2}) \equiv 133.3\ \mathrm{Pa}$

$1\,(\mathrm{bar}) = 10^{5}\,(\mathrm{N/m^2}) \equiv 10^{5}\ \mathrm{Pa}$

Electronic Properties of Some Metals

Material	Effective mass $\left(\frac{m^*}{m_0}\right)_{el}$	Effective mass $\left(\frac{m^*}{m_0}\right)_{opt}$	Fermi energy E_F[eV]	Number of free electrons, N_{eff} $\left[\frac{\text{electrons}}{\text{m}^3}\right]$	Work function (photoelectric) ϕ[eV]	Resistivity $\rho[\mu\Omega\text{cm}]$ at 20° C
Ag		0.95	5.5	6.1×10^{28}	4.7	1.59
Al	0.97	1.08	11.8	16.7×10^{28}	4.1	2.65
Au		1.04		5.65×10^{28}	4.8	2.35
Be	1.6		12.0		3.9	4.0
Ca	1.4		3.0		2.7	3.91
Cs					1.9	20.0
Cu	1.0	1.42	7.0	6.3×10^{28}	4.5	1.67
Fe	1.2				4.7	9.71
K	1.1		1.9		2.2	6.15
Li	1.2		3.7		2.3	8.55
Na	1.0				2.3	4.20
Ni	2.8				5.0	6.84
Zn	0.85		11.0	3×10^{28}	4.3	5.91

Electronic Properties of Some Semiconductors

	Material	Gap energy E_g[eV] 0 K	Gap energy E_g[eV] 300 K	Conductivity $\sigma\left[\frac{1}{\Omega \cdot m}\right]$	Mobility of electrons $\mu_e\left[\frac{m^2}{V \cdot s}\right]$	Mobility of holes $\mu_h\left[\frac{m^2}{V \cdot s}\right]$	Work Function (photoelectric) ϕ[eV]	Effective Mass at 4 K $\frac{m_n^*}{m_0}$	Effective Mass at 4 K $\frac{m_p^*}{m_0}$
Element	C (diamond)	5.48	5.47	10^{-12}	0.18	0.12	4.8	0.2	0.25
	Ge	0.74	0.66	2.2	0.39	0.19	4.6	1.64[a] 0.08[b]	0.04[c] 0.28[d]
	Si	1.17	1.12	9×10^{-4}	0.15	0.045	3.6	0.98[a] 0.19[b]	0.16[c] 0.49[d]
	Sn (gray)	0.08		10^{6}	0.14	0.12	4.4		
III–V	GaAs	1.52	1.42	10^{-6}	0.85	0.04		0.067	0.082
	InAs	0.42	0.36	10^{4}	3.30	0.046		0.023	0.40
	InSb	0.23	0.17		8.00	0.125		0.014	0.40
	GaP	2.34	2.26		0.01	0.007		0.82	0.60
IV–IV	α-SiC	3.03	2.996		0.04	0.005		0.60	1.00
II–VI	ZnO	3.42	3.35		0.02	0.018		0.27	
	CdSe	1.85	1.70		0.08			0.13	0.45

[a] Longitudinal effective mass.

[b] Transverse effective mass.

[c] Light-hole effective mass.

[d] Heavy-hole effective mass.

Ionization Energies for Various Dopants in Semiconductors (Experimental)

Donor ionization energies are given from the donor levels to the bottom of the conduction band. Acceptor ionization energies are given from the top of the valence band to the acceptor levels.

Semiconductor	Dopant		Ionization energy (eV)
	Type	Element	
Ge	Donors	Sb	0.0096
		P	0.012
		As	0.013
	Acceptors	B	0.01
		Al	0.01
		Ga	0.011
		In	0.011
Si	Donors	Sb	0.039
		P	0.045
		As	0.054
	Acceptors	B	0.045
		Al	0.067
		Ga	0.072
		In	0.16
GaAs	Donors	Si	0.0058
		Ge	0.006
		Sn	0.006
	Acceptors	Be	0.028
		Mg	0.028
		Zn	0.031

Magnetic Units

Name	Symbol	em-cgs units	mks (SI) units	Conversions
Magnetic Field Strength	**H**	$\text{Oe} \equiv \frac{\text{g}^{1/2}}{\text{cm}^{1/2} \cdot \text{s}}$	$\frac{\text{A}}{\text{m}}$	$1\frac{\text{A}}{\text{m}} = \frac{4\pi}{10^3}\text{Oe}$
Magnetic Induction	**B**	$\text{G} \equiv \frac{\text{g}^{1/2}}{\text{cm}^{1/2} \cdot \text{s}}$	$\frac{\text{Wb}}{\text{m}^2} = \frac{\text{Kg}}{\text{s} \cdot \text{C}} \equiv \text{T}$	$1\frac{\text{Wb}}{\text{m}^2} = 10^4\ \text{G}$
Magnetization	**M**	$\frac{\text{Maxwell}}{\text{cm}^2} \equiv \frac{\text{g}^{1/2}}{\text{cm}^{1/2} \cdot \text{s}}$	$\frac{\text{A}}{\text{m}}$	$1\frac{\text{A}}{\text{m}} = \frac{4\pi}{10^3}\frac{\text{Maxwells}}{\text{cm}^2}$
Magnetic Flux	ϕ	$\text{Maxwell} \equiv \frac{\text{cm}^{3/2} \cdot \text{g}^{1/2}}{\text{s}}$	$\text{Wb} = \frac{\text{Kg} \cdot \text{m}^2}{\text{s} \cdot \text{C}} = \text{V} \cdot \text{s}$	$1\ \text{Wb} = 10^8\ \text{Maxwells}$
Susceptibility	χ	unitless	unitless	$\chi_{\text{mks}} = 4\pi\chi_{\text{cgs}}$
(Relative) Permeability	μ	unitless	unitless	same value

Conversions Between Various Unit Systems

SI	electrostatic cgs (esu) units	electromagnetic cgs (emu) units	emu–esu conversion
1 (C)	3×10^9 (statcoul) $\equiv \left(\frac{cm^{3/2} \cdot g^{1/2}}{s}\right)$	$\frac{1}{10}$(abcoul) $\equiv (g^{1/2} \cdot cm^{1/2})$	1 (abcoul) = c (statcoul)
1 (V)	$\frac{1}{300}$(statvolts) $\equiv \left(\frac{cm^{1/2} \cdot g^{1/2}}{s}\right)$	10^8 (abvolts) $\equiv \left(\frac{cm^{3/2} \cdot g^{1/2}}{s^2}\right)$	1 (abvolt) $= \frac{1}{c}$(statvolts)
1 (A)	3×10^9 (statamps) $\equiv \left(\frac{cm^{3/2} \cdot g^{1/2}}{s^2}\right)$	$\frac{1}{10}$(abamps) $\equiv \left(\frac{cm^{1/2} \cdot g^{1/2}}{s}\right)$	1 (abamp) = c (statamps)
1 (Ω)	1.113×10^{-12} (statohms) $\equiv \left(\frac{s}{cm}\right)$	10^9 (abohms) $\equiv \left(\frac{cm}{s}\right)$	1 (abohm) $= \frac{1}{c^2}$(statohms)

The equations given in this book can be converted from the cgs (Gaussian) unit system into the SI (mks) system and vice versa by replacing the symbols in the respective equations with the symbols listed in the following table. Symbols which are not listed here remain unchanged. It is imperative that consistent sets of units are utilized.

QUANTITY	mks (SI)	cgs (GAUSSIAN)
Magnetic induction	$\mathbf{B}$	$\mathbf{B}/c$
Magnetic flux	Φ_B	Φ_B/c
Magnetic field strength	$\mathbf{H}$	$c\mathbf{H}/4\pi$
Magnetization	$\mathbf{M}$	$c\mathbf{M}$
Magnetic dipole moment	μ	$c\mu$
Permittivity constant	ε_0	$1/4\pi$
Permeability constant	μ_0	$4\pi/c^2$
Electric displacement	$\mathbf{D}$	$\mathbf{D}/4\pi$

PERIODIC TABLE OF THE ELEMENTS

GROUP IA												IIIA	IVA	VA	VIA	VIIA	VIIIA
1 1.00797 −252.7 −259.2 0.071 1 H Hydrogen	IIA																2 4.0026 −268.9 −269.7 0.126 1 He Helium
3 6.939 1330 180.5 0.53 1 Li Lithium	4 9.0122 2770 1277 1.85 2 Be Beryllium											5 10.811 — (2030) 2.34 3 B Boron	6 12.01115 4830 3727 g 2.26 ±4,2 C Carbon	7 14.0067 −195.8 −210 0.81 ±3,5,4,2 N Nitrogen	8 15.9994 −183 −218.8 1.14 −2 O Oxygen	9 18.9984 −188.2 −219.6 1.505 −1 F Fluorine	10 20.183 −246 −248.6 1.20 Ne Neon
11 22.9898 892 97.8 0.97 1 Na Sodium	12 24.312 1107 650 1.74 2 Mg Magnesium	IIIB	IVB	VB					IB	IIB		13 26.9815 2450 660 2.70 3 Al Aluminum	14 28.086 2680 1410 2.33 4 Si Silicon	15 30.9738 280w 44.2w 1.82w ±3,5,4 P Phosphorus	16 32.064 444.6 119.0 2.07 ±2,4,6 S Sulfur	17 35.453 −34.7 −101.0 1.56 ±1,3,5,7 Cl Chlorine	18 39.948 −185.8 −189.4 1.40 Ar Argon
19 39.102 760 63.7 0.86 1 K Potassium	20 40.08 1440 838 1.55 2 Ca Calcium	21 44.956 2730 1539 3.0 3 Sc Scandium	22 47.90 3260 1668 4.51 4,3 Ti Titanium	23 50.942 3450 1900 6.1 5,4,3,2, V Vanadium					29 63.54 2595 1083 8.96 2,1 Cu Copper	30 65.37 906 419.5 7.14 2 Zn Zinc	31 69.72 2237 29.8 5.91 3 Ga Gallium	32 72.59 2830 937.4 5.32 4 Ge Germanium	33 74.922 613* 817 5.72 ±3,5 As Arsenic	34 78.96 685 217 4.79 −2,4,6 Se Selenium	35 79.909 58 −7.2 3.12 ±1,5 Br Bromine	36 83.80 −152 −157.3 2.6 Kr Krypton
37 85.47 688 38.9 1.53 1 Rb Rubidium	38 87.62 1380 768 2.6 2 Sr Strontium	39 88.905 2927 1509 4.47 3 Y Yttrium	40 91.22 3580 1852 6.49 4 Zr Zirconium	41 92.906 5,3 5400 2468 8.4 Nb Niobium	42 95.94 6,5,4,3,2 5560 2610 10.2 Mo Molybdenum	43 (98) 7 — 2140 11.5 Tc Technetium	44 101.07 2,3,4,6,8 4900 2500 12.2 Ru Ruthenium	45 102.905 2,3,4 4500 1966 12.4 Rh Rhodium	46 106.4 2,4 3980 1552 12.0 Pd Palladium	47 107.870 2210 960.8 10.5 1 Ag Silver	48 112.40 765 320.9 8.65 2 Cd Cadmium	49 114.82 2000 156.2 7.31 3 In Indium	50 118.69 2270 231.9 7.30 4,2 Sn Tin	51 121.75 1380 630.5 6.62 ±3,5 Sb Antimony	52 127.60 989.8 449.5 6.24 −2,4,6 Te Tellurium	53 126.904 183 113.7 4.94 ±1,5,7 I Iodine	54 131.30 −108.0 −111.9 3.06 Xe Xenon
55 132.905 690 28.7 1.90 1 Cs Cesium	56 137.34 1640 714 3.5 2 Ba Barium	57 138.91 3 ★ 3470 920 6.17 La Lanthanum	72 178.49 4 5400 2222 13.1 Hf Hafnium	73 180.948 5 5425 2996 16.6 Ta Tantalum	74 183.85 6,5,4,3,2 5930 3410 19.3 W Wolfram	75 186.2 7,6,4,2,−1 5900 3180 21.0 Re Rhenium	76 190.2 2,3,4,6,8 5500 3000 22.6 Os Osmium	77 192.2 2,3,4,6 5300 2454 22.5 Ir Iridium	78 195.09 2,4 4530 1769 21.4 Pt Platinum	79 196.967 2970 1063 19.3 3,1 Au Gold	80 200.59 357 −38.4 13.6 2,1 Hg Mercury	81 204.37 1457 303 11.85 3,1 Tl Thallium	82 207.19 1725 327.4 11.4 4,2 Pb Lead	83 208.980 1560 271.3 9.8 3,5 Bi Bismuth	84 (210) — 254 9.2) 2,4 Po Polonium	85 (210) — (302) — ±1,3,5,7 At Astatine	86 (222) (−61.8) (−71) — Rn Radon
87 (223) — (27) — 1 Fr Francium	88 (226) 700 5.0 2 Ra Radium	89 (227) 2 ★★ — 1050 — Ac Actinium	104																

★	58 140.12 3,4 3468 795 6.67 Ce Cerium	59 140.907 3,4 3127 935 6.77 Pr Praseodymium	60 144.24 3 3027 1024 7.00 Nd Neodymium	61 (147) 3 — (1027) — Pm Promethium	62 150.35 3,2 1900 1072 7.54 Sm Samarium	63 151.96 3,2 1439 826 5.26 Eu Europium	64 157.25 3 3000 1312 7.89 Gd Gadolinium	65 158.924 3,4 2800 1356 8.27 Tb Terbium	66 162.50 3 2600 1407 8.54 Dy Dysprosium	67 164.930 3 2600 1461 8.80 Ho Holmium	68 167.26 3 2900 1497 9.05 Er Erbium	69 168.934 3,2 1727 1545 9.33 Tm Thulium	70 173.04 3,2 1427 824 6.98 Yb Ytterbium	71 174.97 3 3327 1652 9.84 Lu Lutetium
★★	90 232.038 4 3850 1750 11.7 Th Thorium	91 (231) 5,4 — (1230) 15.4 Pa Protactinium	92 238.03 6,5,4,3 3818 1132 19.07 U Uranium	93 (237) 6,5,4,3 — 637 19.5 Np Neptunium	94 (242) 6,5,4,3 3235 640 — Pu Plutonium	95 (243) 6,5,4, 3 — — 11.7 Am Americium	96 (247) 3 — — — Cm Curium	97 (247) 4,3 — — — Bk Berkelium	98 (249) 3 — — — Cf Californium	99 (254) — — — — Es Einsteinium	100 (253) — — — — Fm Fermium	101 (256) — — — — Md Mendelevium	102 (254) — — — — No Nobelium	103 (257) — — — — Lw Lawrencium

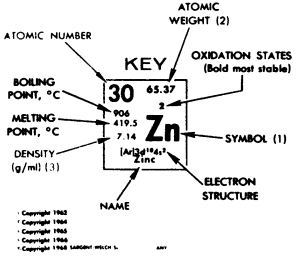

Index